NNT : 2016SACL336

THESE DE DOCTORAT
DE
L'UNIVERSITE PARIS-SACLAY
PREPAREE A UNIVERSITE PARIS SUD

ECOLE DOCTORALE N° 569 ITFA
Innovation thérapeutique: du fondamental à l'appliqué

Spécialité de doctorat: Physiologie, physiopathologie

Par

Marta Lindner

Activation de la phosphodiestérase de type 2 pour traiter l'insuffisance cardiaque

Thèse présentée et soutenue à Châtenay-Malabry, le 12 Octobre 2016

Composition du Jury :

M. Christian POÜS	Professeur, UPSud	Président
Mme Claire LUGNIER	DR Emérite CNRS	Rapporteur
Mme Catherine PAVOINE	CR INSERM	Rapporteur
Mme Liliana CASTRO	Maître de Conférence, UPMC	Examinateur
M. Ali EL-ARMOUCHE	Professeur, Univ. Dresden	Examinateur
M. Grégoire VANDECASTEELE	DR INSERM	Examinateur
M. Rodolphe FISCHMEISTER	DR INSERM	Directeur de thèse

Table of contents

Sommaire

Abstract

Cyclic AMP (cAMP) and cyclic GMP (cGMP) are critical second messengers for the regulation of cardiac function. Intracellular cAMP concentration is regulated by the activities of at least two families of enzymes: adenylyl and guanylyl cyclases, responsible for cAMP and cGMP synthesis and cyclic nucleotide phosphodiesterases (PDEs) that mediate cAMP and cGMP hydrolysis.

Among the PDE superfamily, PDE2 is a dual substrate enzyme that hydrolyzes both cAMP and cGMP and has the unique property to be stimulated by cGMP. It was recently showed that myocardial PDE2 is increased in human and experimental heart failure (HF), while other PDEs (e.g. PDE3 and PDE4) are reduced. However, the pathophysiological consequences of enhanced PDE2 activity in the heart are unknown.

In this context, we generated a transgenic (TG) mouse with a heart specific overexpression of the PDE2A3 isoform (PDE2 TG mouse). Using immunoblotting and radioenzymatic assay we showed that total cardiac cAMP and cGMP PDE activity and specific PDE2 activity was strongly increased in PDE2 TG compared to wild type (WT) mice. Sarcomere shortening, Ca^{2+} transients and the whole L-type Ca^{2+} current ($I_{Ca,L}$) were recorded in adult ventricular myocytes from WT and PDE2 TG mice and isoprenaline (ISO) was used to examine and compare the β-adrenergic (β-AR) response of these parameters. We showed that upon β-AR stimulation, cell contractility, Ca^{2+} transient and $I_{Ca,L}$ were severely blunted. Accordingly, PDE2 overexpression in cardiomyocytes reduced the cAMP levels and abolished the inotropic effect following acute β-AR stimulation. ECG telemetry in PDE2 TG mice showed a marked reduction in resting as well as in maximal heart rate, while cardiac output was completely preserved due to greater contractility. Importantly, PDE2 TG mice were resistant to triggered ventricular arrhythmias and to isoprenaline-induced arrhythmias.

In conclusion, this work demonstrates that PDE2 plays a critical role in the regulation of cardiac excitation-contraction coupling. PDE2 overexpression appears to protect the cardiomyocytes against excessive β-AR drive and reduces the risk of arrhythmias during sympathetic activation. PDE2 activation may thus represent a new subcellular anti-adrenergic and anti-arrhythmic therapeutic strategy in HF.

Key words: phosphodiesterase-2, cAMP, cGMP, β-adrenoceptor signaling, arrhythmias

Résumé

L'AMP cyclique (AMPc) et le GMP cyclique (GMPc) sont des seconds messagers essentiels pour la régulation de la fonction cardiaque. La concentration de l'AMPc intracellulaire est régulée par les activités d'au moins deux familles d'enzymes: les cyclases et guanylyl cyclases, responsable de la synthèse de l'AMPc et du GMPc, et les phosphodiestérases (PDE) qui interviennent dans l'hydrolyse de l'AMPc et du GMPc.

Parmi la superfamille des PDEs, la PDE2 est une enzyme à double substrat qui hydrolyse à la fois l'AMPc et le GMPc et a la propriété unique d'être stimulée par le GMPc. Il a été récemment montré que la PDE2 du myocarde est augmentée dans l'insuffisance cardiaque humaine et expérimentale (IC), tandis que d'autres (par exemple PDE3 et PDE4) sont réduites. Cependant, les conséquences physiopathologiques de l'activité PDE2 renforcée dans le cœur sont inconnues.

Dans ce contexte, nous avons généré des souris transgénique (TG) avec une surexpression spécifique cardiaque de l'isoforme PDE2A3 (souris PDE2 TG).
Grace à l'utilisation de Western blot et de dosage radioenzymatique nous avons montré que l'activité PDE AMPc et l'activité PDE GMPc et l'activité spécifique de PDE2 sont fortement augmentées dans les PDE2 TG par rapport à des souris de type sauvage (WT).
Le raccourcissement cellulaire, les transitoires calciques et le courant calcique de type L ($I_{Ca,L}$) ont été enregistrés dans les myocytes ventriculaires adultes de souris WT et PDE2 TG et l'isoprénaline (ISO) a été utilisée pour examiner et comparer la réponse β-adrénergique (β-AR) de ces paramètres. Nous avons montré que lors de la stimulation β-AR, la contractilité cellulaire, la transitoire Ca^{2+} et l'amplitude du courant $I_{Ca,L}$ sont fortement diminués. En conséquence, la surexpression de la PDE2 dans les cardiomyocytes a réduit les taux d'AMPc et abolit l'effet inotrope après une stimulation β-AR aiguë. L'ECG mesuré par télémétrie chez la souris PDE2 TG a montré une réduction marquée de la fréquence cardiaque au repos ainsi que de la fréquence cardiaque maximale, tandis que le débit cardiaque a est entièrement préservé en raison d'une contractilité plus forte. Fait important, les souris TG PDE2 sont résistantes à des arythmies ventriculaires déclenchées et à des arythmies induites par isoprénaline.

En conclusion, ce travail montre que PDE2 joue un rôle essentiel dans la régulation du couplage excitation-contraction cardiaque. La surexpression de PDE2 semble protéger les cardiomyocytes contre une stimulation excessive β-AR et réduit le risque d'arythmie lors de l'activation sympathique.
L'activation de la PDE2 peut donc représenter une nouvelle stratégie thérapeutique anti-adrénergique et anti-arythmique subcellulaire dans l'insuffisance cardiaque.

Mots clés: phosphodiestérase-2, AMPc, GMPc, signalisation β-adrénergique, arythmies

Abbreviations

AC: Adenylyl cyclase
ACE: Angiotensin-converting enzyme
ACh: Acetylcholine
Ad: Adrenaline
AKAP: A-Kinase Anchoring Protein
cAMP: cyclic adenosine monophosphate
ANP: Atrial natriuretic peptide
AP: Action potential
ATP: Adenosine triphosphate
ATPase: Adenosine triphosphatase
β-AR: Beta-adrenergic receptor
Bay: Bay 60-7550
BNP: Brain natriuretic peptide
Ca^{2+}: Calcium
CaM: Calmodulin
CaMKII: Ca^{2+}/calmodulin-dependent protein kinase
$Ca_v1.2$: Voltage dependent Ca^{2+} channel
CFP: Cyan fluorescent protein
cGMP: cyclic guanosine monophosphate
CICR: Ca^{2+}-induced Ca^{2+}-release
Cil: Cilostamide
CNG: Cyclic nucleotide-gated channels
CNP: C-type natriuretic peptide
CRU: Ca^{2+} release unit
CSQ: Calsequestrin
DAD: Delayed after depolarization
DAG: Diacylglycerol
DP: Developed pressure
EAD: Early after depolarization
ECC: Excitation-contraction coupling
EHNA: Erythro-9-(2-hydroxyl-3-nonyl) adenine
Epac: Exchange factor directly activated by cAMP
FADH: Flavin adenine dinucleotide
FRET: Fluorescence resonance energy transfer
GAF: cGMP, Adenylyl cyclase, Fh1A
GAPDH: Glyceraldehyde 3-phosphate dehydrogenase
G_i: Inhibitory G protein
GPCR: G protein-coupled receptor
GRK: G-protein associated kinase
G_s: Stimulatory G protein
GTP: Guanosine triphosphate
HCN: Hyperpolarization activated Cyclic Nucleotide gated channel
HF: Heart failure
HR: Heart rate
IBMX: 3-isobutyl-1-methylxanthine
$I_{Ca,L}$: L-type Ca^{2+} current
IP3: Inositol trisphosphate
ISO: Isoprenaline or isoproterenol

K^+: Potassium
KO: Knock-out
LTCC: L-type cCa^{2+} channel
mAKAP: muscle AKAP
MAPK: Mitogen-activated protein kinase
MCU: Mitochondrial Ca^{2+} uniporter
Mg^{2+}: Magnesium
MHC: Myosin heavy chain
MLC: Myosin light chain
MOI: Multiplicity of infection
MyBP-C: Myosin binding protein C
NADH : Nicotinamide adenine dinucleotide
NCX: Na^+/Ca^{2+} exchanger
NEP: Neprilysin
NFAT: Nuclear factor of activated T cells
NHR: N-terminal hydrophobic region
NO: Nitric oxide
NOR: Noradrenaline
NOS: Nitric oxide synthase
NP: Natriuretic peptide
PBS: Phosphate buffered saline
PDE: Cyclic nucleotide phosphodiesterase
pGC: Particulate guanylyl cyclase
PGE-R: Prostaglandin E receptor
PI3K: Phosphoinositide 3 Kinase
PKA: cAMP-dependent protein kinase
PKC: Protein kinase C
PKG: cGMP-dependent protein kinase
PKI: Protein kinase inhibitor
PLB: Phospholamban
PLC: Phospholipase C
POP: Popeye family
PP1: Protein phosphatase 1
PP2A: Protein phosphatase 2
(m)PTP: (Mitochondrial) permeability transition pore
RAAS: Renin-angiotensin-aldosterone system
Ro: Ro 20-1724
RyR2: Ryanodine receptor 2
SERCA2: Sarco-endoplasmic reticulum Ca^{2+} ATPase type 2
sAC: Soluble adenylyl cyclase
sGC: Soluble guanylyl cyclase
SNS: Sympathetic nervous system
SNP: Parasympathetic nervous system
SR: Sarcoplasmic reticulum
TG: Transgenic
tmAC: transmembrane adenylyl cyclase
Tn: Troponin
TnC: Troponin C
TnI: Troponin I
TnT: Troponin T
TNF-α: Tumor necrosis factor α

T-tubule: transverse tubule
UCR: Upstream conserved regions
UP: Uniporter
WT: Wild type
YFP: Yellow fluorescent protein
Zn^{2+}: Zinc

List of figures

List of tables

Introduction

I. The heart

I.1 Anatomy of the heart

The heart is an organ in human and other animals, which pumps blood through the blood vessels of the cardiovascular system. Blood provides the body with oxygen and nutrients and takes part in removal of metabolic wastes. The human heart beats about 2.5 billion times during average lifetime and pumps about 300 millions liters of blood. Depending on the individual body's needs, the heart can vary its output between 5 and 20 liters per min. The heart is located in the middle compartment of the chest directly under the breastbone and is composed mainly of cardiac muscles attached to network of collagen fibers. The mammalian and bird heart is divided into four compartments: upper left and right atria; lower left and right ventricles (Figure 1). The right atrium and ventricle are separated from the left atrium and ventricle by a wall, called septum. Blood low in oxygen enters the right atrium from superior and inferior vena cava and passes to the right ventricle. Oxygenated blood returns to the left ventricle through the left atrium and is pumped out through the aorta and pulmonary artery. To prevent the heart from blood backflow, the heart has valves that close automatically. The valve between the right atrium and right ventricle is named the right atrioventricular valve (AV) or tricuspid valve. The valve between left atrium and left ventricle is called the mitral valve. When blood returns from the tissues, fills the atria, as atrial pressure increases above that of the ventricles, the valves open, filling the ventricles with blood. As the ventricles contract, blood is forced back against the valve, pushing them closed. The valve between the left ventricle and the aorta is named the aortic valve. During the left ventricle (LV) contraction (systole), pressure rises in the left ventricle. When the pressure in the LV rises above the pressure in the aorta, aortic valve opens and allows blood to exit the LV. The valve between the right ventricle (RV) and the pulmonary artery is named the pulmonary valve. Pulmonary valve opens in ventricular systole, when the pressure in RV rises above the pressure in the pulmonary artery. At the end of ventricular systole, the pressure in the pulmonary artery closes the pulmonary valve.

Each beat starts in sinoatrial (SA) node localized in the posterior wall of the right atrium. The action potential in the SA node is initiated by depolarizing ion channel and pump currents, and is conducted to the adjacent atrium resulting in atrial contraction. The action potential is then conducted directly to the atrioventricular (AV) node. From the AV node the action potential spreads to the AV bundle. Fibers of the AV bundle branch out forming Purkinje

fibers. When an impulse reaches the ends of the Purkinje fibers, ventricular muscle contracts (Anon, n.d.).

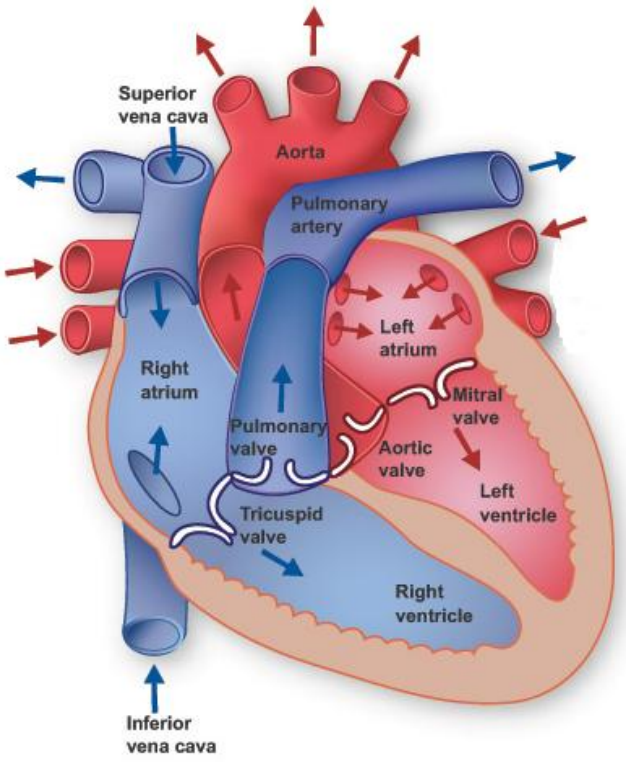

Figure 1: Anatomy of the heart.
Section through the human heart showing the atria, ventricles, valves and circulatory system. (Modified from http://www.texasheart.org)

I.2 Cardiac excitation-contraction coupling

Cardiac excitation-contraction coupling (ECC) is the process by which electrical stimulation of the cardiomyocytes leads to the heart contraction. Ca^{2+} ions play an important and essential role in this process acting as second messengers, direct activators of the myofilaments during contraction.

I.2.1 Structures involved in cardiac ECC

I.2.1.1 Sarcomere and T-tubules

A sarcomere is the basic unit of striated muscle (Figure 2). Highly ordered organization of striated muscle is essential for fast development of force and motion during the heart contraction. In the sarcomeres, the contractile filaments such as actin and myosin are integrated in paracrystalline order by a group of proteins called sarcomeric cytoskeleton. This group of cytoskeletal proteins plays important architectural, mechanical and signaling roles (Gautel & Djinović-Carugo, 2016).

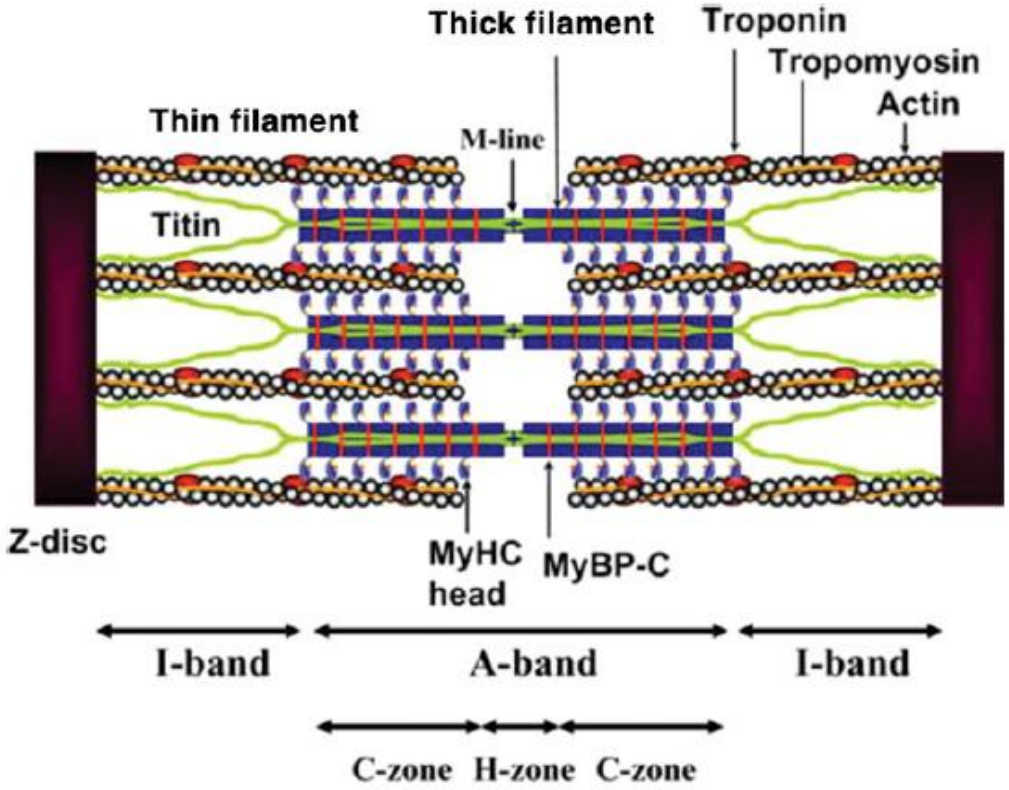

Figure 2: Schematic structure of a sarcomere.
Tropomyosin forms α-helical double strands located along the grooves of actin double strands. Troponin is linked to the specific regions of each tropomyosin in the regular intervals of 38 nm. Myosin heavy chain (MHC) is a protein containing globular head domain with actin binding and ATP hydrolytic sites. Myosin-binding protein C (MyBP-C) is a thick filament which forms 7-9 transverse stripes at a regular distance of 43 nm located in the C-zone of the sarcomere A-band. Titin is the third myofilament located in Z-disc and M-line (Morimoto, 2008).

The transverse tubules (T-tubules) are invaginations of external membrane of skeletal and cardiac muscle and allow depolarization of the membrane to quickly penetrate to the interior of the cell (Orchard & Brette, 2008). The transverse T-tubules of mammalian ventricular cardiomyocytes were first time described by Lindner in 1957 (Lindner, 1957) and the first report of axial T-tubules was done in 1971 (Sperelakis & Rubio, 1971). The transverse tubules are rich in ion channels. Most of the Ca^{2+} ions enter the cell via Ca^{2+} channels located in the T-tubular network. The T-tubules are not just involved in Ca^{2+} influx, but also in Ca^{2+} extrusion and the Na^{+}/Ca^{2+} exchanger (NCX) is also highly expressed in the T-tubules. In addition, the SR Ca^{2+} ATPase is highly expressed in the proximity of the T-tubules, indicating that the greater importance of Ca^{2+} extrusion is close to the Ca^{2+} influx pathway at the T-tubules (Ibrahim *et al.*, 2011). In rat ventricular cardiomyocytes T-tubules represent 3.6% of cellular volume and up to 64% of total sarcolemma (Soeller & Cannell, 1999). It seems that

there is a relation between heart rate and density of T-tubule network. In large animals (e.g pigs) T-tubules density is lower than in small mammals (e.g. mice) which have higher heart rate than bigger mammals. The explanation of this occurrence is that the Ca^{2+} homeostasis (increase and decrease of cytosolic Ca^{2+}) appears faster in animals with higher heart rates (Orchard & Brette, 2008).

I.2.1.2 Sarcoplasmic reticulum

The sarcoplasmic reticulum (SR) is a system of membrane-bounded tubules that surrounds muscle fibrils, first time described by Bennett and Porter and Palade (Bennett & Porter, 1953; Porter & Palade, 1957). The main role of SR is to keep balance between Ca^{2+} storage, release and reuptake in skeletal and cardiac muscle. This balance is achieved through three major classes of SR Ca^{2+}-regulatory proteins:

1) luminal-Ca^{2+} binding proteins, e.g. calsequestrin, involved in Ca^{2+} storage;
2) SR Ca^{2+} release channels, e.g. ryanodine receptors and IP3 receptors, for Ca^{2+} release;
3) sarcoplasmic reticulum Ca^{2+}-ATPases type 2 (SERCA2) for Ca^{2+} reuptake (Rossi & Dirksen, 2006).

Mammalian SR can be arranged into at least three structural and functional elements: longitudinal or "free" SR (fSR), the junctional SR (jSR) and corbular SR (cSR). The longitudinal network is the part of the SR membrane where Ca^{2+} is pumped into the SR via SERCA2. Both jSR and cSR consist of functional clusters of RyRs or 'Ca^{2+} release units' (CRUs). CRUs are localized in the proximity to LTTCs and activated by Ca^{2+} influx from LTCCs, causing Ca^{2+} sparks to produce global Ca^{2+} signals.

cSR is located in ventricular myocytes but is less important than in atrial myocytes. cSR can play a role as a secondary Ca^{2+} amplification system in response to Ca^{2+} diffusion from jSR release (Shiels & Galli, 2014).

I.2.1.3 Myofilaments

The sarcomere is the principal element of the muscle (Figure 2). This repeating unit dominates the anatomy of striated muscles. Each sarcomere is bound by two Z-discs (forming the Z-lines), two I-bands that are regions surrounding the Z-lines, and an A-band between the two I-bands, which is composed of one H-zone and tow C-zones. The Z-line (*Zwinschenscheibe*) appears as a sequence of dark lines and anchors the actin thin fiber from adjacent units. The A-band (*anisotropic*) is the region containing the full length of a single

thick filaments. Within the A-band is a brighter region, the H-zone (*heller*). Within the H-zone is the M-line (*Mittelscheibe*) formed of components of sarcomeric cytoskeleton (Hwang & Sykes, 2015). Without an external force, passive sarcomere length of cardiac myocytes is about 1.9 µm (Granzier & Labeit, 2004).

Thick filaments are composed of 300 to 400 molecules of myosin. Myosins are actin-dependent motor proteins using energy going from ATP hydrolysis to move along actin fibers. The family of myosin consists partially of 20 structurally and functionally different classes and in human genome nearly 40 myosin genes are expressed and encoding 12 classes of proteins. Most myosins are composed of three different regions: 1) NH_2 head domain binding actin and hydrolyzing ATP, 2) neck domain consisting of one or more IQ motifs binding light chains (binding e.g. calmodulin), 3) COOH-terminal tail mediating interactions with cargo molecules and/or dimerization of heavy chains (Krendel & Mooseker, 2005).

The thin filament group is composed of three molecular units: F-actin, tropomyosin and troponin (Robertson *et al.*, 2010). Actin was discovered for the first time in 1942 by Straub (Straub, 1942). A major component of the thin filament is the fibrous form of actin, F-actin. Actin occurs as dynamic equilibrium between polymerized F-actin and monomeric G-actin. One adenosine nucleotide strongly binds to actin and polymerization that occurs during transition from G to F-actin activates ATPase (Oda *et al.*, 2009). Troponin is a protein complex composed of troponin C (TnC), troponin I (TnI) and troponin T (TnT). Troponin C is a Ca^{2+}-binding protein containing two E-F hand motifs in terminal domains. The C-terminal domain of cTnC binds 2 cations, Mg^{2+} or Ca^{2+}, during the contraction-relaxation cycle of the heart. Troponin I interacts with F-actin and inhibits contraction. Troponin T is a scaffold protein that tethers troponin to the thin filament by association with tropomyosin and TnI (Robertson *et al.*, 2010).

I.2.1.4 Mitochondria

Mitochondria are cytosolic double-membrane bound organelles called ‘powerhouse’ of the cell because they generate most of the cell’s energy supply. In addition, mitochondria play an important role in ion homeostasis, redox signaling, apoptotic and necrotic cell death and control of cell growth and cell cycles. In cardiomyocytes, mitochondria represent about 35% of total cell volume and they are localized in the proximity to the main sites of energy consumption: the myofilaments and SR SERCA2. Mitochondria participate in ECC with their ability to maintain cellular pools of ATP, phosphocreatine and NADH, they also store Ca^{2+}

and shape the cytosolic Ca^{2+} signal. The mitochondrial inner membrane is rich in systems of channels and transporters for Ca^{2+} uptake and removal that allows to stock Ca^{2+} ions in the mitochondrial matrix compartment (Maack & O'Rourke, 2007).

Under physiological conditions, glucose is converted to pyruvate which enters mitochondria and is converted into acetyl-coenzyme A (CoA) by pyruvate dehydrogenase complex (PDC). Fatty acids are transformed to fatty acyl-CoA and carnitine-acyltranslocase is responsible for transporting fatty acid across the inner mitochondrial membrane. Acyl-CoA enters β-oxidation, resulting in the formation of NADH and $FADH_2$. NADH is involved in redox reactions in the inner mitochondrial membrane transporting electrons from one reactions to another. The respiratory chain provides the free energy for the ATP generation from ADP.

Mitochondria are important for cell contraction and relaxation because of their efficient machinery for Ca^{2+} transport and ability to store Ca^{2+}. Cardiac contraction is regulated by an elevation of cytosolic Ca^{2+} ($[Ca^{2+}]_i$). The main mechanism of Ca^{2+} efflux in mitochondria is Na^+-dependent via mitochondrial Na^+/Ca^{2+} exchange (mNCX). This antiporter utilizes the Na^+ gradient across the inner membrane. The second way of Ca^{2+} extrusion is via the mitochondrial permeability transition pore (mPTP). This mechanism is based on strong increase in the permeability of the inner mitochondrial membrane to ions with molecular mass up to 1.5 kDa. mPTP is regulated by high concentration of Ca^{2+} in the matrix, oxidative stress and depolarization (Dedkova & Blatter, 2013).

Relaxation occurs upon removal of Ca^{2+} ions from cytoplasm via: 1) SERCA2, 2) sarcolemmal NCX, 3) sarcolemmal Ca-ATPases, and 4) mitochondrial Ca^{2+} uptake. Mitochondrial Ca^{2+} uptake involves the mitochondrial Ca^{2+} uniporter (MCU), a rapid mode of Ca^{2+} uptake (RaM), the mitochondrial ryanodine receptor type 1 (mRyR1) and a recently described leucine-zipper-EF-band-containing transmembrane protein 1 (LETM1). All channels involved in Ca^{2+} uptake are localized to the inner mitochondrial membrane. The most known mechanism of Ca^{2+} uptake is via MCU forced by the large electrochemical gradient. MCU is regulated by several cations, lanthanides, adenine nucleotides and ruthenium compounds (Dedkova & Blatter, 2013).

I.2.2 Excitation

Each beat of the heart is initiated by a pulse of electrical excitation in a group of pacemaker cells. This electrical pulse is initiated by the electrochemical gradient in the surface membrane of each cardiomyocyte. During rest (diastole), the cell membrane is selectively accessible to K^+ ions, so the membrane potential of ventricular cardiomyocyte is about -80 mV, close to

equilibrium potential of K^+ ions (-90 mV). During electrical excitation, the cell membrane starts to be permeable to Na^+ ions, the opening of Na^+ and Ca^{2+} channels brings positive charges inside the cell which leads to depolarization of the membrane potential towards positive values (40 mV or more). Each cell behaves like a dipole and the electrical membrane potential of a cell rapidly rises and falls. The resulting electrical signal is called 'action potential' (Marbán, 2002).

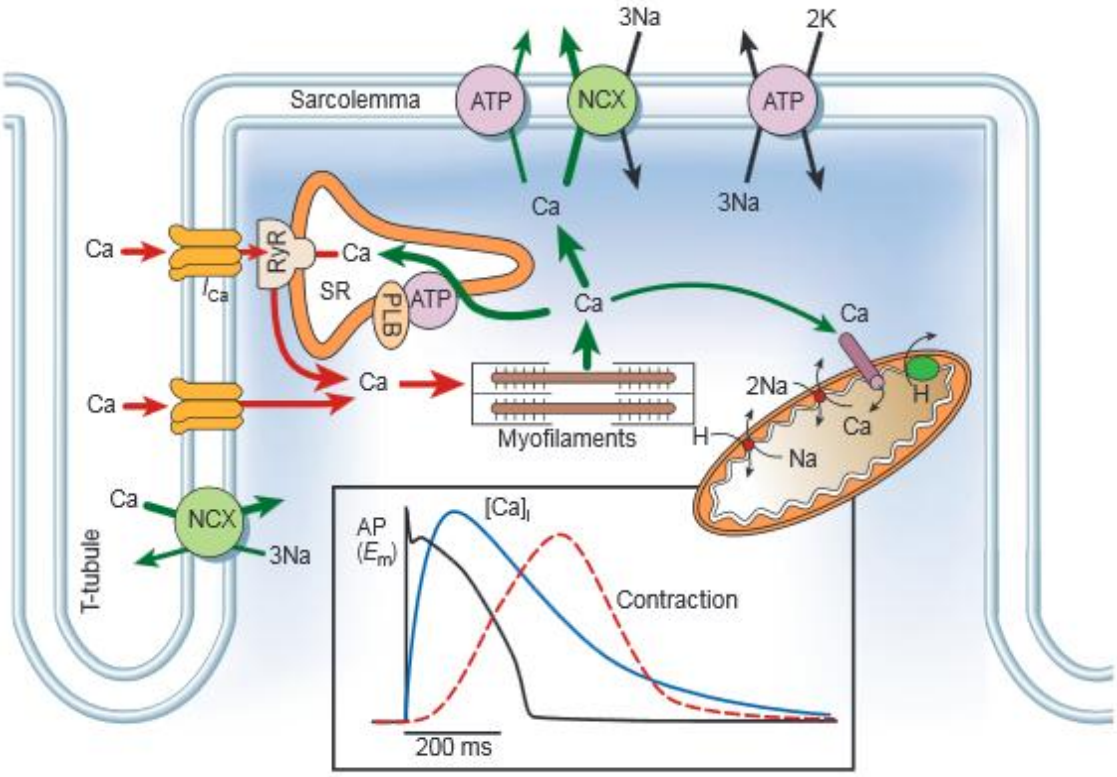

Figure 3: The movement of Ca^{2+} in ventricular myocytes with the key ion channels and pumps.
The graph shows the time course of an action potential, Ca^{2+} transient and contraction in a rabbit ventricular myocytes. Ca, Calcium; NCX, Na^+/Ca^{2+} exchange; ATP, ATPase; PLB, phospholamban, SR, sarcoplasmic reticulum, RyR, ryanodine receptors. (From: (Bers, 2002)).

During the cardiac action potential Ca^{2+} enters the cell through depolarization-activated L-type Ca^{2+} channels (LTCC) generating an inward L-type Ca^{2+} current ($I_{Ca,L}$). Ca^{2+} entry activates adjacent ryanodine receptors (RyRs) to release further Ca^{2+} from the SR where it is stored. The combination of Ca^{2+} influx via $I_{Ca,L}$ and 'Ca^{2+}-induced Ca^{2+}-release' (CICR) from the SR raises cytosolic Ca^{2+} concentration, allows Ca^{2+} to bind to the myofilament protein troponin C and initiates contraction (Figure 3) (Bers, 2002).

I.2.3 Contraction

Molecular mechanism of contraction based on the sliding filament theory was described first time by Huxley in 1954 (Huxley & Hanson, 1954). This theory is based on cyclic interactions between myosin and actin driven by hydrolysis of ATP. Contraction of muscle appears when the thin filaments (actin) slide past the thick fibers (myosin). The crossbridge hypothesis is used to explain this process: it states that actin and myosin filaments create a protein complex, forming a sort of cross-bridge between the two filaments. The myosin head possesses an ATPase activity that allows to convert chemical energy in the form of ATP to mechanical energy, generating force and movement.

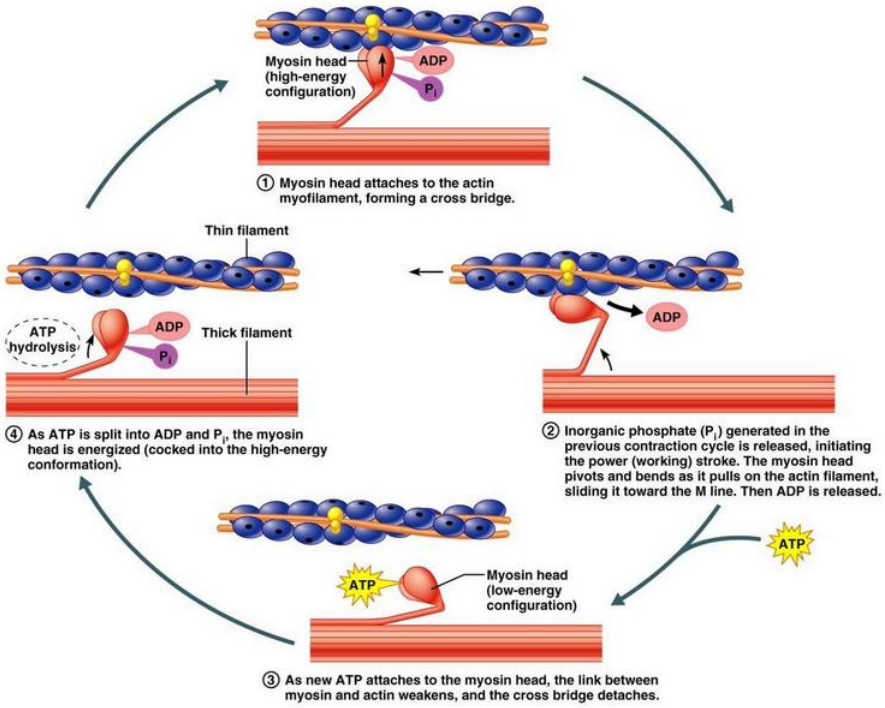

Figure 4: Molecular mechanism of muscle contraction.
In presence of ATP, ADP and Pi are located in the head of myosin. Actin binding to myosin releases ADP and Pi initiating the power stroke resulting in movement of myosin along the thin filament. The cycle is stopped in the absence of ATP. New ATP binds to myosin decreasing its affinity to the actin filament. Separation of myosin and actin results in ATP hydrolysis to ADP and Pi and new cycle starts.

The contraction cycle begins with myosin tightly bound to actin. This interaction activates the myosin ATPase and the energy generated from the hydrolysis of ATP to ADP+Pi (inorganic phosphate) is rapidly converted to mechanical force resulting in movement of myosin along the thin filament by about 5 nm. The products of hydrolysis (ADP+Pi) remain bound to the myosin head. Myosin head rebinds at a new position on the thin filament resulting in the release of ADP+Pi producing the ‘power stroke’ in which the myosin head comes back to the

initial conformation sliding the actin filament toward the M line of the sarcomere (Figure 4). The contraction of cardiac muscle occurs when Ca^{2+} concentration increases in the cytosol from approximately 10^{-7} to 10^{-5} M. The increasing Ca^{2+} concentration gives a signal for contraction via the action of two proteins: tropomyosin and troponin that bind to the actin filaments. Each tropomyosin is bound to troponin formed of troponin C, troponin I and troponin T. The complex of tropomyosin with troponins blocks the interaction of myosin with actin when the concentration of Ca^{2+} in the cytosol is low preventing muscle contraction. At high concentrations, Ca^{2+} binds to troponin C and this leads to conformational changes in the complex resulting in contraction (Cooper, 2000).

I.2.4 Relaxation

Relaxation to occur requires a reduction in cytosolic Ca^{2+} level, allowing Ca^{2+} to dissociate from troponin. This process involves Ca^{2+} transport out of the cytosol by the following pathways: 1) SR Ca^{2+}-ATPase type 2 (SERCA), 2) sarcolemmal Na^{+}/Ca^{2+} exchange (NCX), 3) sarcolemmal Ca^{2+}-ATPase and 4) mitochondrial Ca^{2+} uniport (MCU). The sarcolemmal NCX and sarcolemmal Ca^{2+}-ATPase transport Ca^{2+} out of the cell, SERCA2 allows to restore SR Ca^{2+} reserve and mitochondrial Ca^{2+} uniport allows the passage of Ca^{2+} from a the cytosol into the mitochondrial matrix. To keep steady state conditions in the cell, during each action potetial, Ca^{2+} influx must be balanced by Ca^{2+} efflux (Bers, 2002). However, the importance of the different pathways for Ca^{2+} extrusion varies among species. In rabbit ventricular cardiomyocytes, SERCA2 is responsible for removing 70% of Ca^{2+} ions, while NCX removes 28% and MCU only 1%. In rat and mouse ventricular myocytes, the activity of SERCA2 is higher than in rabbit cells (~92%), while the activity of NCX is lower (~7%).

I.3 Regulation of ECC

The force of cardiac contraction is regulated by intrinsic way as an interplay between length-dependent changes in cardiac function and changing myocardial contractility (Starling's 'law of the heart' and 'Family of Starling Curves'). Heart can be also regulated via the autonomic nervous system.

I.3.1 Frank-Starling law

The principal mechanism represented by the Frank-Starling law is based on intrinsic property of myocardium by which increased ventricular volume results in increased performance during contraction. In other words, increasing volume of blood stretches the ventricular wall causing cardiac muscles contracting more forcefully. The stretching of the muscle filaments increases cardiac contraction by augmentation the Ca^{2+} sensitivity of the myofilaments.

Increase in Ca^{2+} sensitivity leads to a greater number of actin-myosin crossbridges. The force that any single cardiac filament develops is proportional to the initial sarcomere length. Larger or smaller sarcomere length than the optimal values will decrease the force of the muscle contraction.

I.3.2 Neurohormonal regulation of heart function

Even if the heart possesses a special contractile protein-machinery that allows to generate mechanical force, the force and rate of contraction are regulated by the autonomic nervous system, namely the sympathetic system and parasympathetic system (Figure 5).

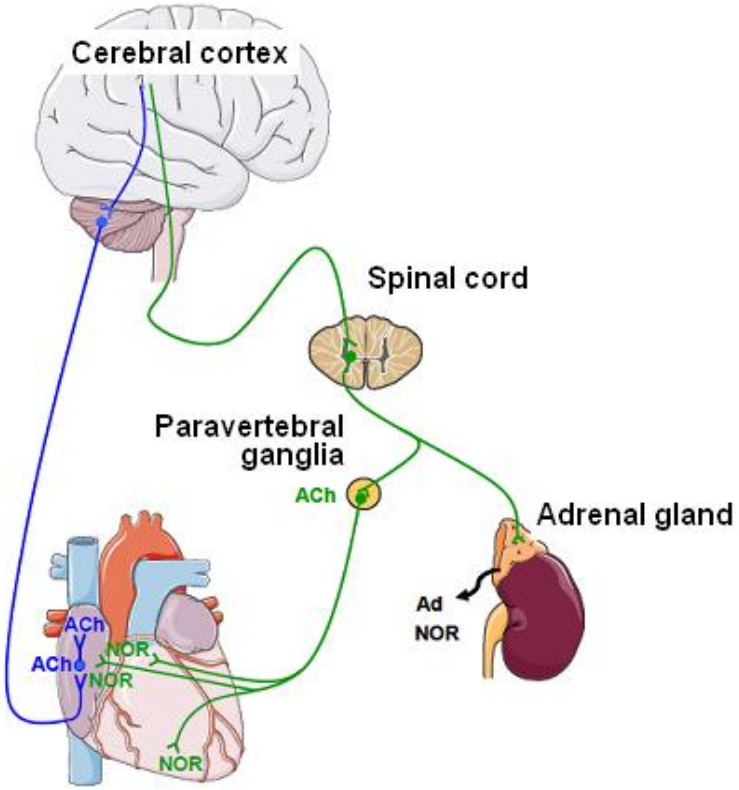

Figure 5: Autonomic regulation of the heart.
The diagram shows the two nervous systems that regulate heart rate and force of contraction. In green, the sympathetic nervous system; in blue, the parasympathetic nervous system. ACh, acetylcholine, Ad, adrenaline, NOR- noradrenaline (Modified from thesis of Nolwenn Merlet, http://www.sudoc.abes.fr/DB=2.1/SRCH?IKT=12&TRM=159710308).

The parasympathetic nervous system decreases heart rate through release of the neurotransmitter acetylcholine (ACh) that raises the threshold for spontaneous action potential generation. In contrast, the sympathetic system increases the rate and force of contraction which is mediated through release of catecholamines like adrenaline (Ad) and noradrenaline

(NOR). This leads to the sinoatrial node (SAN) stimulation and increase in firing rate of action potentials (AP) (Soni *et al.*, 2014).

The sympathetic and parasympathetic nervous system comprises a great number of molecular components like second messengers: cAMP, cGMP, inositol trisphosphate (IP3), diacylglycerol (DAG), which leads to phosphorylation and dephosphorylation of many proteins involved in ECC: LTCCs, RyRs, PLB that regulates the activity of SERCA2, and contractile proteins: TnI and MyBP-C. These signaling pathways predominantly involve α- and β-receptors, which are activated by catecholamines that bind to extracellular sites of various isoforms of GPCRs.

II. Cyclic AMP signaling in the heart

Cyclic AMP was the first discovered second messenger. cAMP was identified by Earl Sutherland in 1958 (Rall & Sutherland, 1958) who won a Nobel Prize in Physiology and Medicine in 1971 for his discovery regarding the mechanisms of action of hormones via second messengers, mainly cAMP.

Cyclic AMP plays a very important role in the cellular response to many hormones like glucagon or adrenaline and neurotransmitters that cannot pass through the plasma membrane. Cyclic AMP is strongly involved in modulating the contractile function of cardiac muscle by activation of cyclic AMP-dependent protein kinases (PKA) which are responsible for phosphorylation of key proteins in E-C coupling.

Intracellular cAMP concentration is regulated by the activities of at least two enzymes: adenylyl cyclase (AC) responsible for cAMP synthesis and cyclic nucleotide phosphodiesterases (PDEs) responsible for cAMP degradation (Fimia & Sassone-Corsi, 2001).

II.1 G-protein coupled receptors (GPCRs)

β-adrenergic receptors are a class of G protein-coupled receptors (GPCRs). GPCRs play an important role in the regulation of the cardiovascular system by interactions with hormones, neurotransmitters and growth factors (Tang & Insel, 2004). GPCRs are known also as a superfamily of the seven-transmembrane (7TM) receptors. β-adrenergic receptors possess

seven transmembrane α-helices (7TMH) connected with intracellular and extracellular loops. The extracellular region (EC) of receptor is responsible for ligand binding and the intracellular (IC) region of receptor is a place of interactions with G-proteins, arrestins and other downstream effectors (Latek *et al.*, 2012).

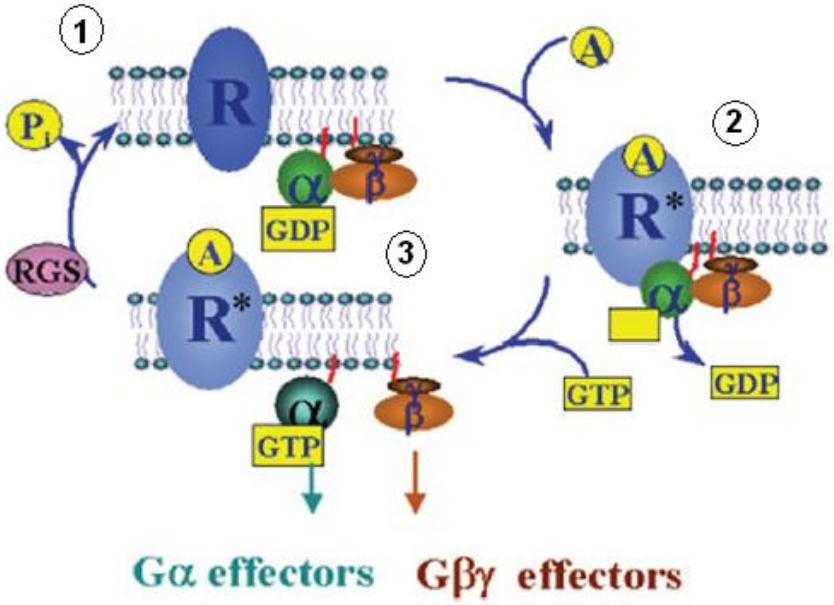

Figure 6: GPCR-mediated G-protein activation.
The diagram shows GTPase cycle in three steps: 1) The interaction between a cell surface receptor with endogenous ligand promotes the coupling of receptor with intracellular heterotrimeric G protein, 2) The receptor-G protein coupling leads to the exchange of GDP for GTP, 3) Gα–GTP subunit dissociates from Gβγ and receptor, both units are ready to modulate the activity of intracellular effectors. Termination of signal occurs when GTP is removed from Gα subunit by the GTPase activity of Gα subunit (Cabrera-Vera *et al.*, 2003).

The cellular or physiological response mediated by a GPCR requires interactions of the receptor with heterotrimeric guanine nucleotide-binding proteins (G proteins). G-proteins are composed of three units: α, β and γ. In inactive state, GDP is bound to Gα subunits. During receptor activation GDP is released and GTP binds to α subunit. Gα-GTP dissociates from receptor and Gβγ subunit. Then, both Gα-GTP and Gβγ are ready to activate or inhibit downstream effectors of signaling pathway (Figure 6) (Cabrera-Vera *et al.*, 2003).

II.2 β-adrenergic receptors

β-adrenergic receptors (β-ARs) belong to the superfamily of GPCRs and their stimulation by sympathetic nervous system or circulating catecholamines is implicated in metabolic regulation, peripheral blood circulation, central neural activities and muscle contraction.

In the heart, acute β-AR stimulation is the most powerful mechanism of cardiac output regulation in response to a flight-or-fight situation. Chronic β-AR stimulation is part of physiological and pathological heart remodeling. Three subtypes of receptor are expressed in cardiac myocytes: β_1, β_2, β_3, where β_1 and β_2 play a dominant role in ECC (Woo & Xiao, 2012).

β_1-AR is the predominant receptor subtype in the mammalian heart. In general, the ratio β_1:β_2-AR is around 70%:30% in the atria and 80%:20% in the ventricles (Brodde *et al.*, 2006).

β-ARs are involved in many different signaling pathways (Figure 7). β_1-AR is the main expressed receptor in healthy cardiomyocytes. β_2-ARs are overexpressed in the failing heart, while the expression of β_1-AR is decreased. Both β_1- and β_2-AR pathways involve the stimulatory G proteins ($G\alpha_S$) leading to increase in contractility. β_2-ARs can interact also with inhibitory G-proteins ($G\alpha_i$) pathway opposing the positive inotropic effects and activating a cell survival pathway. The expression of β_3-ARs is very low in the healthy heart, but β_3-ARs are upregulated in heart failure (HF) and exert both positive and negative inotropic effects in the failing hearts (Najafi *et al.*, 2016).

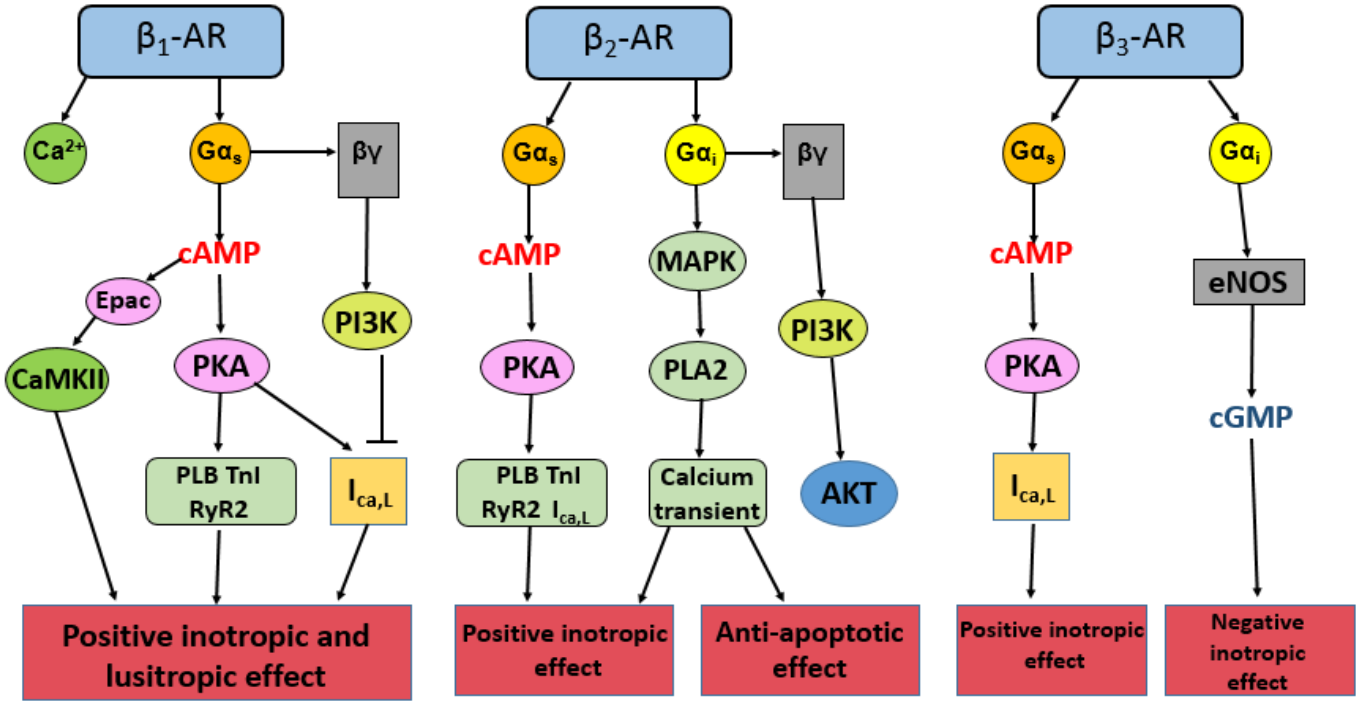

Figure 7: β-adrenergic signaling pathway.
The diagram shows pathways activated by β-adrenergic receptor subtypes and their physiological effects (inspired by (Steinberg, 1999)).

II.2.1 β_1-adrenergic receptor

β_1-ARs are the most studied subtype of β-ARs. β_1-ARs are located on the surface of cardiomyocytes. They are involved in the production of cAMP. cAMP activates exchange proteins directly activated by cAMP (Epac) and PKA. This leads to phosphorylation of key proteins of ECC: LTCCs, phospholamban (PLB), ryanodine receptors (RyR), Troponin T and I, resulting in positive inotropic, chronotropic and lusitropic effect (Fu & Xiang, 2015). However, previous studies showed that β_1-AR stimulation increases activity of phosphatidyl inositol 3-kinase (PI3K) via $G\alpha_s$ and $G\beta\gamma$ proteins in adult rat cardiomyocytes. Increased PI3K activity negatively regulates β_1-AR mediated contractile response. This leads to a decrease in $I_{Ca,L}$ and intracellular Ca^{2+} without phosphorylation of myofilaments involved in EC coupling. The PI3K-dependent inhibition of β_1-AR can be implicated in agonist-induced desensitization of receptor and can lead to HF (Leblais *et al.*, 2004).

Chronic stimulation of β_1-ARs by catecholamines exerts a toxic effect on the heart. Mouse model with overexpression of human β_1-ARs showed a presence of early hypertrophy and interstitial fibrosis with decrease in cardiac function. β_1-ARs mediate pro-apoptotic signalling

via PKA and Ca^{2+} calmodulin-dependent protein kinase (CaMKII), but the role of PKA in apoptotic pathway is not well known (Baker, 2014).

The second mouse model showing β_1-AR-induced toxicity is a model lacking β_1-ARs. This study showed that β_1-ARs are involved in catecholamine induced increase in contraction and stimulation of β_1-ARs activates CaMKII signaling pathway. In addition, mice leaking β_1-ARs showed preserved cardiac function after myocardial infarction (Yoo *et al.*, 2009).

II.2.2 β_2-adrenergic receptors

While β_1-ARs are the predominant subtype of β-AR in the heart, β_2-ARs are expressed in many cell types: mainly in cardiac myocytes and vascular and pulmonary smooth muscle cells, where they are responsible for the regulation of inotropy, chronotropy, vasodilation and bronchodilation. In the heart, β_2-ARs similar to β_1-ARs promote cAMP production resulting in positive inotropic and chronotropic effect (Taylor & Bristow, 2004).

Stimulation of β_2-ARs produces different effects than β_1-AR stimulation. In contrast to β_1-ARs which lead to a rather uniform distribution of cAMP (Fu *et al.*, 2013), β_2-AR-mediated production of cAMP is highly localized (Nikolaev *et al.*, 2006). β_2-ARs are specifically concentrated inside caveolae(Rybin *et al.*, 2000; Xiang *et al.*, 2002). cAMP production upon β_2-AR stimulation is limited by phosphodiesterases (PDEs) (Jurevičius *et al.*, 2003; Nikolaev *et al.*, 2006). The compartmentation of β-AR signaling defines the spatial activation of PKA anchored through A kinase anchoring proteins, thus β_2-ARs activate a specific pool of PKA, which is localized in the close proximity to protein targets (Dodge-Kafka, 2006). β_2-ARs form a complex with L-type Ca^{2+} channels, G proteins, caveolin and AKAPs, PKA and phosphatases like calcineurin and phosphatase 2A (Davare *et al.*, 2001). This complex provides the specificity, efficacy and rapidity of Ca^{2+} channels modulation (Flynn & Altier, 2013).

Study on mouse model with overexpression of the human β_2-AR shows markedly elevated myocardial relaxation and reduced PLB protein level without changes in SR Ca^{2+} or calsequestrin (Rockman *et al.*, 1996). Another study shows that β_2-AR overexpression does not change contractile parameters and has no effect on mortality in β_2-AR transgenic model (Milano *et al.*, 1994). The second animal model used to study function of β_2-ARs is a mouse model with β_2-AR deletion. Targeted deletion of β_2-ARs in mice has no significant effect on resting heart rate, blood pressure or cardiac output. Also, left ventricular functional response to exercise remains unchanged. During exercise on treadmill β_2 knockout mice exercised for a longer time than wild-type littermates without significant difference in heart rate responses to

exercise. β_2 knockout mice became hypertensive; hypertension was probably associated with peripheral vasoconstriction (Bernstein, 2002).

In addition, β_2-AR stimulation, in contrast to β_1-AR stimulation, has anti-apoptotic effect and β_2-ARs are important regulators during chronic activation of the adrenergic system. This difference between β_1 and β_2-AR stimulation can be explained by the interactions of β_2-ARs with inhibitory G proteins (Daaka *et al.*, 1997).

II.2.3 β_3-adrenergic receptors

β_3-AR mRNA was detected in the human heart but with much lower expression than β_1 and β_2-ARs (Michel *et al.*, 2010). β_3-ARs were first characterised in 1989 (Emorine *et al.*, 1989). Most studies focused on β_3-AR function in adipose tissue. In contrast to β_1 and β_2-ARs, the gene coding the β_3-AR has introns (Gauthier *et al.*, 2000). The structure of β_3-AR shows only 51% identity with β_1-ARs and 46% with β_2-ARs (Imbrogno *et al.*, 2015). In mammalian cardiovascular system, β_3-AR is expressed in the myocardium and the coronary microarteries (Dessy *et al.*, 2004). In the mammalian heart, β_3-ARs are more expressed in atrial cells than in ventricular myocytes (Moniotte *et al.*, 2001). In human ventricular myocytes, β_3-ARs stimulation produces negative inotropic effect associated with increase in intracellular cGMP after activation of nitric oxide synthase (NOS) by inhibitory G proteins (Gauthier *et al.*, 1996, 1998). While in human atrium, β_3-ARs activation is either ineffective (Christ *et al.*, 2011) or exerts a positive effect on $I_{Ca,L}$ and contractility (Skeberdis *et al.*, 2008).

In contrast to β_1 and β_2-ARs, the selectivity of ligands for β_3-ARs is less clear. It was shown that β_3-ARs in the human heart has higher affinity for noradrenaline than adrenaline. Well known antagonists for β_1 and β_2-ARs like propranolol, atenolol, pindolol, etc. bind also to β_3-ARs, but with much lower affinity (Imbrogno *et al.*, 2015).

β_3-ARs seems to be upregulated in human HF, while β_1 and β_2-ARs are downregulated or desensitized. It can be a compensatory upregulation of β_3-ARs to avoid further myocyte damage. In addition, β_3-ARs upregulation can act on vessel tone resulting in decrease in the peripheral vascular resistance and the afterload of failing hearts (Gauthier *et al.*, 2000).

II.2.4 Desensitization of β-adrenergic receptors

Desensitization is a process of loss of receptor responsiveness induced by long term exposure to catecholamines. This process can be ‘agonist-specific’ or ‘agonist non-specific’.

Agonist non-specific desensitization (Figure 8A) is mediated by phosphorylation of β-ARs by PKA, protein kinase C (PKC) and G protein-coupled receptor kinase (GRK) on the plasma membrane of the cardiomyocytes. PKA and PKC-mediated phosphorylation of β-ARs directly leads to conformational changes of receptor and prevents the interactions with G proteins and further signal transduction.

The agonist-specific desensitization of β-ARs (Figure 8B) is initiated by phosphorylation of six members of GRK. GRK family is composed of three subfamilies: 1) rhodopsin kinases (GRK1 and 7), 2) β-AR kinases (GRK2 and 3), 3) GRK4 subfamily (GRK4, 5 and 6) (Najafi *et al.*, 2016). GRK 2, 3 and 5 are expressed in the heart. GRK 5 is a membrane associated form and GRK 2 and 3 are mainly localized in the cytoplasm. It has been shown that correlation between hyperactive sympathetic nervous system and β-ARs desensitization is linked mainly to elevated GRK2 expression (Huang *et al.*, 2011). Study with GRK2 knockout mice showed that mice died early during embryonic period, because of HF and hypoplasia, suggesting that GRK2 plays a fundamental role in cardiac development (Jaber *et al.*, 1996).

In both mechanisms of desensitization, β-ARs phosphorylation promotes binding to β-arrestins (Najafi *et al.*, 2016). β-arrestins are small family of proteins that block interactions between β-ARs and G proteins preventing further signaling. β-arrestins use mechanism that involve PDEs which degrade the second messenger, cAMP. β-arrestins interact with PDE4 type D (Baillie *et al.*, 2003). This interactions of β-arrestins with PDE4D decreases a local pool of cAMP and leads to loss of cAMP-induced activation of PKA resulting in reduction of downstream effects of PKA on cell contractility, motility and transcription (Najafi *et al.*, 2016).

In contrast to β_1 and β_2-ARs, β_3-ARs are lacking in PKA and GRK phosphorylation site resulting in resistance to short-term agonist-specific desensitization (Rozec & Gauthier, 2006).

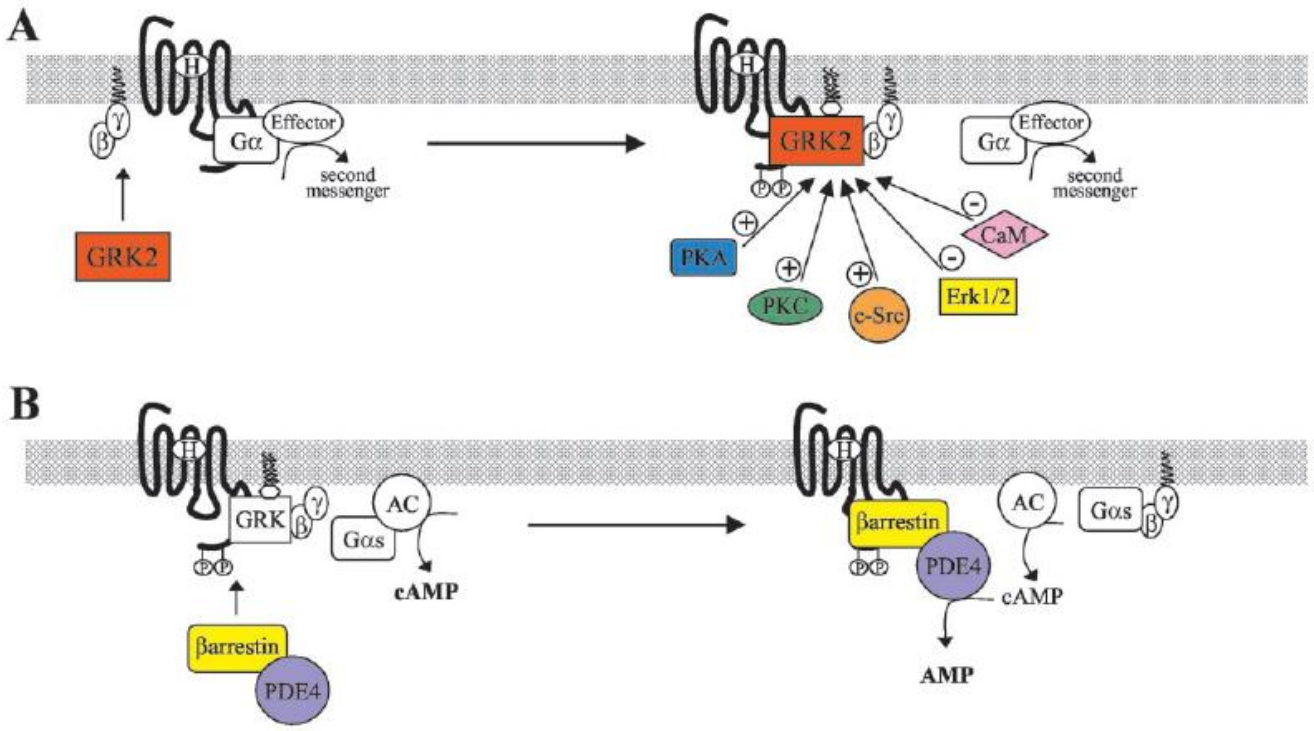

Figure 8: Regulation of β-AR desensitization by GRK and β-arrestins.
A) Receptor activation is followed by binding of GRK2 and Gβγ to the receptor β-AR. The activity of GRK2 can be increased by protein kinase A (PKA), protein kinase C (PKC) and c-Src. GRK2 activity can be decreased by phosphorylation by Erk1/2 or its binding to Ca^{2+}/calmodulin (CaM), B) β-AR activates the effector, adenylyl cyclase (AC) to produce cAMP. After phosphorylation of receptor by GRK, β-arrestin binds to the receptor, translocating PDE4 with it. This places PDE4 on the membrane, reducing local pool of cAMP and prevents further signaling (modified from (Kohout & Lefkowitz, 2003)).

II.3 Adenylyl cyclases

Adenylyl cyclases (ACs) are enzymes that catalyze cAMP synthesis. In mammals, ACs exist as transmembrane adenylyl cyclases (tmACs) or soluble adenylyl cyclases (sAC) anchored at various locations within the cell forming with PDEs local cAMP signaling pool . In mammals, nine isoforms of tmAC exist and they differ in their patterns of expression and regulatory properties (Table 1) (Hanoune & Defer, 2001).

AC enzymes catalyze reaction of intramolecular cyclization of ATP to cAMP with release of pyrophosphate (Steegborn, 2014). All nine isoforms of tmACs are composed of two catalytic domains, C1 and C2, in a single protein chain. Catalytic domains are located downstream of a six membrane helices (M1 and M2) forming pseudoheterodimer, where C1 and C2 domains have low affinity to each other.

Group	Isoform	Activators	Inhibitors	Tissue Distribution
1	AC1	$G_S\alpha$, FSK, Ca^{2+}/CaM	$G_i\alpha$, Gβγ, CaM kinase IV, P-site analogs	Brain, retina
	AC3	$G_S\alpha$, FSK, Ca^{2+}/CaM	CaM kinase II, P-site analogs	Olfactory neurons, brain
	AC8	$G_S\alpha$, FSK, Ca^{2+}/CaM	P-site analogs	Brain
2	AC2	$G_S\alpha$, FSK, Gβγ, PKC	P-site analogs	Brain, olphactory bulb
	AC4	$G_S\alpha$, FSK, Gβγ	P-site analogs	Kidney, brain, liver
	AC7	$G_S\alpha$, FSK, Gβγ, PKC	P-site analogs	Heart>brain>kidney, testis, liver
3	AC5	$G_S\alpha$, FSK, PKC, PKCζ	Giα, PKA, Gβγ, Ca^{2+}, P-site analogs	Brain>heart
	AC6	$G_S\alpha$, FSK	Giα, PKA, PKC, Ca^{2+}, P-site analogs	Heart>brain>kidney, testis, liver
4	AC9	$G_S\alpha$	Calcineurin, P-site analogs	Skeletal muscle, brain, lungs, liver

Table 1: Classification of mammalian tmACs following their regulation by endogenous modulators and tissue expression (Pavan *et al.*, 2009).
$G_S\alpha$: G stimulatory-protein α subunit, FSK: forskolin, Gβγ: G-protein βγ subunit, PKC: protein kinase C, CaM: calmodulin, Giα: G inhibitory-protein α subunit, PKA: protein kinase A, PKC: protein kinase C.

Mammalian C1 and C2 domains are located a head to tail by antiparallel coupling forming two distinct pockets at the interface. One pocket binds ATP and is a place where cyclization occurs. The second pocket is non-catalytic and is the site for forskolin binding. The cyclization reaction requires four residues. Two aspartate residues are located in C1 domain and bind two Mg^{2+} ions, two other residues, arginine and asparagine, are located in the C2 domain (Linder & Schultz, 2008).

Mammalian sAC contains two heterologous catalytic domains (C1 and C2) located in the amino terminus of the protein. C-terminus of sAC consists of an auto inhibitory region, canonical P-loop and leucine zipper sequences. Similarly to tmACs, sAC binds two metal cations in the catalytic site, which are responsible for ATP binding and cyclization. sAC is most active in the presence of Mn^{2+} and in contrast to tmACs, activity of sAC is insensitive to G proteins and forskolin, but can be modulated by Ca^{2+} and HCO^{3-} (Tresguerres *et al.*, 2011).

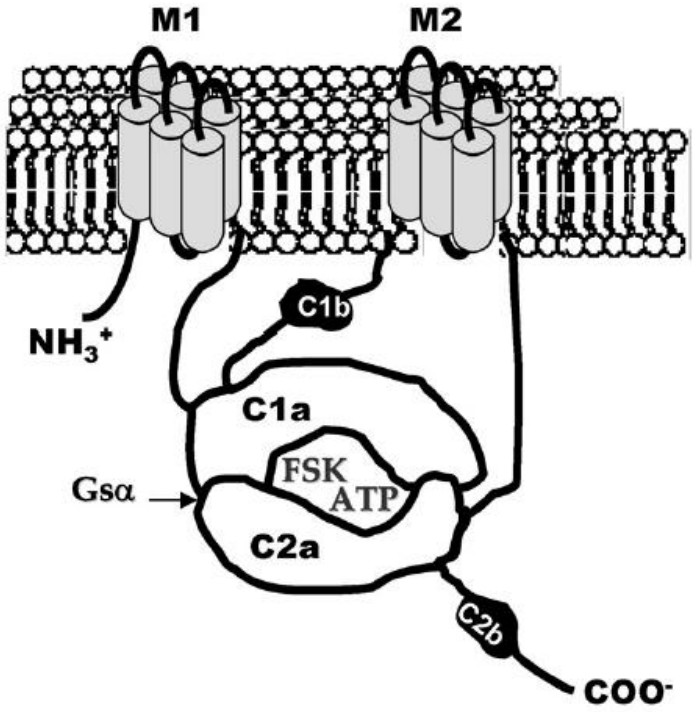

Figure 9: Schematic structure and membrane topology of transmembrane adenylyl cyclases.
M1 and M2 are anchors of a six membrane helices domains. C1a and C2a are the cytoplasmic catalytic domains with two active sites to bind ATP and forskolin (FSK). C1b is the cytoplasmic-linker domain and C2b is the second non-catalytic domain present only in AC1, AC2, AC3 (Pavan *et al.,* 2009).

All isoforms of tmACs are expressed in the heart, except AC8. AC5 and AC6 are the most expressed in the heart with AC5 being dominant. AC1 is expressed only in sinoatrial node controlling pacemaker function. Isoforms 2, 3, 4, 5/6 and 7 are mainly located in cardiac fibroblasts. The most expressed isoforms in the heart are AC5 and 6 and they may serve different functional roles (Efendiev & Dessauer, 2011; Guellich *et al.,* 2014)A mouse model with deletion of AC5 showed that basal cardiac functions remained unchanged, but left ventricle ejection fraction was decreased under isoproterenol condition. AC5 disruption leads to total loss of acetylcholine-mediated inhibition and to decrease in Ca^{2+}-induced inhibition of cAMP production. Studies with AC5 KO models showed that deletion of AC5 can be protective against HF under stress conditions (Yan *et al.,* 2007*b*). Cardioprotective effect is associated with elevated level of Bcl-2 and reduction in myocardial apoptosis (Okumura *et al.*, 2003; Sadana & Dessauer, 2009).

Studies with AC6 knockout mice showed that deletion of AC6 leads to decrease in cAMP level in left ventricle under basal and stress conditions, reduction in PKA and Akt activity and phospholamban phosphorylation resulting in abnormalities in Ca^{2+} transient (Sadana &

Dessauer, 2009). In addition, AC6 is overexpressed in fetal hearts and decreases progressively with age to obtain low level of expression in adult hearts. Expression profile of AC5 is exactly opposite to that of AC6 (Espinasse *et al.*, 1995).

II.4 Effectors of cAMP

Generally, cardiac effects of cAMP are attributed to the activation of cAMP-dependent protein kinase A (PKA). cAMP can also act via 2 other effectors: exchange protein directly activated by cAMP (Epac) and hyperpolarization-activated cyclic nucleotide-gated channels (HCN).

II.4.1 Protein kinase A

II.4.1.1 Structure and regulation

PKA is a threonine/serine kinase and its activity depends on the cellular level of cAMP. PKA catalyzes the reaction of transfer γ-phosphate of ATP to threonine or serine residues. The PKA phosphorylation is essential for many processes including contraction, metabolism and gene expression. PKA is composed of two catalytic (C) and two regulatory (R) subunits, forming heterotetramer in its inactive state (Rababa'h *et al.*, 2015). Each of the two regulatory subunits has two sites A and B to cooperatively bind cAMP. In the inactive state, only B site is exposed to bind cAMP. cAMP binding to B site facilitates cAMP binding to the A site. Binding of four cAMP molecules to the two regulatory domains results in conformational changes and dissociation of enzyme into R subunit dimer with four cAMP molecules and two C monomers (Figure 10). C subunit monomers are catalytically active and are able to phosphorylate serine and threonine residues of substrate proteins (Taskén & Aandahl, 2004).

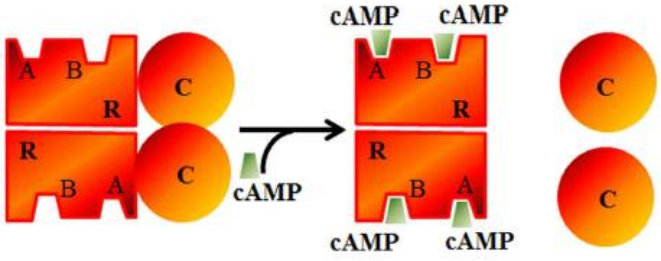

Figure 10; Schematic structure of PKA.
In the absence of cAMP, catalytic subunits (C) and regulatory subunits (R) form the inactive holoenzyme. cAMP binding induces the catalytic subunits dissociation from the regulatory subunits and phosphorylation of specific substrate proteins (Boularan & Gales, 2015).

PKA holoenzyme exists in 2 types, type I and type II, determined on the basis of their elution from ion exchange column. They are composed of different R subunits: RI and RII. It was also shown that there are two RI subunits, RIα and RIβ, and two RII subunits, RIIα and RIIβ (Turnham & Scott, 2016). These two classes of PKA differ in their affinity for cAMP with activation constant of 50-100 nM for PKA type I and 200-400 nM for PKA type II. RI and RII subunits show also different expression profile in cells and tissue and they are involved in different cAMP-dependent responses.

II.4.1.2 Targets of PKA in the heart

Signal transduction by PKA is involved in many cellular responses including metabolism, gene expression and contraction (Walsh & Van Patten, 1994). PKA is activated by β-AR signaling and phosphorylates many of the components involved in ECC (Figure 11) including PLB, TnI, LTCCs, MyBP-C, RyR2 and PDE4D3 (Rababa'h *et al.*, 2015).

PKA dependent phosphorylation of these ECC components leads to increase in Ca^{2+} current $I_{Ca,L}$, SR Ca^{2+} uptake and release, SR Ca^{2+} content and the dissociation of Ca^{2+} from the myofilaments allowing the heart to contract and relax (Rababa'h *et al.*, 2015).

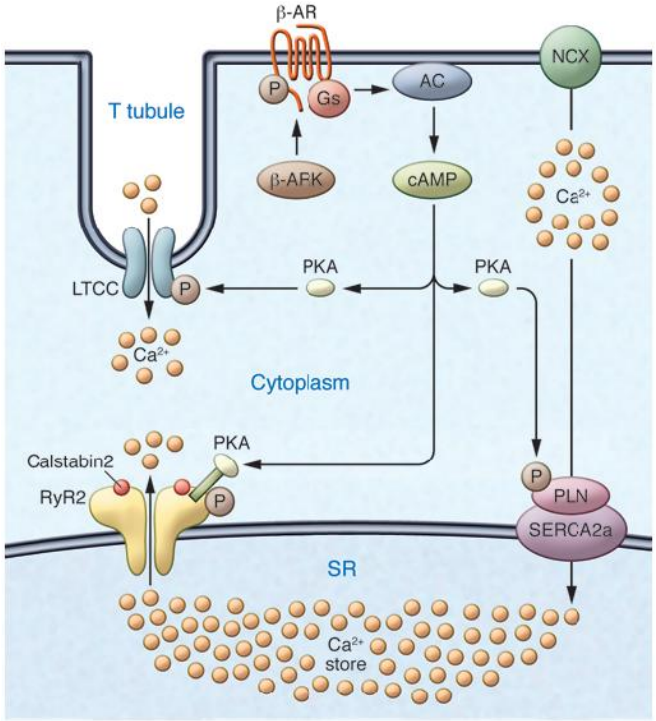

Figure 11: Signal transduction mediated by PKA in ECC.
Activation of β-ARs allows for the activation of adenylyl cyclase (AC), mediated by specific G proteins (Gs) and the generation of cAMP, which activates PKA. PKA phosphorylates key components of ECC: L-type Ca channels (LTCCs), ryanodine receptors (RyR2), phospholamban (PLN) (modified from (Marks, 2013)).

- L-type Ca^{2+} channels (LTTCs)

L-type Ca^{2+} channels (LTCCs) are essential in ECC. They are involved in the generation of the mechanical and electrical properties of the heart muscle. There are four types of LTCCs: Ca_v 1.1-1.4. The LTCC is composed of four different α_1 subunits together with β, $\alpha_2\delta$ and γ subunits. α_1 subunits form a pore for ion conduction composed of four homologous domain (I-IV), each contains six transmembrane segments (Figure 12). $Ca_v1.2$ is the primary LTCC expressed in ventricular myocytes, while both $Ca_v1.2$ and $Ca_v1.3$ are also expressed in atrial and sinoatrial cells (Bers & Perez-Reyes, 1999; Harvey & Hell, 2013).

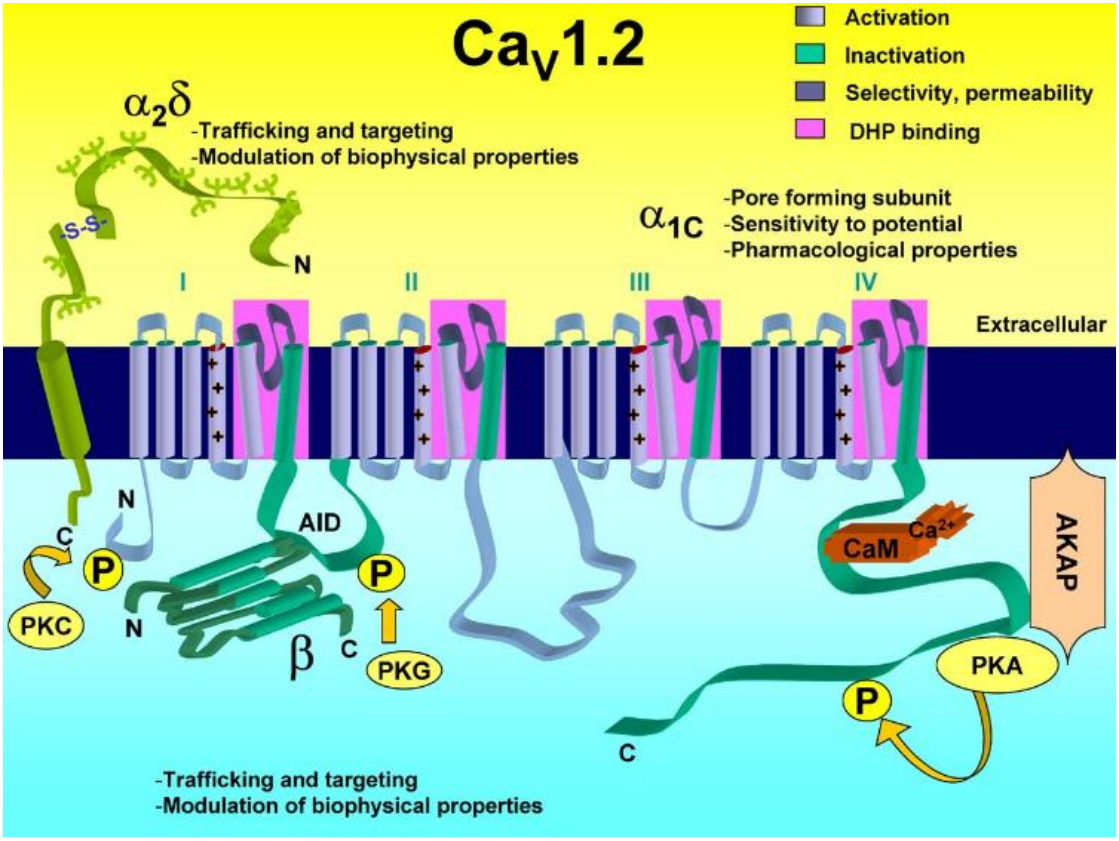

Figure 12: Structure of the cardiac L-type Ca^{2+} channel $Ca_v1.2$.
The purple segments are responsible for channel activation and segment 6 (green) for channel inactivation. Channel is regulated by the complex Ca^{2+}/calmodulin (CaM), by PKA, PKC, PKG and CaMKII phosphorylation and by glycosylation of the α2δ subunit (Brette *et al.*, 2006).

PKA phosphorylation of LTCCs increases activity of LTCCs, resulting in an increase $I_{Ca,L}$ current and Ca^{2+} entry into the cell which leads to increased heart contraction in response to stress, fear or exercise. Serine 1700 is a key site of PKA-dependent phosphorylation (Fu *et al.*, 2014). PKA phosphorylates also serine 1928, but this has little or no effect on β-AR stimulation of LTCCs (Fuller *et al.*, 2010). Recent studies on mice with Serine1700-to-Alanine mutation showed that amino acids substitution reduced basal $Ca_v1.2$ current in cardiomyocytes to 37% of its wild type (WT) values and only 33% under isoprenaline (ISO)

stimulation associated with cardiac hypertrophy and reduction in maximal stress-induced exercise capacity *in vivo*. Mutation of this PKA-phosphorylation has less impact on contraction than on $Ca_v1.2$ current. These studies demonstrated that Serine1700 is essential for the β-AR stimulation of Ca^{2+} current (Fu *et al.*, 2014). In addition, phosphorylation of Serine1700 leads to conformational changes in C-terminal domain of $Ca_v1.2$ resulting in its auto-inhibition (Hell, 2010).

- Ryanodine receptor

Ryanodine receptors (RyRs) are Ca^{2+} release channels and play a crucial role in ECC. They are highly expressed in the SR membrane in the close proximity of L-type Ca^{2+} channels within the transverse T-tubules. This localization of RyRs and LTCCs is important for high fidelity of the Ca^{2+}-induced SR Ca^{2+}-release resulting in Ca^{2+} transient (Houser, 2014). Three isoforms of RyRs were discovered: RyR1, RyR2 and RyR3. RyR1 isoform is found mainly in skeletal muscle, RyR2 in cardiac muscle and RyR3 is a brain isoform (Lanner *et al.*, 2010). RyRs are homotetramers with high molecular weight (>2 MDa). RyRs form a macromolecular complex with component that are relevant to RyR phosphorylation. RyRs are linked to the Ca^{2+}-binding protein, calsequestrin (CSQ), responsible for activation or inhibition of channel activity. RyRs in the heart are also associated with FKBP12.6 protein that stabilizes RyR channel function and is involved in coupled gating between neighboring RyR channels (Marx *et al.*, 2000; Ozawa, 2010). RyRs have also binding sites to calmodulin (CaM), responsible for modulating Ca^{2+} release. Phosphatases PP1 and PP2 are also involved in forming the macromolecular complex and are responsible for RyRs dephosphorylation (Figure 13).

Three phosphorylation sites have been determined: serine 2808, serine 2814 and serine 2030. Under ISO stimulation, PKA phosphorylates serine 2808 and 2030 and Serine 2814 is phosphorylated by CaMKII. Under basal conditions, without β-adrenergic stimulation only serine 2808 is phosphorylated by PKA. Phosphatase 1 is responsible for dephosphorylation of serine 2808/2814, phosphatase 2 only for serine 2814 dephosphorylation (Xiao *et al.*, 2005; Huke & Bers, 2008).

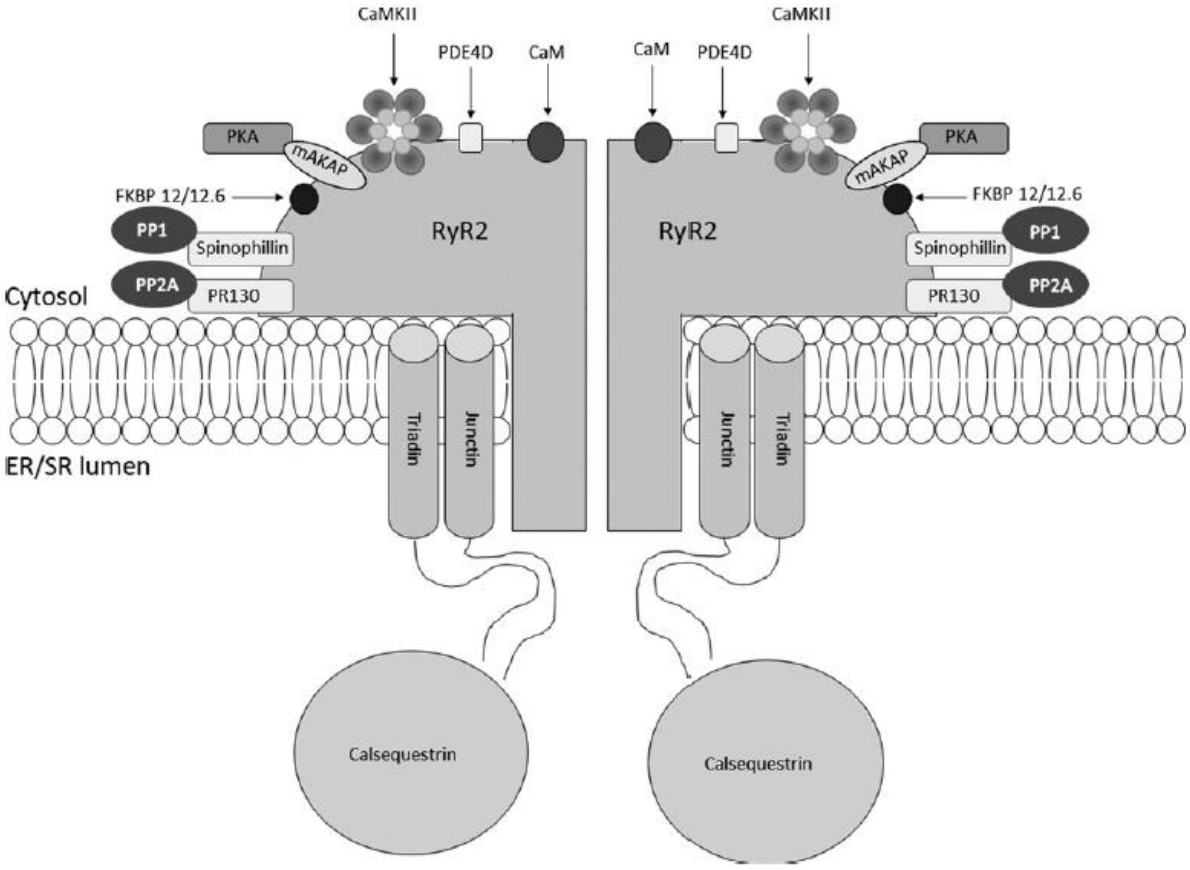

Figure 13: Structure of the RyR2 macromolecular complex.
RyR is composed of four identical subunits (only two are shown). Many proteins and enzymes are associated with RyR2 including calmodulin (CaM), Ca^{2+}/CaM-dependent kinase II (CaMKII), FKBP 12/12.6 and phosphodiesterase 4D (PDE4D). PKA is bound by targeting protein, muscle A kinase anchoring protein (mAKAP). Phosphatases PP1 and PP2 are also associated with the cytoplasmic domain (O'Brien *et al.*, 2015).

The pathophysiological role of PKA phosphorylation of RyR2 at serine 2808 remains controversial. Some studies performed in mice with total ablation of serine 2808 showed no effect on Ca^{2+} transient and a normal response of cellular function to β-adrenergic stimulation. Also, aortic banded mice with phosphorylation site ablation developed cardiac hypertrophy and systolic dysfunction similar to WT mice, suggesting that PKA phosphorylation is not strongly involved in maladaptive remodeling of the heart during chronic β-adrenergic stress (Benkusky *et al.*, 2007). However, mutations of RyR2 at several other sites are linked to ventricular tachycardia and sudden death (Jiang *et al.*, 2004).

- Phospholamban

SERCA is a 110 kDa transmembrane protein, primarily expressed in the heart and involved in Ca^{2+} uptake by the SR initiating relaxation. In the heart, SERCA activity is regulated by phospholamban, a 52-amino acid protein, that is phosphorylated by PKA and CaMKII and dephosphorylated by protein phosphatase 1 (Haghighi *et al.*, 2014). Phospholamban (PLB) can be phosphorylated on serine 16 by PKA, PKG and PKC and on threonine 17 by CaMKII. Phospholamban when dephosphorylated inhibits SERCA activity. Phosphorylation of PLB relieves the inhibition on SERCA and leads to increase in SR Ca^{2+} uptake (Mattiazzi & Kranias, 2014).

Studies on transgenic mice with cardiac specific overexpression of SERCA showed that enhanced activity of SERCA leads to increase in contraction and relaxation under basal and ISO conditions (He *et al.*, 1997). Animal model with SERCA deletion demonstrated that decrease in SERCA results in alterations in Ca^{2+} homeostasis and in decrease in myocyte contractility in heterozygous mice and in early embryonic lethality in homozygous mice, suggesting that SERCA pump level is a critical determinant of heart contractility (Ji *et al.*, 2000).

Cardiac specific overexpression of PLB leads to inhibition of SR Ca^{2+} transport, decrease in systolic Ca^{2+} levels and contraction of ventricular myocytes under basal conditions. *In vivo* studies in these mice showed also a decrease in fractional shortening and depressed left ventricular functions (Kadambi *et al.*, 1996). PLB deletion results in enhanced myocardial performance and Ca^{2+} cycling without changes in heart rate (Luo *et al.*, 1994).

- Contractile proteins

PKA-mediated phosphorylation of myofilaments results in increase in the intrinsic rate of myofibril relaxation associated with the shortening of the cardiac twitch during β-AR stimulation. Myofibral relaxation occurs via phosphorylation of TnI and MyBP-C (Kentish *et al.*, 2001).

TnI can be phosphorylated on the same phosphorylation site by PKA, PKG, PKCβ, PKCδ and PKD1 (Solaro *et al.*, 2013). TnI is phosphorylated at serine 22/23 in mice and serine 23/24 in human located in N-terminal domain of TnI. PKA-mediated phosphorylation results in reduction of myofilament Ca^{2+} sensitivity. It was also shown that phosphorylation increases crossbridge cycling rate and shortening velocity and this can contribute to β-AR induced lusitropy (Layland *et al.*, 2005).

MyBP-C has three phosphorylation sites, serine 273, serine 282 and serine 302, which are phosphorylated by PKA, CaMKII and PKC. PKA phosphorylates MyBP-C on all three phosphorylation sites, while PKC only on serine 273 and 302 (Kentish *et al.*, 2001). PKA-mediated phosphorylation on serine 282 results in decrease in myofibril Ca^{2+} sensitivity which leads to acceleration of relaxation by increasing the rate of thin filament deactivation.

II.4.1.3 Subcellular targeting of PKA

During β-adrenergic signaling, PKA is localized to distinct intracellular compartments in the proximity to its substrate. A kinase anchoring protein (AKAPs) are involved in recruiting PKA to specific subcellular *loci* (Calejo & Taskén, 2015). Over 14 different AKAPs were identified in the heart tissue and they play a dual role: they act as scaffolding proteins that localize PKA to specific cellular compartments and they increase signal transduction through substrate phosphorylation. AKAPs consist of i) a PKA anchoring domain, which interacts with the N-terminal dimerization and docking groove of the PKA regulatory subunits, ii) a targeting domain which allows to locate PKA in the proximity to its substrate, and iii) binding sites for other molecules involved in signaling pathways (Rababa'h *et al.*, 2015). In the heart, AKAPs interact with PKA and PDE4D3 forming a supramolecular complex. This results in a negative feedback loop mechanism where PDE4D3 phosphorylation increases cAMP hydrolysis and turns off PKA activity (Calejo & Taskén, 2015).

II.4.2 Other effectors of cAMP

II.4.2.1 Exchange factor Epac

In 1998, a new family of cAMP effector proteins named exchange protein directly activated by cAMP (Epac) or guanine-nucleotide-exchange factor directly activated by cyclic AMP (cAMP-GEF) was discovered (de Rooij *et al.*, 1998; Kawasaki *et al.*, 1998). The family of Epac consist of 2 isoforms: Epac 1 known also as RAPGEF3 or cAMP-GEF-I and Epac 2 known as RAPGEF4 or cAMP-GEF-II and they act as guanine-nucleotide exchange factors for the small G proteins, Rap1 and Rap2. Epac is a family of proteins with molecular weight between 105 and 115 kDa and they are composed of N-terminal regulatory region and C-terminal catalytic region (Lezoualc'h *et al.*, 2016). The regulatory region has auto-inhibitory properties and contains a Dishevelled Egl-10 Pleckstrin domain (DEP) and a cyclic nucleotide binding domain (CNBD, one for Epac1 and two for Epac2. The C-terminal catalytic region is composed of a Ras Exchange motif domain (REM) and a Ras association domain (RA) and a

CDC-25-homology domain responsible for guanine nucleotide exchange activity (Chen *et al.*, 2014).

Rap proteins belongs to the RAS family of small G proteins. They exist as inactive guanosine diphosphate (GDP)-bound state and active guanosine triphosphate (GTP)-bound state. At the basal state, in the absence of cAMP, Epac has an auto-inhibitory conformation, such as N-terminal region folds on the top of C-terminal catalytic region, blocking an active site. cAMP binding induces conformational changes in Epac, freeing the active site (Figure 14). Rap binding to Epac, leads to exchange of GDP to GTP and activation of G proteins (Gloerich & Bos, 2010).

Epac1 and Epac2 are expressed in almost all mature and developing tissues with different expression profiles. High expression of Epac1 was found in the heart, central nervous system, adipose tissue, blood vessels, ovary, uterus and kidney; Epac2 is highly expressed in central nervous system, adrenal glands and pancreas (Chen *et al.*, 2014).

Epac proteins are involved in many cellular functions including cell adhesion, cell-cell junction, cell differentiation and proliferation, exocytosis/secretion, gene expression, apoptosis, cardiac hypertrophy and phagocytosis (Cheng *et al.*, 2008).

In the heart, under β-AR stimulation, Epac interacts with Rap, phospholipase Cε (PLCε), protein kinase Cε (PKCε), CaMKII and regulates SR Ca^{2+} release in mouse cardiac myocytes. Stimulation of Epac with β_1-AR the specific agonist 8-pCPT-2'-O-Me-cAMP leads to a decrease in the $[Ca^{2+}]_i$ transient amplitude and it is associated with increase in cardiomyocyte contraction via phosphorylation of MyBP-C and TnI by PKCε and CaMKII (Laurent *et al.*, 2012). In addition, Epac is involved in cardiac hypertrophy. Epac1 and Epac2 were shown to be increased in experimental mouse and rat models of hypertrophy with chronic ISO infusion or thoracic aorta constriction. The hypertrophic effect seems to be CaMKII-dependent and correlated with PLCε stimulation by Epac resulting in inositol trisphosphate (IP3) production and increase in intracellular Ca^{2+}, which is responsible for cardiac hypertrophy and arrhythmias. It is proposed that Epac can activate CaMKII and hypertrophic signaling by Ca^{2+} release from the nuclear envelope via the IP3 receptor (Métrich *et al.*, 2009).

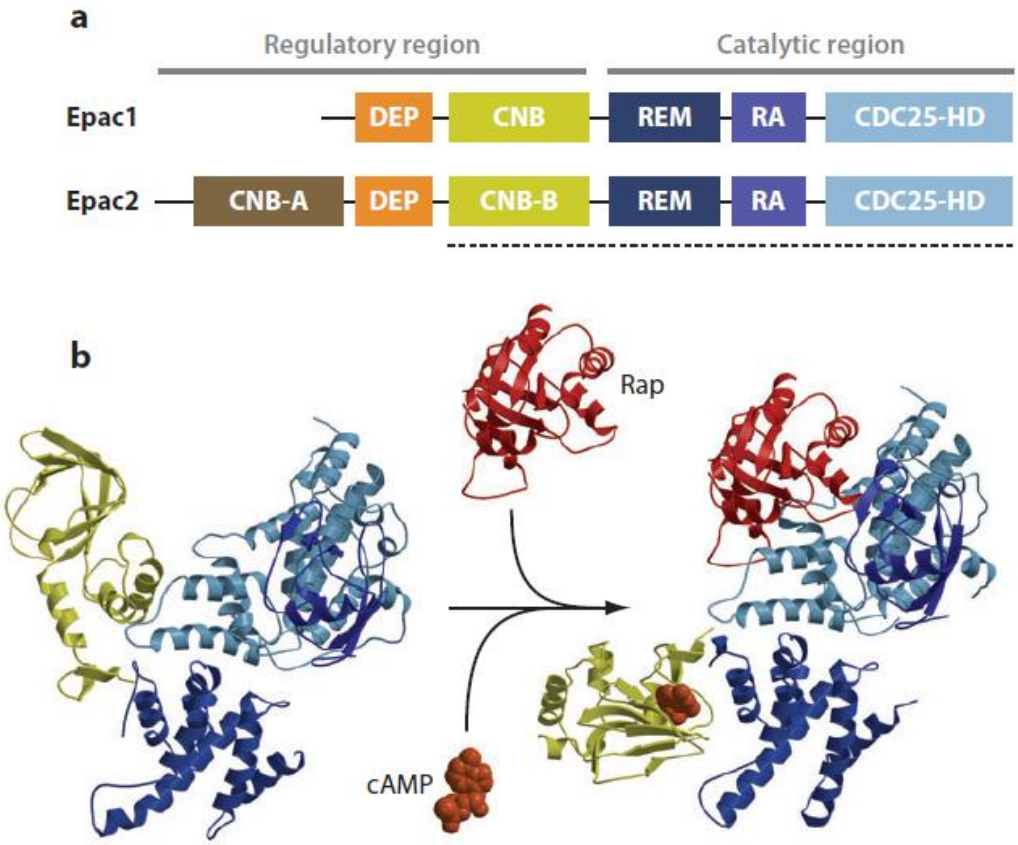

Figure 14: Structure and activation mechanism of Epac proteins.
a) Structure of Epac1 and Epac2 proteins. DEP: Dishevelled, Egl-10 and Pleckstrin, CNB: cyclic nucleotide binding, REM: Ras exchange motif, RA: RAS association domain, CDC25 HD- CDC25 homology domain.
b) Mechanism of Epac activation by cAMP. Crystal structure of inactive Epac2 and active Epac2 in complex with Rap and cAMP (Gloerich & Bos, 2010).

II.4.2.2 CNG and HCN channels

Hyperpolarization-activated cyclic nucleotide-gated (HCN) channels are cation channels activated by hyperpolarized membrane potentials and regulated by intracellular cyclic nucleotides (Herrmann *et al.*, 2015). In the heart, HCN channels are mainly involved in the regulation of sinoatrial function. They provide an inward current which is a major component of slow diastolic depolarization (SDD) in sinoatrial cells. HCN channels regulation by cAMP plays an essential role in the control of heart rate through the autonomous nervous system (Wahl-Schott *et al.*, 2014). Four isoforms of HCN channels (1-4) are expressed in neurons. Isoforms 1, 2 and 4 are expressed in the heart.

Cyclic nucleotide-gated (CNG) channels belong to the superfamily of voltage-gated ion channels that are directly activated by cAMP or cGMP binding. They are mainly involved in visual and olfactory signal transduction in vertebrates (Podda & Grassi, 2014). These channels are not expressed to a significant level in the heart.

II.4.2.3 Popeye domain containing protein family

In 1999, a novel class of cAMP effectors, the popeye domain containing protein family, was discovered through substractive hybridization. Three genes of popeye family (POP) were detected in human and mouse: POP1, POP2 and POP3 (Andrée *et al.*, 2000). All three isoforms are expressed in the heart. POP1 is highly expressed in atrial and ventricular chambers in the embryonic hearts and decreases in ventricle during postnatal period. POP2 is expressed at the same level in the ventricle and atrium. POP3 expression is higher in ventricles than atria. The highest level of expression of POP1 and 2 was found in the sinoatrial and atrioventricular nodes (Schindler & Brand, 2016). Popeye genes are also expressed in the autonomic and central nervous system, epithelial cells, gastrointestinal tract, retina and lens (Schindler *et al.*, 2012). Popeye proteins are membrane proteins composed of three-pass transmembrane regions with extracellular amino-terminus containing two glycosylation sites. Popeye proteins play many roles in multiple tissues: they are involved in epithelial function and are important in the formation and maintenance of epithelial monolayers, they regulate intracellular junctions in the heart, they control vesicular transport and fusion and by interactions with caveolin-3 they control the number and size of caveolae. Popeye proteins are involved in heart rate regulation. Loss of cardiac POP1 and POP2 leads to arrhythmias with the occurrence of sinus pauses resulting in strong decrease in heart rate causing bradycardia. Popeye proteins are modulated by cAMP. cAMP binding leads to conformational changes of POP proteins and exposure of binding site for proteins interacting with Popeye (Schindler & Brand, 2016).

II.5 cAMP degradation

Activity of cyclic nucleotide phosphodiesterases (PDEs) was described in 1962 by Butcher and Sutherland (Butcher & Sutherland, 1962). PDEs are a family of enzymes that catalyze the hydrolysis of the 3’ cyclic phosphate bonds of adenosine and/or guanosine 3’5’-cyclic monophosphate (Bender & Beavo, 2006). PDEs are divided into eleven families in term of their physicochemical and regulatory properties (Table 2). All eleven families are encoded by twenty-one genes displaying a complex structure with multiple promoters (Conti & Beavo, 2007). Three families hydrolyze only cAMP (PDE4, 7 and 8), three other are selective only for cGMP (PDE5, 6 and 9) and the other hydrolyze both cAMP and cGMP (PDE1, 2, 3, 10 and 11) (Lugnier, 2006; Bender & Beavo, 2006). In the heart, seven families of PDEs are expressed: PDE1 activated by Ca^{2+}/calmodulin, PDE2 stimulated by cGMP, PDE3 inhibited by cGMP, PDE4 selective for cAMP, PDE5 selective for cGMP, PDE8 selective for cAMP

	Isoform	Substrate specificity	K_m cGMP (µM)	K_m cAMP (µM)	Properties	IBMX sensibility	Expression profile
PDE1	**PDE1A**	cAMP<cGMP	2.6-3.5	72.7-124	Simulated by Ca^{2+}/ calmodulin	YES	Smooth muscle, heart, lungs, brain, sperm
	PDE1B	cAMP<cGMP	1.2-5.9	10-24			Smooth muscle, neurons, lymphocyte, macrophage
	PDE1C	cAMP=cGMP	0.6-2.2	0.3-1.1			Smooth muscle, brain, heart, olfactory epithelium
PDE2	**PDE2A**	cAMP=cGMP	10	30	Simulated by cGMP	YES	Brain, heart, macrophage, endothelium, adrenal glands
PDE3	**PDE3A**	cAMP>cGMP	0.02-0.15	0.18	Inhibited by cGMP	YES	Heart, vascular smooth muscle, oocytes, kidney
	PDE3B	cAMP>cGMP	0.28	0.38			Heart, vascular smooth muscle, macrophages, lymphocytes, hepatocyte beta cells, heart
PDE4	**PDE4A**	cAMP>cGMP		2.9-10	Selective for cAMP	YES	Ubiquitous
	PDE4B	cAMP>cGMP		1.5-4.7			Ubiquitous
	PDE4C	cAMP>cGMP		1.7			Lungs, testicles, brain
	PDE4B	cAMP>cGMP		1.2-5.9			Ubiquitous
PDE5	**PDE5A**	cAMP<cGMP	2.9-6.2	290	Selective for cGMP	YES	Vascular smooth muscle, adipocyte, kidney, brain, lungs, heart
PDE6	**PDE6A/B**	cAMP<cGMP	15	700	Selective for cGMP	YES	Retina, pineal gland
	PDE6C	cAMP<cGMP	17	610			Retina, pineal gland
PDE7	**PDE7A**	cAMP>cGMP		0.1-0.2	Selective for cAMP	YES	Immune cells, heart, skeletal muscle, endothelial cells
	PDE7B	cAMP>cGMP		0.03-0.07	Selective for cAMP		Brain, heart, liver, skeletal muscle, pancreas, testicles
PDE8	**PDE8A**	cAMP>cGMP		0.06	Selective for cAMP	NO	Testicles, spleen, small intestine, ovary, colon, kidney, heart
	PDE8B	cAMP>cGMP		0.1	Selective for cAMP		Brain, thyroid
PDE9	**PDE9A**	cAMP<cGMP	0.7-0.17	230	Selective for cGMP	NO	Kidney, brain, spleen, prostate, gastrointestinal tissue
PDE10	**PDE10A**	cAMP<cGMP	13-14	0.22-1.1	Inhibited by cAMP	YES	Brain, testicles, heart, thyroid, pituitary gland
PDE11	**PDE11A**	cAMP=cGMP	2.0-3.2	2.0-3.2	Non selective	YES	Skeletal muscle, prostate, testicles, salivary glands, thyroid, liver

Table 2: Eleven families of phosphodiesterases (Inspired by (Lugnier, 2006; Bender & Beavo, 2006).

with high affinity, and PDE9 selective for cGMP with the highest affinity among all PDE families (Azevedo *et al.*, 2014).

II.5.1 Structure, localization and regulation of phosphodiesterases

The 11 families of PDEs are all composed of a catalytic domain localized in the C-terminus of the protein. This catalytic domain is similar between families, showing 25 to 35% of homology in amino acids sequence. All catalytic domains are composed of 16 helices, they have an active site formed at the junction of helices and they contain a substrate binding pocket with two metal binding sites (for zinc or magnesium) on the top, coordinated by two histidine and two aspartic residues, that are highly conserved among all PDEs family (Bender & Beavo, 2006).

PDEs contain also one or several regulatory domains located in the N-terminus, characteristic for each family. The regulatory region can contain a domain for ligand binding, oligomerization, kinase phosphorylation, a domain for Ca^{2+}/calmodulin binding, GAF domain (named derived from cGMP-activated PDEs, adenylyl cyclase, Fh1A), UCR region (upstream conserved regions), PAS domain (named after 3 proteins forming this domain: period, arylhydrocarbon receptor nuclear translocator, single minded) (Figure 15) (Conti & Beavo, 2007).

II.5.1.1 Phosphodiesterase type 1

PDE1 family was the first discovered dual-substrate esterase. PDE1 is encoded by three genes: PDE1A, PDE1B and PDE1C (Lee & Kass, 2012). PDE1A and PDE1B hydrolyze cGMP with a higher affinity than cAMP and PDE1C hydrolyzes cAMP and cGMP with similar affinity. PDE1 has a unique property for being activated by Ca^{2+}/calmodulin and contains two domains for Ca^{2+}/calmodulin binding in the N-terminal regulatory complex. PDE1 activity can be also modulated by PKA- or CaMKII-phosphorylation, suggesting that PDE1 may be a point of interactions among different signaling pathways. PDE1A isoform is highly expressed in the brain and vascular smooth muscle cells and also was found in spermatozoa. PDE1B isoform is mainly expressed in human brain (neuronal cells of the cerebellum, hippocampus, caudate and Purkinje cells) and also in heart and skeletal muscle. PDE1C was mainly found in the heart and brain (Lugnier, 2006).

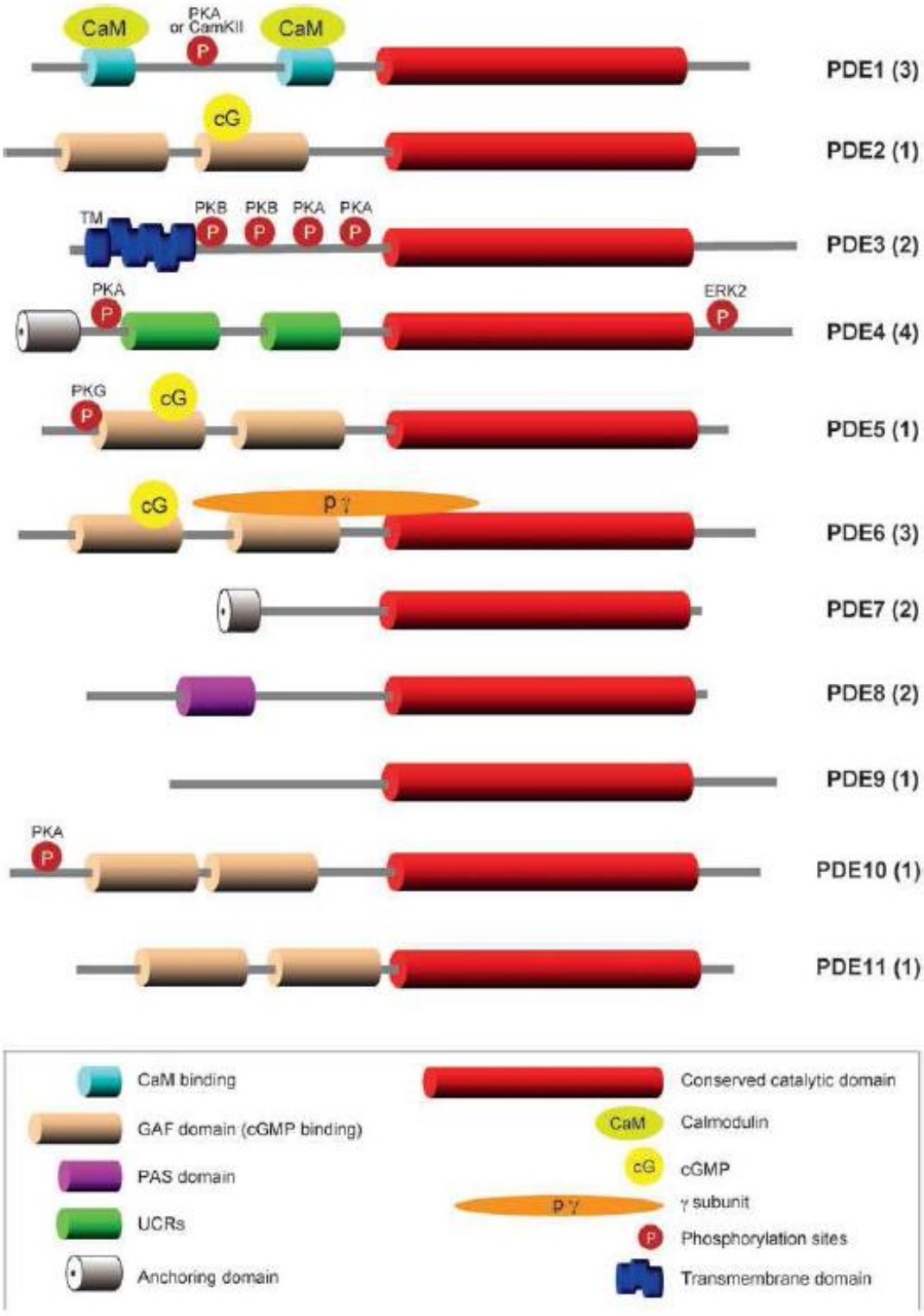

Figure 15: Schematic structure of the 11 phosphodiesterase (PDE) families.
Catalytic domain (red) is located in C-terminus and is highly conserved in all PDE families. The 11 families of PDEs differ in their N-terminal regulatory domain. On the right of each structure, the name of the PDE family and the corresponding number of genes are shown (Conti & Beavo, 2007).

In human myocardium, PDE1C is the most expressed isoform and is located along the Z- and M- lines of cardiac myocytes (Vandeput *et al.*, 2007). In rat heart, PDE1A represents

approximately 80% of total PDE1 activity, while PDE1C only 20%. In contrast, in rat failing cardiomyocytes PDE1A expression was significantly elevated, suggesting that PDE1A decreases level of cGMP and PKG activity, resulting in cardiac hypertrophy development (Miller *et al.*, 2009).

II.5.1.2 Phosphodiesterase type 2

PDE2 is a dual substrate enzyme, hydrolyzing both cAMP and cGMP with similar V_{max} and K_m (Bender & Beavo, 2006). PDE2 is encoded by a single gene *pde2A* which is present in 3 splicing variants: *pde2a1*, *pde2a2* and *pde2a3*. All three isoforms contain the same C-terminal domain but different N-terminal sequences that determine cytosolic or membrane localization (Lugnier, 2006). PDE2 has a unique property of being activated by cGMP binding. cAMP-hydrolyzing activity (V_{max}) is increased 2 to 6 fold in the presence of low concentration of cGMP and this is associated with increase in PDE2 affinity to cAMP (Osadchii, 2007). The N-terminal region of PDE2 contain a tandem of GAF domains (GAF-A and GAF-B) (Martinez *et al.*, 2002*b*). In PDE2, cGMP binds to GAF-B domain resulting in conformational changes and increase in catalytic activity of the enzyme (Heikaus *et al.*, 2009). PDE2 is mainly expressed in the heart, brain, liver, adrenal medulla, brown adipose tissue, platelets, endothelium and very low expression of PDE2 was also found in lungs (Beavo, 1995; Lugnier, 2006; Bubb *et al.*, 2014).

In the heart, PDE2A is mainly localized in the proximity of membrane structures, Golgi, SR and nuclear envelope, and is involved in crosstalk between cAMP and cGMP signaling and regulation of cAMP pools (Knight & Yan, 2013). PDE2 plays also an important role in modulation of heart rate and contractility by regulating the L-type Ca^{2+} current (Hartzell & Fischmeister, 1986; Rivet-Bastide *et al.*, 1997; Fischmeister *et al.*, 2005).

More detailed functions, structure and regulation of PDE2 are presented in the last chapter (VI. Phosphodiesterase type 2).

II.5.1.3 Phosphodiesterase type 3

PDE3 family is divided into 2 subfamilies: PDE3A and PDE3B. At least three PDE3A-related proteins were found with different molecular mass and N-terminal regions: PDE3A1, PDE3A2 and PDE3A3. In contrast, only one isoform was described for PDE3B subfamily, PDE3B1. PDE3A is mainly expressed in cardiac myocytes, vascular smooth muscle cells and platelets, while PDE3B is highly expressed in adipocytes, hepatocytes and pancreas. The N-terminal region of PDE3 family can contain the N-terminal hydrophobic domain 1 and 2 (NHR1 and NHR2), composed of 200 and 50 amino acids, respectively. The structure of the N-terminal region is responsible for subcellular localization of enzyme. PDE3A1 (136 kDa) has both NHR1 and NHR2 domains and is localized in the particulate fraction. PDE3A2 (118 kDa) contains only the NHR2 domain and is localized in particulate and cytosolic fraction. PDE3A3 (94 kDa) is lacking both NHR1 and NHR2 domains and is localized mainly in the cytoplasm. PDE3B1 has almost an identical structure as PDE3A1 and is also found in the particulate fraction (Degerman *et al.*, 1997*a*; Yan *et al.*, 2007*a*). PDE3 is highly specific for cAMP and is inhibited by cGMP. In the human heart, PDE3A is a major isoform hydrolyzing cAMP and represents more than 50% of the total PDE activity in the cytosol in the absence of Ca^{2+}/calmodulin (Osadchii, 2007). Distinct PDE3A isoforms are phosphorylated in different ways. PKA phosphorylates PDE3A1 on serine 312 and PDE3A2 is phosphorylated by PKC on serine 428 (Movsesian, 2016). In the heart, PDE3 is involved in the regulation of cardiac function. Pharmacological inhibition of PDE3 activity leads to increase in L-type Ca^{2+} current $I_{Ca,L}$ resulting in positive inotropic effect. PDE3 is also involved in mediating the effects of cGMP on cardiomyocytes contraction, together with PDE2 (Kirstein *et al.*, 1995; Rivet-Bastide *et al.*, 1997). cGMP-dependent inhibition of PDE3 results in increase in cAMP level by nitrate donors and atrial natriuretic peptides action, while cGMP-dependent activation of PDE2 antagonizes the cGMP-dependent effects on PDE3 (Maurice *et al.*, 2003).

II.5.1.4 Phosphodiesterase type 4

PDE4 family is the largest family of PDEs encoded by four genes, PDE4A, PDE4B, PDE4C and PDE4D (Lugnier, 2006). PDE4 is highly selective for cAMP and insensitive to cGMP and calmodulin. The four families of PDE4 differ in their N-terminal regulatory regions with conserved, almost identical catalytic regions. PDE4 has a unique N-terminal region containing two upstream conserved regions 1 and 2 (UCR1, UCR2). UCR1 is composed of 55 amino acids and UCR2 of 97 amino acids. UCR1 and UCR2 are separated by linker region 1 (LR1) formed of 33 residues and UCR2 and catalytic domain are separated by LR2 of approximately 28 residues. PKA phosphorylation site is located in UCR1 allowing PKA to activate PDE4 (Eskandari *et al.*, 2015). PDE4 family can be divided into three groups: long isoforms containing UCR1 and UCR2 regions, short isoforms, which have only UCR2 regions and super-short forms, which lack UCR1 and contain a truncated UCR2 regions. It was shown that UCR2 exerts an inhibitory effect on PDE4, thus isoforms lacking in UCR2 region present higher PDE4 catalytic activity (Houslay & Adams, 2003). PDE4C isoform is expressed mainly in skeletal muscle, lung, brain and testis, while PDE4A, B and D are highly expressed in brain, but they are rather ubiquitous (Zhang *et al.*, 2005). In mouse and rat heart, PDE4 represents ~30% of total PDE activity (Abi-Gerges *et al.*, 2009; Leroy *et al.*, 2011), while in human heart PDE4 constitutes only 10% of total PDE activity (Molina *et al.*, 2012; Eschenhagen, 2013). PDE4 is considered to be essential cAMP homeostasis regulator involved in cAMP signal compartmentalization, signaling cross-talk, cell desensitization and adaptation (Conti *et al.*, 2003). PDE4 exerts also effect on cardiac function. In rat heart, pharmacological inhibition of PDE4 leads to increase in contractile functions related to cAMP-mediated elevations in Ca^{2+} transients, SR Ca^{2+} load and phospholamban phosphorylation, without significant effects on $I_{Ca,L}$ and ryanodine receptor 2 (Mika *et al.*, 2013). Elevated basal contractility under PDE4 inhibition was also observed in guinea pig. In rat and dog hearts, PDE4 inhibition results in increase in heart rate (Beca *et al.*, 2011). In rodent heart, PDE4D isoform is associated with ryanodine receptors and studies with PDE4D knockout mice showed that mice lacking PDE4D develop HF and severe arrhythmias (Lehnart *et al.*, 2005). PDE4 is involved also in the generation of cAMP compartments by forming barriers for cAMP diffusion or acting as local sink for cAMP (Jurevicius *et al.*, 2003; Rochais *et al.*, 2004, 2006).

II.5.2 Pharmacological inhibition of phosphodiesterases

Family selective PDE inhibitors play an essential role as a research tool to help understand functional and regulatory roles of PDEs, as well as cyclic nucleotide signaling pathways. Selective PDE inhibitors are also used for treatment of a broad range of diseases with high selectivity and limited side effects as compared to non-selective generation of PDE inhibitors such as caffeine or other xanthine derivatives (Maurice *et al.*, 2014). Selective inhibitors of PDE families are presented in Table 3.

Family	Specificities	Inhibitors	IC_{50}
PDE1	Ca^{2+}/calmodulin-stimulated	Vinpocetine IC224 SCH51866	14 µM 80 nM 13-100 nM
PDE2	cGMP-stimulated	EHNA Bay 60-7550 PDP IC933	1 µM 4,7 nM 0,6 nM 4 nM
PDE3	cAMP-selective cGMP-inhibited	Cilostamide Milrinone Cilostazol OPC-33540	20 nM 150 nM 200 nM 0.3-1.5 nM
PDE4	cAMP-specific	Rolipram Ro 20-1724 Roflumilast Cilomilast	1 µM 2 µM 0.8 nM 120 nM
PDE5	cGMP-specific	Sildenafil Vardenafil Tadalafil	10 nM 1 nM 10 nM
PDE7	Rolipram-insensitive	BRL50481 IC242	260 nM 370 nM
PDE8	IBMX-insensitive Rolipram-insensitive	PF-04957325	0.2-0.7 nM
PDE9	IBMX-insensitive	Bay 73-6691 PF-04447943	55 nM 2.8-18 nM

Table 3: Pharmacology of PDE family-selective inhibitors (inspired by (Bender & Beavo, 2006; Hutson *et al.*, 2011; Keravis & Lugnier, 2012).

Inhibition of PDE1 was shown to improve behavioral functions and leads to increase in striatal dopamine levels. In addition, PDE1 inhibition exerts anti-inflammatory effects and plays beneficial role in Parkinson disease (Sharma *et al.*, 2013). Inhibition of PDE2 leads to increase in cGMP and cAMP impacting cAMP and cGMP signaling pathways. PDE2 inhibitors are investigated for precognitive and anxiolytic actions (Francis *et al.*, 2011). Inhibitors of PDE3 are used in HF but chronic administration of PDE3 inhibitors results in mortality related to occurrence of arrhythmias. PDE3 inhibition exerts anti-inflammatory effects and reduces apoptotic signaling in patients with severe HF (Lanfear *et al.*, 2009). PDE4 inhibitors are used in anti-depressive therapy and for the treatment of respiratory diseases- asthma and chronic obstructive pulmonary disease (COPD) (Keravis & Lugnier, 2012). PDE5 inhibitors are mainly used to improve erectile functions and for the treatment of pulmonary hypertension. PDE5 inhibitors are also used in therapy of pulmonary disease-asthma, chronic bronchitis, emphysema and COPD (Lugnier, 2011; Maurice *et al.*, 2014). Inhibitors of PDE7 can be used in inflammation, asthma and COPD. PDE8 inhibition is involved in regulation of basal rates of steroid production in rodent adrenal cells (Maurice *et al.*, 2014).

II.5.3 cAMP compartmentation

It was considered for a long time that second messengers can diffuse freely in the cytosol of cardiomyocytes. But observations of multiple physiological effects mediated by various external stimuli activating the same second messenger (cAMP) led to the assumpation that these effects were the result of different pools of cAMP with different dynamics depending on their subcellular location (Perera & Nikolaev, 2013). First evidence of intracellular cAMP compartmentation was formulated more than 30 years ago. It was shown that different agonists activating the cAMP signaling pathway via β_1-ARs and prostaglandin E_1 receptor (PGE_1-R) induce different effects. Isoproterenol, a non-selective β-AR agonist, induces an increase in cAMP mainly in microsomal fraction leading to activation of soluble and particulate PKA and enhancement in the force of contraction, while PGE_1 activation promotes an increase in cAMP in the cytosolic fraction and an activation of soluble PKA without any changes in contractile activity (Hayes *et al.*, 1982; Buxton & Brunton, 1983). Later, a study based on LTCC current recording in frog ventricular myocytes with the whole-cell patch clamp combined with a double microperfusion showed that cAMP activated by β_2-AR stimulation does not diffuse throughout the cytoplasm except when PDEs are inhibited (Jurevicius & Fischmeister, 1996) suggesting the formation of discrete pools of intracellular

cAMP. More recently, new techniques such as real-time fluorescent imaging techniques allowed to study intracellular cAMP changes and distribution in intact cardiomyocytes (Goaillard *et al.*, 2001). A study using genetically encoded fluorescence resonance energy transfer (FRET)-based cAMP probes showed that in cardiac myocytes β-AR stimulation induces a specific response leading to an increase in intracellular cAMP that is spatially limited and activation of a selected subset of PKA. cAMP in the restricted pools show a range of action as small as 1 micrometer and free diffusion is limited by PDEs that play a major role in shaping cAMP microdomains (Zaccolo & Pozzan, 2002; Zaccolo, 2006). Several observations suggest that various components of cAMP signaling pathway are localized in discrete regions of plasma membrane such as caveolae and T-tubules allowing for rapid modulation and production of cAMP (Fischmeister *et al.*, 2006). In caveolae, β_1-ARs were shown to be colocalized with AC6, hence providing a rapid and specific signal transduction in cardiac myocytes (Ostrom *et al.*, 2000). β_2-ARs are exclusively localized within caveolae where they regulate LTCCs and augment contractile function (Rybin *et al.*, 2003). As β_2-ARs were shown to activate not only Gs-dependent but also G_i-dependent pathway, the latter might be responsible for confining the cAMP/PKA-dependent signal to the surface membrane (Steinberg, 1999). In T-tubules, LTCCs are present together with Na^+/Ca^{2+} exchanger and other components of cAMP signaling pathway such as ACs and Gs proteins (Brette and Orchard 2003).

It has been shown that PDEs play an important role in cAMP diffusional restriction. In addition, PDEs can be targeted to subcellular compartments of plasma membrane, form multiprotein signaling complexes (Figure 16) and have ability to terminate the cAMP signal in a spatially restricted manner (Baillie *et al.*, 2005; Lissandron & Zaccolo, 2006). PDE2, PDE3 and PDE4 have been shown to be important players in modulating cAMP signals in a specific manner in response to various Gs-coupled receptors (Rochais *et al.*, 2006).

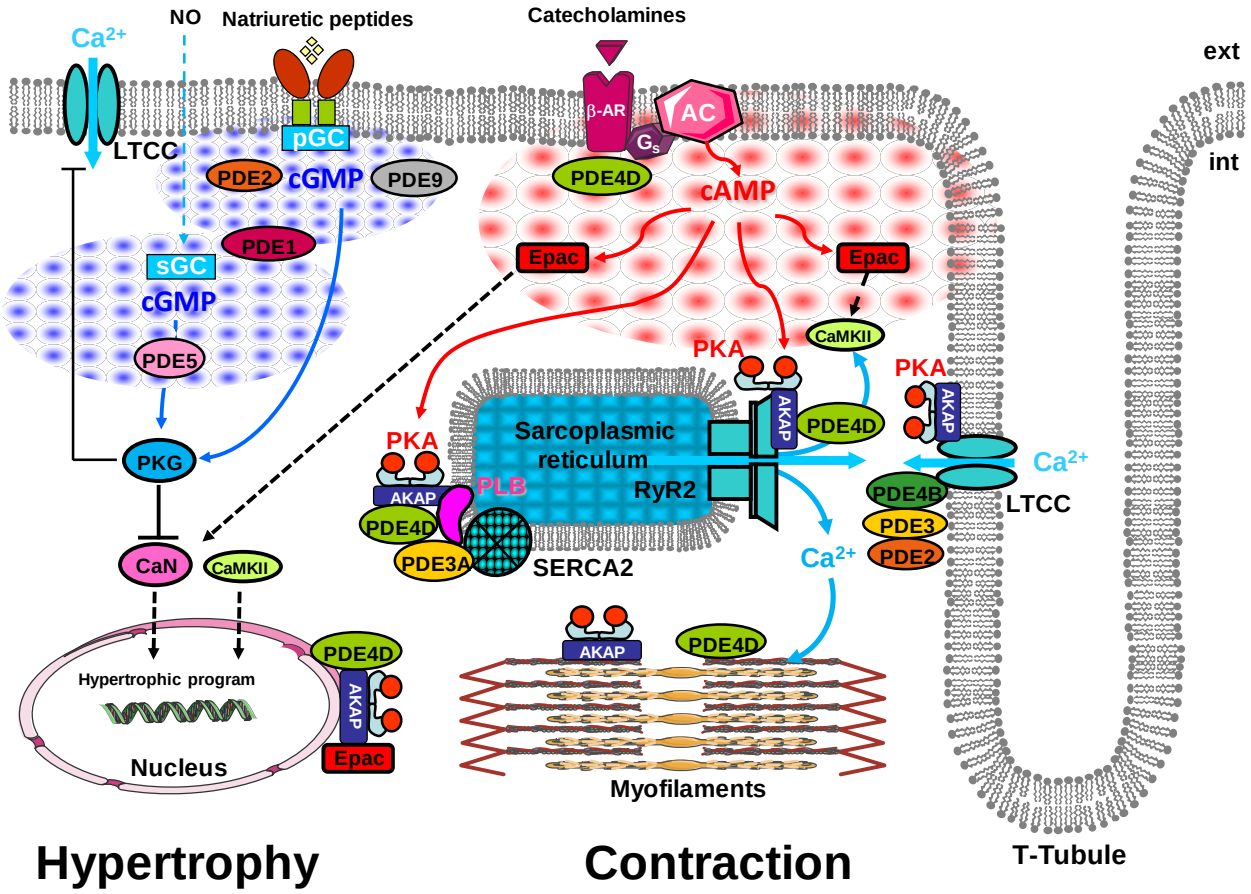

Figure 16: Distribution of PDE isoforms in cyclic nucleotide compartmentation.
Intracellular distribution of PDE isoforms and macromolecular complexes involving PDE activity in cyclic nucleotide compartmentation in cardiac myocytes (Bedioune *et al.*, 2016).

PDE2 has been shown to be localized preferentially in microsomal fractions associated with membrane structure such as plasma membrane, sarcoplasmic reticulum, Golgi and nuclear envelope (Lugnier, 2006). It has been shown that PDE2 highly controls the activity of LTCCs (Fischmeister *et al.*, 2005). The involvement of PDE2 in cAMP compartmentation was originally studied in frog cardiac myocytes. Dittrich et al. showed that stimulation of soluble guanylyl cyclase by NO leads to a strong local decrease in cAMP level in the proximity of LTCCs due to PDE2 activation, but causes only a marginal decrease in cAMP level in the rest of the cell (Dittrich *et al.*, 2001). PDE2 is also involved in regulation of cGMP compartments (Castro *et al.*, 2006).

PDE3 is a cGMP-inhibited PDE, thus cGMP signaling is involved in shaping cAMP compartments resulting in increase in cAMP level (Stangherlin *et al.*, 2011). PDE3 is found in cytosolic and membrane fraction and its localization is species and tissue dependent (Lugnier, 2006). In dog heart, PDE3 is associated with the SR membrane (Lugnier *et al.*, 1993) and PDE3 inhibition results in increase in local cAMP level, PKA activation and PLB

phosphorylation (Kerfant *et al.*, 2007), while in guinea pig and rat, PDE3 is present mainly in cytosolic fraction and exerts a minor effect in cAMP compartmentation (Weishaar *et al.*, 1987).

PDE4 has no effect on basal cAMP levels, but controls cAMP concentration and PKA phosphorylation of key proteins involved in ECC such as LTCCs, RyR2 and PLB upon β-AR stimulation (Mika *et al.*, 2012). Study with a cardiac contraction rate assay showed that PDE4 attenuates the adrenergic signaling of cAMP/PKA for enhancing contraction response (Xiang, 2011). Perinuclear PDE4 is also involved in regulation of cAMP pool near the nucleus and controls import of the catalytic subunits of PKA into the nucleus and hence gene regulation (Dodge *et al.*, 2001). PDE4D3 may form macromolecular complexes with PKA, mAKAP, Epac1 and kinase Erk5. Interestingly, these three enzymes (PKA, PDE4D3, Epac1) respond to cAMP in different concentration spectrum. Whereas PKA responds to nanomolar concentration, PDE4D3 and Epac1 are activated at micromolar concentration of cAMP (Dodge-Kafka *et al.*, 2005).

III. Cyclic GMP signaling in the heart

III.1 Cyclic GMP production

Cyclic guanosine monophosphate (cGMP) is a cyclic nucleotide and first time was purified and identified in rat urine in 1963 by Ashman and colleagues (Ashman *et al.*, 1963). cGMP acts as a second messenger like cAMP. cGMP is a main regulator of ion channel conductance, cell growth, apoptosis, cell mobility and contractility. In the cardiovascular system, cGMP plays an important role in regulation of endothelial and vascular smooth muscle and cardiac myocytes function (Tsai & Kass, 2009). In the heart, intracellular cGMP level is regulated by guanylate cyclases, responsible for cGMP synthesis and PDEs hydrolyzing cGMP (Hammond & Balligand, 2012).

In animal cells, cGMP is synthesized by two classes of guanylyl cyclases (GC): soluble GC (sGC) activated by nitric oxide (NO) and particulate GC (pGC) activated by natriuretic peptides, atrial natriuretic peptide (ANP), brain natriuretic peptide (BNP) and C-type natriuretic peptide (CNP). Then, cGMP activates downstream effectors of cGMP signaling such as cGMP-dependent protein kinase and phosphodiesterases (Gileadi, 2014).

III.1.1 Soluble guanylyl cyclase

Soluble GCs are found in almost all tissues, but the highest expression is observed in brain, kidney and vascular tissue (Potter, 2011). Soluble GC is a αβ heterodimer with a molecular weight of 72 kDa (Poulos, 2006). In human, two types of each subunit exist: α_1 and α_2 for the α subunit and β_1 and β_2 for the β subunit and they are encoded by four different genes: GUCY1A3, GUCY1A2, GUCY1B3, GUCY1B2, respectively (Wobst *et al.*, 2015). Both α_1 and β_1 subunits are rather ubiquitous, while the α2 subunit is mainly expressed in the brain, lung, colon, heart, spleen, uterus and placenta (Derbyshire & Marletta, 2012). α and β subunits form heterodimers and each subunit is divided into three domains: N-terminal domain, central domain, which contains a dimerization region and C-terminal domain, which recognizes substrate and has a catalytic activity of sGC. The N-terminal part of sGC is critical for sGC activity and binds heme, which is a receptor for ligands such as NO and CO. The central domain of sGC is responsible for heterodimer formation. The catalytic part contains the active site located between two catalytic domains of α and β subunits (Pyriochou & Papapetropoulos, 2005).

sGC is part of a regulatory cascade initiated by NO synthase (NOS) activation responsible for oxidation of L-arginine to NO and L-citrulline (Padayatti *et al.*, 2004*a*; Poulos, 2006). NO then binds to sGC and increases it activity by 100 to 300-fold. Upon activation, sGC converts GTP to cGMP and then cGMP can activate downstream effectors (Figure 17). NOS occurs in three isozymes: neuronal NOS (nNOS), inducible NOS (iNOS) and endothelial NOS (eNOS). eNOS and nNOS are activated by Ca^{2+}/calmodulin, while iNOS is Ca^{2+}-independent and is activated by inflammatory stimuli. eNOS is found mainly in endothelial cells and nNOS in neurons and skeletal muscle. All three isozymes of NOS are expressed in cardiac myocytes (Takimoto, 2012).

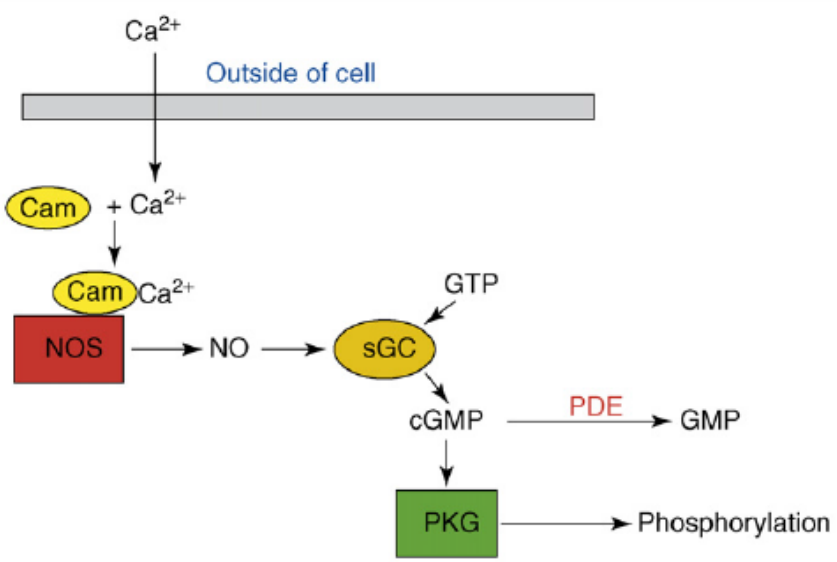

Figure 17: Soluble GC/NO signaling pathway.
Ca^{2+} enters the cell and binds to calmodulin resulting in NOS activation and NO production which activates soluble guanylyl cyclase (sGC). sGC produces cGMP which activates protein kinase G (PKG) resulting in phosphorylation of key components critical to cell signaling processes (Poulos, 2006).

III.1.2 Particulate guanylyl cyclase

Particulate or membrane form of guanylyl cyclases (pGC) are found in almost all tissue, but their distribution and main functions are isoform specific. Seven different isoform of pGCs were identified (GC-A to GC-G) in mammalian cells and their characteristic is presented in Table 4. GC-A is the best known guanylyl cyclase and is the most widely expressed throughout mammalian body in different cell types of the nervous system, immune system, kidney, lung, intestine, testis and heart (Kobiałka & Gorczyca, 2000).

Particulate GCs are composed of an extracellular ligand-binding domain (ECD), which consists of 500 amino acids, a transmembrane domain (TD) of about 50-70 amino acids, an inactive kinase homology domain (KHD) and a GC catalytic domain (CD) of about 250 amino acids (Padayatti *et al.*, 2004*b*; Freihat *et al.*, 2014). Peptide hormones bind to an extracellular domains of GC-A, GC-B and GC-C. Intracellular domains of pGC are responsible for interactions with proteins such as kinases and phosphatases that regulate the activity of the enzyme. Enzyme can be activated by extracellular ligand binding, phosphorylation of KHD domain or interactions with Ca^{2+}-binding proteins. The transmembrane domain is responsible for oligomerization/dimerization, obligatory for the enzyme activation (Kobiałka & Gorczyca, 2000). The kinase homology domain of GCs is responsible for regulation the activity of the catalytic domain (Jaleel *et al.*, 2006).

In addition, particulate GCs can be homologously desensitized after chronic exposure to hormone peptides through cGMP-independent mechanism (Hamad *et al.*, 2003).

Receptor	Ligands	Other regulators of activity	Localization	Function
GC-A	ANP>BNP	ATP	Lung, kidney, brain, thymus, smooth muscle, retina, macrophages, neutrophils, thymocytes, T lymphocytes	Decrease in arterial blood pressure, decrease in blood volume, inhibition of cardiomyocyte growth
GC-B	CNP	ATP	Lung, kidney, brain, thymus, smooth muscle, retina	Endochondral ossification, vascular regeneration
GC-C	Guanylin Uroguanylin	ATP, PKC	Epithelial cells of gastrointestinal tract, kidney, liver, uterus	Increased intestinal and renal water transport, epithelial cell growth and differentiation
GC-D	Unknown	Unknown	Olfactory cell	Odor recognition (?)
GC-E	Unknown	Ca^{2+}/neurocalcin Ca^{2+}/GCAP1-3 ATP	Retina, pineal glands	Vision, survival of cones
GC-F	Unknown	Ca^{2+}/GCAP2-3 Ca^{2+}/GCAP1 (?) ATP (?)	Retina	Vision (?)
GC-G	Unknown	Unknown	Lung, intestine, skeletal muscle	Unknown

Table 4: Ligands, activators, localization and main functions of the various mammalian particulate guanylyl cyclase receptors.
GCAP: guanylyl cyclase-activating protein, PKC- protein kinase C (inspired by (Kobiałka & Gorczyca, 2000; Kuhn, 2003)).

III.2 cGMP targets in cardiac myocytes

cGMP exerts effect on three main groups of cellular targets including cGMP-dependent protein kinase G (PKG), cGMP-gated ion channels and PDEs.

III.2.1 Protein kinase G

In 1969, Kuo and Greengard discovered that protein kinase from lobster tail was activated by cAMP and cGMP in a histone phosphorylation assay (Kuo & Greengard, 1969; Kots *et al.*, 2009). PKG exists in two isoforms PKGI and PKGII and is encoded by two genes *prkg1* and *prkg2*, respectively. PKGI is expressed in two isoforms PKGIα and PKGIβ, encoded by two alternatively spliced exons in the amino terminus (Surks, 2007). PKGI occurs in smooth muscles, platelets, cerebellum, hippocampus, dorsal root ganglia, neuromuscular endplate and kidney at high concentration (>0.1 μM). At low concentration, PKGI isoform is present in cardiac muscle, vascular endothelium, granulocytes, chondrocytes and osteoclasts. PKGIα is mainly expressed in lung, heart, dorsal root ganglia and cerebellum. PKGIβ isoform is

expressed in smooth muscle such as uterus, vessels, intestine and trachea (Hofmann, 2005). PKG is a serine/threonine specific kinase phosphorylating various protein targets. PKG is composed of an N-terminal domain with a leucine-isoleucine zipper, responsible for homodimerization and intracellular localization, an autoinhibitory domain, a regulatory domain, which contains two allosteric cGMP-binding sites, an ATP binding domain and a catalytic domain (Schlossmann & Hofmann, 2005). In the absence of cGMP, the autoinhibitory domain covers the active site of PKG. cGMP binding induces conformational changes that move the autoinhibitory domain away from the active site. It was also shown, that PKG is endogenously activated by phosphorylation of threonine 517 located in the catalytic loop.

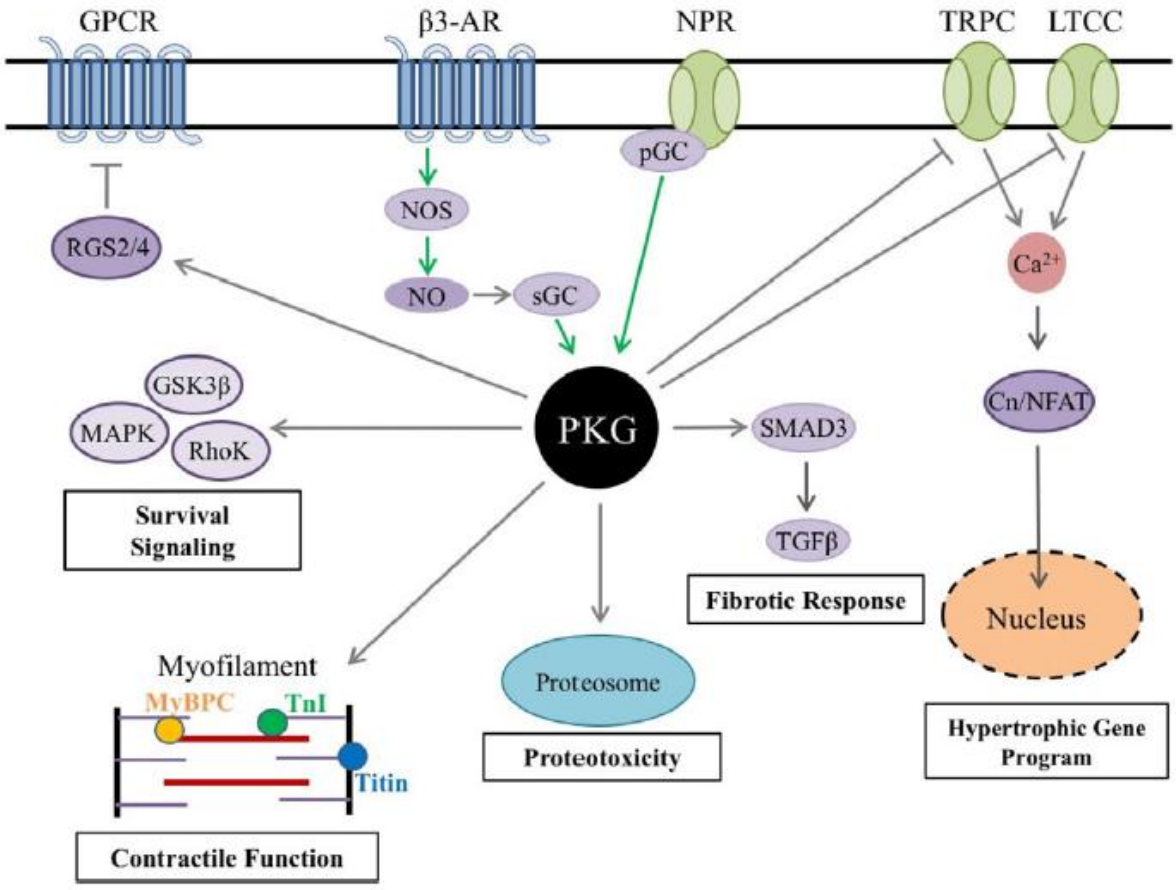

Figure 18: PKG signaling pathway in cardiac myocytes.
GPCR: G-protein coupled receptor, β_3-AR: β_3-adrenergic receptor, NPR: natriuretic peptide receptor, TRPC: transient receptor potential canonical, LTCC: L-type Ca^{2+} channels, pGC: particulate guanylyl cyclase, NOS: nitric oxide synthase, NO: nitric oxide, sGC: soluble guanylyl cyclase, RGS: regulator of G protein signaling, GSK-3β: glycogen synthase kinase 3β, MAPK: mitogen-activated protein kinase, TGFβ: transforming growth factor β, Cn: calcineurin, NFAT: nuclear factor of activated T cells, MyBP-C: myosin binding protein C, TnI: troponin I (from (Kirk *et al.*, 2016)).

In the heart, when PKG is activated by cGMP binding, PKG phosphorylates protein target on the serine/threonine residues. The protein targets can be divided into four groups: 1) intracellular Ca^{2+} regulation and signaling, 2) sarcomere myofilament proteins, 3) transforming growth factor β (TGFβ) and fibrosis factors, and 4) activation of other survival pathways (Figure 18) (Kirk *et al.*, 2016).

As mentioned before, PKG phosphorylates protein targets involved in ECC including LTCCs, TnI and PLB.

III.2.1.1 LTCCs

PKG was shown to phosphorylate LTCCs (Jiang *et al.*, 2000; Yang *et al.*, 2007). A number of studies showed that cGMP/PKG mediated phosphorylation leads to inhibition of LTCCs (Méry *et al.*, 1991). In rabbit cardiomyocytes, LTCC has two potential PKG phosphorylation sites, on serine 533 and serine 1371. PKG-dependent phosphorylation on serine 533 leads to inhibition of LTCCs (van der Heyden *et al.*, 2005). Two different mechanisms for LTCC inhibition have been reported: direct phosphorylation of LTCCs by PKG and PKG-dependent activation of a phosphatase, resulting in channels dephosphorylation (Keef *et al.*, 2001). PKG-mediated inhibition of LTCCs is in line with results obtained with transgenic mice overexpressing PKG-I, which augments NO/cGMP inhibition of single LTCC activity (Schröder *et al.*, 2003).

III.2.1.2 Troponin I

PKG phosphorylates TnI at the same phosphorylation sites as PKA on serine 23 and 24 (Blumenthal *et al.*, 1978; Lincoln & Corbin, 1978), but with much less efficiency than PKA (Lincoln & Corbin, 1978). PKG phosphorylation of TnI leads to reduction in myofilament Ca^{2+} responsiveness (Layland *et al.*, 2002) with additional effects such as reduction of LTCC current or increased SR Ca^{2+} uptake (Layland *et al.*, 2005). These effects were absent under pharmacological inhibition of PKG (Kaye *et al.*, 1999) and in PKG-I knockout mice (Wegener *et al.*, 2002). In addition, cardiac specific overexpression of PKG-I results in increase in cardiac relaxation and confirming the role of PKG phosphorylation in the regulation of cardiac function (Wollert *et al.*, 2003).

III.2.1.3 Phospholamban

PKG phosphorylates PLB on serine 16 (Kranias & Hajjar, 2012). PKG-dependent phosphorylation plays an essential role in the modulation of smooth muscle contraction and is also involved in a positive inotropic and lusitropic effect in mammalian heart (Mattiazi et al 2005). It has been also suggested that pharmacological activation of PKG with the cGMP analogue 8-bromo-cGMP leads to an increase in phosphorylation of PLB and activation of SERCA, resulting in reduction in the cytosolic Ca^{2+} oscillations and preventing excessive myofibril activation during reperfusion (Inserte *et al.*, 2014). PLB once phosphorylated by PKG reduces intracellular Ca^{2+} concentration by dissociating from SERCA. Then, SERCA is ready to pump Ca^{2+} ions back into the SR (Kranias & Hajjar, 2012).

III.2.2 Cyclic nucleotide phosphodiesterase

In addition to cGMP synthesis, cGMP is degraded by PDEs that control intracellular cGMP levels. Five PDEs are responsible for cGMP hydrolysis- PDE1, PDE2, PDE3, PDE5 and PDE9, but the activity of only three of them is regulated by cGMP. PDE2 and PDE5 are stimulated by cGMP and PDE3 is inhibited by cGMP (Figure 19) (Zhang & Kass, 2011).

PDE5 is encoded by a single gene *pde5a* and is expressed as three isoforms, PDE5A1, PDE5A2 and PDE5A3 that differ in their N-termini. The highest expression of PDE5A is observed in vascular smooth muscle, lung and corpus cavernosum and low expression of PDE5A was found in systemic arteries and in the heart (Kass, 2012). PDE5 is phosphorylated by PKG-I on serine 102 in human and serine 92 in mouse, and also by PKA (Corbin *et al.*, 2000). Phosphorylation of PDE5 occurs when cGMP is bound to the regulatory domains (Turko *et al.*, 1998). PKG-mediated phosphorylation of PDE5 leads to increase in enzyme activity and represents a feedback mechanism to limit amplitude and duration of a cGMP signal in cells that express PDE5 (Mullershausen *et al.*, 2003). PDE5 contains two highly homologous GAF domains (GAF-A and GAF-B). It was shown that high-affinity cGMP binding occurs only to the GAF-A domain. cGMP binding is stabilized by PKG-dependent phosphorylation of a nearby serine (Kass *et al.*, 2007). In cardiac myocytes, PDE5 is localized in a striated banding pattern, colocalized with α-actinin in the Z-disk (Kass, 2012). It was demonstrated that in this localization, PDE5 controls the cGMP pool produced by sGC, while cGMP produced via pGC is under the control of PDE2 (Castro *et al.*, 2006). Chronic NOS activity was shown to be required for PDE5 localization to Z-band region in the proximity of β-AR-complex signaling proteins (Takimoto *et al.*, 2005*a*).

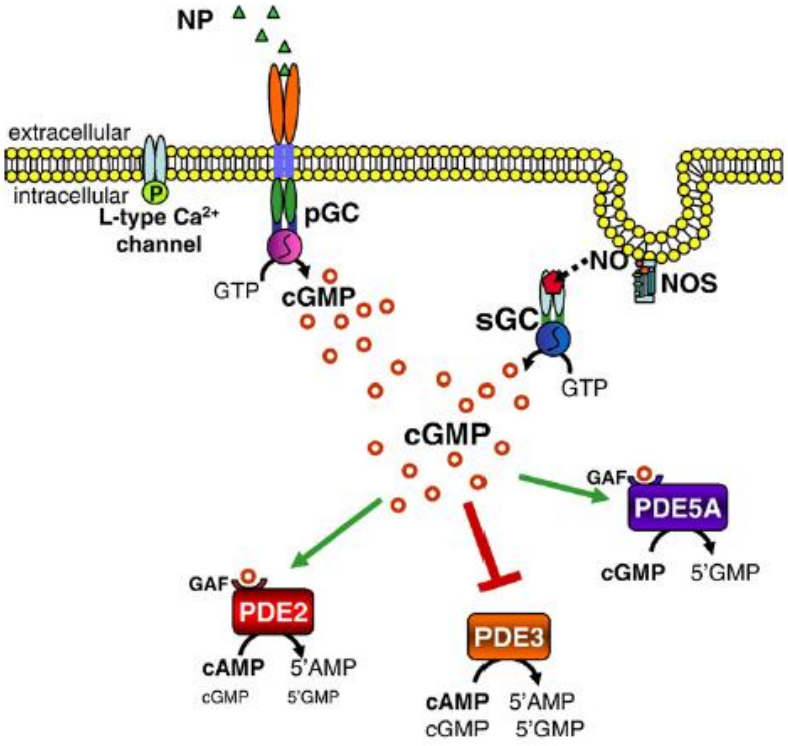

Figure 19: cGMP signaling pathway.
cGMP is produced by particulate (pGC) and soluble (sGC) guanylyl cyclases upon natriuretic peptide and nitric oxide activation. cGMP then activates (green arrow) or inhibits (red arrow bar) various PDE isoforms (modified from (Tsai & Kass, 2009)).

PDE3 structure, localization and splice variants were described in the chapter §II.6.1: Structure, localization and regulation of PDEs. PDE3 is a PDE isoform inhibited by cGMP. PDE3 does not have allosteric cGMP-binding domains such as PDE2 and PDE5. PDE3 catalytic sites have high affinity for both cAMP and cGMP, but the V_{max} is 4-10 times higher for cAMP than for cGMP. Thus, cGMP regulates PDE3 catalytic activity through competition with cAMP at the catalytic sites (Rybalkin *et al.*, 2003). Cyclic GMP-dependent inhibition of PDE3 results in increase in cAMP and activation of PKA (Degerman *et al.*, 1997*a*).

PDE2 is a dual substrate enzyme, hydrolyzing both cAMP and cGMP. PDE2 has a property for being stimulated by cGMP. This cGMP-dependent stimulation is due to the presence of two GAF domains (GAF-A and GAF-B). In contrast to PDE5, cGMP binds with high affinity to PDE2 GAF-B domain (Wu *et al.*, 2004), while GAF-A domain is involved in enzyme dimerization (Martinez *et al.*, 2002*b*). cGMP binding to GAF-B domain leads to decrease in the apparent K_m for cAMP, resulting in activation of the cAMP-hydrolyzing activity of the enzyme (Martinez *et al.*, 2002*a*). More detailed regulation of PDE2 is described in the last chapter VI.2: Regulation of expression and activity of PDE2.

PDE1 is a dual-specificity enzyme that hydrolyzes cAMP and cGMP in a competitive manner. PDE1 is encoded by three PDE1 genes, *PDE1A*, *PDE1B* and *PDE1C*. PDE1A and PDE1B isoforms have higher affinity for cGMP, while PDE1C isoform has similar affinity both substrates. The majority of cGMP-hydrolytic activity is attributable to PDE1, together with PDE3, in normal and failing human hearts. PDE1C is the predominant PDE1 isoform expressed in human myocardium. Susceptibility of PDE1 to competitive inhibition by cAMP and cGMP suggests that PDE1 may have a role in the integration of cAMP and cGMP signaling pathways (Vandeput *et al.*, 2007, 2009).

PDE9A was for the first time cloned and characterized in 1998 (Fisher *et al.*, 1998; Soderling *et al.*, 1998). PDE9A has the highest affinity and selectivity for cGMP. PDE9A is mainly expressed in the brain, gut and kidney, however mRNA is also detectable in the heart. Basal gene expression is low in neonatal myocytes but increases with agonist or mechanical stimulation.

Opposite to PDE5, PDE9A regulates cGMP pool coupled to NPs, but not NO-stimulated cGMP. It can be related to intracellular localization and co-localization with t-tubular membranes. PDE9A protein expression is increased in LV myocardium from human with HF or LV hypertrophy. Selective pharmacological or genetic inhibition of PDE9 protects the heart against pathological neurohormonal response (Lee *et al.*, 2015).

III.3 cGMP signaling in cardiac hypertrophy

Cardiac hypertrophy is the enlargement of the heart in response to chronic pressure or volume overload caused by different disease conditions such as hypertension, coronary artery disease or valvular heart (Opie *et al.*, 2006; Weeks & McMullen, 2011; Hou & Kang, 2012). At the cellular level, hypertrophy is characterized by increase in cell size, protein synthesis and heightened organization of the sarcomere (Frey *et al.*, 2004). Cardiac hypertrophy eventually leads to contractile dysfunction, ventricular dilation and finally to heart failure (Mann, 1999; Frey & Olson, 2003). One of the molecular mechanisms of hypertrophy involves calcineurin/NFAT signaling pathway. Calcineurin is activated by an increase in intracellular concentration of Ca^{2+}. Once activated calcineurin dephosphorylates its downstream effectors including nuclear factor of activated T cells (NFAT) within the cytoplasm. Dephosphorylated NFAT translocates to the nucleus and is involved in Ca^{2+}-inducible gene expression with other transcription factors. Ca^{2+}-calcineurin-NFAT pathway can interact with other pathway such as PKC and mitogen-activated protein kinases (MAPK), resulting in hypertrophic

response (Molkentin, 2004). Cardiac hypertrophy is controlled also by counter regulatory signaling pathway including cGMP production by nitric oxide (NO) and natriuretic peptides (NPs) (Calderone *et al.*, 1998). It was shown that anti-hypertrophic effect of NO is via activation of soluble guanylyl cyclase and cGMP synthesis (Wollert *et al.*, 2003). NO and cGMP, acting via PKGI, inhibit calcineurin/NFAT pathway and prevent NFAT nuclear translocation and transcriptional activity (Fiedler & Wollert, 2004). The second anti-hypertrophic mechanism involves the action of natriuretic peptides. As discussed above, NPs are hormones responsible for regulation of salt-water balance and blood pressure by promoting renal sodium and water excretion (Song *et al.*, 2015). The plasma concentration of ANP and BNP is increased in patients with HF and cardiac hypertrophy suggesting their compensatory role in HF because of their diuretic, natriuretic and vasodilating actions (Nishikimi *et al.*, 2006). Consequently, ANP and BNP are used as prognostic biomarkers in cardiovascular events. Elevated ANP and BNP levels were positively and significantly correlated with cardiovascular mortality and adverse cardiovascular outcomes (Gupta & Wang, 2015). Studies with ANP and BNP deficiency in mice confirmed the anti-hypertrophic effect of NPs. Mice lacking ANP developed chronic hypertension and cardiac hypertrophy (Lopez *et al.*, 1995; Knowles *et al.*, 2001). In contrast to ANP-deficient mice, mice lacking BNP did not develop hypertrophy, but interstitial cardiac fibrosis, responsible for abnormal myocardial stiffness and ventricular dysfunction (Tamura *et al.*, 2000). These results suggest that ANP and BNP play distinct roles in cardiovascular system.

IV. cAMP and cGMP signaling crosstalk

In the mammalian heart, cAMP and cGMP are essential second messengers that mediate the activity of several neurotransmitters. The β-adrenergic and NO/cGMP/PKG pathways have opposite physiological effects on cardiac function. cAMP is responsible for increasing force and frequency of cardiac contraction via PKA activation, while cGMP regulates vasorelaxation and decreases cardiac contractility via PKG activation (Stangherlin & Zaccolo, 2012). PDEs play an important role in the compartmentation of both cyclic nucleotides and in the crosstalk of cAMP and cGMP signaling pathways. PDEs are also under the control of cAMP and cGMP which exert a feedback regulation of the rate of degradation of these two second messengers (Figure 20) (Fischmeister *et al.*, 2006).

Thirty years ago, cGMP was shown to exert an opposite effect to cAMP on $I_{Ca,L}$ in frog cardiomyocytes via activation of a PDE (Hartzell & Fischmeister, 1986; Fischmeister & Hartzell, 1987). Since then, PDE2 was shown to mediate the inhibitory effect of NO on $I_{Ca,L}$ upon β-AR stimulation in various species, including human (Méry *et al.*, 1993*b*; Kirstein *et al.*, 1995; Méry *et al.*, 1995; Rivet-Bastide *et al.*, 1997). cGMP was also shown to modulate cAMP signal in rabbit atrioventricular nodal (AV) cells (Han *et al.*, 1996). In this study, PDE2 activated by NO/cGMP was proposed to be involved in the muscarinic cholinergic attenuation of $I_{Ca,L}$ upon activation by isoproterenol. In rat neonatal cardiomyocytes, β_3-ARs were shown to activate NO generation, resulting in sGC activation and production of cGMP that activates PDE2 and reduces cAMP concentration (Mongillo *et al.*, 2006). In contrast, PDE5 inhibition results in increase in cytosolic cGMP and PKG activation, but not whole-cell β-AR response (Zhao *et al.*, 2016). Other studies showed involvement of PDE3 in cAMP-cGMP crosstalk. PDE3 is a cGMP-inhibited PDE and cGMP acts as competitive inhibitor of PDE3 (Degerman *et al.*, 1997*b*). In human atrial cells, cGMP-dependent inhibition of PDE3 induces an increase in $I_{Ca,L}$ at low concentrations of cGMP but this effect is overcome by cGMP-activation of PDE2 at higher cGMP concentrations, leading to a decrease in $I_{Ca,L}$ (Vandecasteele G, Verde I, Rucker-Martin C, Donzeau-Gouge P, Fischmeister R. Cyclic GMP regulation of the L-type Ca^{2+} channel current in human atrial myocytes. *J Physiol*. 2001;533:329-340).In guinea pig cardiac sinoatrial cells, cGMP-dependent inhibition of PDE3 leads to an increase in the delayed rectifier K^+ currents through an elevation of intracellular cAMP levels and subsequent activation of PKA (Shimizu *et al.*, 2002).

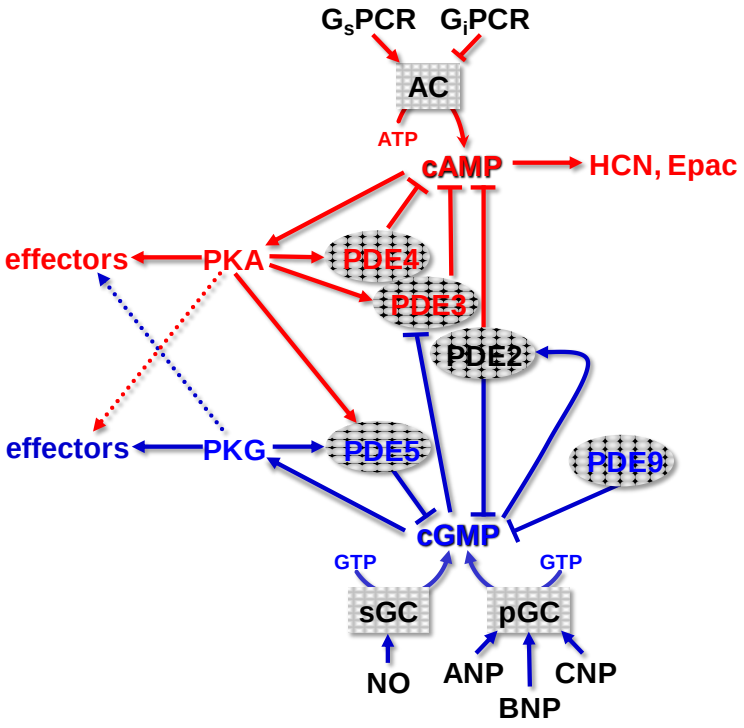

Figure 20: cAMP and cGMP signaling pathways in cardiomyocytes.
The diagram illustrates the enzymes involved in cAMP and cGMP synthesis and degradation and the complex interactions between the 2 signaling pathways in cardiomyocytes (in red for cAMP, in blue for cGMP) (adapted from Fischmeister *et al.*, 2006).

Studies on cGMP signals on the cAMP response to ISO in rat ventricular myocytes showed that cGMP signal do not change the whole cellular cAMP response, but alter the cAMP signals locally. Increase in cGMP results in increase in the cAMP pool activated by PKAI-RI and in decrease in the cAMP pool activated by PKA-RII. This effect is associated with local PDE2 and PDE3 activities. PDE2 activity is rather coupled to the PKA-RII compartment, while PDE3 is preferentially localized in the proximity of the PKA-RI compartment in which cGMP-dependent activation of PDE2 and cGMP-mediated inhibition of PDE3 exert opposing effects of cGMP on local cAMP signals (Stangherlin *et al.*, 2011).

It was also demonstrated that cAMP-mediated signaling is affected by natriuretic peptides (ANP, BNP, CNP) and their receptors (NPR-A and NPR-B). BNP acting through NPR-A and CNP acting through NPR-B lead to increase in β_1-AR signaling in failing rat ventricles via cGMP-dependent PDE3 inhibition (Qvigstad *et al.*, 2010; Levy, 2013). NPR-B stimulation leads to increase in total cAMP concentration, inotropic responses, apoptosis mediated through β_1-ARs and also results in increased phosphorylation of PLB and TnI. These effects were comparable with those of a selective PDE3 inhibition with cilostamide. cGMP-mediated

inhibition of PDE3 overcomes the ability of PKG to attenuate PKA-mediated effects on cardiac function (Qvigstad *et al.*, 2010).

V. Heart failure

Heart failure (HF) is one of the most common causes of mortality and morbidity around the world. Each year, approximately 500 000 new cases are diagnosed in the United States and two million of new cases worldwide, leading to a prevalence of over 22 million across the globe. HF affects 10 people per 1000 over the age of 65. 78% of patients have at least two hospitalization per year, leading to an annual cost of 10-38 billion dollars (Kemp & Conte, 2012).

V.1 Pathophysiology of heart failure

Heart failure is a disease in which the heart is unable to pump blood sufficiently to meet the body's needs. HF is associated with risk factors such as hypertension, diabetes, coronary artery disease, obesity, sleep apnea, valvular heart disease, myocardial infarction and amyloidosis. There are two types of HF, HF with decreased ejection fraction (less than 45%) caused by systolic dysfunctions, destruction of cardiac myocytes or their molecular components, characterized by reduction in cardiac contractility. The second type of HF is HF with preserved ejection fraction, caused by diastolic dysfunctions and leading to impaired cardiac relaxation and abnormal ventricular filling (Kanwar *et al.*, 2016).

In human HF, cardiac β-AR dysfunctions is observed, characterized at the molecular level by selective decrease in β_1-AR density at the plasma membrane and by uncoupling of the membrane β_1-ARs and β_2-ARs from G proteins (Lymperopoulos *et al.*, 2013). Perturbations at the cellular level in human HF include impaired Ca^{2+}-handling, extracellular matrix modifications, myofilament dysfunctions, reduction in SERCA2 expression and reduction in phosphorylation of PLB by PKA (El-Armouche & Eschenhagen, 2009). Modifications of the extracellular matrix are characterized by an increased stiffness caused by abundance of collagen type I (van der Velden, 2011).

Myocardial systolic dysfunctions are associated with neurohormonal hyperactivity, acting as a compensatory mechanism, to maintain cardiac output during decrease of cardiac function. This mechanism includes increase in secretion and in circulating level of certain catecholamines, mainly epinephrine and norepinephrine released by cardiac nerve terminals.

Elevation in catecholamine levels results in chronically elevated stimulation of the cardiac β-AR system and exert detrimental effects on the failing hearts (El-Armouche & Eschenhagen, 2009). Hyperactive neurohormonal system was reported to be cardiotoxic and causes interstitial fibrosis, reduction in β-AR mediated inotropic responses, promotes cardiac apoptosis and induces contractile dysfunction through left ventricular dilation (Lymperopoulos *et al.*, 2013). During compensated hypertrophy, the Frank-Starling mechanism leads to increase in cardiac output by increasing ventricular volume and wall thickness through ventricular remodeling. This helps to maintain tissue perfusion with augmented mean arterial pressure through activation of neurohormonal system (Kemp & Conte, 2012).

V.2 Treatment of heart failure

The aim of pharmacological therapy of HF is to relieve symptoms and signs, improve quality of live, prevent hospitalization and improve survival. First-line therapy for people with HF can include treatment with beta-blockers, inhibitors of phosphodiesterases, nitrovasodilators, Ca^{2+} channel blockers, angiotensin receptor blockers, diuretics, ivabradine, digoxin or a new medical agent with a double action, LCZ 696 (Gu *et al.*, 2010).

V.2.1 β-blockers

β-blockers were first time used in 1973 when a single bolus injection was administered to a 59-year old woman with tachycardia to reduce the heart rate. In 1975, seven patients were treated with β-blockers in first clinical studies. All seven patients had an improvement of cardiac functions shortly after starting treatment. In 1980, Bristow et al demonstrated that the adenylyl cyclase response to β-AR blockade was attenuated in patients with HF compared with controls (Bristow *et al.*, 1986; Swedberg, 1998). It was shown that chronic sympathetic activation acts as inotropic and chronotropic support to the failing hearts, but has also deleterious effects such as direct cardiotoxic effects of catecholamines on myocardium, activation of the renin-angiotensin-aldosterone system and elevation in myocardial oxygen demand and β-blockade can be beneficial in the treatment of chronic HF (Denbow, 2000). β-blockers can be divided into three generations that differ in their receptor selectivity, vasodilating properties and metabolism (Gorre & Vandekerckhove, 2010). First generation of β-blockers competitively block both the β_1-ARs and β_2-ARs (propranolol, nadolol, timolol). Second generation has higher affinity for β_1-ARs than β_2-ARs (atenolol, metoprolol, bisoprolol). The third generation can be subtype-selective (celiprolol, nebivolol) and non-

selective (bucindolol, carvedilol, labetalol). Non-selective third generation of β-blockers block also α_1-ARs resulting in peripheral vasodilation (Lymperopoulos *et al.*, 2013). Chronic therapy with β-blockers showed beneficial effects including amelioration of symptoms, reverse cardiac remodeling, improvement in left ventricular systolic functions and coronary blood flow to the heart, reduction in risk of arrhythmias, protection of the heart against cardiotoxic overstimulation by catecholamines and improvement of survival (Zafrir & Amir, 2012; Lymperopoulos *et al.*, 2013).

V.2.2 Inhibitors of PDEs

In acute HF, inotropes such as β-AR agonists (dobutamine, dopamine) or inhibitors of phosphodiesterase 3 (milrinone) seem to improve clinical symptoms and hemodynamics. Treatment with inotropes results in increase in intracellular cAMP level and increase in cardiac output and have been used as a short-term bridge to other forms of therapy, e.g. transplantation or in patients with chronic advanced HF (Parissis *et al.*, 2007). More recently, inhibitors of PDE5 have been used as a cGMP-raising agents in vascular smooth muscle and a lot of studies focus on inhibitors of PDE5 as potential therapeutic strategy in HF (Movsesian *et al.*, 2009; Kass, 2012).

In 1980, Milrinone was approved for short-term intravenous use. Milrinone is a bipyridine derivative, which leads to increase in intracellular cAMP level, resulting in increase in intracellular Ca^{2+} concentration and contractility and myocardial relaxation. Increased cAMP exerts a vasodilatory effect in arterial and venous circulation leading to decrease in systemic and pulmonary vascular resistance, decrease in left and right ventricular filling pressure and increase in cardiac output (Bayram *et al.*, 2005). However, milrinone treatment was associated with acceleration of disease progression and development of serious ventricular arrhythmias (Packer *et al.*, 1991). Milrinone increases also myocardial oxygen demand and may lead to myocardial ischemia (Petersen & Felker, 2008).

PDE5 inhibition (Sildenafil, Vardenafil, Tadalafil) increases cGMP bioavailability and improves heart functions (Wang *et al.*, 2015). Takimoto et al showed that chronic treatment with sildenafil significantly attenuated the left ventricular hypertrophy in mice with transverse aortic constriction. Treatment with sildenafil decreased chronic pressure overload in LV chamber, myocyte hypertrophy and improved cardiac function (Takimoto *et al.*, 2005*b*). In experimental models of myocardial disease, elevated PDE5 expression and activity were observed and related to oxidative stress. It was also shown that PDE5 is upregulated in human failing hearts and hypertrophy (Kass, 2012). Preclinical studies showed beneficial effects of

PDE5 inhibition by blocking adrenergic, hypertrophy and pro-apoptotic signaling. Chronic treatment with PDE5 inhibitors has also favorable effect on lung diffusion capacity and exercise performance. In addition, clinical trials showed the safety, efficacy and tolerability of PDE5 inhibitors on morbidity and mortality in patients with systolic or diastolic HF (Kanwar *et al.*, 2016). Currently, three PDE5 inhibitors are used for treatment of erectile dysfunction and sildenafil and tadalafil are used in therapy of pulmonary arterial hypertension (Das *et al.*, 2015).

V.2.3 Vasodilators

Vasodilators that are nitrates (nitroglycerin, isosorbide mononitrate, isosorbide dinitrate and sodium nitroprusside) are a first-line agents for acute HF (Singh *et al.*, 2016). Acute HF is characterized by increased left ventricular filling pressure and high or normal blood pressure. In this case, treatment with vasodilators can improve both hemodynamics and symptoms (Hollenberg, 2007).

Nitrovasodilators can be divided into two groups: first group of agents that release NO spontaneously (sodium nitroprusside) and the second group of agents that need an enzymatic process to form NO (isosorbide mononitrate, isosorbide dinitrate and nitroglycerine). NO activates sGC and leads to production of cGMP. Then, intracellular cGMP inhibits Ca^{2+} entry into the cell resulting in decrease in intracellular Ca^{2+} concentration and in smooth muscle relaxation. NO can also activate K^{+} channels causing hyperpolarization and relaxation. Finally, NO acting via cGMP can activate PKG which activates myosin light chain phosphate resulting in relaxation and dilation. Nitrates at low doses promote only venous dilation, but at higher doses induce arteries (including the coronary arteries) dilation. Thus, nitrates cause balanced vasodilation and reduce elevated left ventricular filling pressures (Piper & McDonagh, 2014).

V.2.4 Ca^{2+} channel blockers

The Ca^{2+} channel blockers are a heterogeneous group of agents (nifedipine, nicardipine, nimodipine, felodipine, isradipine, amlodipine, dilitiazem, bepridil, mibefradil) with various effects on heart muscle, sinus node function, atrioventricular conduction, peripheral blood vessels and coronary circulation. The Ca^{2+} channel blockers are used for treatment of congestive HF. This group of agents have a strong arteriolar dilator effect resulting in reduction in systemic vascular resistance and left ventricular afterload. Combination of Ca^{2+}

channel blockers with vasodilators improve exercise tolerance and ejection fraction and survival in patients with mild-to-moderate HF. This group of drugs has also anti-ischemic effect and can be used in treatment of myocardial ischemia (Elkayam *et al.*, 1993; Elkayam, 1998).

V.2.5 ACE inhibitors and angiotensin receptor blockers

The renin-angiotensin-aldosterone system (RAAS) acts as a compensatory mechanism in HF. In early phase of HF, RAAS activation induces water and salt retention resulting in vasoconstriction in peripheral arteries, myocardial contractility and keeps cardiac output within normal limits. Chronic activation of RAAS has adverse effects on the cardiovascular system including heart remodeling and progression of HF. Renin converts angiotensinogen, synthesized in tissue and liver to angiotensin I and then angiotensin-converting enzyme (ACE) converts angiotensin I to angiotensin II, biologically active form. Angiotensin exerts its effect by binding to two receptors, angiotensin type I and angiotensin type II, both are found in heart tissue. Current RAAS inhibition includes use of ACE inhibitors (e.g. Captopril, Perindopril, Enalapril, Ramipril) and angiotensin type II blockers (e.g. Losartan, Olmesartan, Valsartan, Fimosartan, Eprosartan, Irbesartan, Telmisartan). Inhibition of ACE also leads to an increase in bradykinin which stimulates the production and secretion of NO. This leads to vasodilation by decreasing vascular resistance, improve the hemodynamics and systolic function by reverse remodeling and increase the exercise capacity (Kılıçkıran Avcı *et al.*, 2014; Arumugam *et al.*, 2016).

V.2.6 LCZ 696

The natriuretic peptides (NPs) ANP, BNP and CNP play an essential role in cardiovascular health, they promote vasodilation and oppose acute effects of volume overload by suppressing the sympathetic and RAAS activity. Neprilysin (NEP) is an enzyme that degrades NPs. NEP belongs to a neutral endopeptidase family and is expressed mostly in kidneys. It degrades also other vasoactive peptides (e.g. bradykinin) and vasoconstrictors (endothelin-1 and angiotensin II). Thus, physiological effect of NEP depends on the balance between its actions on vasodilating and vasoconstricting peptides (Andersen *et al.*, 2016). It was shown that combination of NEP inhibition with ACE inhibition leads to greater inhibition of bradykinin and higher increase in bradykinin level than with NEP or ACE inhibition alone. Recently, a novel pharmacological agent (LCZ696, Novartis) with a dual action as angiotensin receptor

inhibitor and NEP inhibitor has been developed. LCZ696 increases RAAS blockade and leads to beneficial effects of NPS without increasing side effects (Volpe *et al.*, 2016).

VI. Phosphodiesterase type 2

VI.1 Structure, function and subcellular localization of PDE2

PDE2 is an enzyme that hydrolyzes both cAMP and cGMP with similar kinetic constants (30 µM for cAMP and 10 µM for cGMP) and with a maximal hydrolysis velocity (V_{max}) of ~120 µmol/min/mg protein. However, the rate of cAMP hydrolysis is increased up to 30-fold by low concentrations of cGMP (Beavo *et al.*, 1971; Terasaki & Appleman, 1975; Erneux *et al.*, 1980; Martins *et al.*, 1982). Therefore, PDE2 has also been termed cGMP-dependent phosphodiesterase or cGMP-stimulated PDE. PDE2 is a homodimer of two monomers (103 kDa each) composed of a regulatory segment with two GAF domains (GAF-A and GAF-B) and a catalytic domain (Figure 21) (Martinez *et al.*, 2002*b*). The N-terminal regulatory domain of PDE2 is a place for alternative splicing resulting in three different isoforms of PDE2 that differ in their subcellular localization. The GAF-B domain is responsible for cGMP binding with high affinity resulting in allosteric activation of PDE2 (Stroop *et al.*, 1989; Charbonneau *et al.*, 1990; Wu *et al.*, 2004). cAMP binds to GAF-B domain as well but with very low affinity without significant changes in catalytic activity (Beavo *et al.*, 1971; Wu *et al.*, 2004). In the GAF-A domain, the key cGMP binding sites are poorly conserved suggesting that GAF-A domain cannot bind cyclic nucleotides and is involved only in dimerization of PDE2 (Martinez *et al.*, 2002*b*). In contrast, a recent study on solved crystal structure of an almost full length PDE2 shows that tandem of GAF-A and GAF-B domains is involved in dimerization of holoenzyme, not only GAF-A domain (Pandit *et al.*, 2009).

The catalytic domain of PDE2 shares the common structure with all PDEs and is composed of the helices that form an active site with two divalent metal ions (Zn^{2+} and Mg^{2+}) (Iffland *et al.*, 2005). A glutamine residue (Gln 859 in the human PDE2) in the catalytic site plays an important role in determining nucleotide specificity of PDEs in general. In PDEs that degrades only cAMP, Gln residue adopts arrangement that favors hydrogen bonding to the adenine base. In cGMP-specific PDEs, the orientation of glutamine residues allows the formation of hydrogen bonds with the guanine-base. In PDE2, the glutamine residue can occur in two orientations, because of dual specificity to the enzyme (Zhang *et al.*, 2004).

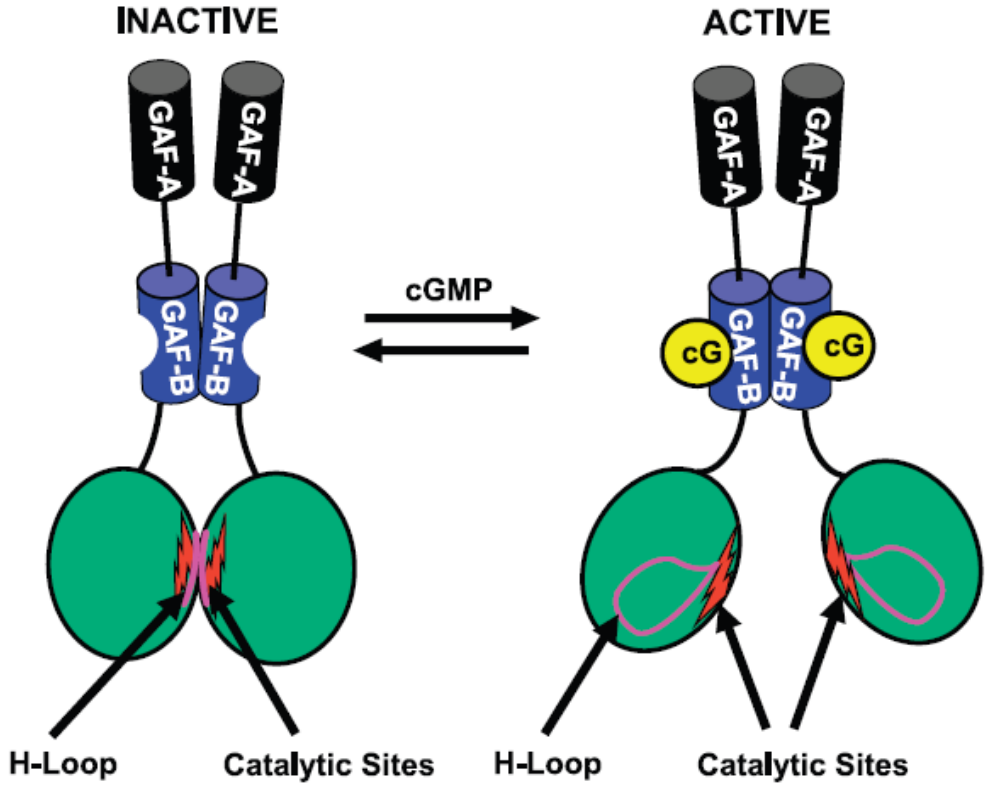

Figure 21: cGMP-induced activation of PDE2.
In the inactive state, the arrangement of the two C domains (green) in the dimer blocks substrate access to the catalytic sites. cGMP binding to GAF-B in each subunit results in a conformational change that leads to the disruption of the dimer interface in the C domain. Then substrate can reach easily the catalytic pocket (Francis *et al.*, 2011).

PDE2 is mainly expressed in brain, where it is mainly responsible for regulation of cGMP and cAMP levels (Juilfs *et al.*, 1997; Wykes *et al.*, 2002; Lin *et al.*, 2010) and is involved in regulation of memory and emotion formation processes (Boess *et al.*, 2004). PDE2 expressed in the heart is implicated in ECC and attenuation of β-adrenergic signaling in cardiac myocytes (Hartzell & Fischmeister, 1986; Vandecasteele *et al.*, 2001). PDE2 is also present in adrenal glands and controls aldosterone secretion (MacFarland *et al.*, 1991; Nikolaev *et al.*, 2005). PDE2 is less expressed in peripheral tissues, however it is involved in thrombin-dependent activation of platelets (Dickinson *et al.*, 1997) and proliferation of vascular endothelial cells and in angiogenesis (Favot *et al.*, 2003; Diebold *et al.*, 2009).

PDE2 is encoded by a single gene *pde2a* but exists in three isoforms: PDE2A1, PDE2A2, PDE2A3 that differ in their N-terminal regulatory domain and subcellular localization. PDE2A1 is localized in the cytoplasm, while PDE2A2 and PDE2A3 are associated with membrane structures (Sonnenburg *et al.*, 1991; Rosman *et al.*, 1997). In brain, immunostaining for PDE2A shows that PDE2 is mainly detected in limbic system such as

cortical areas, hippocampus, amygdale, olfactory bulb, the adrenal cortex and at lipid rafts in neurons (Omori & Kotera, 2007). In cardiomyocytes, PDE2 is confined to membrane compartment with the sarcomeric Z-lines (Lugnier *et al.*, 1999; Mongillo *et al.*, 2006; Omori & Kotera, 2007). In addition, it has been shown that PDE2A mRNA transcription and activity differ between right and left ventricle and are significantly lower in RV compared to LV (Soler *et al.*, 2015). In the liver, PDE2 is associated with Golgi-endosomal fractions (Geoffroy *et al.*, 1999). PDE2 is also localized in mitochondrial matrix in brain and liver tissue (Acin-Perez *et al.*, 2011).

VI.2 Regulation of expression and activity of PDE2

So far, the regulation of PDE2 gene expression is not well known. It has been shown that PDE2A expression is induced by macrophage colony, a stimulating factor in human monocytes differentiating into peritoneal macrophages (Bender *et al.*, 2004). It was also demonstrated that expression of PDE2A gene is regulated exclusively by tumor necrosis factor-α (TNF-α) in a p53 MAPK-dependent manner in human umbilical vein endothelial cells (HUVEC). TNF-α rapidly increases PDE2A activity resulting in a decrease in cyclic nucleotide accumulation (Seybold *et al.*, 2005). Vascular endothelial growth factor (VEGF) plays also an important role in regulation of PDE2A expression in HUVEC. Treatment of HUVEC with VEGF leads to significant increase in PDE2A expression by 47% (Favot *et al.*, 2003). Study on obese rats with a missense mutation in the leptin receptor gene shows a transcriptionally upregulated PDE2 level in brown adipose tissue of these animals. However, the relation between PDE2 upregulation and the leptin receptor mutation remains unknown (Coudray *et al.*, 1999).

PDE2 activity is regulated by cGMP at low concentrations via binding to the GAF-B domain. cGMP binding increases cAMP hydrolysis by 5 to 30 fold. A study on the x-ray crystallographic structure of dimerized PDE2 construct composed of GAF-A/B tandem and catalytic domain shows the mechanism of PDE2 activation. In the absence of cyclic nucleotides, catalytic domain occurs in a closed conformation in which the substrate binding pocket of catalytic domain is occluded by the H-loop. cGMP binding to the GAF-B domain causes movement and H-loop swings out of the substrate binding pocket to allow substrate access (Pandit *et al.*, 2009).

It has been shown that Ca^{2+}/phospholipid-dependent protein kinase (PKC) stimulates PDE2 activity in a liver Golgi-endosomal fraction. Treatment with 4β-phorbol 12-myristate 13 acetate, which is activator of PKC, stimulates PDE2 activity via serine/threonine

phosphorylation but it has not yet been established directly (Geoffroy *et al.*, 1999). Another study shows that nerve growth factor (NGF) inhibits PDE2 activity in PC12 cells resulting in over 50% loss of PDE2 activity. Moreover, NGF leads to an increase in PDE2 associated phosphoproteins at concentrations producing a loss of PDE2 activity (Bentley *et al.*, 2001).

So far, there is no direct evidence that PDE2 activity is regulated by post-translational modifications. However, some studies show an increase in PDE2 activity in a model of hypertrophy without any changes in PDE2 mRNA levels, suggesting a post-translational modifications or reduction in PDE2 protein degradation (Yanaka *et al.*, 2003; Mokni *et al.*, 2010).

There are known inhibitors of PDE2A activity which are useful tools for determining its cellular functions. IBMX, which is a non-specific, broad spectrum inhibitor of PDEs, inhibits PDE2 with a Ki in the range of 8-18 µM in the presence of cGMP (Erneux *et al.*, 1982). The first specific PDE2 inhibitor found is EHNA (erythro-9-(2-hydroxyl-3-nonyl) adenine) which has an IC_{50} of ~0.8 µM for human PDE2 and more than 100 µM for other PDEs (Méry *et al.*, 1995; Podzuweit *et al.*, 1995). Recently, a large number of highly specific and selective PDE2 inhibitors has been developed including oxinodol with IC_{50} of 40 nM (Chambers *et al.*, 2006), PDP (9-(6-Phenyl-2-oxohex-3-yl)-2-(3,4-dimethoxybenzyl)-purine-6-one with IC_{50} of 0.6 nM (Seybold *et al.*, 2005). An inhibitor that is commercially available is Bay 60-7550 (2-[(3,4-dimethoxyphenyl)methyl)]-7-[(1R)-1-hydroxyethyl]-4-phenylbutyl]-5-methyl-imidazol[5,1-f][1,2,4]triazin-4(1H)-one] with IC_{50} of 5 nM for recombinant human PDE2A (Boess *et al.*, 2004).

VI.3 PDE2 as potential target in heart failure

PDE2 is stimulated by cGMP to increase hydrolysis of cAMP and this plays an important role as a feedback mechanism restoring the basal level of the cyclic nucleotide upon hormonal stimulation (MacFarland *et al.*, 1991; Lugnier, 2006). PDE2 is expressed in both ventricular and atrial myocytes, from frog to human (Bender & Beavo, 2006). It was shown in frog ventricular myocytes (Dittrich *et al.*, 2001) and human atrial myocytes (Rivet-Bastide *et al.*, 1997) that PDE2 stimulated by cGMP depletes cAMP in the vicinity of LTCCs resulting in inhibition of $I_{Ca,L}$. Real time measurements of cyclic nucleotide concentrations in intact cardiomyocytes showed that PDE2 is involved in maintaining compartmentalized pools of cyclic nucleotides and shapes the cAMP response to catecholamines via the β_3-AR/NO/cGMP pathway to suppress myocyte inotropy (Mongillo *et al.*, 2006; Bender & Beavo, 2006). In adult rat ventricular myocytes, PDE2 also controls cGMP concentrations: it exclusively

controls pool of cGMP generated by pGC activation at the sarcolemmal membrane and participates in the control of the pool of cGMP generated by sGC, together with PDE5 (Castro *et al.*, 2006).

PDE2 seems to be important in cardiac pathologies, which are accompanied by severe neurohormonal dysregulation. Published studies showed that PDE2 is upregulated in a rat model of induced hypertrophy in response to pressure overload (Yanaka *et al.*, 2003; Mokni *et al.*, 2010). More recently, Mehel et al showed that PDE2 mRNA and protein level is upregulated in patients with end-stage dilated cardiomyopathy or ischemic cardiomyopathy (Mehel *et al.*, 2013). PDE2 abundance, activity and transcript levels were also upregulated in animal models of HF. Using the chronic isoprenaline infusion model (El-Armouche A, Gocht F, Jaeckel E, Wittkopper K, Peeck M, Eschenhagen T. Longterm beta-adrenergic stimulation leads to downregulation of protein phosphatase inhibitor-1 in the heart. European journal of heart failure 2007;9:1077-80), they showed that pathological β-AR overstimulation alone is sufficient to induce higher PDE2 abundance and activity to a similar extent as observed in human end-stage HF, clearly indicating that PDE2 upregulation is a consequence of pathological β-AR overstimulation.. The same authors showed that adenoviral overexpression of PDE2 dramatically blunted β-AR inotropic responses, cellular hypertrophy and arrhythmogenic events in isolated ventricular myocytes , yet without affecting basal contractility (Mehel *et al.*, 2013).

These studies suggest that PDE2 may play a protective role in myocardial remodeling during hypertrophy as well as in decompensated stages of HF. The observed increased expression and activity of PDE2 in the failing heart is likely to play a role in the desensitization machinery of the β-AR signaling pathway. They postulated that this constitutes a potentially important defense mechanism during cardiac stress, in particular, during excessive β-AR drive.

Objectives

cAMP is an essential second messenger in neurohormonal regulation of cardiac function. Heart failure is characterized by disruption of cAMP signaling pathway due to chronic activation of the adrenergic pathway, leading to β-adrenergic receptor desensitization. So far, heart failure caused by damage to the heart that has developed over time cannot be cured. It can only be treated to improve symptoms. Nowadays, the treatment that increases cAMP level such as milrinone improves short-term cardiac performance but increases mortality because of a Ca^{2+} overload that leads to arrhythmias and sudden death. Treatment with β-blockers reduces the action of catecholamines on cAMP level and reduces mortality, but is effective in only 40-50% of patients with HF and is unable to improve the ability to exercise resulting in a reduction in a quality of life.

PDE2 is the only PDE being activated by cGMP to increase cAMP hydrolysis and it was demonstrated that PDE2 is upregulated in HF suggesting its potential role in cardiac pathology. To explore the pathophysiological consequences of enhanced PDE2 activity and its potential therapeutic value in HF, we created for the first time a transgenic mouse with a heart specific overexpression of the PDE2A3 isoform in collaboration with Prof. Ali El-Armouche (Institute of Pharmacology, University of Technology, Dresden, Germany). The animal model was validated by checking the overexpression of the transcript by qRT-PCR, increased protein level by Western Blot and elevated PDE2 activity by the radioenzymatic assay. The hypothesis of my thesis is that the activation of PDE2 may be beneficial to cardiac function.

The first objective of my thesis was to evaluate the role of PDE2 overexpression on cardiac function *in vivo* and *ex vivo*. In collaboration with Prof. Ali El-Armouche, the effect of PDE2 overexpression on heart rate and cardiac function was studied using echocardiography and telemetry (subcutaneously implanted ECG transmitters) that allows to record parameters over 24 h. The exercise capacity of mouse was tested using graded treadmill exercise protocol. Then, we tested effect of PDE2 overexpression on cardiac function upon chronic isoproterenol administration (subcutaneously implanted osmotic minipumps) using echocardiography. Here, for the first time we showed that PDE2 transgenic (TG) mice have a lower heart rate and increased heart contractility than their WT littermates. To determine, whether higher contractility is due to lower heart rate, we performed experiments using Langendorff perfused heart technique. The hearts isolated from PDE2 TG and WT mice were

electrically paced at the same rate (450 beats per min) and contractility (developed pressure) was measured.

The second objective of my thesis was to determine the role of PDE2 overexpression on cellular level, *in vitro*. We evaluated the role of PDE2 overexpression on overall cAMP signaling and ECC using electrophysiology techniques. In isolated adult mouse cardiomyocytes, we measured intracellular cAMP concentration using a Förster resonance energy transfer (FRET)-based sensor. We also measured the sarcomere shortening and Ca^{2+} transient using a Ca^{2+} sensor (Fura-2-AM) and the IonOptix system. We quantified a number of spontaneous arrhythmic events and we evaluated SR Ca^{2+} leak and SR Ca^{2+} load with tetracaine and caffeine, respectively using IonOptix system. The L-type Ca^{2+} current was recorded with patch-clamp technique.

Materials and methods

I. Animal model

I.1 Transgenic mice with PDE2 overexpression

PDE2 TG mice were generated by using a plasmid containing the murine sequence of the splice variant PDE2A3 (NM_001008548.3). Expression was set under the control of the human α-myosin heavy chain promoter to ensure cardiac specificity (Subramaniam et al., 1991). Transgenesis was achieved by pronucleus injection of linearized plasmids into isolated zygotes of a FVB/N donor strain. Successful transformation of the offspring was assessed by PCR and PDE2 protein level was determined by immunoblot analysis. Resulting founder lines were crossed into a C57Bl/6 background. Handling and genotyping of mice were realized in the Animal core facility, University of Paris Sud, UMS-IPSIT.

All experiments were carried out according to the European Community guiding principles in the care and use of animals (2010/63/UE, 22 September 2010), the local Ethics Committee (CREEA Ile-de-France Sud) guidelines and the French decree n°2013-118, 1st February 2013 on the protection of animals used for scientific purposes (JORF n°0032, 7 February 2013 p2199, text n°24). Authorizations were obtained from Ministère Français de l'Agriculture, de l'Agroalimentaire et de la Forêt (agreement N° B 92-019-01).

I.2 Experimental model of hypertrophy

Cardiac hypertrophy was induced in mice by chronic administration of the β-AR agonist-isoproterenol (ISO). Implantation of ISO-minipumps was done in the platform ANIMEX in Châtenay-Malabry.

WT and PDE2 TG mice (10 weeks old, 25g) were divided into two groups. One group received ISO with a daily dose of 60 mg/kg, while the control group obtained physiological serum (NaCl 0.9%). Two groups were treated during 14 days. Treatments were administrated with mean flow of 0.76 µl per hour using osmotic minipumps Alzet® (Model 2001 Alza Corporation, Paolo Alto, USA). The minipumps offer constant administration of drugs. Mice were anaesthetized with isoflurane (3% induction and 2% maintenance delivered through a mask). Mouse was fixed on the operating table, skin was shaved and disinfection of the skin was done. Then, a 1 cm incision between the scapulae was done. Using blunt scissors, a subcutaneous pocket was prepared and was approximately 1 cm longer than the pump. The pump's outlet was introduced into the forward direction of the subcutaneous pocket to avoid

interactions between the administered drug and wound healing. The subcutaneous pocket was closed by two interrupted sutures.

All minipumps were weighed before implantation and after sacrifice at the end of the treatment protocol to be sure that minipumps were functional and the drug was successfully delivered.

Echocardiography was performed before, 2 and 4 weeks after minipumps implantation. 5 weeks after implantation, mice were sacrificed. Body, heart, lungs weight and tibia length were measured.

II. Exercise capacity test

To measure exercise capacity in WT and PDE2 TG mice, mice were subjected to forced treadmill activity. Before the start of experiment, all mice were acclimatized to the treadmill running exercise by 12 min activity in the treadmill apparatus. The training started 4 days before the day of experiment and mice ran 2 min at 10 m/min, then 4 min at 13 m/min, 2 min at 15 m/min, 2 min at 16.5 m/min and 2 min at 18 m/min at a 4% slope. Next, the mice had training 3 days before the day of experiment as follows: running 2 min at 13 m/min, 2 min at 16 m/min, 2 min at 18 m/min, 4 min at 20 m/min and 2 min at 22 m/min at a 4% slope. During training and experiments, pressurized air, triggered at the end of each running sequence was used to maintain the running motivation.

On the day of experiment, all mice were warmed up by running 6 min at 10 m/min. Then, to measure the maximal aerobic running performance, the mice were exercised until they were no longer able to maintain the increasing speed of treadmill. The speed was increased by 3.3 m/min every 1.5 min to reach the speed of 30 m/min at a 4% slope. Then, the treadmill speed was increased by 3.3 m/min every 1 min at a 4% slope.

At the end of experiment, maximal running distance was calculated for each mouse.

III. Langendorff perfused heart

III.1 Principle

The isolated mammalian heart preparation was described first time by Oscar Langendorff in 1898 (Langendorff, 1898). This technique allows the examination of cardiac contractile strength and heart rate including the role of temperature, oxygen and Ca^{2+} ions. A general principal of the method is to deliver physiological solutions or pharmacological agents into the heart through a cannula inserted in the ascending aorta. The backwards pressure closes the aortic valve, preventing the perfusion fluid to enter into the left ventricle. As a consequence, the total perfusate enters to coronary arteries (Skrzypiec-Spring *et al.*, 2007).

III.2 Experimental set-up

Isolated adult mouse heart was perfused at constant pressure (75 mmHg). The key component of the system is a compliance chamber, that keeps a constant pressure. The compliance chamber is warmed to 37°C and filled with a perfusate oxygenated via a glass tube gas disperser with a gas mixture of 95% O_2 - 5% CO_2. The perfusate level in the compliance chamber is maintained by controlling the emptying and filling column with a solution. The solution enters the compliance chamber using high-fidelity peristaltic pump (Figure 22). Once the heart is cannulated, the coronary flow can be measured by probe connected to the perfusion cannula (Transonic Systems, Ithaca, NY). The cannulated heart was placed in a water-jacketed bath and warmed to 37°C. Isovolumic pressure in the mouse heart was achieved by insertion of a small latex balloon in the left ventricle. The heart was electrically stimulated at 450 and 650 beats per min using stimulating platinum filament placed on the surface of the right ventricle. The experimental set-up of Langendorff perfused heart method is presented in Figure 22. All parameters were registered using acquisition system (software IOX, Emka Technologies).

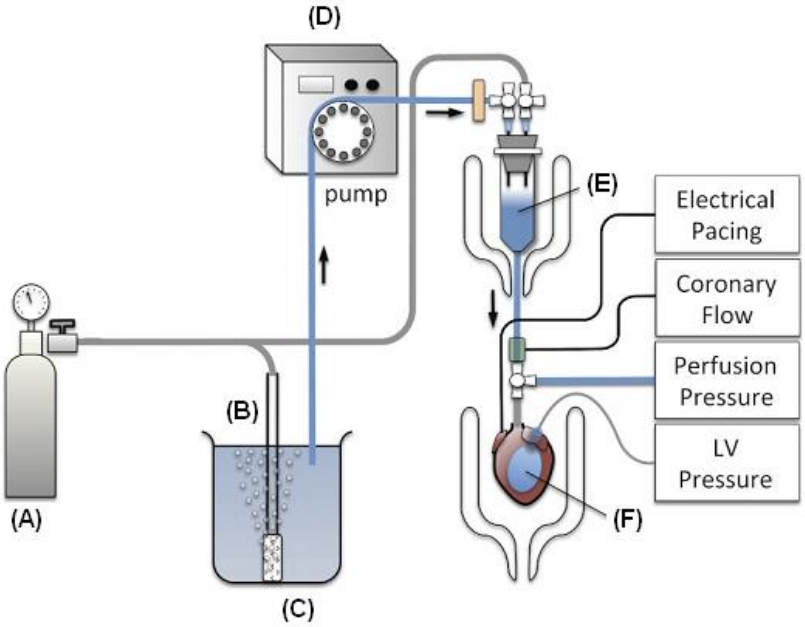

Figure 22: Experimental set-up of Langendorff perfused heart.
95%O_2–5%CO_2 tank (A), gas dispersion tube (B), perfusion solution (C), peristaltic pump (D), compliance chamber (E), balloon (F), (modified from (Liao *et al.*, 2012)).

III.3 Experimental protocol

Mice were anaesthetised with the intraperitoneal injection of pentobarbital (CEVA Santé Animale, 150 mg/kg). The heart was quickly removed after thoracotomy and placed into a solution for dissection containing (in mM): NaCl 116, D-glucose 15, $NaHCO_3$ 25, KCl 4.7, KH_2PO_4 1.2, $MgSO_4$ 1.2, $CaCl_2$ 0.4, at 4°C, oxygenated (95% O_2–5% CO_2). Solution for dissection and KREBS solution were prepared freshly before each experiment with ultra pure water and filtered through membrane with pores of 0.45 µm. Then, the aorta was cannulated as quickly as possible (to minimize time of ischemia) and perfused in retrograde manner by Langendorff method with Krebs solution containing (in mM): NaCl 116, D-glucose 11, $NaHCO_3$ 25, KCl 4.7, KH_2PO_4 1.2, $MgSO_4$ 1.2, $CaCl_2$ 1.2, Pyruvate 2, EDTA 0.1, warmed to 37.0±0.5°C.

The latex balloon filled with water and ethanol (90/10) connected to a pressure transducer (Statham gauge Ohmeda, Bilthoven, The Netherlands) was introduced into the left ventricle after crossing the mitral valve. The signal obtained by this device allows to measure force developed by left ventricle over time. The pressure inside the balloon was progressively increased using a micro syringe to find optimal conditions for cardiac muscle to contract more forcefully (Frank-Starling mechanism). 10 min after stabilization of cardiac parameters, the

heart was electrically stimulated using platinum electrode at 450 beats per min (bpm) placed on the surface of the right ventricle. When cardiac functions were recorded, electrical stimulation was stopped and after stabilization of cardiac parameters, the heart was perfused with ISO at increasing concentrations: 0.03, 0.1, 0.3, 1, 3, 10, 30 and 100 nM.

Different ISO solutions were diluted in KREBS and ISO was infused to the heart using an electric syringe pump (Harvard Apparatus pump 11) with flow representing 5% of aortic flow. Each of ISO solution was prepared at a concentration 20 times higher than the test solution to correct for the dilution factor. During perfusion of the heart with the last concentration of ISO (100 nM), when all parameters reached steady state, the heart was electrically stimulated at 650 bpm and then, the electrical stimulation was stopped to obtain the maximal pressure developed by left ventricle and the maximal heart rate.

IV. Isolation of adult mouse ventricular cardiomyocytes

Male mice 10 to 14-week-old were anesthetized by intraperitoneal injection of pentothal (150 mg/kg) and the heart was quickly removed and placed into a cold Ca^{2+} free Tyrode's solution containing (in mM): NaCl 113, KCl 4.7, $MgSO_4$ 4, KH_2PO_4 0.6, NaH_2PO_4 0.6, BDM 10, $NaHCO_3$ 1.6, HEPES 10, Taurine 30, D-glucose 20, adjusted to pH 7.4. The ascending aorta was cannulated and the heart was perfused with oxygenated Ca^{2+} free Tyrode's solution at 37°C during 4 min using retrograde Langendorff perfusion apparatus. Enzymatic dissociation was realized by perfusion with Ca^{2+} free Tyrode's solution containing liberase TM research grade (Roche Diagnostics) for 10 min at 37°C. Then, the heart was removed and placed into a dish containing Tyrode's solution supplemented with 0.2 mM $CaCl_2$ and 5 mg/ml BSA (Sigma-Aldrich). Then, the ventricles were separated from the atria, cut into small pieces, and triturated with a pipette to disperse the myocytes. The supernatant was removed and the cells were suspended in Tyrode's solution containing 0.5 mM $CaCl_2$ and 5 mg/ml BSA. The procedure was repeated once and the cells were suspended in Tyrode's solution supplemented with 1 mM $CaCl_2$ for IonOptix and patch clamp experiments or in medium I (Table 5) for FRET experiments. Freshly isolated ventricular myocytes were plated in 35 mm culture dishes coated with laminin (10 µg/ml) and stored at room temperature until use. All experiments were done in room temperature within 6 hours after cardiomyocytes isolation.

	Medium I	**Medium II**
Medium MEM (51200, Gibco)	Yes	Yes
BDM (2,3-butanedione	10 mM	10 mM

monoxime)		
BSA	1 mg/ml	-
L-Glutamine	2 mM	2mM
ITS (1X) **Insulin** **Transferrin** **Selenium**	 10 mg/L 5.5 mg/L 5 µg/L	 10 mg/L 5.5 mg/L 5 µg/L
Penicillin-Streptomycine	2%	2%
SVF	5%	-
pH at 21°C	7.6	7.6

Table 5: Composition of culture medium I and II used for adult mice ventricular cardiomyocytes.

V. Sarcomere shortening and Ca^{2+} transient measurements

V.1 Principle

Photometric system IonOptix (IonOptix, Milton, MA, USA) was used for combined measurement of fluorescence and contraction with a CCD camera (*cooled charge coupled*, IonOptix, Myocam CCD100M) and photomultiplier tubes. This system allows to measure simultaneously sarcomere length and changes in intracellular Ca^{2+} level.

V.2 Fluorescent Ca^{2+} indicator Fura-2-AM

Isolated mouse ventricular myocytes were loaded with Ca^{2+} indicator Fura-2-AM (Fura-2-acetoxymethyl ester,) at concentration of 3 µM during 15 min. Then, the cells were washed with physiological Ringer K^+ solution (Table 6). Fura-2-AM crosses the plasma membrane and intracellular esterases cleave the ester group to release Fura-2-free acid, that binds to free intracellular Ca^{2+}. Fura-2 is excited at 340 and 380 nm light and the emission ratio measured at 512 nm is directly related to the intracellular concentration of Ca^{2+}. Dissociation constant of Fura-2 for Ca^{2+} is 0.14 µM.

	Solutions (in mM)			
	Ringer K^+	Ringer $0Na^+/0Ca^{2+}$	Ringer $0Na^+/0Ca^{2+}$ + tetracaine	Ringer $0Na^+/0Ca^{2+}$ + caffeine
HEPES	10	10	10	10
NaCl	121.6	-	-	-
LiCl	-	121.6	121.6	121.6
Glucose	5	5	5	5
Na pyruvate	5	-	-	-
Li pyruvate	-	5	5	5
$NaHCO_3$	4.013	-	-	-
Li_2CO_3	-	4.013	4.013	4.013
Na_2HPO_4	0.8	-	-	-
LiH_2PO_4	-	0.8	0.8	0.8
KCl	5.4	5.4	5.4	5.4
$CaCl_2$	1.0	-	-	-
$MgCl_2$	1.8	1.8	1.8	1.8
pH at 21°C	7.4 (NaOH)	7.4 (LiOH)	7.4 (LiOH)	7.4 (LiOH)
Tetracaine	-	-	1	-
Caffeine	-	-	-	10

Table 6: Composition of Ringer solutions used for measurements of Ca^{2+} transient, cell shortening, SR Ca^{2+} leak and load.

Ringer K^+ solution was used to measure Ca^{2+} transient and cell shortening, the three other Ringer solutions were used to assess SR Ca^{2+} leak and load.

V.3 Experimental set-up

Observation of the sample was done using epifluorescence microscope (Nikon DIAPHOT 300). Cardiomyocytes showed clear striation observed with microscope (40x oil objective). Under the light microscope, sarcomere length corresponds to the distance from the middle of one light band to the middle of the next. Cardiomyocytes were electrically stimulated with biphasic field pulses (5V, 4 ms) at a frequency of 0.5 Hz. A CCD camera connected to the microscope allows to follow fast morphological changes of a single cell. The illumination system (Xenon lamp, Xenon Short Arc lamp, Ushio, Saint-Ouen-L'Aumone, France) is equipped with an dichroic mirror («*HyperSwitch*») that offers two excitation light sources at 340 and 380 nm. A dichroic mirror splits Fura-2 emission (<585 nm) to a photomultiplier and incidents red light (>585 nm) to the camera (Figure 23). Software Ion Wizard 6.0 was used to record experiments.

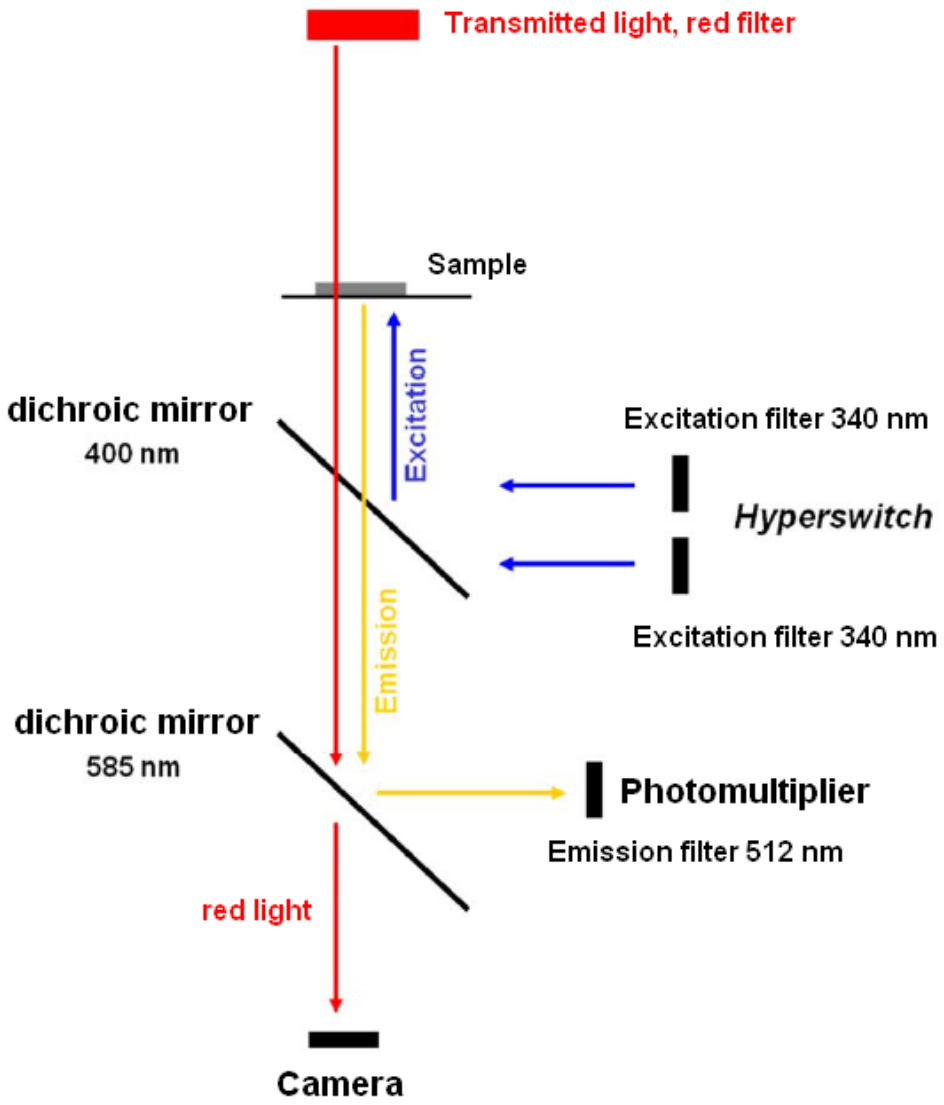

Figure 23: Experimental set-up to measure simultaneously sarcomere shortening and Ca^{2+} transient.

V.4 Experimental protocols

All experiments on adult mouse ventricular myocytes were done at controlled room temperature (22±2°C).

Isolated cardiomyocytes were washed with Ringer K^+ (Table 6) after loading with Fura-2-AM. Then, the cells were paced by field stimulation at 0.5 Hz in Ringer K^+ solution for few minutes until cellular Ca^{2+} transients reached a steady state. ISO at concentration of 3 nM, followed by concentration of 10 and 100 nM was applied through a system of external infusion. A perfusion system composed of 8 capillaries was placed in the proximity of the experimental set-up. Each capillary contained a different test solution and could be turned on

manually to allow solution to flow by gravity onto the cell. All solutions were prepared with Ringer K^+ supplemented with 1 mM Ca^{2+}. Presence of spontaneous Ca^{2+} waves was assessed during the application of successive concentrations of ISO.

The effect of PDE2 inhibition was tested with the selective PDE2 inhibitor, Bay 60-7550 added on the top of ISO at a concentration of 100 nM.

SR Ca^{2+} leak and load were measured according to a dedicated protocol (Shannon *et al.*, 2002). Fura-2 loaded cardiomyocytes were stimulated at 0.5 Hz in normal Ringer K^+ for few minutes. Then, Ringer K^+ was replaced for 30 s by a 0 Na^+/0 Ca^{2+} Ringer supplemented with 10 mM EGTA. This condition allows to measure intracellular Ca^{2+} levels in a closed system without trans-sarcolemmal Ca^{2+} fluxes. Then, after 30 seconds, the cell was perfused again with normal Ringer K^+ and paced at 0.5 Hz until Ca^{2+} transient amplitude and sarcomere shortening reached steady-state. Then, the electrically stimulation was stopped and the cell was perfused with a 0 Na^+/0 Ca^{2+} solution supplemented with the RyR2 blocker, tetracaine at a concentration of 10 mM. Tetracaine was then washed out for at least 1 min and caffeine at a concentration of 10 mM was applied to evaluate the total SR Ca^{2+} content.

V.5 Data processing

The Ion Wizard software allows to measure sarcomere shortening. The sarcomere length was measured from a user-defined region of interest (ROI). All the calculations were performed on a density trace derived from the ROI. Each pixel in the image represents a value that indicates its brightness (0 for black, and 255 for white). As a consequence of alternating dark and light A and I bands, the density trace has a sinusoidal appearance. Using periodic signal, the frequency can be evaluated, by a mathematical function called a *Fourier Transform*. In the frequency domain, the wavelength is represented by a peak, that shifts to a higher frequency, when the cell contracts. The mean sarcomere length in the ROI is determined every $1/240^{th}$ second (camera's speed). Increase in Ca^{2+} concentration in the cell results in an increase in fluorescence emitted by the Fura-2 at 512 nm in response to excitation at 340 nm (F_{340}) and in decrease of fluorescence emitted at the same wavelength in response to excitation at 380 nm (F_{380}). The ratio of emitted fluorescence intensities at 340 and 380 nm excitation is used to assess the intracellular changes in Ca^{2+} concentration.

V.6 Data analysis

Averages of 5 to 10 contractions and Ca^{2+} transients were determined using IonWizard software for each experimental condition. For each mean trace, the amplitude and kinetic parameters were measured with software (Figure 24). Ca^{2+} transient amplitude (ΔR) was

measured by the twitch amplitude (difference between the end-diastolic and the peak systolic ratios) divided by the end-diastolic ratio, corresponding to the percentage of variation in the Fura-2 ratio. Sarcomere shortening (ΔL) was assessed by its percentage of variation, which is obtained by dividing the twitch amplitude (difference between the systolic and the diastolic sarcomere length) by the end-diastolic sarcomere length. For both parameters, the kinetics of relaxation were assessed by measuring the time-to-50% relaxation from the time to peak.

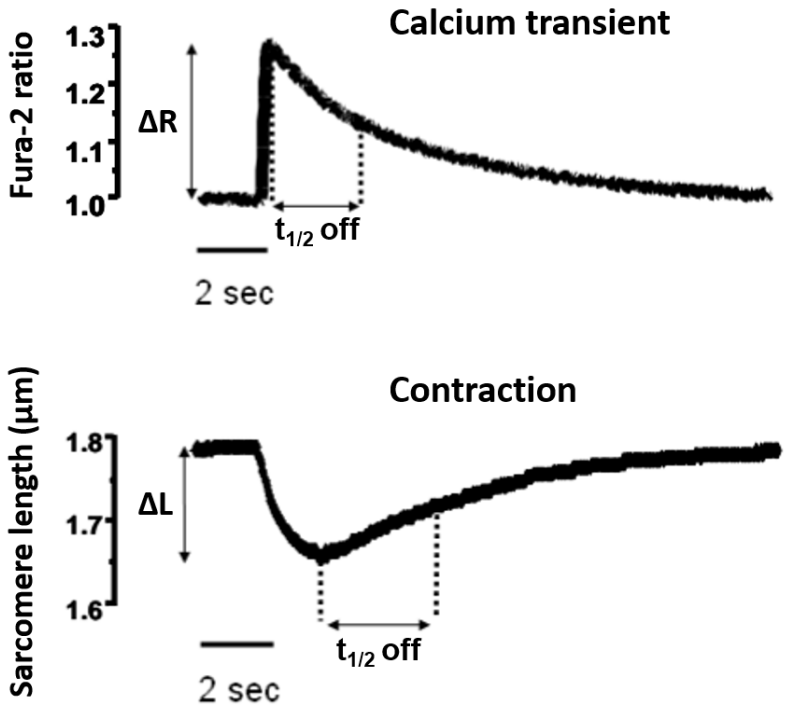

Figure 24: Determination of amplitude and kinetic parameters calculated for Ca^{2+} transients and sarcomere shortening.

VI. Fluorescence resonance energy transfer (FRET) imaging

VI.1 Principle

Fluorescence (or Förster) resonance energy transfer (FRET) was described first time by Förster in 1948. It is a process where energy is transferred nonradiativly from excited molecular fluorophore (donor) to another fluorophore (acceptor). The second concept of FRET is treating an excited fluorophore as an oscillating dipole that can undergo an energy exchange with a second dipole which has a similar resonance frequency. FRET depends on the distance between the two fluorophores. The distance depends on the spectral characteristics of the fluorophores, but generally the distance over which energy can be

transferred is in the range of 10-100 Å. FRET is used mainly to determine the structure, conformational changes and interactions between molecules, but also as in our case, to measure concentrations of small molecules or enzyme activity.

VI.2 Experimental set-up

The cells in Ringer K^+ (Table 6) are visualized using an inverted microscopy (Nikon TE) with a 40x oil objective and connected to a software (Metafluor, Molecular Devices, Sunnyvale, CA, USA) controlling camera CCD (*Cooled charge coupled*, Sensicam PE; PCO, Kelheim, Germany). A fluorescent cell is selected and the tip of the perfusion system is placed in the close proximity of the cell. CFP is excited during 300 msec with a Xenon lamp (100 W, Nikon, Champigny sur Marne, France) using a filter 440/20BP (*band pass*) and dichroic mirror 455LP (*long pass*). An image separator (Optosplit II emission splitter; Cairn Research, Faversham, UK) equipped with a dichroic mirror 495LP and 2 filters: BP 470/30 (for CFP) and 535/30 (for YFP) allow to separate CFP and YFP images. Image acquisition is done by the camera every 5 seconds.

VI.3 FRET sensor – H187

The H187 FRET sensor is a recombinant protein containing a cAMP binding domain from the protein Epac localised between two different fluorophores: mTurquoise2 (CFP) and 2 Venus (YFP) (Klarenbeek *et al.*, 2011, 2015).

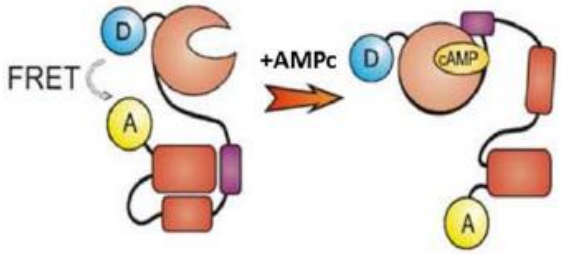

Figure 25: Functioning of the H187 cAMP-FRET sensor.
In conditions of low cAMP concentration, the donor (D) is in close proximity of the acceptor (A) and FRET is maximal. When cAMP rises, the second messenger binds to Epac, inducing a conformational change that disrupts FRET (Klarenbeek *et al.*, 2011).

The cAMP binding domain has a Q270E mutation, which leads to an increase in affinity for cAMP in comparison with other commonly used Epac2-camp probes. In addition, the turquoise-Venus-Venus combination provides a fluorescence emission with higher intensity than standard CFP/YFP combination. In the absence of cAMP, FRET occurs between two fluorophores. When cAMP concentration increases in the proximity of the probe, cAMP binding to the probe causes conformational changes of the probe, leading to decrease in FRET

that is proportional to the increase in cAMP (Figure 25). cAMP concentration is directly proportional to the equation CFP/[YFP-(0.6*CFP)].

VI.4 Adenoviral infection

The cells were infected with adenovirus suspended in medium II (Table 5). The number of active virus particles per cell is defined by MOI (multiplicity of infection). Adult mouse ventricular myocytes isolated from WT and PDE2 TG mice were infected with MOI 1000 (expression during 24 h). Ventricular myocytes were kept in culture medium in the absence of serum to minimize the effect of cellular dedifferentiation. After adenoviral infection, cells had still their typical appearance and clearly visible striations.

VI.5 Experimental protocol

After 24 h of infection with H187 adenovirus, the cells were washed once and kept in Ringer K^+ solution. ISO at concentration of 30 nM was applied briefly (15 second) in the absence or presence of PDE2 inhibitor.

VI.6 Data analysis

Mean fluorescence intensity was measured in a region of interest of defined cell. Background noise was subtracted from intensity of CFP and YFP. CFP/YFP ratio was calculated as % of increase over basal level. Image ratio was obtained using Image J 1.44a software (NIH, USA).

VII. L type Ca^{2+} current measurement – the patch clamp technique

VII.1 Principle

The patch clamp technique was described first time by Neher and Sakmann in 1976, who received the Nobel Prize of medicine and physiology in 1991. This technique allows to detect the current that passes through ion channels in different cell types. The tip of a fire-polished glass micropipette is pressed against a cell in order to electrically isolate a small patch of membrane. Applying suction to the interior of micropipette results in occurrence of a very high-resistance seal (“gigaohm seal”) between the pipette and the membrane. The first possible configuration of patch clamp is named “cell-attached” configuration. The second configuration called “inside-out” can be used to study the effects of cytoplasmic constituents on channel activity. The third configuration, used in my experiments, is known as “whole-cell”, it allows to measure channel current in the entire cell membrane. The last configuration

is “outside out”. The pipette in whole cell configuration can be withdrawn slowly from the cell, this stretches the membrane between the pipette and the cell until it finally breaks. Then the membrane seals at the tip of the pipette forming a membrane vesivle with its extracellular surface facing the bathing medium. This configuration allows to study effects on channels of agents that can act on the extracellular surface.

VII.2 Solutions

Three different solutions were used to record the L-type Ca^{2+} current $I_{Ca,L}$ with the whole-celle patch clamp technique (Table 7). The osmolarity of these solutions was between 300 and 310 mosm.

	Concentrations (in mM)		
	Intracellular solution	**0 Ca^{2+} extracellular solution**	**1.8 mM Ca^{2+} extracellular solution**
NaCl	-	140	140
KCl	130	4	4
HEPES	10	10	10
EGTA	0.05	-	-
Glucose	-	10	10
$MgCl_2$	4.013	1.1	1.1
$CaCl_2$	-	-	1.8
Na_2-phosphocreatine	5	-	-
Na_2-ATP	3.075	-	-
Na-GTP	0.416	-	-
pH at 21°C	7.3 (KOH)	7.4 (NaOH)	7.4 (NaOH)

Table 7: Compositions of the solutions used in whole-cell patch clamp experiments in adult mouse ventricular myocytes.

VII.3 Experimental setup

The patch-clamp setup is a combination of mechanical equipment: inverted microscope (Olympus, model IMT-2), micromanipulators (model P-30, Sutter Instruments, Novato, CA, USA) allowing the tip of patch clamp pipette to make a contact with the cell membrane, and electrical equipment: amplifier (model Axopatch 200B, Axon Instruments, USA), oscilloscope (Axon Instruments, USA), computer interface which allows to digitize and record the traces of the ionic currents flowing through ion channels in the cell membrane. Glass pipette were made of borosilicate glass (model 1-000-1000, external diameter 1.44 mm and internal diameter 1.05 mm, Drummond Scientific, Broomall, PA, USA). They were fire-poloshed before use and had typically a resistance of 1 to 2 MΩ when filled with intracellular

solution (Table 7). A metal electrode in contact with the intracellular solution conducts the electrical changes to a voltage clamp amplifier. All experiments were done at room temperature. Experimental data were recorded with P-clamp software (Clampex, version 10.2, Axon Instruments, USA). Then, the results were analyzed using Clampfit software (version 10.2, Axon Instruments, USA).

VII.4 Experimental protocol

The cells were placed in dishes with external solution without $CaCl_2$. All experiments were performed at room temperature (22±2°C). When the whole-cell configuration was obtained, external solution supplemented with 1.8 mM $CaCl_2$ was applied by the perfusion system and the membrane capacitance (C_m) was measured. To record $I_{Ca,L}$, the cell was depolarized every 8 seconds from -50 mV holding potential to 0 mV during 400 ms. At -50 mV sodium currents are inactivated and potassium currents were blocked by replacing potassium ions by cesium in the extracellular and intracellular solutions. ISO at a concentration of 30 nM was added briefly (15 second) in the presence or absence of PDE2 inhibitor Bay 60-7550. The maximal amplitude of $I_{Ca,L}$ was measured as the difference between peak inward current and the current at the end of the voltage pulse. Average data are presented as mean ± SEM.

VIII. Biochemical methods

VIII.1 Genotyping of WT and PDE2 TG mice

Genotyping is the process of determining differences in genotype of animals by examining the individual's DNA sequence using biological assays. In order to identify mice genetically modified (PDE2 TG), DNA analysis was done from tail biopsy. For tail isolation, a 3 mm segment of the distal part of the tail was obtained from WT and PDE2 TG mice and used for nucleic acid extraction. Tails were placed in eppendorf tubes with 400 µL of digestion buffer containing (in mM) NaOH 25 and EDTA 0.2. Samples were incubated during 80 min at 95°C to digest the tails. After incubation time, tubes with tails were placed on ice during 2 min to stop the digestion. Then, 550 µL of neutralization buffer containing (in mM) Tris-HCl 40 was added to each sample and the tubes were delicately inverted to avoid DNA damage. Samples were centrifuged for 3 min at 4000 rpm. The upper, water phase contains double-stranded DNA. The concentration of DNA was verified by measurement of absorbance at 260 nm.

From the DNA extracts, 2 µL of each samples was used for PCR amplifications. The PCR cocktail (50 µL) contained dNTP mixture at 0.2 mM, 1 µL of each of the primer sets, 0.25 units Taq DNA polymerase and 10x DreamTaq Green Buffer with $MgCl_2$ 20 mM

(Fermentas). The PCR conditions were: incubation at 94°C for 8 min followed by 35 cycles at 94°C for 45 sec, 59°C for 30 sec and 72°C for 30 sec. Cycling was followed by a final extension step at 72°C for 10 min. The PCR primers for PDE2 were: 5' AGTGCTGGGAGAAGAGGTCA (sense), 5' TCATCAGTCGAGCCACTGAC (anti-sense). Amplified products were analyzed on 1% agarose gel (25µl of PCR product/lane). PCR primers were used to amplify a 1000 bp fragment of PDE2.

VIII.2 Extraction of proteins from cardiac tissue

Cardiac tissue was transferred to a tube with ceramic balls and 400-600 µL of lysis buffer containing (in mM): NaCl 150, HEPES 20 (pH 7.4), EDTA 2, glycerol 10%, NP-40 (detergent) 0.5%, microcystin-LR 1µM and cocktail of inhibitors of protease (Roche, Basel, Switzerland) for radioenzymatic assay or with lysis buffer for Western Blot containing (in mM): HEPES 50 (pH 7.4), NaCl 400 mM, Triton X-100 1%, glycerol 10%, EGTA 1, sodium pyrophosphate 10, sodium fluoride 100 (inhibitor of protein phosphatase), sodium orthovanadate 1 (inhibitor of protein phosphatase) and cocktail of inhibitors of protease (Roche, Basel, Switzerland). Cardiac tissue was homogenized using a whipper Precellys 24 (Bertin, France). The heart extracts were transferred to eppendorf tubes and left on ice for 10 min and then, samples were centrifuged for 12 min at 12000 rpm at 4°C and the upper, water phase was directly used or kept in -80°C.

VIII.3 Protein assay

Concentration of proteins was measured by BCA (bicinchoninic acid) assay (Smith *et al.*, 1985). Under alkaline conditions, the peptide bonds reduce Cu^{2+} ions from the copper (II) sulphate to Cu^{+}. BCA has a property to bind Cu^{+} ions and form purple-colour complex, proportional to the amount of proteins present in solution that can be quantified by spectrophotometry at the wavelength of 562 nm.

VIII.4 Western Blot

The phosphorylation level of proteins involved in ECC and total protein level of different isoforms of PDEs were measured with Western Blot. This technique allows to detect specific proteins in a sample of tissue homogenate. Western Blot includes gel electrophoresis to separate denaturated proteins by the length of polypeptides, protein transfer from gel to membrane where they are stained with antibodies specific to the target proteins and, finally, detection step.

VIII.4.1 Polyacrylamide gel electrophoresis (SDS-PAGE)

Proteins are separated according to their molecular weight with denaturating polyacrylamide gel electrophoresis. The samples are diluted in Laemmli loading buffer containing bromophenol blue 0.1%, Tris 30 mM (pH 6.8), β-mercaptoethanol 2.5%, sodium dodecyl sulphate (SDS) 1%, glycerol 10% and incubated 5 min at 95ºC. Proteins are denaturated and charged negatively by SDS and β-mercaptoethanol. The samples are loaded on the electrophoresis gel consisting of a first concentration gel of 5% of acrylamide (5% acrylamide (acrylamide/bisacrylamide 30/0.8), Tris-HCl 0.125 mM (pH 6.8), SDS 0.1%, ammonium persulfate 0.1%, Temed 0.001%) and a second separation gel of 8% (MyBP-C, P-MyBP-C, PDE4A, PDE4B, PDE4D), 10% (PDE3A, PDE3B) of acrylamide (8-15% polyacrylamide, Tris-HCl 375 mM (pH 8,8), SDS 0.1%, ammonium persulfate 0.05%, Temed 0.001%). The samples are concentrated in the first gel under the action of an electrical field of 80 V for 30 min and then separated in the second gel under the action of an electrical field of 120 V during 60 min in a migration buffer (25 mM Tris, 200 mM glycine, 0.1% SDS). A molecular weight marker migrates at the same time with samples.

VIII.4.2 Protein transfer onto the membrane

At the end of electrophoresis, proteins within the gel are transferred onto the membrane made of polyvinylididene difluoride (PVDF, Hybond-P (Amersham Pharmacia Biotech, Orsay, France)) that acts as a support for immunostaining. First, the membrane is dehydrated with ethanol and equilibrated with a transfer buffer (40 mM Glycine, 25 mM Tris, 20% methanol). The positively charged membrane is in contact with the gel and retains the negatively charged proteins. The transfer occurs at 120 V for 1 hour 30 min at 4ºC. To verify the quality of the sample loading, the membrane is stained with Ponceau S Red (B6008, Sigma, Saint-Louis, MO, USA) dissolved in 3% of trichloroacetic acid.

VIII.4.3 Immunostaining and revelation

The membrane is blocked of non-specific binding with 5% milk dissolved in TBS-Tween buffer (Tris-HCl 50 mM (pH 7.4), NaCl 0.15 M, Tween 20 0.1%). Then, the membrane is incubated overnight at 4ºC with primary antibodies specifically directed against proteins of interest. After several washing of the membrane with TBS-Tween buffer, the membrane is incubated for 1 hour at room temperature with appropriate secondary antibodies coupled to horseradish peroxidise (HRP). The membrane is incubated in the dark for 5 min with the substrate for horseradish peroxydase (Kit ECL, Amersham Pharma biotechnologies). The reaction product produced luminescence in proportion to the amount of proteins.

Then, the membrane is dehybridized with Re-blot Plus solution (Millipore, Saint Quentin-en-Yvelines, France) to eliminate hooked antibodies. After a new step of membrane saturation, the membrane is incubated with new primary antibodies directed against calsequestrin (CSQ) or Glyceraldehyde 3-phosphate dehydrogenase (GAPDH), which are reference proteins. The next steps are the same as described before: incubation with the primary antibodies and revelation.

VIII.4.4 Analysis and quantification

The intensity of the various bands is quantified using Image J 1.44a (NIH). The ratio of the intensity of protein of interest/CSQ or GAPDH is calculated for samples from WT and PDE2 TG mice. At least three heart samples of each group were used for Western Blot and results are presented as mean ± SEM.

VIII.4.5 Antibodies

Primary antibodies directed against proteins involved in ECC and different isoforms of PDEs are listed below:

- Anti-myosin binding protein C (MyBP-C): polyclonal antibodies produced in a goat, diluted 1/2000 in a blocking solution (Santa Cruz Biotechnology, Santa Cruz, CA, USA).
- Anti-phospho-myosin binding protein C (P-MyBP-C): polyclonal antibodies produced in a rabbit, directed against phosphorylated serine 282 of MyBP-C, diluted 1/2000 in a blocking solution (Alexis Biochemicals, San Diego, CA, USA).
- Anti-phosphodiesterase type 2 (PDE2): polyclonal antibodies produced in a goat, diluted 1/500 in a blocking solution (Santa Cruz Biotechnology, Santa Cruz, CA, USA).
- Anti-phosphodiesterase type 3A (PDE3A): polyclonal antibodies produced in a rabbit, diluted 1/10000 in a blocking solution, generously provided by Dr Chen Yan (University of Rochester Medical Center, Rochester, New York, USA).
- Anti-phosphodiesterase type 3B (PDE3B): polyclonal antibodies produced in a rabbit, diluted 1/1000 in a blocking solution, generously provided by Dr Alessandra Ghigo (University of Torino, Torino, Italy) (Perino *et al.*, 2011).
- Anti-phosphodiesterase type 4A (PDE4A): polyclonal antibodies produced in a rabbit, diluted 1/5000 in a blocking solution, generously provided by Prof. Marco Conti (University of California San Francisco, San Francisco, USA).

- Anti-phosphodiesterase type 4B (PDE4B): polyclonal antibodies produced in a rabbit, diluted 1/1000 in a blocking solution, generously provided by Prof. Marco Conti (University of California San Francisco, San Francisco, USA).
- Anti-phosphodiesterase type 4D (PDE4D): polyclonal antibodies produced in a mouse, diluted 1/10000 in a blocking solution, generously provided by Prof. Marco Conti (University of California San Francisco, San Francisco, USA).
- Anti-calsequestrin (CSQ): polyclonal antibodies produced in a rabbit, diluted 1/2500 in a blocking solution (Affinity Bioreagents, Golden, CO, USA).
- Anti- glyceraldehyde 3-phosphate dehydrogenase (GAPDH): polyclonal antibodies produced in a rabbit, diluted 1/1000 in a blocking solution (Cell signaling, Danvers, MA, USA).
- Secondary antibody anti-rabbit coupled with HRP: diluted 1/10000 in TBS-Tween buffer (Santa Cruz Biotechnology, Santa Cruz, CA, USA).
- Secondary antibody anti-goat coupled with HRP: diluted 1/10000 in TBS-Tween buffer (Santa Cruz Biotechnology, Santa Cruz, CA, USA).
- Secondary antibody anti-mouse coupled with HRP: diluted 1/10000 in TBS-Tween buffer (Santa Cruz Biotechnology, Santa Cruz, CA, USA).

VIII.5 cAMP and cGMP measurements by radioenzymatic assay

The hydrolytic cAMP or cGMP PDE2 hydrolytic activity was measured with radioenzymatic assay described by Thompson and Appleman (Thompson & Appleman, 1971). The method is based on the hydrolysis of H^3-labelled 3'5'cAMP or 3'5'cGMP by PDEs present in heart extract and then, conversion of nucleotides to nucleosides by 5'-nucleotidase from snake venom. After that, samples are passed over an anion exchange columns to separate reaction products of unhydrolyzed substrate. Then radioactivity is measured and is proportional to PDE activity.

cAMP or cGMP-hydrolytic activity was measured in heart extracts. Heart extract is incubated in a reaction buffer containing (in mM): Tris-HCl 10 (pH 8) 10 mM, $MgCl_2$ 10 mM, β-mercaptoethanol 5, cAMP 1 µM (or cGMP 5 µM), and 10^5 cpm [^{3}H]-cAMP or [^{3}H]-cGMP, for 25 min at 33°C. Then, the reaction is stopped with a solution, containing (in mM) Tris-HCl 200 (pH 8.6), EDTA 100 (pH 8), followed by an incubation of samples in a boiling water bath for 1 min. The reaction product (5'-AMP or 5'-GMP) is incubated with snake venom (*crotalus atrox*) for 20 min at 33°C. The adenosine or guanosine was separated on anion exchange columns using 2 ml of resine AG1-X8 (Biorad, Hercules, CA, USA) and

recuperated in vials containing scintillation liquid. The measurement of labelled adenosine or guanosine was done with a β-counter.

Two series of tubes without heart extract were prepared: one for calculating "total radioactivity" (the radioactivity was measured directly on the reaction product without separating samples on anion exchange columns) and the second to determine the "blanc" (radioactivity was measured after separation on anion exchange columns).

The amount of proteins used in the assay was determined by the percentage of nucleotide hydrolysis (it should be between 7 and 20%), in the absence of inhibitor, according to the equation:

% hydrolysis = [(X-blank)/(total radioactivity-blank)x100],

where X = radioactivity of control sample.

To evaluate activity due to PDE2, the experiment is carried out in the absence or presence of selective PDE2 inhibitor, Bay 60-7550 (100 nM). The difference between the total activity and the residual hydrolytic activity observed in the presence of Bay 60-7550 corresponds to the PDE2-cAMP or cGMP-hydrolytic activity (Figure 26).

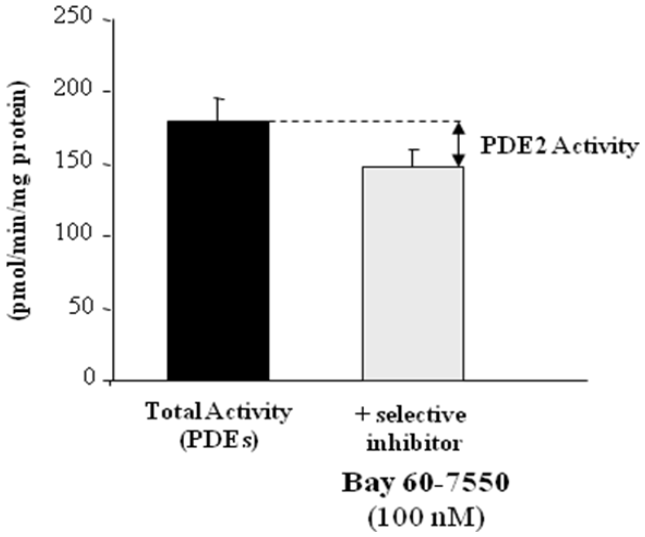

Figure 26: Determination of PDE2-cAMP-cGMP hydrolytic activity.
Activity of PDE2 was calculated as difference between total activity and the activity in the presence of PDE2 inhibitor Bay 60-7550.

VIII.6 Measurement of genes expression by quantitative RT-PCR

This technique based on polymerase chain reaction allows to quantify the level of gene expression of the considered genes using a complementary DNA (cDNA). In our study, we measured gene expression of two hypertrophy markers, ANP and BNP.

VIII.6.1 Extraction of RNA

Measurement of the level of gene expression in WT and PDE2 TG mice required an extraction of total RNA from ventricular tissue removed during sacrifice. About 30 mg of tissue is homogenised in 1 mL of Trizol solution (Gibco BRL, USA) at 4°C using a whipper Precellys 24 (Bertin, France). This solution containing phenol and guanidine isothiocyanate is used for lysis of cell membrane, conserving nucleic acid intact. The heart homogenate is treated with 200 µL of chloroform and then centrifuged for 15 min at 4°C at 10,000 G to separate RNA that is in water phase from proteins present in organic phase. Water phase is treated with isopropyl alcohol overnight at -20°C to precipitate RNA, then centrifuged for 15 min at 4°C at 12,000 G to obtain a RNA pellet. Then, supernatant is removed and pellet is washed with ethanol 75%, dried and dissolved in 20 µL of pure water (DNAse and RNAse free) and stored in -80°C.

The total RNA concentration is determined by measurement of absorbance at 260 nm with a NanoDrop 2000c apparatus (Thermo Fisher Scientific). It was established that 1 unit of absorbance at 260 nm is equivalent to 40 µg/ml of RNA. An additional measurement of absorbance at 280 nm was used to determine the purity of RNA content. The $Absorbance_{260}/Absorbance_{280}$ is a good indicator of the purity of the samples, since all values lower than 1.5 and greater than 2 indicates contamination with proteins or nucleic acids.

VIII.6.2 Inverse transcription

Quantitative PCR technique requires a preliminary step, inverse transcription, resulting in the production of cDNA from RNA. This step was done using a modified reverse trancriptase from Moloney Murine Leukemia Virus (MMLV). Initiation of reaction requires also primers type “random” that hybridize randomly with mRNAs present in the reaction buffer. In addition, the presence of RNAse inhibitor in the buffer limits degradation of RNA.

The reverse transcription reaction was performed in a volume of 25 µL per well containing 5 µL reaction buffer, 1.25 µL of enzyme and 18.75 µL of H_2O. The reaction MIX was prepared for all the wells. After 5 min of incubation at 25°C, the reaction was carried out by incubation for 30 min at 42°C (optimal temperature for enzyme, reverse transcriptase). Finally, the enzyme was deactivated by incubation for 5 min at 85°C.

The reaction was done on 96-well plates using a thermo cycler CFX 96 (Biorad) that allows to define a program with different desired temperature ranges.

VIII.6.3 Quantitative PCR using technology « SYBR Green »

The quantitative PCR technology is based on the same rules as conventional PCR but gives an advantage to monitor real-time amplification of a target gene. The quantification depends on fluorescent intercalator, in this case « SYBR Green » that is incorporated between the bases of double-strained DNA. This incorporation translates results in fluorescence emission. Thus, for each new formed molecule of DNA, the signal of fluorescence increases. The level of fluorescence is directly proportional to the number of new formed DNA molecules and refers to the level of mRNA expression. The specific amplifications depend on primers. The primers used in this method were designed with software Primer 3 and verified with software BLAST. The "sense" and "anti-sense" primers were chosen in two different exons to detect contamination with genomic DNA.

PCR reaction was performed on 96-well plates, total volume of reaction was 15 µL composed of 12.5 ng cDNA, 0.5 µM of each primer and SYBR-Green master mix containing dNTPs (mixture of four deoxyribonucleotides), SYBR-Green buffer and Taq-polymerase using a CFX-96 real-time PCR machine (BioRad). First step was enzyme activation (30 sec at 95°C), followed by 50 cycles. Each cycle included first step-denaturation (30 sec at 95°C) and second step-hybridization-elongation (20 sec at 60-62°C depending on genes). Negative controls were done without cDNA to check the exogenous contamination. At the end of protocol, the melting curve of formed product was performed to verify the specificity of PCR reaction.

VIII.6.4 Analysis

Quantification of gene expression level was done by calculating the "threshold cycle" (Ct) corresponding to the number of cycles required for detecting the SYBR-Green fluorescence. C_t is inversely proportional to the logarithm of the cDNA concentration presents in the sample. For each sample, RNA concentration was determined according to its C_t and a linear standard curve (6 points from 50 ng to 1.5625 ng of each samples for each gene).

In order to overcome errors between different samples, these values were normalized to the expression of stable reference genes. Results are presented as mean±SEM.

IX. Statistics

Results are presented as mean±SEM. Data sets were compared by Student's t-test, one-way ANOVA followed by Newman Keuls multiple comparison, or Fisher's exact test according to the experimental setting. P values of less than 0.05 were considered statistically significant.

Results

Cyclic AMP and cGMP are critical second messengers involved in the regulation of cardiac function. Intracellular level of cAMP and cGMP is controlled by opposite actions of different families of enzymes: ACs and GCs responsible for production of cAMP and cGMP and PDEs that degrade these second messengers.

Among the PDE superfamily expressed in the heart, PDE2 is a dual substrate enzyme, hydrolysing both cAMP and cGMP and has the unique property to be activated by cGMP to stimulate cAMP hydrolysis (Beavo *et al.*, 1971; Martinez *et al.*, 2002*b*). Thus, PDE2 is involved in cAMP/cGMP crosstalk. It has been demonstrated that myocardial PDE2 is upregulated in human and experimental HF and this upregulation is a direct consequence of chronic β-AR overstimulation and β-AR desensitization (Mehel *et al.*, 2013). However, the pathophysiological consequences of elevated PDE2 activity on cardiac functions remain unclear.

In our study, in collaboration with Prof. Ali El-Armouche, we offer for the first time characterization of a cardiac PDE2 TG mouse line to determine short and long term effects of PDE2 upregulation in the heart.

First aim of our studies was to evaluate the consequences of pharmacological PDE2 inhibition and to test the effect of PDE2 overexpression on heart rate and cardiac functions *in vivo*. Then, we studied the effect of PDE2 overexpression under acute β-AR stress, *in vivo,* and animals were monitored for arrhythmic events such as ventricular extra systoles (VES), salvos and ventricular tachycardia (VT). The last aim of our studies was to determine how PDE2 overexpression affects intracellular cAMP levels, Ca^{2+} cycling and Ca^{2+} handling proteins. Then we studied the cellular mechanisms involved in antiarrhythmic action of PDE2 in the ventricular myocardium.

The results of our work are presented in the article:

I. Article: Cyclic nucleotide phosphodiesterase 2 protects against catecholamine-induced arrhythmias and preserves contractile function after myocardial infarction

This article is in revision in *Circulation Research*.

Cyclic Nucleotide Phosphodiesterase 2 Protects against Catecholamine-induced Arrhythmias and Preserves Contractile Function after Myocardial Infarction

Running title: *Vettel et al., PDE2 in arrhythmia and contractile function*

Christiane Vettel, PhD*; Marta Lindner*; Matthias Dewenter, MD*; Kristina Lorenz, PhD; Constanze Schanbacher; Merle Riedel, MD; Simon Lämmle, PhD; Simone Meinecke, MD; Fleur Mason, PhD; Samuel Sossalla, MD; Andreas Geerts; Michael Hoffmann; Frank Wunder, PhD; Fabian J. Brunner, MD; Thomas Wieland, PhD; Hind Mehel, PhD; Sarah Karam, PhD; Patrick Lechêne, BSc; Jérôme Leroy, PhD; Grégoire Vandecasteele, PhD; Michael Wagner, MD; Rodolphe Fischmeister, PhD[†,#]; Ali El-Armouche, MD[†,#]

From the Institute of Experimental and Clinical Pharmacology and Toxicology, University Medical Center Mannheim, Heidelberg University, Germany (C.V., T.W.); Department of Pharmacology, University Medical Center Göttingen (UMG) Heart Center, Georg August University Medical School Göttingen, Germany (C.V., M.D., M.R., S.M.); UMR-S 1180, INSERM, Université Paris-Sud, Université Paris-Saclay, Châtenay-Malabry, France (M.L., H.M., S.K., P.L., J.L., G.V., R.F.); Department of Molecular Cardiology and Epigenetics, University Hospital Heidelberg, Germany (M.D.); Institute of Pharmacology and Toxicology, University of Würzburg and Leibniz-Institut für Analytische Wissenschaften – ISAS – e.V., Dortmund, Germany (K.L., C.S.), Comprehensive Heart Failure Center, University of Würzburg, and West German Heart and Vascular Center Essen, Germany (K.L.); Institute of Pharmacology, University of Technology Dresden, Germany (S.L., M. W., A.EA.); Department of Cardiology and Pneumology, Center of Molecular Cardiology, UMG Heart Center, Georg August University Medical School Göttingen, Germany (F.M., S.S.); Department of Internal Medicine III: Cardiology and Angiology, University of Kiel, Germany (S.S.); BAYER Pharma AG, Wuppertal, Germany (A.G., M.H., F.W.); University Heart Center, Department of General and Interventional Cardiology, University Medical Center Hamburg-Eppendorf (F.J.B.). DZHK (German Centre for Cardiovascular Research), partner sites Heidelberg/Mannheim, Göttingen and Hamburg/Kiel/Lübeck, Germany (C.V., M.D., M.R., S.M., F.M., S.S., F.J.B., T.W.)

*[†]These authors contributed equally

[#]**Correspondence to**: Ali El-Armouche, Institute of Pharmacology, University of Technology Dresden, Medical Faculty Carl Gustav August, Fetscherstr. 74, 01307 Dresden, Germany. Phone: +49 351 458 6300, Fax: +49 351 458 6315; e-mail: ali.el-armouche@tu-dresden.de OR Rodolphe Fischmeister, INSERM UMR-S 1180, Université Paris-Sud, Faculté de Pharmacie, 5, Rue J.-B. Clément, F-92296 Châtenay-Malabry Cedex, France. Phone: 33.1.46.83.57.57; Fax 33.1.46.83.54.75; e-mail: rodolphe.fischmeister@inserm.fr

Word Count: 7675

Journal subject codes: Remodeling, Animal models of human disease, Arrhythmias-basic studies

Abstract

Rationale: Phosphodiesterase 2 (PDE2) is a dual substrate esterase, which has the unique property to be stimulated by cGMP, but primarily hydrolyses cAMP. Myocardial PDE2 is upregulated in human heart failure (HF), but its role in the heart is unknown.

Objective: To explore the role of PDE2 in cardiac function and heart disease.

Methods and Results: Pharmacological inhibition of PDE2 (BAY 60-7550, BAY) led to a significant positive chronotropic effect on top of maximal β-adrenoceptor (β-AR) activation in healthy mice. Under pathological conditions induced by chronic catecholamine infusions, BAY reversed both the attenuated β-AR mediated inotropy and chronotropy. Conversely, ECG telemetry in heart specific PDE2 transgenic mice (TG) showed a marked reduction in resting as well as in maximal heart rate, while cardiac output was completely preserved due to greater cardiac contraction. This well tolerated phenotype persisted in elderly TG with no indications of cardiac pathology or premature death. Molecular studies on the cardiomyocyte level showed lower β-AR stimulation of contractility, Ca^{2+} transients and L-Type Ca^{2+} current. During arrhythmia provocation induced by catecholamine injections, TG animals were resistant to triggered ventricular arrhythmias. Accordingly, Ca^{2+}-spark analysis in isolated TG cardiomyocytes revealed remarkably reduced Ca^{2+}-leakage and lower basal phosphorylation levels of Ca^{2+}-cycling proteins including ryanodine receptor type 2. Moreover, TG demonstrated attenuated ventricular dysfunction and a strong trend toward prolonged survival after myocardial infarction.

Conclusion: Endogenous PDE2 contributes to heart rate regulation. Greater PDE2 abundance protects against arrhythmias and improves contraction force after severe cardiac insult. Activating myocardial PDE2 may thus represent a novel intracellular anti-adrenergic therapeutic strategy protecting the heart from arrhythmia and contractile dysfunction.

Key words: cyclic nucleotide phosphodiesterase, β-adrenoceptors, heart rate, arrhythmia

Nonstandard Abbreviations and Acronyms

AR	adrenoceptor
BAY	PDE2-inhibitor BAY 60-7550
BPs	systolic blood pressure
BPd	diastolic blood pressure
bpm	beats per minute
BW	body weight
cAMP	cyclic adenosine monophosphate
cGMP	cyclic guanosine monophosphate
CO	cardiac output
CSQ	calsequestrin
DOBU	dobutamine
FAS	fractional area shortening
HF	heart failure
HR	heart rate
$I_{Ca,L}$	L-type Ca^{2+} channel current
ISO	isoproterenol
IVA	ivabradine
LAD	left anterior descending coronary artery
LTCC	L-type Ca^{2+} channel
LVW	left ventricular weight
METO	metoprolol
MI	myocardial infarction
NCX	sodium-calcium exchanger
NO	nitric oxide
NP	natriuretic peptide
PDE	cyclic nucleotide phosphodiesterase
PLB	phospholamban
RYR2	ryanodine receptor type 2
SCaW	spontaneous Ca^{2+} waves
SR	sarcoplasmic reticulum
TG	PDE2-transgenic
VT	ventricular tachycardia
WT	wildtype

Heart failure (HF) is among the most common causes of morbidity and mortality worldwide. A characteristic feature of this pathophysiological condition is a chronic activation of the sympathetic nervous system[1]. Although initially aimed to maintain cardiac output, constant stimulation of β-adrenoceptors (β-ARs) results in molecular and structural changes, such as hypertrophy, cardiac fibrosis, and electromechanical dysfunction. This process creates a setting for lethal cardiac arrhythmias, which may account for approximate 40% of deaths in patients with HF[2, 3]. Moreover, increased resting heart rate and lower heart rate variability are significant prognostic risk factors for mortality and cardiovascular outcome[4, 5]. The sympathetically stressed heart responds with desensitization mechanisms which involve the reduction of functional β_1-AR and the redistribution β_2-AR at the plasma membrane[6, 7], but also a modulation in abundance and/or activity of intracellular key effectors, downstream of receptor activation[8, 9]. Even though β-AR desensitization may further compromise contractile performance, it nevertheless appears to be a protective adaptation against catecholamine toxicity[10]. Accordingly, pharmacological blockade of receptor activation by β-blockers to date is a central strategy in attenuating HF progression[11]. In this context, the extent of heart rate reduction by β-blockers appears to be of particular importance for the clinical outcome in HF[12]. However, not all patients receive or tolerate the necessary dose to substantially improve prognosis[13].

In contrast to β-AR signaling, which is mainly mediated by the second messenger cyclic adenosine monophosphate (cAMP), the actions of cyclic guanosine monophosphate (cGMP) generated by either natriuretic peptides (NP) or nitric oxide (NO) are considered to be beneficial in HF partially because they may oppose cAMP-induced stress remodeling[14-17]. Both cAMP and cGMP are regulated in level and subcellular distribution by cyclic nucleotide hydrolyzing phosphodiesterases (PDEs). Their degradation is a highly compartmentalized process, allowing the distinction of different extracellular stimuli to maintain the specificity of downstream target activation[18]. Among the PDE families expressed in the heart, PDE2 has the unique property to be activated by cGMP via binding of the nucleotide to a regulatory GAF-B domain located at its N-terminus[19, 20]. The conformational change induced by this allosteric mechanism increases cAMP hydrolysis 10- to 30-fold thus staging PDE2 in the center of a negative cGMP/cAMP crosstalk[21]. Evidence for such a crosstalk regarding the cardiovascular system includes the cGMP-mediated decrease in ventricular and atrial L-type Ca^{2+} channel current ($I_{Ca,L}$) in various species including man[22, 23], β_3-AR-dependent regulation of protein kinase A in cardiomyocytes[24], and the ANP-mediated reduction in aldosterone production in adrenal glomerulosa cells[25]. Unlike the described downregulation of cAMP-degrading PDE3 and some isoforms of PDE4[26, 27], myocardial PDE2 is upregulated in human HF. We showed that the upregulation of ventricular PDE2 is a direct consequence of chronic β-AR overstimulation and part of the β-AR desensitization machinery[28]. However, the consequences of higher abundance and activity of PDE2 on cardiac function are largely unknown.

In the present study, we show that in healthy hearts, PDE2 tonically reduces heart rate, but controls both β-AR chronotropic and inotropic responsiveness under stressed conditions *in vivo*. Moreover, we generated a cardiac PDE2-transgenic (TG) mouse line to evaluate short and long term effects of chronically increased PDE2 activity in the heart. Our study reveals that greater PDE2 abundance lowers heart rate without impairment of cardiac contractility *in vivo* and protects against ventricular arrhythmias by preventing Ca^{2+}-leakage from the sarcoplasmic reticulum (SR). In experimental myocardial infarction, higher PDE2 abundance improved ventricular function and may even prolong survival.

Methods

For a detailed description of methods including surgical procedures see Online Supplement Material.

Chronic isoproterenol administration: Isoproterenol (ISO, 30 µg/g/d, Sigma-Aldrich) was delivered to mice by subcutaneously implanted osmotic minipumps (Alzet, model 2002).

Application of dobutamine, BAY 60-7550 and metoprolol for echocardiographic experiments: Anesthetized mice were analyzed by echocardiography first under basal conditions and then 5 min after the injection of dobutamine (DOBU, i.p., 10 mg/kg). When indicated, BAY (i.p., 3 mg/kg) was applied 10 min post DOBU injection, and after an additional period of 10 min cardiac function was again echocardiographically monitored. For metoprolol studies, doses from 1 to 100 mg/kg (i.p.) were cumulatively applied with 10 min intervals between injections and echocardiographic measurements.

Generation of PDE2 transgenic mice: PDE2-TG mice were generated by using a plasmid containing the murine sequence of the splice variant PDE2A3 (NM_001008548.3). Expression was set under the control of the human α-myosin heavy chain promoter to ensure cardiac specificity[29]. Transgenesis was achieved by pronucleus injection of linearized plasmids into isolated zygotes of a FVB/N donor strain. Successful transformation of the offspring was assessed by PCR and overexpression levels were determined by immunoblot analysis. Resulting founder lines were crossed into a C57Bl/6 background.

ECG-telemetry recordings and arrhythmia provocation: ECGs were recorded in freely moving unrestrained mice. Arrhythmia provocation was performed by double injections of isoproterenol (ISO, i.p. 2 mg/kg) separated by an interval of 30 min; analysis was performed for 90 min after the first injection.

Isolation of adult mouse ventricular myocytes: Adult mouse ventricular myocytes were isolated by Langendorff perfusion using a Ca^{2+}-free Tyrode's solution containing liberase as described previously[30].

cAMP measurements by FRET: Adult mouse ventricular myocytes mice were infected with an adenovirus encoding the Epac-S^{H187} cAMP FRET probe for 24 h[31]. Changes in cAMP levels were assessed by YFP/CFP emission ratios.

Patch-Clamp studies: L-type Ca^{2+} currents ($I_{Ca,L}$) were recorded in the whole-cell configuration of the patch-clamp technique[32].

Ca^{2+} spark analysis: Ca^{2+} spark measurements were performed on a laser scanning confocal microscope (LSM 5 Pascal, Zeiss). Fluorescence images of Fluo-3 AM (10 µmol/L, Molecular Probes) loaded ventricular myocytes were recorded in the line-scan mode.

Measurement of Ca^{2+} transients, sarcomere shortening, SR Ca^{2+} leak and load: Isolated mouse ventricular cardiomyocytes were loaded with 3 µmol/L Fura-2 AM (Invitrogen). Sarcomere shortening and Fura-2 ratio (measured at 512 nm upon excitation at 340 and 380 nm) were simultaneously recorded using spectrofluorimeter coupled with a video detection system (IonOptix) as previously described[32]. Myocytes were electrically stimulated at a frequency of 0.5 Hz.

Immunoblot analysis: Protein samples were prepared from pulverized ventricular myocardium and lyzed in a buffer containing 30 mmol/L Tris/HCl (pH 8.8), 5 mmol/L EDTA, 30 mmol/L NaF, 3% SDS, and 10% glycerol. Samples were separated in denaturizing acrylamide gels and subsequently transferred onto nitrocellulose or PVDF membranes. After blocking the membranes with Roti®-block (Carl Roth) for 1 h, the incubation with anti-calsequestrin (1:1,000, ThermoScientific), anti-SERCA2a, anti-PDE2 (each 1:200, Santa

Cruz), anti-pPLB-S16, anti-pPLB-T17, anti-PLB, anti-pRYR2-S2808, anti-pRYR2-S2814 (each 1:5,000, Badrilla), and anti-RYR2 (1:2,000, Sigma-Aldrich) was carried out over night at 4°C. After incubation with appropriate secondary antibodies for 1 h, proteins were visualized by enhanced chemoluminescence (VersaDoc, Biorad) and quantified with Quantity One software (Biorad).

Ligation of the anterior descending artery

At the age of 10-14 weeks, mice were subjected to permanent ligation of the left anterior descending coronary artery (LAD) to induce myocardial infarction. After anesthesia was induced using 10% ketamine/ 2% xylazine i.p., the chest was opened between the third and the fourth rib. A 8−0 silk suture was used to occlude the LAD. Animals received buprenorphine (0.05–0.1 mg/kg, s.c.) for post-operative analgesia. ECG-telemetry recordings were performed for 2 weeks after LAD ligation.

Statistics: Results are presented as mean±SEM. Data sets were compared by Student's *t*-test, one-way ANOVA followed by Newman Keuls multiple comparison test, two-way ANOVA, Fisher's exact test or Pearson correlation according to the experimental setting. P values of less than 0.05 were considered statistically significant.

Results

Consequences of pharmacological PDE2 inhibition on cardiac function in vivo

To characterize the contribution of PDE2 to cardiac function under chronic β-AR stimulation *in vivo*, we subjected mice to ISO infusions (30 mg/kg/d for 7d) or NaCl (0.9%) as control. As expected, ISO treated animals developed prominent cardiac hypertrophy, indicated by an increase in left ventricular weight to body weight ratio from 3.6±0.2 to 4.7±0.1 mg/g ($p<0.05$, Suppl. Fig. 1). After chronic ISO treatment, the positive chronotropic and ionotropic effects of DOBU were abrogated, indicating desensitization of the β-ARs (Fig. 1). This was completely reversed by inhibition of PDE2 with BAY (3 mg/kg), restoring β-AR responsiveness to the level observed in the control group (Fig. 1). Interestingly, PDE2 inhibition also had an effect on control mice, almost doubling the impact of β-AR stimulation on heart rate (HR) over the average basal HR of 424±18 bpm from 95±29 to 170±23 bpm (Fig. 1B). The dosage of 3 mg/kg was chosen according to recent publications regarding *in vivo* experiments in rodents[33] and unpublished pharmacokinetic studies provided by BAYER. This restriction of PDE2 to chronotropic regulation under physiological conditions was supported by a study on beagle dogs treated with increasing doses of BAY (3, 10, and 30 mg/kg). In line with the murine model, the inhibition of PDE2 predominantly resulted in acceleration of HR (10 mg/kg: +20%; 30 mg/kg: +28%, Suppl. Fig. 2A), while stroke volume (SV), cardiac output (CO) and systolic (BPs) as well as diastolic blood pressures (BPd) remained largely unchanged (Suppl. Fig. 2B). Taken together, the role of PDE2 seems restricted to HR regulation under physiological conditions, while its stress-induced upregulation contributes to the desensitization of both β-AR-induced increases in HR and contraction force.

Effect of PDE2 overexpression on heart rate and cardiac function

To gain insight into the consequences of higher cardiac PDE2 levels, we generated transgenic (TG) mouse lines which overexpress PDE2 about 6- to 15-fold specifically in cardiomyocytes (Fig. 2H; Suppl. Fig. 3, 4). The low expressing (6-fold) line TG-4808 did not show any overt phenotype (Suppl. Fig. 3). In contrast, the ~10-fold overexpressing line TG-4320 (Fig. 2H) analyzed at 2 months displayed a substantial lower basal and dobutamine (DOBU)-stimulated maximal HR compared to wildtype (WT) with an average difference of 77±17 and 98±14 bpm, respectively (Fig. 2B). Basal contraction force measured as fractional area shortening (FAS) was higher in TG-4320 than in WT (37±1% vs. 32±1%), while maximal DOBU-stimulated contractility remained unaffected (80±3% in WT and 77±2% in PDE2-TG, Fig. 2A). In line with this, the lower HR combined with higher basal contraction produced a cardiac output virtually identical to that of WT controls (Fig. 2C). The higher contraction force in TG-4320 was not associated with cardiac hypertrophy as left ventricular weight to body weight ratio or heart weight to tibia length did not differ between WT and PDE2-TG mice (Fig. 2G, 3C). PDE2-TG displayed preserved susceptibility to β-AR blockade by metoprolol regarding the decrease both in HR and FAS with IC_{50} values that paralleled WT controls (Fig. 2D-F, Suppl. Fig. 5). Interestingly, while maximal doses of metoprolol (100 mg/kg) reduced HR to a similar extent in WT and PDE2-TG (332±15 and 306±8 bpm, respectively), FAS of PDE2-TG was higher under β−AR blockade compared to WT controls (31±2% in WT *vs.* 44±2% in PDE2-TG, Fig. 2D, F). The specific phenotype of lower HR with preserved cardiac performance was confirmed in a second independent transgenic line (TG-4811) with even higher overexpression levels (15-fold, Suppl. Fig. 4) excluding possible insertion artefacts. In accordance with recently published guidelines for transgenic mice[34] the lower expressing TG-4320 was chosen for the following experiments and will hence be referred to as PDE2-TG or TG.

Next, we analyzed the effects of PDE2 abundance on cardiac morphology and performance throughout most of the animals' life span including elderly mice. Notably, during 18 months of serial echocardiography, low HR and higher cardiac performance were preserved with no indication of functional decline, maladaptive remodeling or premature death (Fig. 3). The prominent impact on basal HR prompted us to investigate the effect of PDE2 on HR

regulation by telemetric ECG recordings in unrestrained, freely moving mice. Circadian analysis over the course of 24 h confirmed significantly lower HR in PDE2-TG animals during low activity daytime (Δ105±17 bpm) as well as high activity nighttime (Δ90±24 bpm, Fig. 4A, B and Suppl. Fig. 6A, B). Accordingly, analysis of the respective RR intervals recorded for 24 h showed longer average intervals in PDE2-TG demonstrated by a rightward shift of the Gaussian distribution curve (Fig. 4C). The difference in RR pattern was further confirmed by Poincaré analysis (Suppl. Fig. 6C, D). Notably, the broadening of the RR distribution as well as the significantly higher standard deviation from average RR-intervals indicate higher HR variability in PDE2-TG compared to WT animals (Fig. 4D). Thus, overexpression of PDE2 recapitulates the classical shift in sympathetic/parasympathetic balance as observed during an increased parasympathetic control of HR regulation[35]. However, PDE2-TG displayed the same relation of HR and physical activity as WT littermates, indicating preserved chronotropic competence (Fig. 4E). Basal heart rate reduction with maintained autonomic control has been allocated to a decrease in hyperpolarization-activated cyclic nucleotide-gated (HCN) channels activity[36]. Therefore we investigated the impact of HCN-blocker ivabradine (IVA; i.p. 5 µg/g) on heart beat frequency (Fig. 4F, Suppl. Fig. 6E). WT and TG animals showed similar susceptibility to IVA treatment displaying no significant difference in either lowest HR (348±23 and 319±17 bpm, respectively) or average HR reduction (158±10 bpm for WT and 128±14 for TG).

Impact of PDE2 overexpression on cAMP levels and Ca^{2+} cycling

To study the cellular mechanisms involved in PDE2 action, we investigated how PDE2 overexpression affects intracellular cAMP levels ($[cAMP]_i$). For that, we assessed real time changes in β-AR-induced $[cAMP]_i$ by FRET measurements in isolated ventricular myocytes infected with an adenovirus expressing the FRET-based cAMP probe Epac-S^{H187} [31]. The response to a 15 s application of ISO (30 nmol/L) was markedly blunted in PDE2-TG myocytes which showed an average change over basal of 17% compared to an average of 120% displayed by WT animals (Fig. 5A).

Next, we analyzed the consequences of the reduced accumulation of $[cAMP]_i$ on cellular Ca^{2+} handling in PDE2-TG mice. In line with previous publications, PDE2 overexpression markedly attenuated the β-AR induced increase in $I_{Ca,L}$ from 35% in WT to 8% in PDE2-TG (Fig. 5B), while basal $I_{Ca,L}$ amplitude remained unaffected (data not shown). This effect was fully reversed by PDE2 inhibition with BAY (Fig. 5C). Accordingly, Ca^{2+} transient and contractility analysis in field stimulated isolated ventricular myocytes revealed an attenuation of the β-AR response to ISO, while basal contractility and Ca^{2+} transients were similar between WT and PDE2-TG mice (Suppl. Fig. 7). SR Ca^{2+} load and fractional release were evaluated during the SR leak protocol (see below) by rapid application of 10 mmol/L caffeine. As expected, SR Ca^{2+} load as well as the fraction of released Ca^{2+} from the SR during systole significantly increased in WT derived ventricular myocytes after β-AR stimulation. In contrast, the ISO-induced increase in fractional SR Ca^{2+} release was absent in PDE2-TG, while SR Ca^{2+} content was not affected neither under basal nor stimulated conditions (Fig. 5D, E). This observation is in line with the lower β-AR response of systolic Ca^{2+} amplitude and force development measured in myocytes from PDE2-TG (Suppl. Fig. 7).

Arrhythmia provocation

To test the effect of greater PDE2 abundance under acute β-AR stress, animals received two injections of ISO (2 mg/kg) separated by an interval of 30 min[37]. As expected from echocardiographic analysis (Fig. 2B) and HR/activity correlation (Fig. 4E), PDE2-TG displayed a lower maximal HR upon β-AR stimulation (693±9 bpm in WT *vs*. 610±5 bpm in PDE2-TG), while chronotropic adaptation, i.e. absolute increase over basal HR, was maintained (157±18 bpm and 154±11 bpm, respectively, Fig. 6A, B). ECG was monitored for arrhythmic events such as ventricular extra systoles (VES), salvos and ventricular tachycardia (VT) over a period of 90 min after the first injection. All animals tested developed VES with frequency of occurrence increasing starting approximately 15 min after the second

injection of ISO (Suppl. Fig. 8A). The total number of VES was significantly lower in PDE2-TG (73±12 in WT *vs.* 30±9 in PDE2-TG, Fig. 5C). Importantly, only 1 out of 7 TG animals displayed severe arrhythmic events in form of VTs, while VTs were common incidents in WT animals where 6 out of 7 animals were affected (Fig. 6D, E). This finding was further confirmed *in vitro* where isolated WT ventricular myocytes exposed to ISO showed frequent occurrences of spontaneous Ca^{2+} waves (sCaW) which were abrogated in myocytes isolated from PDE2-TG mice (Fig. 6F, G).

Ca^2 leak and Ca^{2+} handling proteins

Since ISO-induced arrhythmias are to a large extent caused by an increased diastolic Ca^{2+} leak from the sarcoplasmic reticulum (SR) via the ryanodine receptor (RYR2)[38-40], analysis of Ca^{2+} sparks was conducted to estimate Ca^{2+} leakage. PDE2-TG animals revealed a trend to a lower number of sparks under basal conditions and a complete abrogation of the increase in spark frequency after application of ISO, indicating the likely underlying cause of the reduced arrhythmia burden of PDE2-TG mice after ISO injection (Fig. 7A, B). This was further confirmed by assessing the SR Ca^{2+} leak as the difference between the Fura-2 ratio with and without RYR2 blocker tetracaine (1 mmol/L), using a $0Na^{+}/0Ca^{2+}$ solution to prevent Ca^{2+} extrusion by the Na^{+}/Ca^{2+} exchanger (Suppl. Fig. 9).

To explore the molecular mechanisms of a reduced Ca^{2+} leak, we performed immunoblot analysis of key Ca^{2+} handling proteins (Fig. 7C-G). Consistent with the preserved SR Ca^{2+} load in PDE2-TG mice (Fig. 5D), we did not find differences between WT and PDE2-TG mice in regard to the expression of SERCA2a, PLB or RYR2. PLB phosphorylation was significantly reduced at S16 and milder also at T17. Most strikingly, we found a reduction of RYR2 receptor phosphorylation at the described Ca^{2+}/calmodulin-dependent kinase II (CaMKII) phosphorylation site, S2814, which has been linked to diastolic Ca^{2+} leakage, but not at the putative PKA site S2808.

Arrhythmia development and cardiac function after myocardial infarction

To induce myocardial infarction (MI), mice were subjected to ligation of the left anterior descending artery (LAD). While infarct size was similar in both groups (Fig. 8C), PDE2-TG were markedly protected against ventricular failure with an ejection fraction of 47±5% compared to 31±4% in WT (Fig. 8A, B) at 14d after MI. The overall VT incidence was only slightly and not significantly lower in PDE2 TG than in WT: 62.5% of the WT and 53.3% of PDE2-TG developed VTs in the first 40 h following MI (Fig. 8E). However, only 30% of WT with VTs survived the first 7d, whereas none of the PDE2-TG with VTs suffered from an early death (Fig. 8F). Moreover, all early WT deaths were preceded by VTs, while PDE2-TG did not show this correlation (Fig. 8G). Further analysis of WT and PDE2-TG VT quality suggested a tendency towards long VTs (>20s) in WT animals with early deaths (3 out of 7), which occurred neither in WT survivors nor in PDE2-TG (Suppl. Fig. 10, Fig. 8H). Overall, over 86% of PDE2-TG survived the early phase post MI, while only 56% of WT animals endured more than 7d (Fig. 8D, p=0.06). No further deaths occurred in either group between day 8 and day 14 (endpoint of intervention).

Discussion

Myocardial PDE2 is upregulated in human as well as in experimental HF but its physiological and pathological role in the heart remained unknown. Here, we show that heart rate regulation is the predominant physiological role of PDE2. Specific inhibition of PDE2 in dogs and mice led to an exclusive increase in HR, while overexpression of PDE2 resulted in its decrease. Under chronic β-AR activation, however, PDE2 contributes to myocardial β-AR desensitization, protecting the heart from excessive sympathetic stress. Moreover, under acute β-adrenergic stress, higher PDE2 abundance effectively protects against ventricular arrhythmia without compromising contractile performance *in vivo*. In the setting of MI, PDE2 TG showed improved ventricular function compared to WT.

Role of PDE2 in heart rate regulation

The modern concept of heartbeat initiation is based on the mutual interplay between ion channels of the cell membrane ("membrane clock") and cellular Ca^{2+} cycling ("Ca^{2+} clock")[41, 42]. The most prominent targets of sympathetic HR modulation are the funny current (I_f), mediated by cAMP-dependent regulation of HCN channels and PKA-dependent phosphorylation of L-type Ca^{2+} channels (LTCC) as well as of SR Ca^{2+} cycling proteins[43]. So far, PDE2 has been shown to contribute to myocardial Ca^{2+} cycling by modulating $I_{Ca,L}$ not only in ventricular, but also in atrial and sinoatrial nodal cells[22, 23, 44]. These findings are consistent with the attenuated β-AR responsiveness regarding $I_{Ca,L}$ and SR Ca^{2+} release observed in PDE2-TG derived ventricular myocytes. Moreover, the close interplay between $I_{Ca,L}$, RYR2-mediated Ca^{2+} release and SERCA/PLB-dependent filling of the SR suggests that PDE2 is involved in the regulation of the Ca^{2+} clock[42]. However, while in the ventricular myocardium *in vivo* contraction force was unaffected in PDE2-TG, PDE2-TG exhibited lower basal as well as maximal heart rates, but retained β-AR induced control of pacemaker activity. This particular chronotropic phenotype has remarkable parallels with a cardiac cAMP-binding deficient HCN4 mutation analyzed in mice and humans[45, 36]. Notably, while HCN-blockade with IVA had no effect in mice expressing the mutated channel[45], PDE2-TG mice were still sensitive to IVA treatment indicating a remaining contribution of I_f to basal heart rate regulation. This study shows for the first time, that PDE2 is a major player in HR regulation *in vivo*, most likely by affecting both membrane and Ca^{2+} clock.

Role of PDE2 in propensity to arrhythmia and in contractility

There is substantial evidence that generation of delayed afterdepolarizations due to increased diastolic Ca^{2+} leak from the SR via RYR2 and the subsequent depolarizing activity of the Na^+/Ca^{2+} exchanger (NCX) is the main underlying mechanism for triggered arrhythmias[46]. A central role in this dysfunction of Ca^{2+} cycling has been attributed to the phosphorylation of RYR2 at the CaMKII site S2814 and the associated facilitation of diastolic Ca^{2+}-release[39, 40, 47]. Our conclusion that PDE2-TG are less susceptible to arrhythmia provocation induced by acute β-AR stimulation due to a significantly lower Ca^{2+}-spark frequency as well as lower RYR2-S2814 phosphorylation fits well to this model. At the cardiomyocyte level, efficacy of β-AR-induced increase in sarcomere shortening was significantly attenuated, as were efficacy and potency of β-AR-induced stimulation of Ca^{2+}-transients. Notably, at baseline and at low ISO concentrations, contractile parameters were normal (Suppl. Fig. 8). However, the *in vitro* findings regarding force development did not entirely recapitulate the actual phenotype of PDE2-TG mice. Our *in vivo* data clearly demonstrate that PDE2 overexpression was associated with a normal contractile reserve and rather improved contraction force. This was even maintained when HR was reduced to an identical level (332±15 *vs*. 306±8 bpm) induced by acute β-blockade (Fig. 2 D-F) indicating that the lower basal HR per se e.g. via augmented filling in diastole cannot completely explain the hypercontractile phenotype. Despite lower PLB-phosphorylation, SR load did not appear affected in PDE2-TG. Longer diastolic intervals and the reduced Ca^{2+} leak may therefore be sufficient for maintaining adequate SR Ca^{2+} filling and preservation of cardiac function *in vivo*, even in the presence of reduced SERCA activity[47]. In summary, PDE2

overexpression offers a potential of dual protection by limiting HR without affecting chronotropic adaptation and by attenuating ventricular SR Ca^{2+}-release with the benefit of lower arrhythmia susceptibility. The effect of PDE2 overexpression is therefore similar to β-blocker treatment but without depression of contractile performance.

PDE2 in cardiac remodeling

A very recent publication proposed that in context of cardiac remodeling processes, chronic inhibition of PDE2 leads to a reduction of pathological hypertrophic growth[48]. While this contradicts our earlier findings that adenoviral overexpression of PDE2 antagonizes β-AR induced cellular hypertrophy (Mehel et al., 2013; Wagner et al. 2016, Naunyn-Schmiedeberg's archives of pharmacology), we observed a small but not significant increase in cardiac size in PDE2-TG mice as compared to WT (Fig. 2G, 3C). Therefore, we cannot completely rule out a minor increase of heart size due to PDE2 overexpression. Consistently, heart weight was also ~10% higher in PDE2-TG mice after MI compared to WT (Suppl. Fig. 11). However, preservation of cardiac function and size up to an advanced age (Fig. 3) strongly argues against pathological hypertrophy. Moreover, we offer proof that high abundance of PDE2 significantly protects against acute and chronic β-AR stress and maintains contractile function after MI.

Potential limitations

A general limitation of transgenic “overexpressors” is potential spill over within subcellular compartments, where the protein of interest may be not physiologically located. This is even more critical when examining PDEs, which control highly compartmentalized cAMP pools and redistribution phenomena under pathological conditions have been reported[49, 50]. Despite designing our experiments following general recommendations for state-of-the-art phenotyping of transgenic mice[34], we are not able to fully exclude artificial compartmentation effects. However, the specificity of the phenotype and its striking similarities to *in vivo* studies of endogenous PDE2 from mice and larger animals offers a valid approach for analyzing the pathophysiological role of PDE2 in heart function. A second limitation is that the role played by each PDE isoform varies among mammalian species[51, 52] and accordingly, our results may not recapitulate the situation in humans in all details.

Clinical perspective: PDE2 as a downstream target of cGMP pools

The current therapeutic strategies for HF and prevention of sudden cardiac death are only moderately effective. Despite all efforts, a lack of understanding of the pathophysiological mechanisms underlying HF and arrhythmias has hindered the development of more effective, rational therapeutic approaches. Recently, the publication of the PARADIGM-HF trial, which demonstrated the successful introduction of the compound LCZ696 (a combination of a standard Angiotesin-II-receptor-1 blocker and an inhibitor of the NP-degrading enzyme neprilysin), has once again shifted the enhancement of cGMP-signaling into the focus of HF therapy. One remarkable result of the study was a significant protection from sudden cardiac death[53, 54]. The importance of the NP signaling pathway was further emphasized in a study by the Kass group showing that the inhibition of cGMP-degrading PDE9 protects against HF progression by specifically targeting the ANP/BNP-coupled cGMP pool[15, 55]. PDE2 is a central component of the cGMP/cAMP crosstalk and as our study demonstrates effectively protects against ventricular arrhythmia during excessive sympathetic stress and improved ventricular function after a severe cardiac insult. It may therefore constitute an up to now unconsidered link between ANP/BNP-coupled cGMP enhancement and the protection against toxic sympathetic effects by acting as a cGMP controlled intracellular sympathetic blockade. Thus, PDE2 is worth being considered a key element in recent encouraging therapeutic approaches and accordingly its direct activation may offer an alternative strategy in a promising new field of HF therapy.

Acknowledgments: We wish to thank Roland Blume, Ursel Leonard, Daniela Wolter, Marcel Zoremba (University Medical Center Göttingen), and Stefano Gaburro (DSI) for their technical support. Further, Florence Lefebvre for cell isolation, and Pauline Robert and Valérie Domergue-Dupont (Animal core facility, University of Paris-Sud, UMS-IPSIT*)* for handling and genotyping of mice.

Funding sources: This study was supported by Deutsche Forschungsgemeinschaft Grants DFG EL 270/7-1 (to A. El-Armouche), DFG WA 2586/4-1 (to M. Wagner), SFB 1002 (to A. El-Armouche), and IRTG 1816 (to C. Vettel, and A. El-Armouche), by the Investment for the Future program ANR-11-IDEX-0003-01 within the LABEX ANR-10-LABX-0033 (to R. Fischmeister and M. Lindner) and the German Centre for Cardiovascular Research.

Disclosures: None

References

1. Cohn JN, Levine TB, Olivari MT, Garberg V, Lura D, Francis GS, Simon AB, Rector T. Plasma norepinephrine as a guide to prognosis in patients with chronic congestive heart failure. *The New England journal of medicine*. 1984;311:819-823
2. Tomaselli GF, Zipes DP. What causes sudden death in heart failure? *Circulation research*. 2004;95:754-763
3. Coronel R, Wilders R, Verkerk AO, Wiegerinck RF, Benoist D, Bernus O. Electrophysiological changes in heart failure and their implications for arrhythmogenesis. *Biochim Biophys Acta*. 2013;1832:2432-2441
4. Fox K, Ford I, Steg PG, Tendera M, Robertson M, Ferrari R, investigators B. Heart rate as a prognostic risk factor in patients with coronary artery disease and left-ventricular systolic dysfunction (beautiful): A subgroup analysis of a randomised controlled trial. *Lancet*. 2008;372:817-821
5. Bilchick KC, Berger RD. Heart rate variability. *Journal of cardiovascular electrophysiology*. 2006;17:691-694
6. Bristow MR, Ginsburg R, Minobe W, Cubicciotti RS, Sageman WS, Lurie K, Billingham ME, Harrison DC, Stinson EB. Decreased catecholamine sensitivity and beta-adrenergic-receptor density in failing human hearts. *The New England journal of medicine*. 1982;307:205-211
7. Nikolaev VO, Moshkov A, Lyon AR, Miragoli M, Novak P, Paur H, Lohse MJ, Korchev YE, Harding SE, Gorelik J. Beta2-adrenergic receptor redistribution in heart failure changes camp compartmentation. *Science*. 2010;327:1653-1657
8. El-Armouche A, Eschenhagen T. Beta-adrenergic stimulation and myocardial function in the failing heart. *Heart failure reviews*. 2009;14:225-241
9. Tilley DG, Rockman HA. Role of beta-adrenergic receptor signaling and desensitization in heart failure: New concepts and prospects for treatment. *Expert review of cardiovascular therapy*. 2006;4:417-432
10. Bristow MR. Pathophysiologic and pharmacologic rationales for clinical management of chronic heart failure with beta-blocking agents. *The American journal of cardiology*. 1993;71:12C-22C
11. Effect of metoprolol cr/xl in chronic heart failure: Metoprolol cr/xl randomised intervention trial in congestive heart failure (merit-hf). *Lancet*. 1999;353:2001-2007
12. Flannery G, Gehrig-Mills R, Billah B, Krum H. Analysis of randomized controlled trials on the effect of magnitude of heart rate reduction on clinical outcomes in patients with systolic chronic heart failure receiving beta-blockers. *The American journal of cardiology*. 2008;101:865-869
13. Swedberg K, Komajda M, Bohm M, Borer JS, Ford I, Dubost-Brama A, Lerebours G, Tavazzi L, Investigators S. Ivabradine and outcomes in chronic heart failure (shift): A randomised placebo-controlled study. *Lancet*. 2010;376:875-885
14. Lee DI, Vahebi S, Tocchetti CG, Barouch LA, Solaro RJ, Takimoto E, Kass DA. Pde5a suppression of acute beta-adrenergic activation requires modulation of myocyte beta-3 signaling coupled to pkg-mediated troponin i phosphorylation. *Basic Res Cardiol*. 2010;105:337-347
15. Lee DI, Zhu G, Sasaki T, Cho GS, Hamdani N, Holewinski R, Jo SH, Danner T, Zhang M, Rainer PP, Bedja D, Kirk JA, Ranek MJ, Dostmann WR, Kwon C, Margulies KB, Van Eyk JE, Paulus WJ, Takimoto E, Kass DA. Phosphodiesterase 9a controls nitric-oxide-independent cgmp and hypertrophic heart disease. *Nature*. 2015;519:472-476
16. Nagayama T, Hsu S, Zhang M, Koitabashi N, Bedja D, Gabrielson KL, Takimoto E, Kass DA. Sildenafil stops progressive chamber, cellular, and molecular remodeling and improves calcium handling and function in hearts with pre-existing advanced hypertrophy caused by pressure overload. *J Am Coll Cardiol*. 2009;53:207-215
17. Wang H, Kohr MJ, Traynham CJ, Ziolo MT. Phosphodiesterase 5 restricts nos3/soluble guanylate cyclase signaling to L-type Ca^{2+} current in cardiac myocytes. *J Mol Cell Cardiol*. 2009;47:304-314

18. Mika D, Leroy J, Vandecasteele G, Fischmeister R. Pdes create local domains of camp signaling. *J Mol Cell Cardiol*. 2012;52:323-329
19. Martinez SE, Wu AY, Glavas NA, Tang XB, Turley S, Hol WG, Beavo JA. The two gaf domains in phosphodiesterase 2a have distinct roles in dimerization and in cgmp binding. *Proc Natl Acad Sci U S A*. 2002;99:13260-13265
20. Wu AY, Tang XB, Martinez SE, Ikeda K, Beavo JA. Molecular determinants for cyclic nucleotide binding to the regulatory domains of phosphodiesterase 2a. *J Biol Chem*. 2004;279:37928-37938
21. Martinez SE, Beavo JA, Hol WG. Gaf domains: Two-billion-year-old molecular switches that bind cyclic nucleotides. *Molecular interventions*. 2002;2:317-323
22. Dittrich M, Jurevicius J, Georget M, Rochais F, Fleischmann B, Hescheler J, Fischmeister R. Local response of L-type Ca^{2+} current to nitric oxide in frog ventricular myocytes. *J Physiol*. 2001;534:109-121
23. Vandecasteele G, Verde I, Rucker-Martin C, Donzeau-Gouge P, Fischmeister R. Cyclic gmp regulation of the L-type Ca^{2+} channel current in human atrial myocytes. *J Physiol*. 2001;533:329-340
24. Mongillo M, Tocchetti CG, Terrin A, Lissandron V, Cheung YF, Dostmann WR, Pozzan T, Kass DA, Paolocci N, Houslay MD, Zaccolo M. Compartmentalized phosphodiesterase-2 activity blunts beta-adrenergic cardiac inotropy via an no/cgmp-dependent pathway. *Circulation research*. 2006;98:226-234
25. MacFarland RT, Zelus BD, Beavo JA. High concentrations of a cgmp-stimulated phosphodiesterase mediate anp-induced decreases in camp and steroidogenesis in adrenal glomerulosa cells. *J Biol Chem*. 1991;266:136-142
26. Ding B, Abe J, Wei H, Huang Q, Walsh RA, Molina CA, Zhao A, Sadoshima J, Blaxall BC, Berk BC, Yan C. Functional role of phosphodiesterase 3 in cardiomyocyte apoptosis: Implication in heart failure. *Circulation*. 2005;111:2469-2476
27. Abi-Gerges A, Richter W, Lefebvre F, Mateo P, Varin A, Heymes C, Samuel JL, Lugnier C, Conti M, Fischmeister R, Vandecasteele G. Decreased expression and activity of camp phosphodiesterases in cardiac hypertrophy and its impact on beta-adrenergic camp signals. *Circulation research*. 2009;105:784-792
28. Mehel H, Emons J, Vettel C, Wittkopper K, Seppelt D, Dewenter M, Lutz S, Sossalla S, Maier LS, Lechene P, Leroy J, Lefebvre F, Varin A, Eschenhagen T, Nattel S, Dobrev D, Zimmermann WH, Nikolaev VO, Vandecasteele G, Fischmeister R, El-Armouche A. Phosphodiesterase-2 is up-regulated in human failing hearts and blunts beta-adrenergic responses in cardiomyocytes. *J Am Coll Cardiol*. 2013;62:1596-1606
29. Subramaniam A, Jones WK, Gulick J, Wert S, Neumann J, Robbins J. Tissue-specific regulation of the alpha-myosin heavy chain gene promoter in transgenic mice. *J Biol Chem*. 1991;266:24613-24620
30. Borner S, Schwede F, Schlipp A, Berisha F, Calebiro D, Lohse MJ, Nikolaev VO. Fret measurements of intracellular camp concentrations and camp analog permeability in intact cells. *Nature protocols*. 2011;6:427-438
31. Klarenbeek J, Goedhart J, van Batenburg A, Groenewald D, Jalink K. Fourth-generation epac-based fret sensors for camp feature exceptional brightness, photostability and dynamic range: Characterization of dedicated sensors for flim, for ratiometry and with high affinity. *PloS one*. 2015;10:e0122513
32. Leroy J, Richter W, Mika D, Castro LR, Abi-Gerges A, Xie M, Scheitrum C, Lefebvre F, Schittl J, Mateo P, Westenbroek R, Catterall WA, Charpentier F, Conti M, Fischmeister R, Vandecasteele G. Phosphodiesterase 4b in the cardiac L-type Ca^{2+} channel complex regulates Ca^{2+} current and protects against ventricular arrhythmias in mice. *The Journal of clinical investigation*. 2011;121:2651-2661
33. Masood A, Huang Y, Hajjhussein H, Xiao L, Li H, Wang W, Hamza A, Zhan CG, O'Donnell JM. Anxiolytic effects of phosphodiesterase-2 inhibitors associated with increased cgmp signaling. *The Journal of pharmacology and experimental therapeutics*. 2009;331:690-699

34. Davis J, Maillet M, Miano JM, Molkentin JD. Lost in transgenesis: A user's guide for genetically manipulating the mouse in cardiac research. *Circulation research*. 2012;111:761-777
35. Hayano J, Sakakibara Y, Yamada A, Yamada M, Mukai S, Fujinami T, Yokoyama K, Watanabe Y, Takata K. Accuracy of assessment of cardiac vagal tone by heart rate variability in normal subjects. *The American journal of cardiology*. 1991;67:199-204
36. Schweizer PA, Duhme N, Thomas D, Becker R, Zehelein J, Draguhn A, Bruehl C, Katus HA, Koenen M. Camp sensitivity of hcn pacemaker channels determines basal heart rate but is not critical for autonomic rate control. *Circulation. Arrhythmia and electrophysiology*. 2010;3:542-552
37. Wittkopper K, Fabritz L, Neef S, Ort KR, Grefe C, Unsold B, Kirchhof P, Maier LS, Hasenfuss G, Dobrev D, Eschenhagen T, El-Armouche A. Constitutively active phosphatase inhibitor-1 improves cardiac contractility in young mice but is deleterious after catecholaminergic stress and with aging. *The Journal of clinical investigation*. 2010;120:617-626
38. Neef S, Maier LS. Novel aspects of excitation-contraction coupling in heart failure. *Basic Res Cardiol*. 2013;108:360
39. Respress JL, van Oort RJ, Li N, Rolim N, Dixit SS, deAlmeida A, Voigt N, Lawrence WS, Skapura DG, Skardal K, Wisloff U, Wieland T, Ai X, Pogwizd SM, Dobrev D, Wehrens XH. Role of ryr2 phosphorylation at s2814 during heart failure progression. *Circulation research*. 2012;110:1474-1483
40. van Oort RJ, McCauley MD, Dixit SS, Pereira L, Yang Y, Respress JL, Wang Q, De Almeida AC, Skapura DG, Anderson ME, Bers DM, Wehrens XH. Ryanodine receptor phosphorylation by calcium/calmodulin-dependent protein kinase ii promotes life-threatening ventricular arrhythmias in mice with heart failure. *Circulation*. 2010;122:2669-2679
41. DiFrancesco D. The role of the funny current in pacemaker activity. *Circulation research*. 2010;106:434-446
42. Lakatta EG, Maltsev VA, Vinogradova TM. A coupled system of intracellular Ca^{2+} clocks and surface membrane voltage clocks controls the timekeeping mechanism of the heart's pacemaker. *Circulation research*. 2010;106:659-673
43. Lyashkov AE, Vinogradova TM, Zahanich I, Li Y, Younes A, Nuss HB, Spurgeon HA, Maltsev VA, Lakatta EG. Cholinergic receptor signaling modulates spontaneous firing of sinoatrial nodal cells via integrated effects on pka-dependent Ca^{2+} cycling and i(kach). *American journal of physiology. Heart and circulatory physiology*. 2009;297:H949-959
44. Hua R, Adamczyk A, Robbins C, Ray G, Rose RA. Distinct patterns of constitutive phosphodiesterase activity in mouse sinoatrial node and atrial myocardium. *PloS one*. 2012;7:e47652
45. Alig J, Marger L, Mesirca P, Ehmke H, Mangoni ME, Isbrandt D. Control of heart rate by camp sensitivity of hcn channels. *Proc Natl Acad Sci U S A*. 2009;106:12189-12194
46. Bers DM. Cardiac sarcoplasmic reticulum calcium leak: Basis and roles in cardiac dysfunction. *Annual review of physiology*. 2014;76:107-127
47. Neef S, Dybkova N, Sossalla S, Ort KR, Fluschnik N, Neumann K, Seipelt R, Schondube FA, Hasenfuss G, Maier LS. Camkii-dependent diastolic SR Ca^{2+} leak and elevated diastolic Ca^{2+} levels in right atrial myocardium of patients with atrial fibrillation. *Circulation research*. 2010;106:1134-1144
48. Zoccarato A, Surdo NC, Aronsen JM, Fields LA, Mancuso L, Dodoni G, Stangherlin A, Livie C, Jiang H, Sin YY, Gesellchen F, Terrin A, Baillie GS, Nicklin SA, Graham D, Szabo-Fresnais N, Krall J, Vandeput F, Movsesian M, Furlan L, Corsetti V, Hamilton GM, Lefkimmiatis K, Sjaastad I, Zaccolo M. Cardiac hypertrophy is inhibited by a local pool of camp regulated by phosphodiesterase 2. *Circulation research*. 2015
49. Perera RK, Sprenger JU, Steinbrecher JH, Hubscher D, Lehnart SE, Abesser M, Schuh K, El-Armouche A, Nikolaev VO. Microdomain switch of cgmp-regulated phosphodiesterases leads to anp-induced augmentation of beta-adrenoceptor-

stimulated contractility in early cardiac hypertrophy. *Circulation research*. 2015;116:1304-1311
50. Zhang M, Takimoto E, Lee DI, Santos CX, Nakamura T, Hsu S, Jiang A, Nagayama T, Bedja D, Yuan Y, Eaton P, Shah AM, Kass DA. Pathological cardiac hypertrophy alters intracellular targeting of phosphodiesterase type 5 from nitric oxide synthase-3 to natriuretic peptide signaling. *Circulation*. 2012;126:942-951
51. Fischmeister R, Castro LR, Abi-Gerges A, Rochais F, Jurevicius J, Leroy J, Vandecasteele G. Compartmentation of cyclic nucleotide signaling in the heart: The role of cyclic nucleotide phosphodiesterases. *Circulation research*. 2006;99:816-828
52. Zaccolo M, Movsesian MA. Camp and cgmp signaling cross-talk: Role of phosphodiesterases and implications for cardiac pathophysiology. *Circulation research*. 2007;100:1569-1578
53. McMurray JJ, Packer M, Desai AS, Gong J, Lefkowitz MP, Rizkala AR, Rouleau J, Shi VC, Solomon SD, Swedberg K, Zile MR, Committees P-H, Investigators. Dual angiotensin receptor and neprilysin inhibition as an alternative to angiotensin-converting enzyme inhibition in patients with chronic systolic heart failure: Rationale for and design of the prospective comparison of arni with acei to determine impact on global mortality and morbidity in heart failure trial (paradigm-hf). *European journal of heart failure*. 2013;15:1062-1073
54. McMurray JJ, Packer M, Desai AS, Gong J, Lefkowitz MP, Rizkala AR, Rouleau JL, Shi VC, Solomon SD, Swedberg K, Zile MR, Investigators P-H, Committees. Angiotensin-neprilysin inhibition versus enalapril in heart failure. *N Engl J Med*. 2014;371:993-1004
55. Kuhn M. Cardiology: A big-hearted molecule. *Nature*. 2015;519:416-417

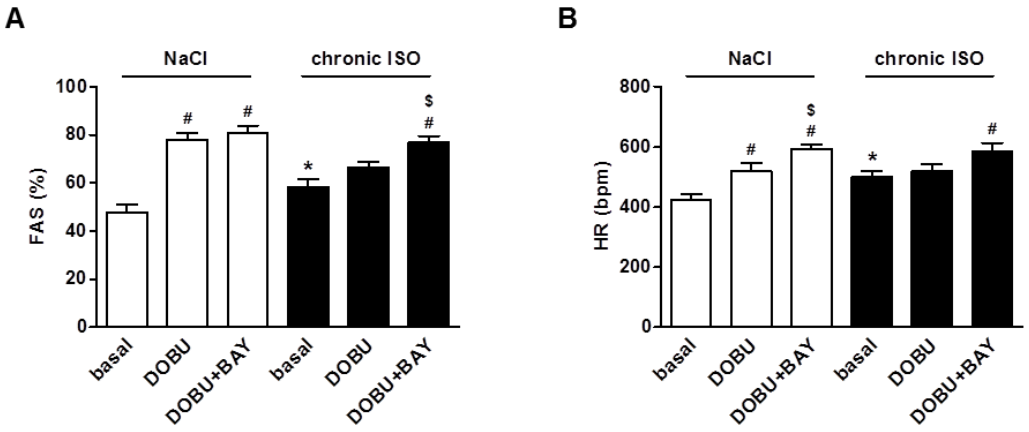

Figure 1. PDE2 regulates heart rate and blunts β-AR-induced inotropy in animals chronically treated with ISO. Effect of PDE2 inhibition in mice exposed to chronic ISO infusions for 7 d (30 mg/kg*d) or treated with vehicle (0.9% NaCl). Animals were anaesthetized and monitored by echocardiography under basal conditions, 2-7 min after dobutamine (10 mg/kg i.p., DOBU) injection and 10 min after application of the PDE2 inhibitor BAY 60-7550 (3 mg/kg i.p., BAY) on top of DOBU (DOBU+BAY). (A) Fractional area shortening (FAS). (B) Heart rate (HR); n=7-8 for each group. Statistical significance was determined by one-way ANOVA followed by Newman-Keuls multiple comparison test. *$p<0.05$ *vs.* NaCl, $^{\#}p<0.05$ *vs.* respective basal, and $^{\$}p<0.05$ *vs.* DOBU.

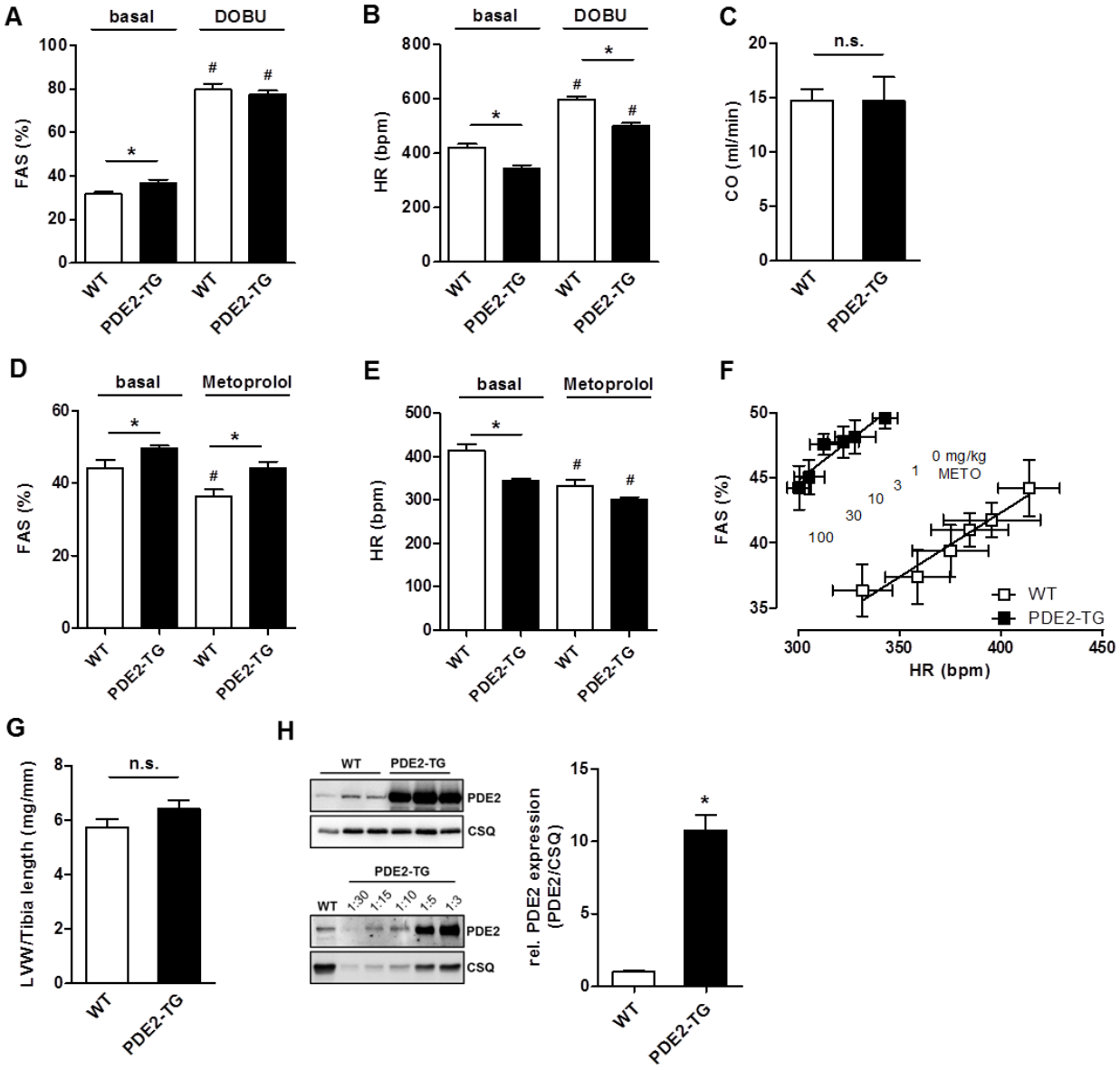

Figure 2. Higher basal contractility and lower heart rate in PDE2-TG. Echocardiographic determination of fractional area shortening (FAS, A), heart rate cardiac (HR, B) and output (CO, C), and in anaesthetized 2 month old mice. Animals were treated with 10 mg/kg dobutamine (DOBU, i.p.) 2 min prior to measurements when indicated; n=7-9 for each group. Effect of metoprolol (100 mg/kg, i.p.) on (D) FAS and (E) HR in anaesthetized animals. (G) Correlation between the reduction of FAS and HR in the presence of increasing metoprolol doses (METO 0, 1, 3, 10, 30 and 100 mg/kg); n=5 for each group. (G) Left ventricular weight (LVW) calculated from the echocardiographic data and normalized to tibia length. (H) Lysates prepared from ventricular myocardium were analyzed by immunoblot with the indicated specific antibodies. PDE2 expression was normalized to calsequestrin (CSQ) and given relative to WT. (E) Representative immunoblots and (F) quantification; n=7-9 for each group. Statistical significance was determined by One-way ANOVA followed by Newman-Keuls multiple comparison test (A, B, D, E) and Student's *t*-test to compare the two genotypes on basal level (A-E, G,H). *p<0.05 *vs*. WT, $^{\#}$p<0.05 *vs.* respective basal.

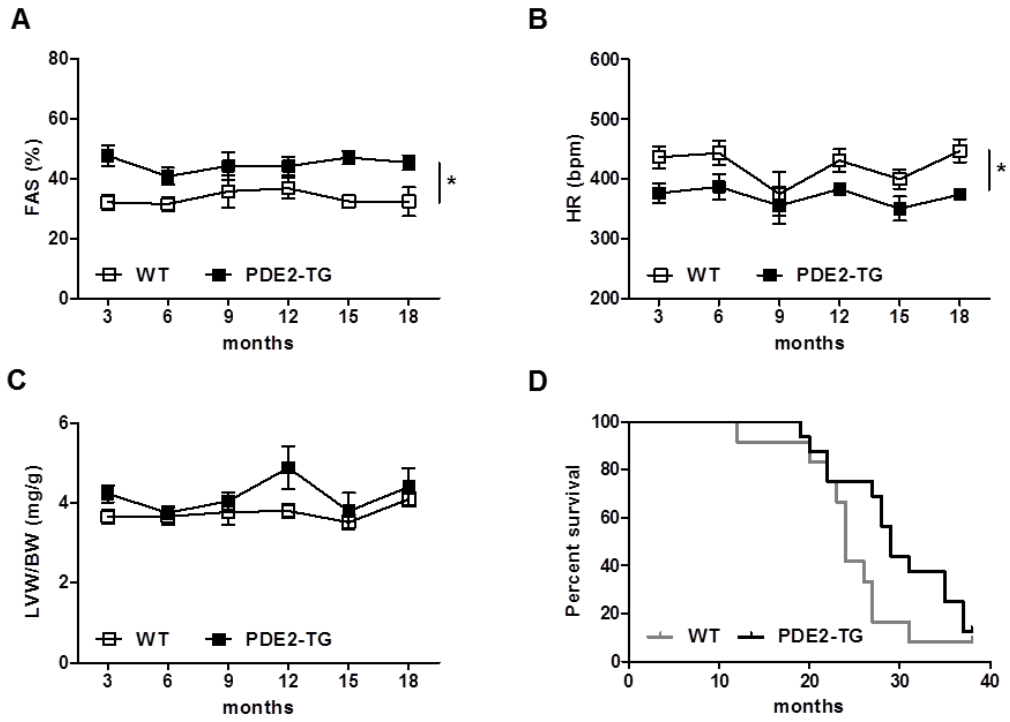

Figure 3. Preserved phenotype of higher basal contractility and lower heart rate in elderly PDE2-TG. Echocardiographic determination of fractional area shortening (FAS, A), and heart rate (HR, B) in anaesthetized 3-18 month old mice. (C) Left ventricular weight (LVW) was calculated from the echocardiographic data and normalized to body weight (BW); n=6 for each group. Statistical significance was determined by Two-way ANOVA. *p<0.05 *vs*. WT. (D) Longevity study of WT (n=12) and PDE2-TG (n=16). The study was terminated after 38 months. Average life span of WT=24 and PDE2-TG=29 months.

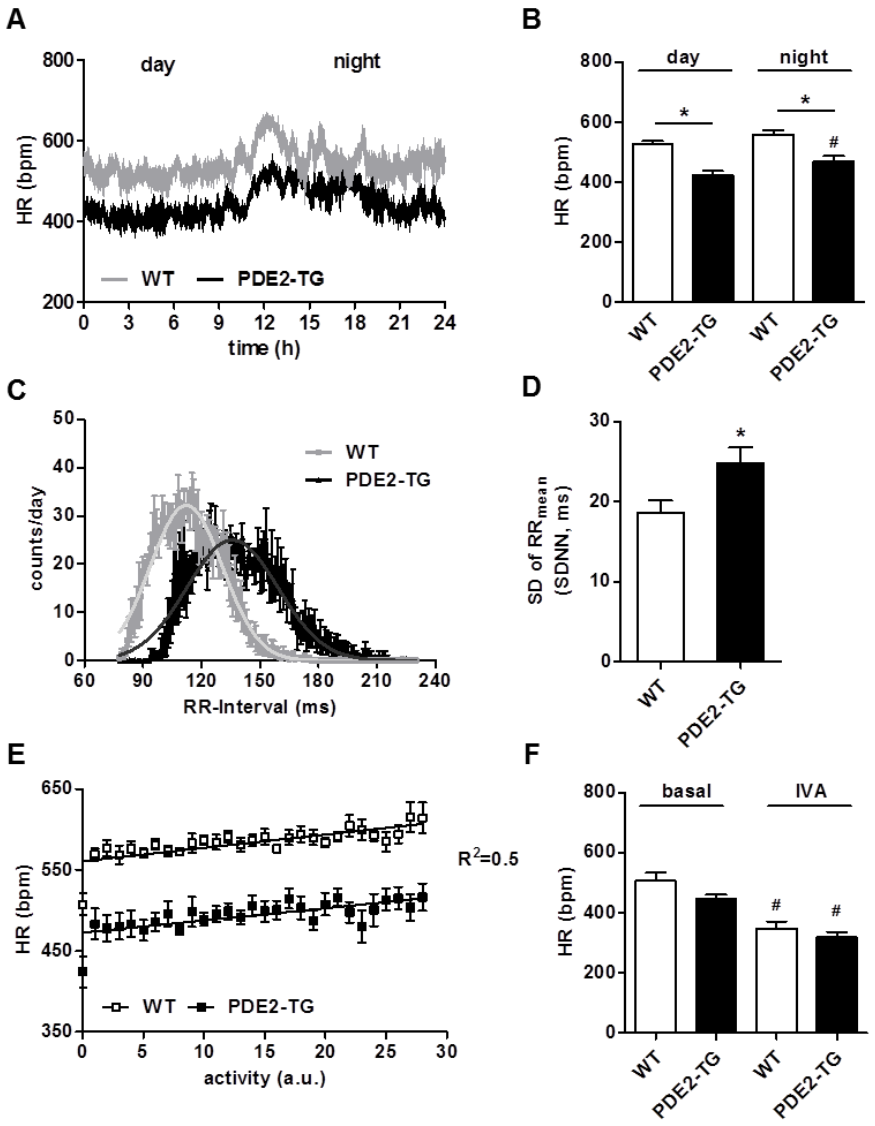

Figure 4. PDE2 transgenic mice show higher heart rate variability and normal chronotropic adaptation. Animals (n=4-5 per genotype) were monitored by ECG-telemetry for a period of 72 h to calculate average changes in heart rate (HR) and heart rate variability of a 24 h cycle. Frequencies and activity were tracked as averages of 1 min intervals. (A) Average circadian changes in heart rate over a period of 24 h. (B) Average heart rate during day and night periods. (C) Heart rate variability given as occurrence of RR-intervals during one 24 h recording with Gaussian distribution curve calculated for each group. (D) Standard derivation of average RR-intervals (SDNN). (E) Correlation between heart rate and activity. (F) Average HR over a period of 20 min prior (0-20 min) and after ivabradine (IVA, 5 mg/kg, i.p.) injection (10-30 min). Statistical significance was determined by one-way ANOVA followed by Newman-Keuls multiple comparison test and Student's *t*-test to compare the two genotypes (D). *p<0.05 *vs*. WT, #p<0.05 *vs*. day (B) or respective basal (F).

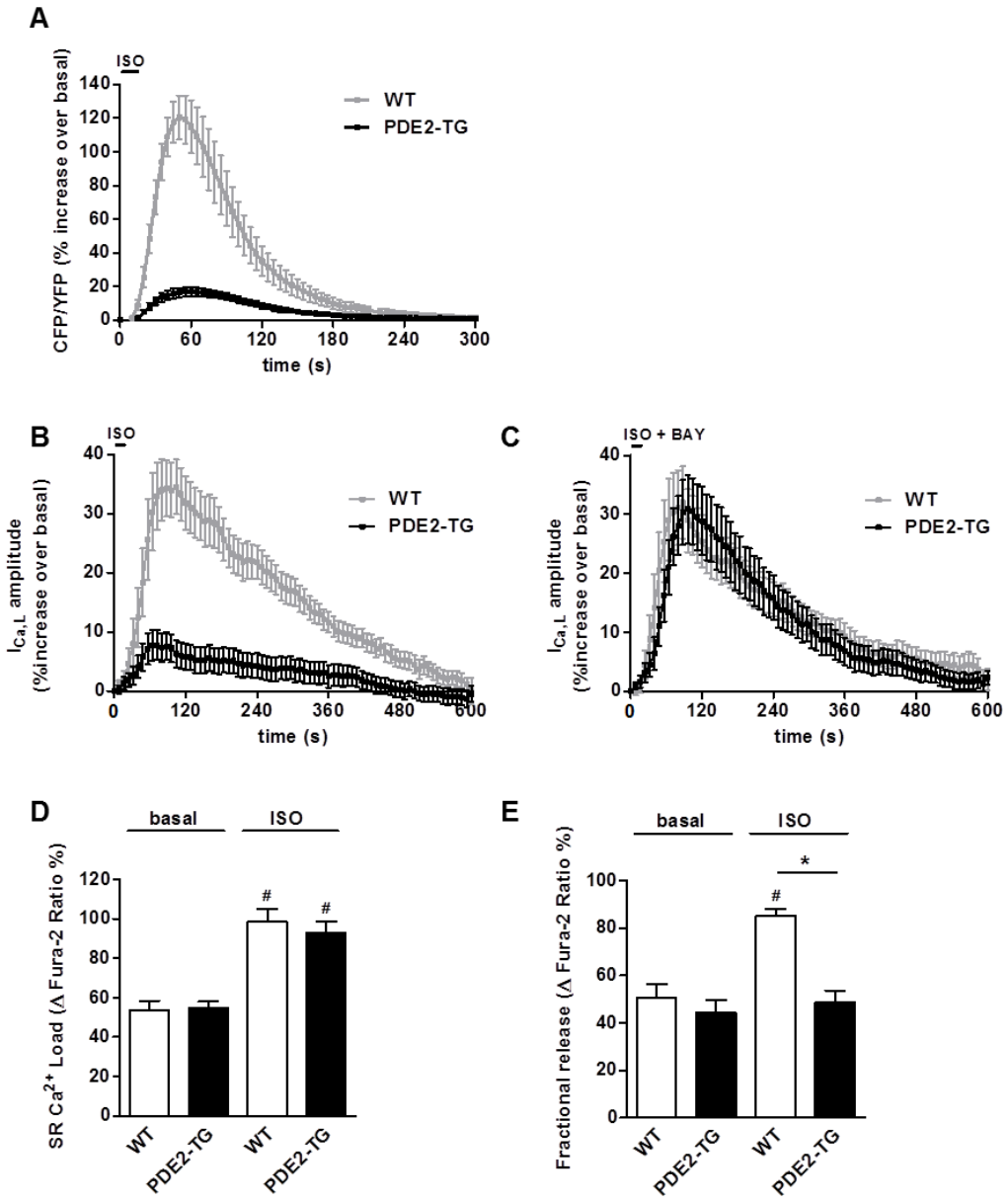

Figure 5. Ventricular myocytes from PDE2-TG mice show reduced β-AR-response, but normal SR Ca^{2+} load. (A) Normalized average time course of $[cAMP]_i$ in response to a 15 s application of ISO (30 nmol/L) in WT and PDE2-TG ventricular myocytes infected with an adenovirus expressing the FRET-based cAMP probe Epac-S^{H187}; n=3 animals/genotype with 11-13 cell in each group. (B, C) Normalized average time course of $I_{Ca,L}$ amplitude following ISO pulse stimulation (30 nmol/L, 15 s) in the absence (B) or presence (C) of PDE2 inhibitor BAY 60-7550 (100 nmol/L). The cells were depolarized every 8 s from -50 to 0 mV during 400 ms; n=3 animals/genotype with 10-19 cell in each group. (D) Mean amplitude of SR Ca^{2+} load in the presence or absence of ISO measured as the change in Fura-2 ratio after rapid application of caffeine (10 mmol/L). (E, F) SR Ca^{2+} load and fractional release measured in Fura-2 loaded adult mouse ventricular myocytes paced at 1 Hz, in the presence or absence of ISO (100 nmol/L) (E) Mean fractional Ca^{2+} release in control or ISO calculated as the ratio of Ca^{2+} transient amplitude divided by caffeine-induced response; n=2-3 animals/genotype with 7-11 cells in each group. Statistical significance was determined by One-way ANOVA followed by Newman-Keuls multiple comparison test. *p<0.05 *vs*. WT, $^{\#}$p<0.05 *vs*. respective basal.

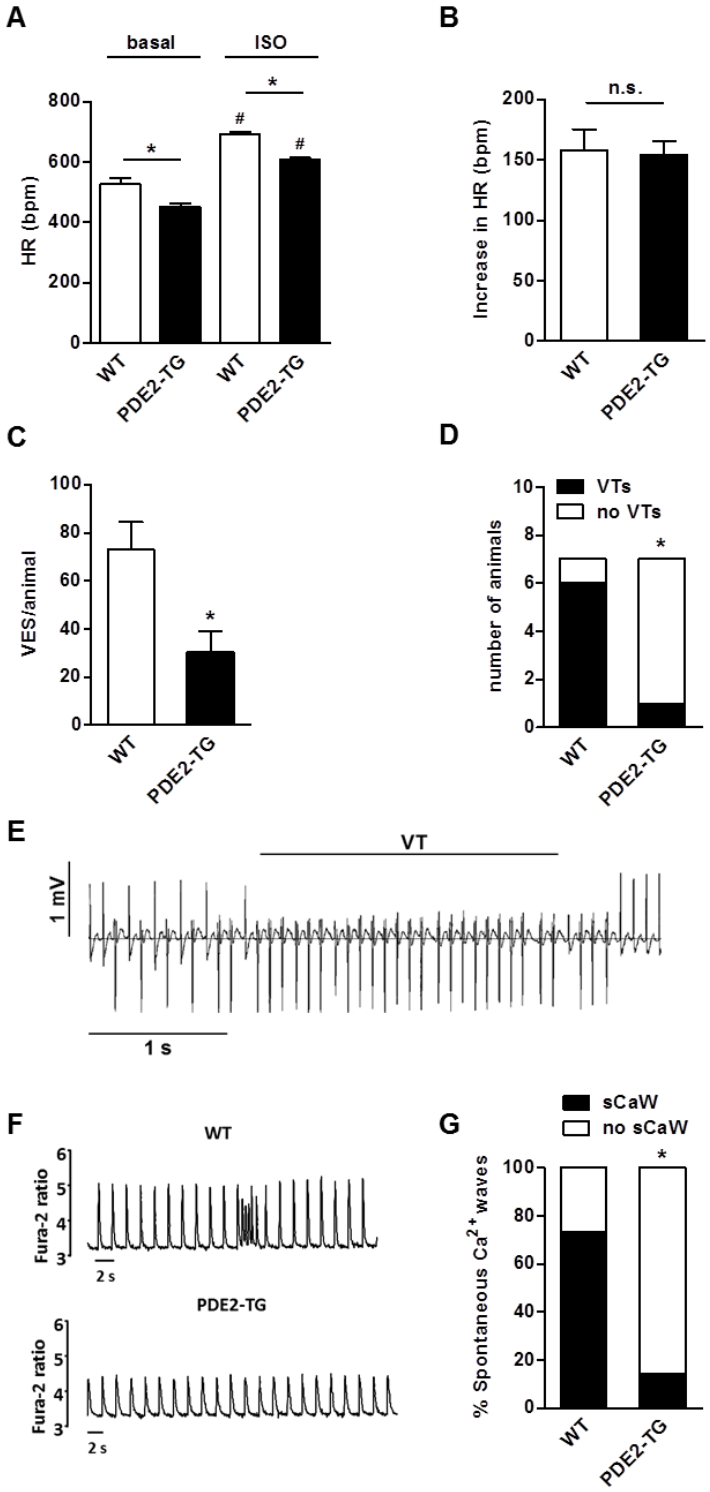
A
basal
ISO
HR (bpm)
WT
PDE2-TG
B
n.s.
Increase in HR (bpm)
C
VES/animal
D
VTs
no VTs
number of animals
E
VT
1 mV
1 s
F
WT
PDE2-TG
Fura-2 ratio
2 s
G
sCaW
no sCaW
% Spontaneous Ca2+ waves

Figure 6. PDE2 transgenic mice show the same absolute increase in heart rate after β-AR stimulation, but lower susceptibility to arrhythmic events. Heart rate was monitored after double ISO injection (2 mg/kg, i.p.; time interval between injections: 30 min) and analyzed for ventricular extra systoles (VES), salvos and ventricular tachycardia (VT) over a period of 90 min after the first application; n=7. (A) ISO-induced increase in heat rate (HR) calculated as an average of 5 s intervals. (B) Absolute increase over basal heart rate. (C) Total number of VES per animal. (D) Number of animals with VTs; n=7. (E) Representative trace of a WT animal showing VTs; with bigeminy (alternations of sinus beat and VES) before onset of VT. (F, G) Effect of PDE2 overexpression on spontaneous Ca^{2+} waves (sCaW) in mouse ventricular cells. (F) Representative traces of Ca^{2+} transients in Fura-2 loaded mouse ventricular cells isolated from WT or PDE2-TG mice paced at 0.5 Hz in the presence of 100 nmol/L ISO. (G) Percent of cells with sCaW in WT and PDE2-TG mice after ISO-treatment; n=3-4 animals/genotype with a total of 16-22 cells in each group. Statistical significance was determined by One-way ANOVA followed by Newman-Keuls multiple comparison test (A), Student's *t*-test to compare the two genotypes (B, C) and Fisher's exact test (D, G) to compare occurrence of events. *$p<0.05$ *vs*. WT, $^{\#}p<0.05$ *vs*. respective basal.

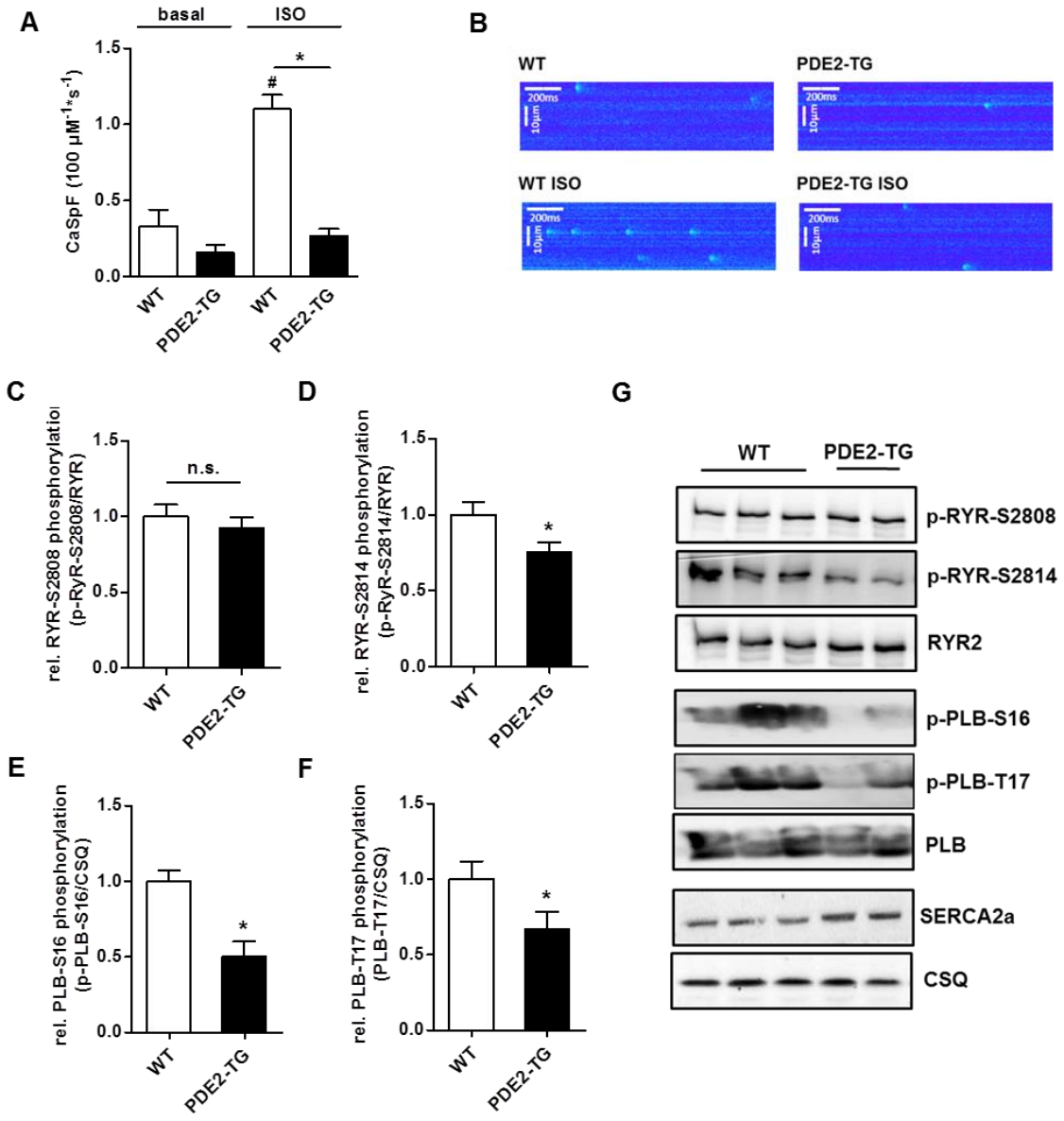

Figure 7. PDE2 transgenic mice show reduction in Ca^{2+} leak and phosphorylation of Ca^{2+} handling SR proteins in ventricular myocardium. (A, B) Ventricular myocytes were loaded with Fluo-3 AM and monitored for Ca^{2+}-sparks by laser scanning confocal microscopy under basal conditions and after stimulation with 100 nmol/L ISO. (A) Quantification of Ca^{2+}-spark frequency (CaSpF) normalized to cell width and scan rate. (B) Representative original recordings, n=4 animals/genotype. (C-G) Lysates prepared from ventricular myocardium were analyzed by immunoblot with the indicated specific antibodies. Protein phosphorylation was normalized to the respective total protein. (C-F) Quantification and (G) representative immunoblots showing additionally the expression levels of sarcolemma Ca^{2+} ATPase 2a (SERCA2a) and calsequestrin (CSQ); n=7-8 for each group. Statistical significance was determined by One-way ANOVA followed by Newman-Keuls multiple comparison test and Student's t-test to compare the two genotypes. *p<0.05 *vs*. WT, $^{\#}$p<0.05 *vs*. respective basal.

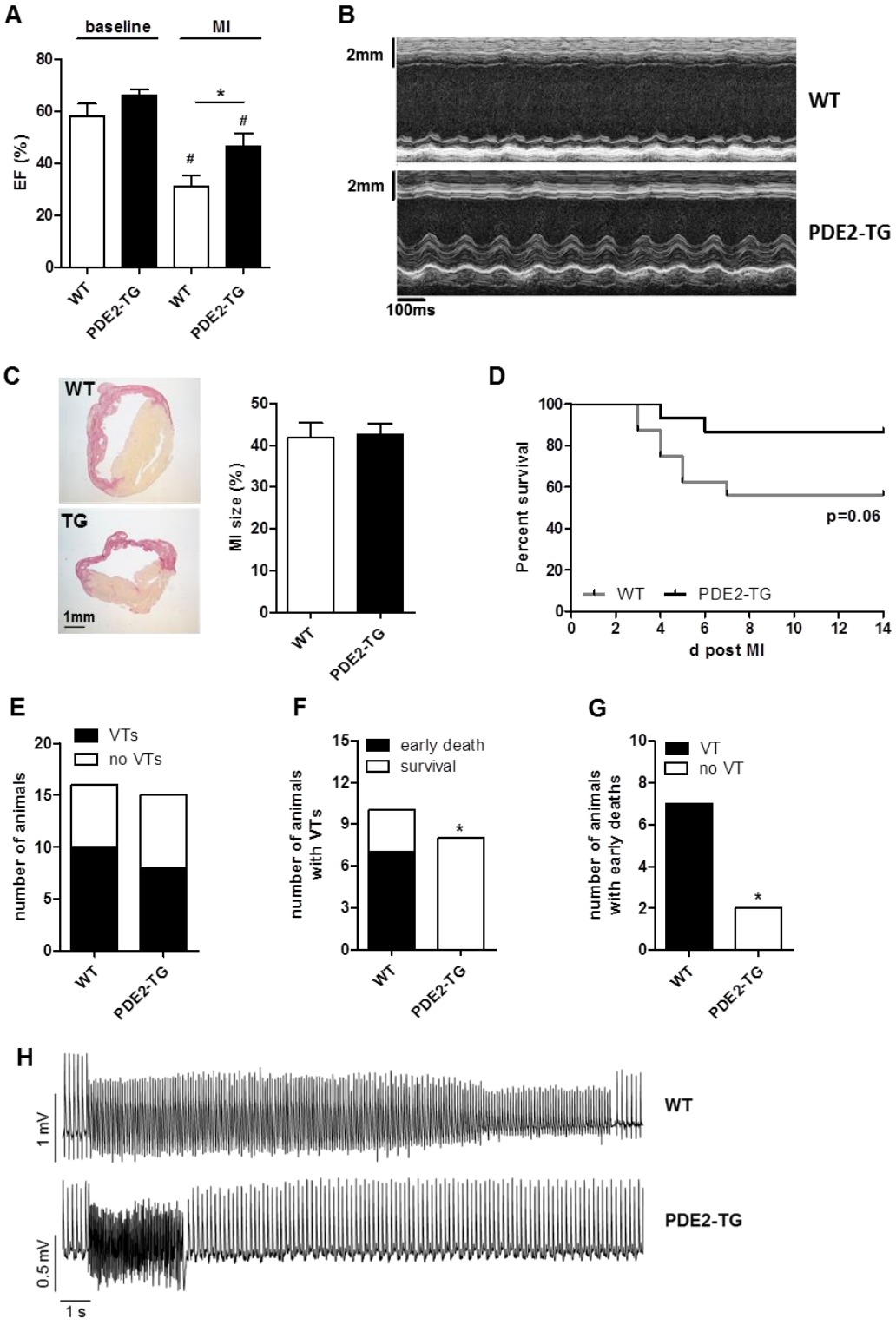
A
baseline
MI
EF (%)
WT
PDE2-TG
B
2mm
WT
PDE2-TG
100ms
C
WT
TG
1mm
MI size (%)
D
Percent survival
p=0.06
d post MI
E
VTs
no VTs
number of animals
F
early death
survival
number of animals with VTs
G
VT
no VT
number of animals with early deaths
H
1 mV
0.5 mV
1 s

Figure 8. PDE2-TG are protected from early death, sustained arrhythmias and decline of heart function after myocardial infarct (MI). (A) Ejection fraction calculated from echocardiographic analysis prior MI (baseline) and at day 14 post MI. (B) Representative M-Mode trace from infarcted area taken 14 d post MI. (C) *Left panel:* Representative Sirius Red staining of heart sections prepared from surviving animals at day 14; *right panel:* quantification of infarct size given as % of total tissue area. (D) % of surviving animals. Study was terminated 14 d post MI. (E, F, G) Analysis of ventricular tachycardia (VT) during the first 40 h post MI and association with early death events. (F) Representative ECG-traces showing a 17 s lasting VT in WT and 4 s in TG animals. Statistical significance was determined by One-way ANOVA followed by Newman-Keuls multiple comparison test (A), Long rank test (B), and Fischer's exact test (F, G). *$p<0.05$ *vs*. WT, $^{\#}p<0.05$ *vs*. respective baseline.

Supplemental Material

Cyclic Nucleotide Phosphodiesterase 2 Protects against Catecholamine-induced Arrhythmias and Preserves Contractile Function after Myocardial Infarction

Running title: *Vettel et al., PDE2 in arrhythmia and contractile function*

Christiane Vettel, PhD*; Marta Lindner*; Matthias Dewenter, MD*; Kristina Lorenz, PhD; Constanze Schanbacher; Merle Riedel, MD; Simon Lämmle, PhD; Simone Meinecke, MD; Fleur Mason, PhD; Samuel Sossalla, MD; Andreas Geerts; Michael Hoffmann; Frank Wunder, PhD; Fabian J. Brunner, MD; Thomas Wieland, PhD; Hind Mehel, PhD; Sarah Karam, PhD; Patrick Lechêne, BSc; Jérôme Leroy, PhD; Grégoire Vandecasteele, PhD; Michael Wagner, MD; Rodolphe Fischmeister, PhD[†,#]; Ali El-Armouche, MD[†,#]

From the Institute of Experimental and Clinical Pharmacology and Toxicology, University Medical Center Mannheim, Heidelberg University, Germany (C.V., T.W.); Department of Pharmacology, University Medical Center Göttingen (UMG) Heart Center, Georg August University Medical School Göttingen, Germany (C.V., M.D., M.R., S.M.); UMR-S 1180, INSERM, Université Paris-Sud, Université Paris-Saclay, Châtenay-Malabry, France (M.L., H.M., S.K., P.L., J.L., G.V., R.F.); Department of Molecular Cardiology and Epigenetics, University Hospital Heidelberg, Germany (M.D.); Institute of Pharmacology and Toxicology, University of Würzburg and Leibniz-Institut für Analytische Wissenschaften – ISAS – e.V., Dortmund, Germany (K.L., C.S.), Comprehensive Heart Failure Center, University of Würzburg, and West German Heart and Vascular Center Essen, Germany (K.L.); Institute of Pharmacology, University of Technology Dresden, Germany (S.L., M. W., A.EA.); Department of Cardiology and Pneumology, Center of Molecular Cardiology, UMG Heart Center, Georg August University Medical School Göttingen, Germany (F.M., S.S.); Department of Internal Medicine III: Cardiology and Angiology, University of Kiel, Germany (S.S.); BAYER Pharma AG, Wuppertal, Germany (A.G., M.H., F.W.); University Heart Center, Department of General and Interventional Cardiology, University Medical Center Hamburg-Eppendorf (F.J.B.). DZHK (German Centre for Cardiovascular Research), partner sites Heidelberg/Mannheim, Göttingen and Hamburg/Kiel/Lübeck, Germany (C.V., M.D., M.R., S.M., F.M., S.S., F.J.B., T.W.)

[#]Correspondence to Ali El-Armouche, Institute of Pharmacology, University of Technology Dresden, Medical Faculty Carl Gustav August, Fetscherstr. 74, 01307 Dresden, Germany. Phone: +49 351 458 6300, Fax: +49 351 458 6315; e-mail: ali.el-armouche@tu-dresden.de OR Rodolphe Fischmeister, INSERM UMR-S 1180, Université Paris-Sud, Faculté de Pharmacie, 5, Rue J.-B. Clément, F-92296 Châtenay-Malabry Cedex, France. Phone: 33.1.46.83.57.57; Fax 33.1.46.83.54.75; e-mail: rodolphe.fischmeister@inserm.fr

Detailed Methods

All experiments were carried out according to the European Community guiding principles in the care and use of animals (2010/63/UE, 22 september 2010), the local Ethics Committee (CREEA Ile-de-France Sud) guidelines and the French decree n° 2013-118, 1st February 2013 on the protection of animals used for scientific purposes (JORF n°0032, 7 February 2013 p2199, text n° 24). Authorizations were obtained from the Niedersächsisches Landesamt für Verbraucherschutz und Lebensmittelsicherheit (Germany) and Ministère Français de l'Agriculture, de l'Agroalimentaire et de la Forêt (agreement N°B 92-019-01).

Application of BAY 60-7550 for cardiovascular analysis, canine animal model
Evaluation of hemodynamic parameters was performed in beagle dogs according to GLP requirements using a dog model described earlier[1]. Both male and female animals were used at an age of 1 to 5.5 years and 9.5 to 16 kg body weight. Briefly, 12 Beagle dogs were subjected to general neuroleptic anesthesia (droperidol + fentanyl) and mechanical ventilation with nitrous oxide/oxygen (1:3). Administration formulations of BAY 60-7550 (BAY) were prepared in ethanol/polyethylene glycol 400 (1:9 v/v) and administered intraduodenally (i.d.) with an administration volume of 1-2 ml/kg in a dose range of 3, 10, and 30 mg/kg (n=3 dogs per group). Three control animals received the vehicle only. Dogs were instrumented with a Millar tip catheter placed into the abdominal aorta for measurement of systemic arterial blood pressure. A second Millar catheter equipped with a pressure and a velocity sensor was introduced into the heart via the left carotid artery. The pressure sensor was located within the left ventricle, the velocity sensor located in the ascending aorta to allow the measurement of stroke volume, left ventricular pressure (LVP) and the determination of left ventricular pressure rise (LV dP/dt), a surrogate for heart contractility. Heart rate was determined by ECG. Cardiac output (CO) and total peripheral resistance were calculated from stroke volume, heart rate and mean arterial blood pressure. At predefined time points at baseline and up to 240 min after administration, cardiovascular parameters were collected, stored and evaluated using P3 Plus Ponemah software (DSI).

Chronic isoproterenol administration
Isoproterenol (ISO, Sigma-Aldrich) was delivered to mice by subcutaneously implanted osmotic minipumps (Alzet, model 2002) that released ISO solved in 0.9% NaCl at a dose of 30 µg/g/d[2]. Anesthesia was performed with isoflurane (1.5% v/v). After 7 days, cardiac function was monitored by echocardiography. The mice used for this study were 2 month old littermates with a FVB/N background. Groups were age and sex matched.

Echocardiography
Animals were kept under light temperature and ECG-controlled anesthesia (isoflurane, 1.5% v/v or pentobarbital 35 mg/kg body weight (i.p.)) during the whole procedure. Echocardiography images (Vevo 770® System or 2100® System (MI), Visual Sonics Inc.) were obtained in a parasternal long and a short axis view at midpapillary and apical (representative M-mode pictures, MI) muscle level at a frame rate of 60 Hz. Long axis images were used to measure left ventricle length (L) during end-diastole (d) and end-systole (s). The thickness of the anterior (AWTh) and posterior wall (PWTh), the left ventricular diameter (LVD), the epicardial (EpiA) and endocardial (EndoA) area of the left ventricular cavity were obtained in the short axis or long axis (MI) view during d and s stages. Parameters were calculated as follows: %Fractional area shortening (%FAS) = (EndoAd – EndAs)/EndAd x 100; systolic volume (SV) = 5/6 x (EndoAd x Ld – EndoAs x Ls); cardiac output CO=SV x HR/1000; left ventricular weight (LVW) = 1.05 x 5/6 x [EpiAs x (Ls + (AWThs + PWThs)/2)) – EndoAs x Ls], where 1.05 is the specific gravity of muscle. %Ejection fraction = 100* ((7.0 / (2.4 + average diastolic diameter)* (average diastolic diameter)^3) – (7.0 / (2.4 + average systolic diameter) * (average systolic diameter)^3) / ((7.0 / (2.4 + average diastolic diameter)* (average diastolic diameter)^3). In MI, measurements were performed before and two weeks after left anterior descending coronary artery ligation.

Longevity study
Animals were kept under standard housing conditions until either natural death or any severe illness occurred (e.g. tumor growth, colic, age related decay etc.). Animals, which fell sick during the study were euthanized according to animal care guidelines to avoid unnecessary pain and counted as a naturally death event. The study was terminated after 38 months with 3 still living individuals. Groups were age and sex matched.

Implantation of ECG transmitters
Mice were anaesthetized with isoflurane (2% v/v) via mask ventilation and placed on a warming plate (37°). After the skin of the anterior thoracic region was depilated and disinfected, a 2 cm long median incision of the thoracic skin was made. The underlying tissue was prepared in order to create subcutaneous space for the ECG-transmitter (Data Sciences International, ETA-F10) and the electrodes. Afterwards, the ECG-transmitter was placed subcutaneously to the back of the mouse, the negative electrode was fixed to the right pectoralis fascia and the positive electrode was fixed 1 cm left to the xiphoid. The wound was closed using resorbable sutures. Alternatively, the transmitters were implanted into the peritoneal cavity. Buprenorphine 0.05 mg/kg s.c. once before starting the surgical procedure and metamizol 300 mg/kg p.o. from 2 days before to 7 days after the surgical procedure were used for intra- and postoperative analgesia. Recordings were started after a recovery time of at least two weeks post subcutaneous implantation of the telemetric transmitter). Recording and analysis parameters were set according to the manufacturer's instructions using P3 Plus software (DSI) or LabChart software (Chart 5.4, AD Instruments) and to conventional arrhythmia/frequency analysis guidelines[3-5]. Heart rate, activity and RR-intervals are given as either an average of 1 min or of 5 s intervals. Details are specified in the respective figure legends.

Isolation of adult mouse cardiomyocytes
Ventricular myocytes were obtained from 10 to 14 week old male mice. Animals were anesthetized by intraperitoneal injection of pentothal (150 mg/kg), and the heart was quickly removed and placed into cold Ca^{2+}-free Tyrode's solution containing (in mmol/L): NaCl 113, KCl 4.7, $MgSO_4$ 4, KH_2PO_4 0.6, NaH_2PO_4 0.6, BDM 10, $NaHCO_3$ 1.6, HEPES 10, Taurine 30, D-glucose 20, adjusted to pH 7.4. The ascending aorta was cannulated and the heart was perfused with oxygenated Ca^{2+}-free Tyrode's solution at 37°C during 4 min. For enzymatic dissociation, the heart was perfused with Ca^{2+}-free Tyrode's solution containing liberase TM research grade (Roche Diagnostics) for 10 min at 37°C. Then the heart was removed and placed into a dish containing Tyrode's solution supplemented with 0.2 mmol/L $CaCl_2$ and 5 mg/ml BSA (Sigma-Aldrich). The ventricles were separated from the atria, cut into small pieces, and triturated with a pipette to disperse the myocytes. Ventricular myocytes were filtered on gauze and allowed to sediment by gravity for 10 min. The supernatant was removed and cells were suspended in Tyrode's solution supplemented with 0.5 mmol/L $CaCl_2$ and 5 mg/ml BSA. The procedure was repeated once and cells were suspended in Tyrode's solution with 1 mmol/L $CaCl_2$. Freshly isolated ventricular myocytes were plated in 35 mm culture dishes coated with laminin (10 µg/ml) and stored at room temperature until use[6].

cAMP measurements by FRET
Adult mouse ventricular myocytes isolated from WT or PDE2-TG mice were infected with an adenovirus encoding the Epac-S^{H187} cAMP FRET probe for 24 h (kindly provided by Dr. Kees Jalink, Cancer Institute, Amsterdam, The Netherlands)[7]. Thereafter, the cells were washed once and maintained in a physiological buffer containing (in mmol/L): NaCl 144, KCl 5.4, $CaCl_2$ 1.8, $MgCl_2$ 1.8, and HEPES 20, pH 7.4 at room temperature. Images were captured every 5 s using the ×40 oil immersion objective of an inverted microscope (Nikon) connected to a Cool SNAP HQ2 camera (Photometrics) controlled by the Metafluor software (Molecular Devices). Cyan Fluorescent Protein (CFP) was excited for 300 ms by a Xenon lamp (Nikon) using a 440/20BP filter and a 455LP dichroic mirror. Dual-emission imaging of CFP and Yellow Fluorescent Protein (YFP) was performed using a Dual-View emission splitter equipped with a 510 LP dichroic mirror and BP filters 480/30 and 535/25 nm, respectively.

The YFP/CFP emission ratio upon 436 nm excitation (filters YFP 535 ± 15 nm, CFP 480 ± 20 nm) was measured. After each measurement, emission values were corrected for bleedthrough of CFP into the YFP channel. The imaging data was analyzed with Excel. All experiments were performed at room temperature.

$I_{Ca,L}$ measurements

The whole-cell configuration of the patch-clamp technique was used to record $I_{Ca,L}$. Pipette resistance was between 1–2 MΩ when filled with internal solution containing (in mmol/L): CsCl 118, EGTA 5, $MgCl_2$ 4, sodium phosphocreatine 5, Na_2ATP 3.1, Na_2GTP 0.42, $CaCl_2$ 0.062 (pCa 8.5), HEPES 10, adjusted to pH 7.3 with CsOH. Extracellular Cs^+-Ringer solution contained (in mmol/L): $CaCl_2$ 1.8, $MgCl_2$ 1.8, NaCl 107.1, CsCl 20, $NaHCO_3$ 4, NaH_2PO_4 0.8, D-glucose 5, sodium pyruvate 5, HEPES 10, adjusted to pH 7.4 with NaOH. For $I_{Ca,L}$ measurement, the cells were depolarized every 8 s from -50 to 0 mV for 400 ms and the maximal amplitude of whole-cell $I_{Ca,L}$ was measured as previously described[8]. The use of -50 mV as holding potential allowed the inactivation of voltage dependent sodium currents. K^+ currents were blocked by replacing all K^+ ions with external and internal Cs^+. Currents were not compensated for capacitance and leak currents. All experiments were performed at room temperature.

Measurements of Ca^{2+} transients, sarcomere shortening, SR Ca^{2+} leak and load

All experiments were performed at room temperature within 6 h after cell isolation. Isolated mouse ventricular cardiomyocytes were loaded with 3 µmol/L Fura-2 AM (Invitrogen) for 15 min in Ringer's solution containing (in mmol/L): KCl 5.4; NaCl 121.6; Na-pyruvate 5; $NaHCO_3$ 4.013; NaH_2PO_4 0.8; $CaCl_2$ 1.0; $MgCl_2$ 1.8; glucose 5 and HEPES 10 (pH 7,4 with NaOH). Sarcomere shortening and Fura-2 ratio (measured at 512 nm upon excitation at 340 and 380 nm) were simultaneously recorded in Ringer's solution, using a double excitation spectrofluorimeter coupled with a video detection system (IonOptix, Milton, MA, USA). Myocytes were electrically stimulated with biphasic field pulses (5 V, 4 ms) at a frequency of 0.5 Hz as previously described[9]. Because arrhythmias depend on the initial quality of cells, cardiomyocytes exhibiting spontaneous Ca^{2+} waves (sCaW) when perfused with control Ringer solution were discarded.

SR Ca^{2+} leak and load were measured according to a dedicated protocol[10]. Fura-2 loaded ventricular myocytes were paced by field stimulation at 0.5 Hz in normal Ringer's for few minutes until cellular Ca^{2+} transients reached a steady state. Directly after the last pulse, normal Ringer's was substituted for 30 s by a $0Na^+/0Ca^{2+}$ Ringer's in which Na^+ was replaced by Li^+ and supplemented with 10 mmol/L EGTA. This condition allowed measuring intracellular Ca^{2+} levels in a closed system without trans-sarcolemmal Ca^{2+} fluxes. Then, the cell was switched back to normal Ringer's and paced at 0.5 Hz until Ca^{2+} transient amplitude and sarcomere shortening reached steady-state. Again, following the last pulse, cells were perfused for 30 s with a $0Na^+/0Ca^{2+}$ solution including 1 mmol/L of the RyR2 inhibitor tetracaine. As a consequence, SR Ca^{2+} leak into the cytoplasm was prevented. SR Ca^{2+} leak was estimated as the difference between the Fura-2 ratio recorded at the end of the $0Na^+/0Ca^{2+}$ Ringer's perfusion with and without tetracaine. At the end of this protocol, tetracaine was washed out for at least 60 seconds and 10 mmol/L caffeine was applied to evaluate the total SR Ca^{2+} content.

Ca^{2+} transient amplitude was measured by dividing the twitch amplitude (difference between the end-diastolic and the peak systolic ratios) by the end-diastolic ratio, thus corresponding to the percentage of variation in the Fura-2 ratio. Similarly, sarcomere shortening was assessed by its percentage of variation, which is obtained by dividing the twitch amplitude (difference between the end-diastolic and the peak systolic sarcomere length) by the end-diastolic sarcomere length. Relaxation was assessed by measuring the time-to-50% relaxation from the time to peak shortening, and the Ca^{2+} transient decay was evaluated by measuring the time-to-50% decay of the Fura-2 ratio from the time to peak ratio. SR Ca^{2+} leak was measured by subtracting the ratio of fluorescence recorded in steady-state in $0Na^+/0Ca^{2+}$ Ringer's with tetracaine from the ratio recorded in steady-state in $0Na^+/0Ca^{2+}$ Ringer's without tetracaine. SR Ca^{2+} load was estimated by dividing the amplitude of the

caffeine-induced twitch (difference between the peak ratio obtained with caffeine and the diastolic ratio measured before tetracaine treatment) by the diastolic ratio. Fractional release was calculated by dividing the Ca^{2+} transient amplitude by the caffeine-induced twitch amplitude, thus corresponds to the fraction of Ca^{2+} released from the SR during a twitch. All parameters were calculated offline using IonWizard 6 (IonOptix).

Ca^{2+} spark analysis

Mice were sacrificed under isoflurane anesthesia (5% v/v) by cervical dislocation. 100 I.U. heparin was administered by intraperitoneal injection prior to isolation, to ensure sufficient perfusion of myocardium. Explanted hearts were retrogradely perfused on a Langendorff system, first with a Ca^{2+} free solution containing (in mmol/L) NaCl 113, KCl 4.7, KH_2PO_4 0.6, $Na_2HPO_4x2H_2O$ 0.6, $MgSO_4x7H_2O$ 1.2, $NaHCO_3$ 12, $KHCO_3$ 10, HEPES 10, taurine 30, BDM 10, glucose 5.5, phenol-red 0.032 (37°C, pH 7.4), followed by the addition of 7.5 mg/ml liberase 1 (Roche diagnostics) and trypsin 0.6% (Life Technologies) as well as 0.125 mmol/L $CaCl_2$. Upon becoming flaccid, ventricular and atrial myocardium were separated. Ventricular myocardium was cut into small pieces and dispersed in solution. Ca^{2+} concentration was increased in steps every 7 min until desired concentration was reached. Cells were plated on laminin-coated recording chambers and left to settle for 20 min.

Isolated mouse ventricular cardiac myocytes were incubated for 15 min at room temperature with a Fluo-3 AM loading buffer (10 µmol/L, Molecular Probes). Experimental solution contained (in mmol/L): KCl 4, NaCl 140, $MgCl_2$ 1, HEPES 5, glucose 10, $CaCl_2$ 2 (pH 7.4, NaOH, room temperature) plus isoproterenol (ISO) 100 nmol/L for the ISO experiments. Myocytes were superfused with experimental solution for 5-10 min before experiments commenced and during experiments to remove excess indicator and to allow time for complete deesterification of Fluo-3 AM. Ca^{2+} spark measurements were carried out on a laser scanning confocal microscope (LSM 5 Pascal, Zeiss) with a 40x oil-immersion objective. Fluo-3 was excited by an argon ion laser (488 nm). Emitted fluorescence was collected through a 505 nm long-pass emission filter. Fluorescence images were recorded in the line-scan mode (width of scan line: 38.4 µm, 512 pixels per line, pixel time: 0.64 µs, number of unidirectional line scans: 10,000, measurement period: 7.68 s). Confocal line scans were performed at rest after a brief period of field stimulation to load the SR (10 pulses, 1 Hz, 20 V). Ca^{2+} sparks were analyzed in SparkMaster for ImageJ. Mean spark frequency (CaSpF) was normalized to cell width and scan rate (100 $\mu m^{-1}*s^{-1}$).

Immunoblot analysis

Protein samples were prepared from pulverized ventricular myocardium and lyzed in buffer containing 30 mmol/L Tris/HCl (pH 8.8), 5 mmol/L EDTA, 30 mmol/L NaF, 3% SDS, and 10% glycerol. Samples were separated in denaturizing acrylamide gels and subsequently transferred onto nitrocellulose or PVDF membranes. After blocking the membranes with Roti®-block (Carl Roth) for 1 h, the incubation with anti-PDE2 (1:1,000, FabGennix), anti-calsequestrin (1:1,000, ThermoScientific), and anti-α-tubulin (1:2,000, Sigma-Aldrich) was carried out over night at 4°C. After incubation with appropriate secondary antibodies for 1 h, proteins were visualized by enhanced chemoluminescence and quantified with Quantity One software (Biorad).

Measurement of infarct size

Hearts were fixed in 4% (m/V) paraformaldehyde and embedded in paraffin. Hearts were sliced transversely (2 µm). Sections of the midpapillary region were stained with Sirius Red as described previously[11]. For the determination of the infarct size, the epicardial and endocardial infarct length and circumference was measured. Infarct size was calculated as follows: [(epicardial infarct length/ epicardial circumference) + (endocardial infarct length/endocardial circumference)/2] * 100 [12].

Supplemental Figures

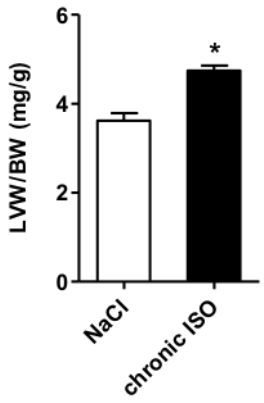

Suppl. Figure 1. ISO infusion induces left ventricular hypertrophy. Relative left ventricular weight (LVW) to body weight (BW) ratio in mice subjected to chronic ISO infusions (30 mg/kg/d for 7d) or NaCl (0.9%) as control; n=7-9. Statistical significance was determined by Student's *t*-test. *p<0.05 *vs*. NaCl.

A

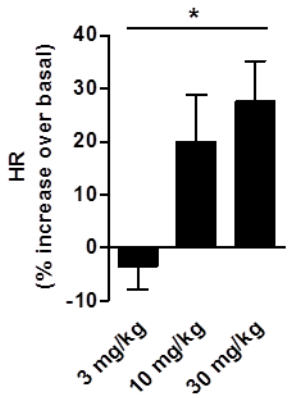

B

	HR beats/min	BPs mmHg	BPd mmHg	LVP mmHg	LV dP/dt mmHg/s	CO l/min	SV ml/beat
basal	78 ± 7.3	123 ± 7.6	71 ± 10.2	105 ± 6.9	2655 ± 133	1.1 ± 0.1	14 ± 2.8
control	74 ± 10.7	118 ± 4.8	68 ± 7.2	102 ± 4.0	2542 ± 68	0.9 ± 0.1	13 ± 2.4
basal	78 ± 3.5	124 ± 5.1	75 ± 5.5	105 ± 4.8	2715 ± 294	0.9 ± 0.1	11 ± 1.3
3 mg/kg	75 ± 2.5	132 ± 7.5	81 ± 6.4	111 ± 6.6	2598 ± 303	0.9 ± 0.1	12 ± 0.9
basal	83 ± 5.3	133 ± 6.7	82 ± 4.0	116 ± 6.4	3562 ± 355	1.1 ± 0.1	13 ± 1.7
10 mg/kg	100 ± 11.6	136 ± 4.6	89 ± 3.5	121 ± 4.9	3489 ± 253	1.2 ± 0.1	12 ± 2.1
basal	78 ± 1.7	126 ± 11.5	79 ± 7.9	110 ± 11.2	3099 ± 477	1 ± 0.2	13 ± 2.4
30 mg/kg	100 ± 7.8	119 ± 10.1	78 ± 6.7	106 ± 9.6	2957 ± 532	1.2 ± 0.4	12 ± 3.4

Suppl. Figure 2. Effect of PDE2-specific inhibitor BAY 60-7550 on hemodynamic parameters in beagle dogs. Effect of PDE2 inhibition in dogs exposed to the indicated doses of BAY 60-7550 (i.d.). Animals were anaesthetized, equipped with catheters (abdominal aorta, left ventricle and ascending aorta) and monitored by echocardiography over a period of 240 min post application. (A) Maximal increase in heart rate (HR) given as % over respective basal HR. (B) Table with assessed hemodynamic parameters at the time point of maximal increase in heart rate (HR): systolic and diastolic blood pressure (BPs, BPd), left ventricular pressure (LVP), cardiac output (CO), stroke volume (SV). Average of n=3 for each group. Statistical significance was determined by one-way ANOVA. *p<0.05 for linear trend.

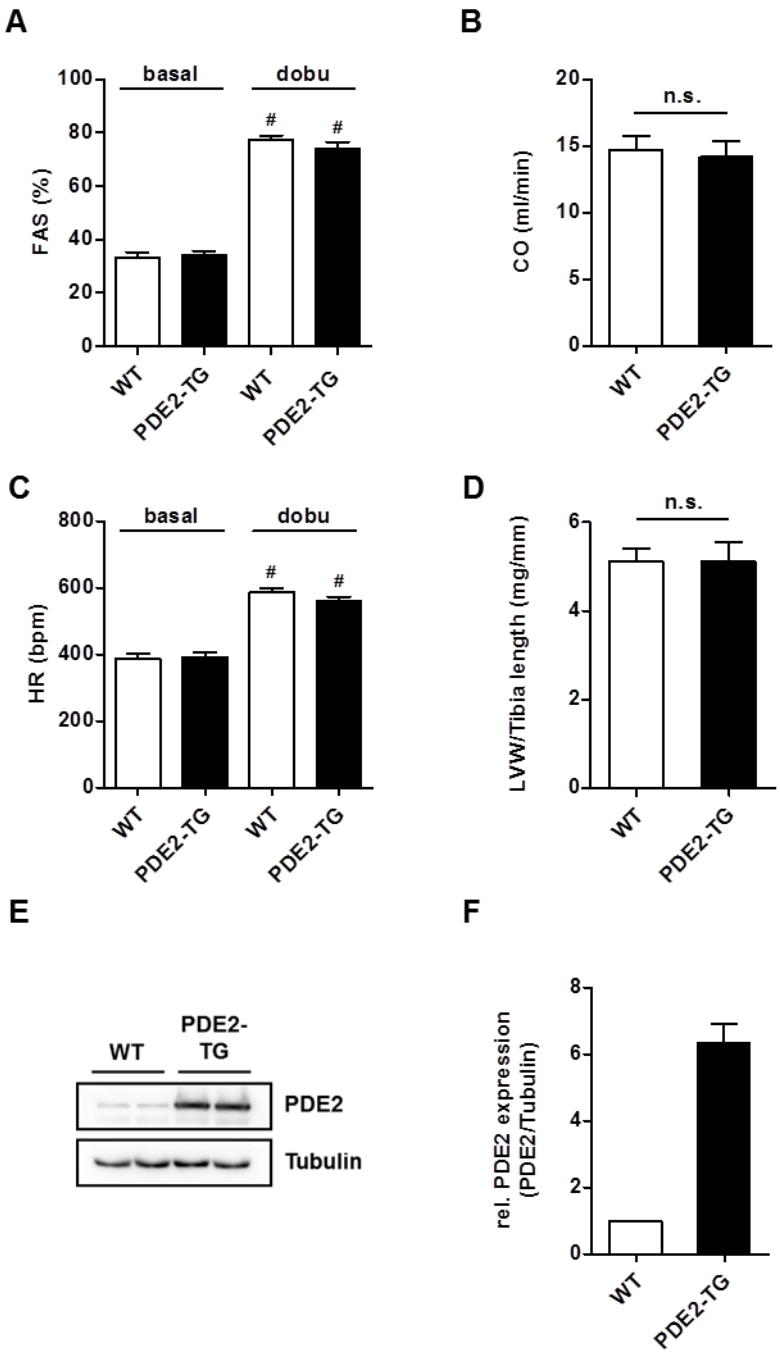

Suppl. Figure 3. Characterization of the lower expressing transgenic mouse line TG-4808. Echocardiographic determination of fractional area shortening (FAS, A), cardiac output (CO, B), and heart rate (HR, C) in anaesthetized 2-18 month old mice. Animals were treated with 10 mg/kg dobutamine (DOBU, i.p.) 2 min prior to measurements when indicated. (D) Left ventricular weight (LVW) calculated from the echocardiographic data and normalized to tibia length; n=12-14 for each group. (E, F) Lysates prepared from ventricular myocardium were analyzed by immunoblot with the indicated specific antibodies. PDE2 expression was normalized to tubulin and given relative to WT. (E) Immunoblots and (F) quantification; n=2 for each group Statistical significance was determined by one-way ANOVA followed by Newman-Keuls multiple comparison Test (A, C) and by Student's *t*-test (B, D). $^{\#}p<0.05$ *vs.* respective basal.

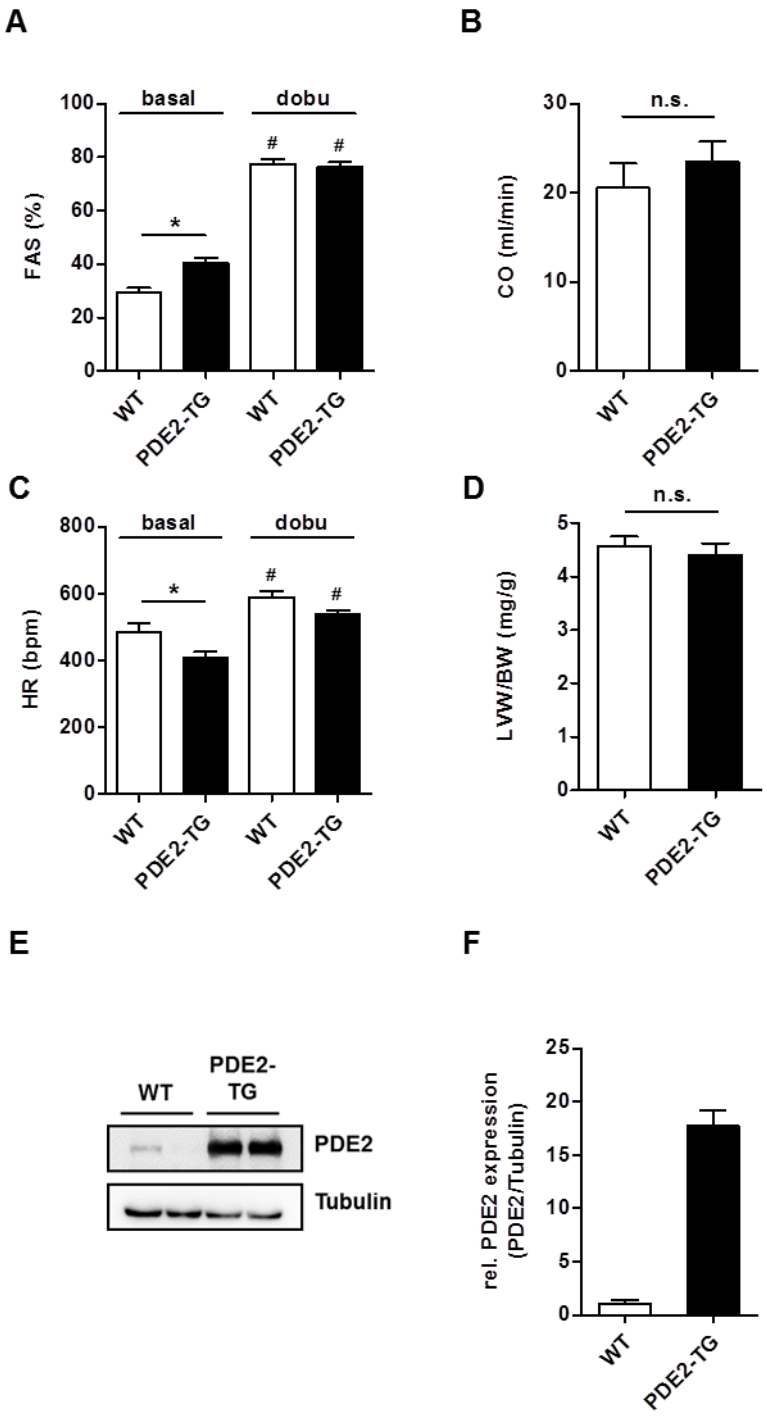

Suppl. Figure 4. Characterization of the higher expressing transgenic mouse line TG-4811. Echocardiographic determination of fractional area shortening (FAS, A), cardiac output (CO, B), and heart rate (HR, C) in anaesthetized 2-18 month old mice. Animals were additionally treated with 10 mg/kg dobutamine (DOBU, i.p.) 2 min prior to measurements when indicated. (D) Left ventricular weight (LVW) calculated from the echocardiographic data and normalized to body weight (BW); n=6-8 for each group. (E, F) Lysates prepared from ventricular myocardium were analyzed by immunoblot with the indicated specific antibodies. PDE2 expression was normalized to tubulin and given relative to WT. (E) Immunoblots and (F) quantification; n=2 for each group. Statistical significance was determined by one-way ANOVA followed by Newman-Keuls multiple comparison test (A, C) and by Student's *t*-test (B, D). *p<0.05 *vs.* WT, #p<0.05 *vs.* respective basal.

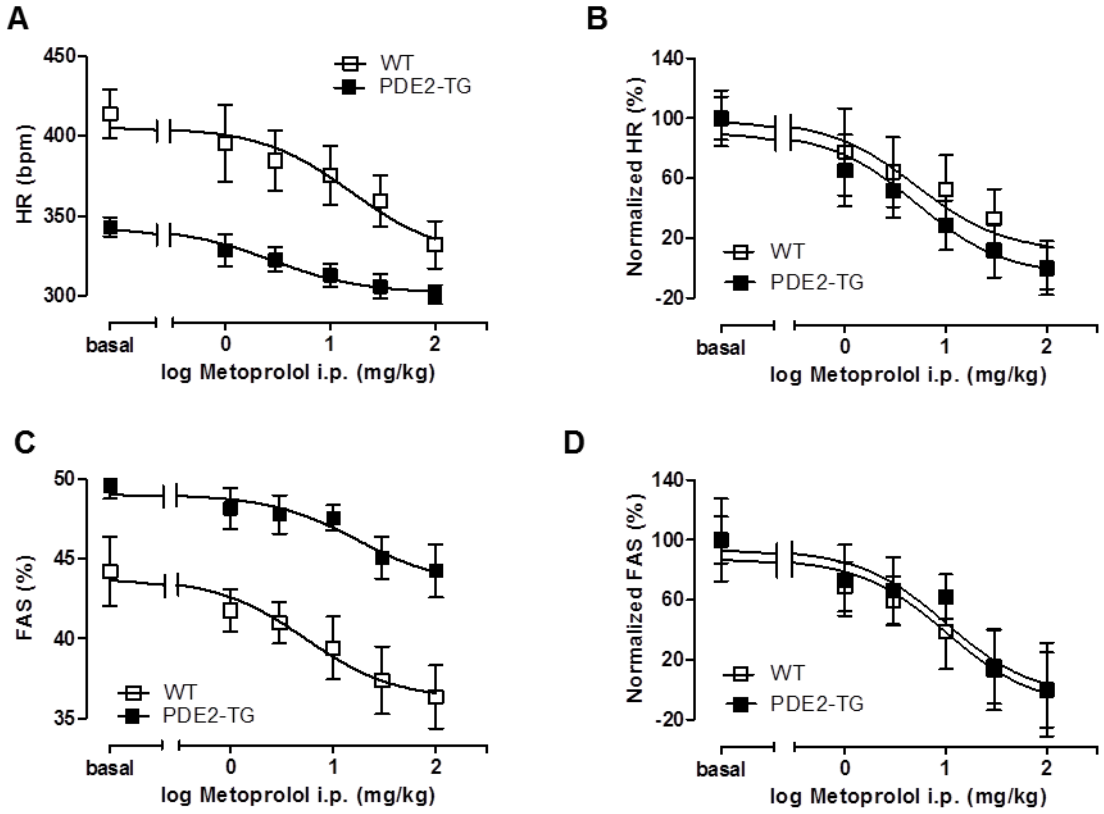

<u>Suppl. Figure 5.</u> Metoprolol reduced heart rate to a similar extent in WT and PDE2-TG, while basal hypercontractility of PDE2-TG was independent of β-AR activity. Echocardiographic determination of heart rate (HR, A) and fractional area shortening (FAS, C) in anaesthetized mice in the presence of increasing metoprolol doses (1, 3, 10, 30, 100 mg/kg, i.p.). (B, D) Normalization of (A, C) to compare logIC_{50} values with lowest values equal 0% and highest values equal 100%. Calculated IC_{50} for HR: 5 mg/kg and FAS: 10 mg/kg metoprolol.

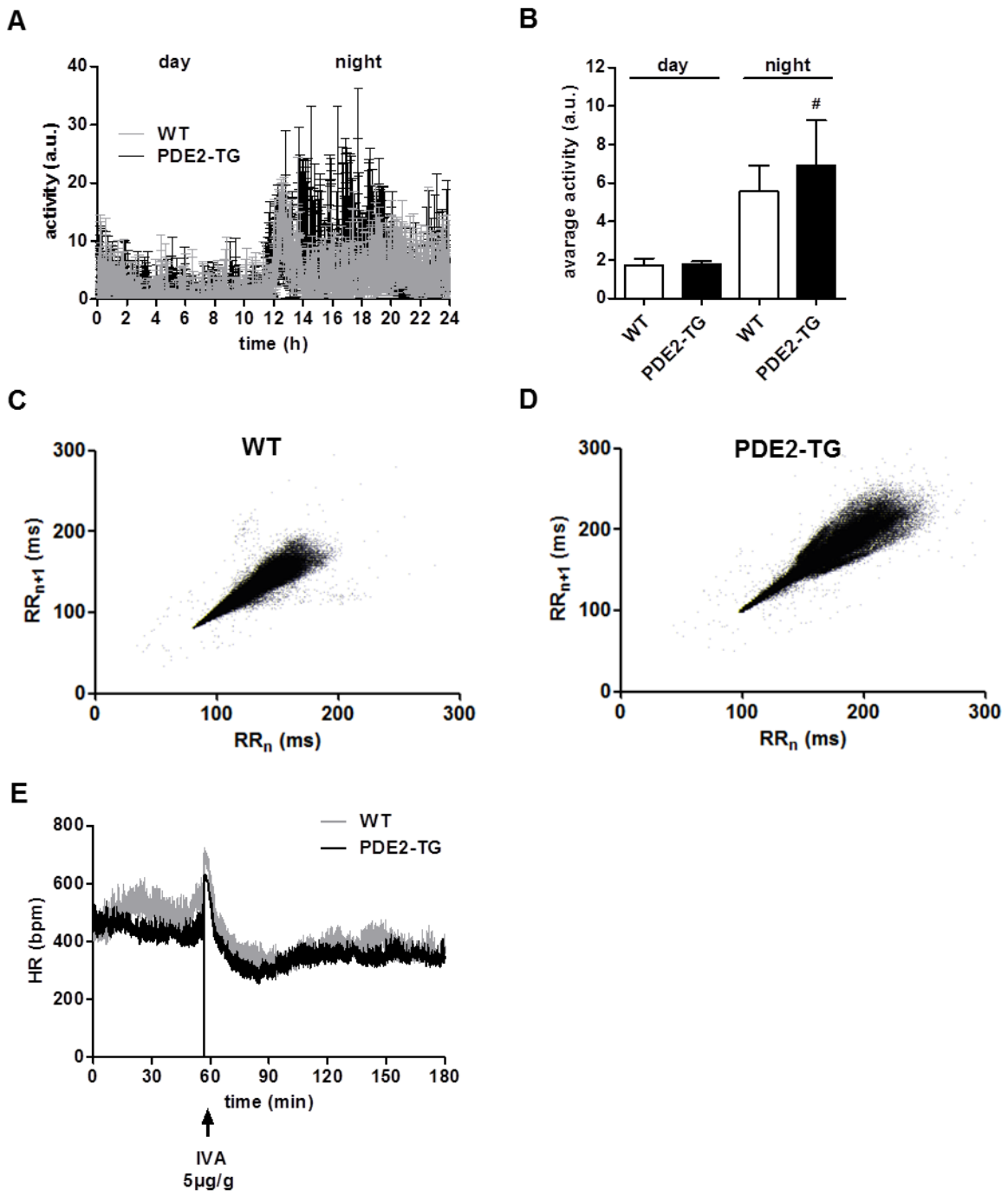

<u>Suppl. Figure 6.</u> ECG-Telemetry: Activity pattern and Poincaré plots of RR intervals documented over a period of 24 h. Application of HCN-Blocker Ivabradine (IVA). Animals (n=4 per genotype) were monitored by ECG-telemetry for a period of 72 h to calculate average changes in activity of a 24 h cycle. Activity was tracked as an average of 1 min intervals. (A) Average circadian changes in activity. (B) Average activity during day and night periods. Statistical significance was determined by one-way ANOVA followed by Newman-Keuls multiple comparison test. $^{\#}p<0.05$ *vs.* respective basal. (C, D) Representative Poincaré plot of a WT an TG animal regarding the distribution of daily RR intervals. Sinus arrest and AV block were excluded. (E) Average traces of IVA-application 45 min prior and 2 h after ivabradine (IVA) injection (5 mg/kg, i.p.). Frequencies were tracked as average of 5 s intervals; n=5.

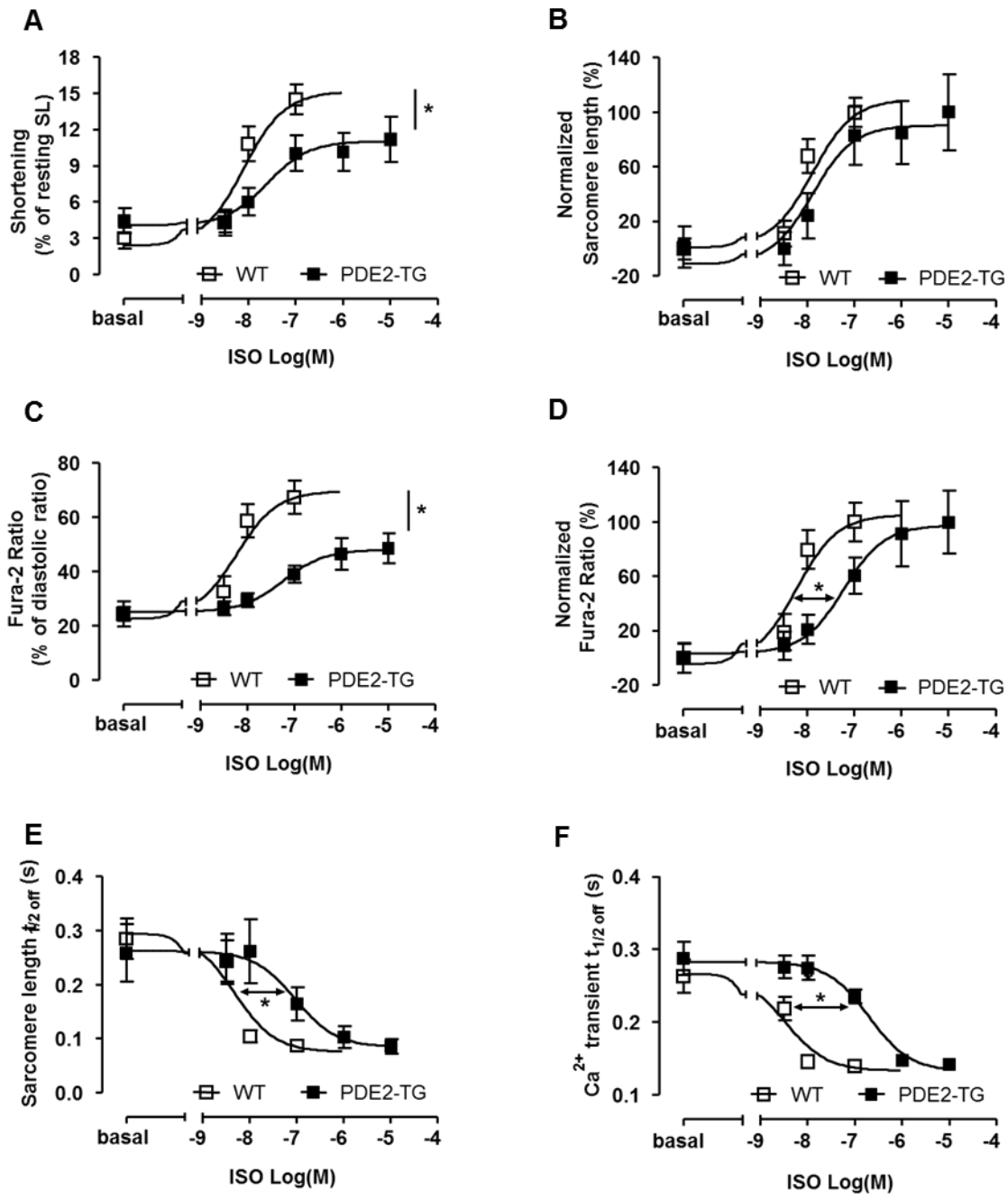

Suppl. Figure 7. PDE2 overexpression attenuates β-AR stimulation of Ca^{2+} transients and sarcomere shortening in cardiomyocytes. Adult ventricular myocytes isolated from WT or PDE2-TG mice were loaded with Fura-2 and stimulated at a frequency of 0.5 Hz in the absence or presence of increasing concentrations of ISO. Sarcomere length and Fura-2 ratio were recorded using an IonOptix System. Concentration-response relationship was extrapolated for WT cardiomyocytes under the assumption that 100 nmol/L ISO is sufficient for maximal responsivness. (A) Average amplitudes of sarcomere shortening. (B) Normalization of (A) to compare $logEC_{50}$ values with lowest values equal 0% and highest values equal 100%. (C) Average amplitudes of Ca^{2+} transients. (D) Normalization of (C) to compare $logEC_{50}$ values with lowest values equal 0% and highest values equal 100%. (E). Average amplitudes of half-time relaxation of sarcomere shortening ($t_{1/2\ off}$). (F) Average amplitudes of half-time relaxation of Ca^{2+} transients ($t_{1/2\ off}$). n=3-6 animals/genotype with 6-20 cells in each group. Data sets were subjected to comparison of fit regarding top values (efficacy) or $logEC_{50}$ (potency). *p<0.05 *vs*. WT.

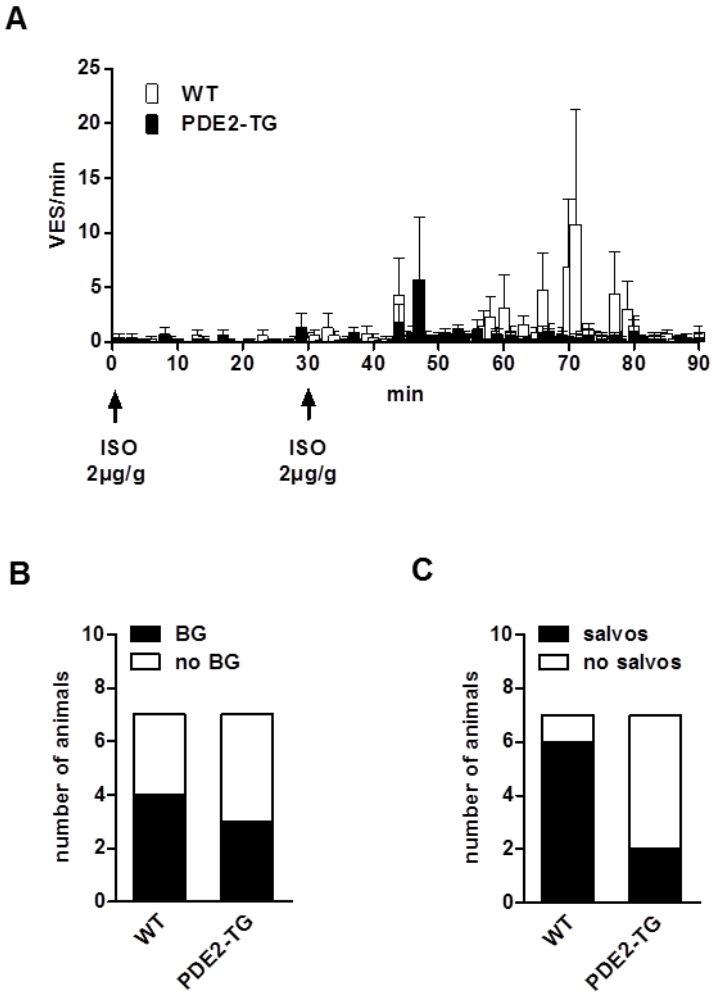

Suppl. Figure 8. Arrhythmia study in healthy mice. Heart rate was monitored after double ISO injection (2 mg/kg, i.p.; time intervall between injections 30 min) and analyzed for arrhythmic events such as ventricular extra systoles, bigeminy, salvos and VTs over a period of 90 min; n=7. (A) Average ISO-induced ventricular extra systoles (VES including salvos and ventricular tachycardia) per minute. Regular occurence of VES 15 min after the second injection of ISO in all animals. (B) Occurrence of bigemeny (BG) and (C) salvos in addition to main Fig. 4. Statistical significance was determined by Fisher's exact test to compare occurrence of events.

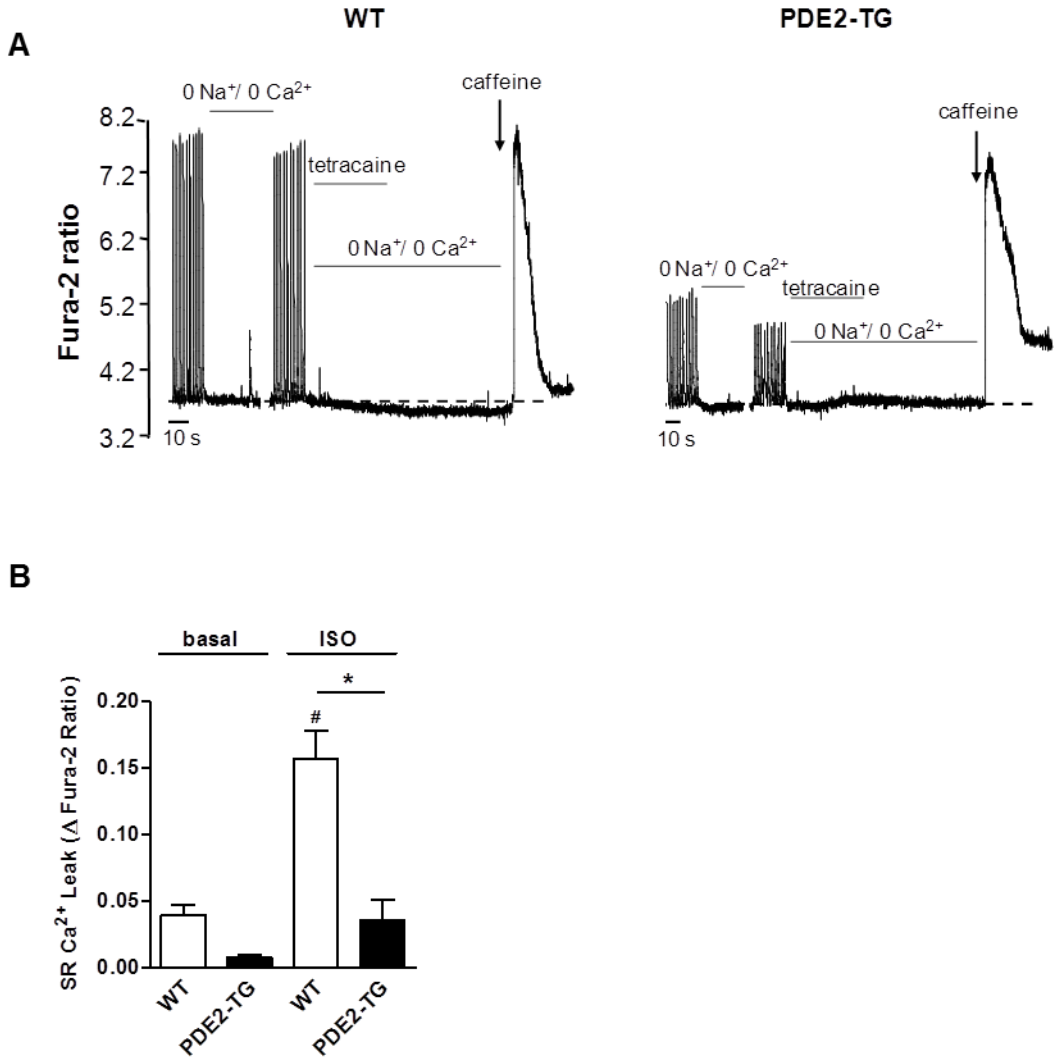

Suppl. Figure 9. SR Ca^{2+} leak (A) Representative traces of Ca^{2+} transients, sarcoplasmic reticulum (SR) Ca^{2+} leak and load measured in Fura-2 loaded adult mouse ventricular myocytes from WT (left) or PDE2-TG mouse (right) paced at 1 Hz, upon ISO (100 nmol/L) application. Tetracaine (1 mmol/L) was used to estimate SR Ca^{2+} leak, caffeine (10 mmol/L) to measure SR Ca^{2+} load. (B) Mean amplitude of the SR Ca^{2+} leak recorded in control or ISO. n=3 animals/genotype with 7-10 cells in each group. Statistical significance was determined by one-way ANOVA followed by Newman-Keuls multiple comparison test. *p<0.05 vs. WT, $^{\#}$p<0.05 *vs*. respective basal.

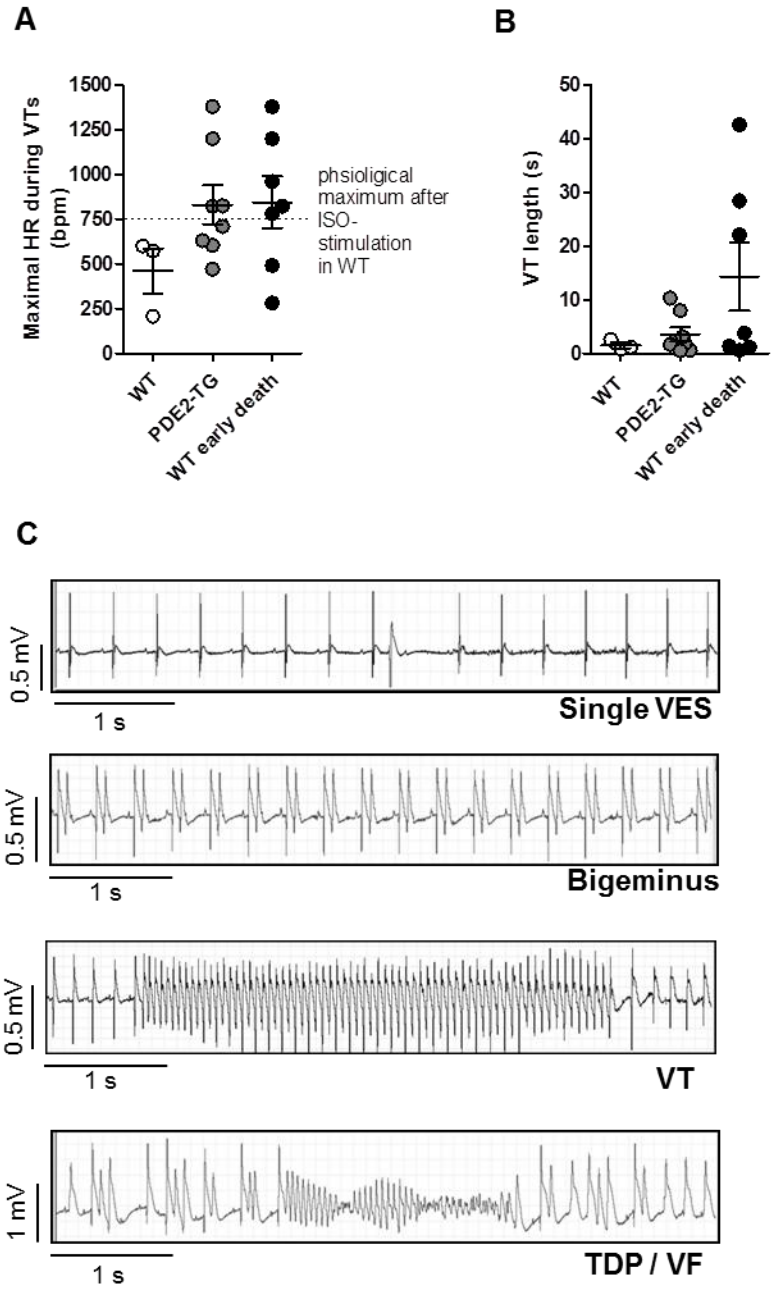

Suppl. Figure 10. Arrhythmic events post MI. (A, B) Qualitative analysis of ventricular tachycardia (VT) during the first 40 h post MI. For VT frequency and length calculations the highest frequency and longest VT of each individual animal was taken into account (n=3 for surviving WT with VT, n=8 for surviving PDE2-TG with VT, n=7 for early death WT with VT). (C) Examples of arrhythmic events. VES, ventricular extra systoles; TDP, torsade de pointes; VF, ventricular fibrillation.

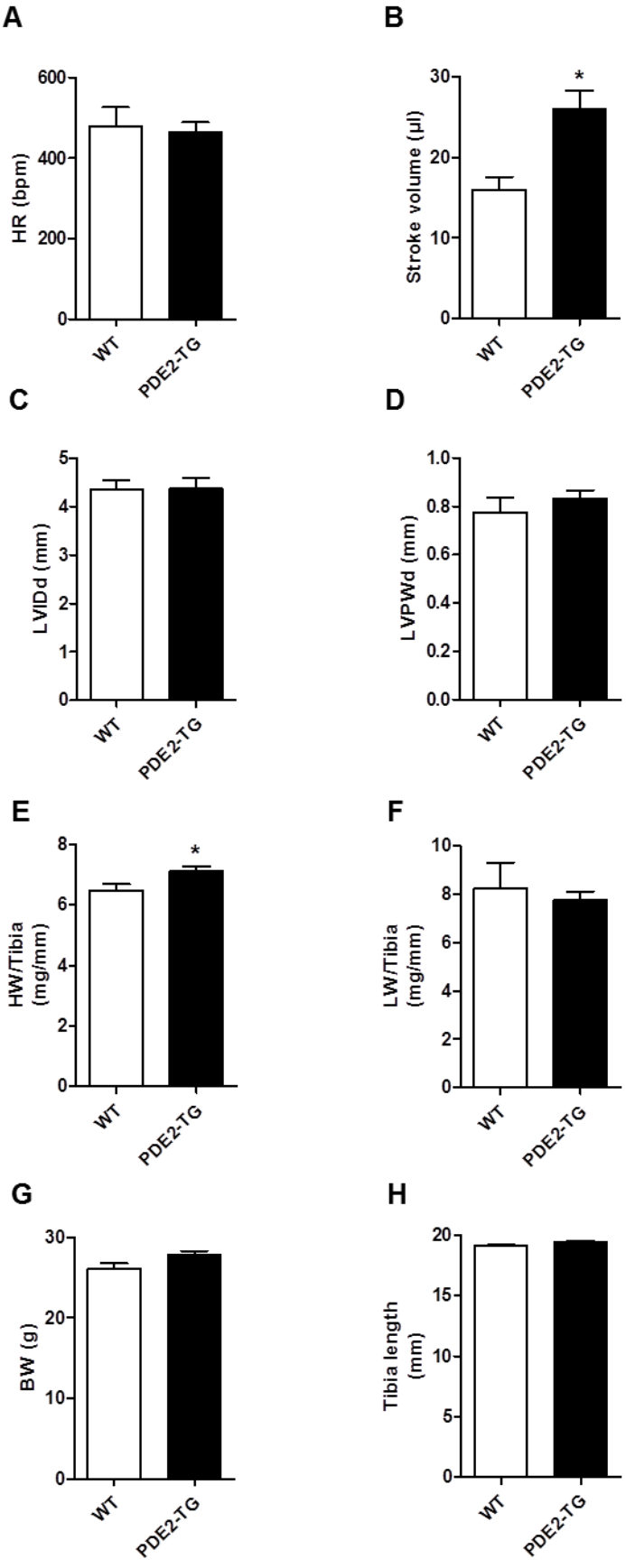
A
HR (bpm)
600
400
200
0
WT
PDE2-TG
B
Stroke volume (µl)
30
20
10
0
*
WT
PDE2-TG
C
LVIDd (mm)
5
4
3
2
1
0
WT
PDE2-TG
D
LVPWd (mm)
1.0
0.8
0.6
0.4
0.2
0.0
WT
PDE2-TG
E
HW/Tibia (mg/mm)
8
6
4
2
0
*
WT
PDE2-TG
F
LW/Tibia (mg/mm)
10
8
6
4
2
0
WT
PDE2-TG
G
BW (g)
30
20
10
0
WT
PDE2-TG
H
Tibia length (mm)
20
15
10
5
0
WT
PDE2-TG

Suppl. Figure 11. Echocardiographic parameters and heat weights after MI. Echocardiographic analysis 14 d post MI of (A) heart rate, (B) stroke volume, (C) left ventricular inner end-diastolic diameter and (D) left ventricular posterior wall end-diastolic diameter**.** Biometric data included determination of (E) heart weight (HW) to tibia length ratios, (F) lung weight (LW) to tibia length ratios, (G) body weight (BW) and (H) tibia length. Statistical significance was determined by Student's *t*-test. *p<0.05 *vs.* WT.

Supplemental References

1. Vormberge T, Hoffmann M, Himmel H. Safety pharmacology assessment of drug-induced qt-prolongation in dogs with reduced repolarization reserve. *Journal of pharmacological and toxicological methods*. 2006;54:130-140
2. El-Armouche A, Wittkopper K, Degenhardt F, Weinberger F, Didie M, Melnychenko I, Grimm M, Peeck M, Zimmermann WH, Unsold B, Hasenfuss G, Dobrev D, Eschenhagen T. Phosphatase inhibitor-1-deficient mice are protected from catecholamine-induced arrhythmias and myocardial hypertrophy. *Cardiovasc Res*. 2008;80:396-406
3. Heart rate variability. Standards of measurement, physiological interpretation, and clinical use. Task force of the european society of cardiology and the north american society of pacing and electrophysiology. *European heart journal*. 1996;17:354-381
4. Thireau J, Zhang BL, Poisson D, Babuty D. Heart rate variability in mice: A theoretical and practical guide. *Experimental physiology*. 2008;93:83-94
5. Walker MJ, Curtis MJ, Hearse DJ, Campbell RW, Janse MJ, Yellon DM, Cobbe SM, Coker SJ, Harness JB, Harron DW, et al. The lambeth conventions: Guidelines for the study of arrhythmias in ischaemia infarction, and reperfusion. *Cardiovasc Res*. 1988;22:447-455
6. Borner S, Schwede F, Schlipp A, Berisha F, Calebiro D, Lohse MJ, Nikolaev VO. Fret measurements of intracellular camp concentrations and camp analog permeability in intact cells. *Nature protocols*. 2011;6:427-438
7. Klarenbeek J, Goedhart J, van Batenburg A, Groenewald D, Jalink K. Fourth-generation epac-based fret sensors for camp feature exceptional brightness, photostability and dynamic range: Characterization of dedicated sensors for flim, for ratiometry and with high affinity. *PloS one*. 2015;10:e0122513
8. Verde I, Vandecasteele G, Lezoualc'h F, Fischmeister R. Characterization of the cyclic nucleotide phosphodiesterase subtypes involved in the regulation of the L-type Ca^{2+} current in rat ventricular myocytes. *British journal of pharmacology*. 1999;127:65-74
9. Leroy J, Richter W, Mika D, Castro LR, Abi-Gerges A, Xie M, Scheitrum C, Lefebvre F, Schittl J, Mateo P, Westenbroek R, Catterall WA, Charpentier F, Conti M, Fischmeister R, Vandecasteele G. Phosphodiesterase 4b in the cardiac L-type Ca^{2+} channel complex regulates Ca^{2+} current and protects against ventricular arrhythmias in mice. *The Journal of clinical investigation*. 2011;121:2651-2661
10. Shannon TR, Ginsburg KS, Bers DM. Quantitative assessment of the SR Ca^{2+} leak-load relationship. *Circulation research*. 2002;91:594-600
11. Lorenz K, Schmitt JP, Schmitteckert EM, Lohse MJ. A new type of erk1/2 autophosphorylation causes cardiac hypertrophy. *Nature medicine*. 2009;15:75-83
12. Takagawa J, Zhang Y, Wong ML, Sievers RE, Kapasi NK, Wang Y, Yeghiazarians Y, Lee RJ, Grossman W, Springer ML. Myocardial infarct size measurement in the mouse chronic infarction model: Comparison of area- and length-based approaches. *Journal of applied physiology*. 2007;102:2104-2111

II. Conclusions

In our study, we showed that in mice exposed to chronic ISO infusion, the positive chronotropic and inotropic effects of dobutamine were abrogated, suggesting desensitization of the β-ARs. These effects were reversed upon inhibition of PDE2 with Bay 60-7550 (Bay), restoring β-AR responsiveness. Inhibition of PDE2 with Bay had also an effect on control mice, doubling the impact of β-AR stimulation on heart rate.

These results suggest that the role of PDE2 seems to be restricted to heart rate regulation under physiological conditions.

Then, we showed that PDE2 overexpression displayed a significant decrease in basal heart rate and β-AR stimulated maximal heart rate and increase in basal contraction measured as fractional area shortening.

Next, we showed that PDE2 overexpression affects intracellular cAMP levels, the response to a short application of ISO was markedly blunted in PDE2 TG myocytes. PDE2 overexpression markedly attenuated the β-AR induced increase in $I_{Ca,L}$, Ca^{2+} transient and contractility in isolated cardiomyocytes from PDE2 TG mice. Then we showed that expression of SERCA2a, PLB and RyR2 remains unchanged in PDE2 TG mice, but PLB phosphorylation at S16 and T17 was significantly reduced. We also observed a reduction of RyR2 phosphorylation at CaMKII phosphorylation site.

The results of our studies let us assume that PDE2 upregulation in the heart can be an important defence mechanism by antagonizing β-AR/cAMP mediated cardiac toxicity. We think that PDE2 overexpression in the heart may represent a new, potential therapeutic strategy in HF.

The additional studies showing the effect of PDE2 overexpression on exercise capacity, heart remodelling (fibrosis measurements), cardiac hypertrophy are presented in the next chapter (Additional results).

III. Additional results

III.1 cAMP- and cGMP-hydrolytic activity of PDE2

Overexpression of PDE2 in the heart was confirmed with PDE2 assay. We measured cAMP- and cGMP-hydrolytic activity.

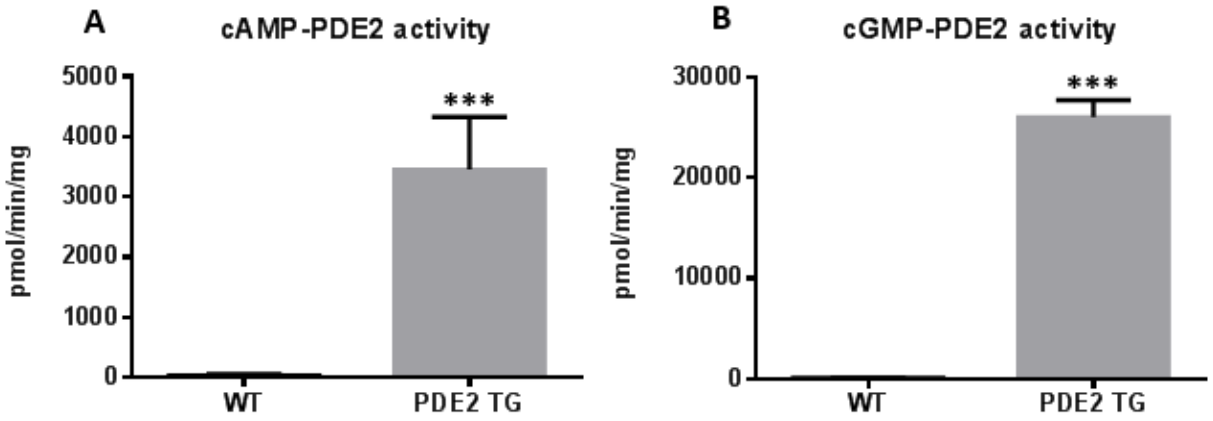

Figure 27: PDE2 activity in heart extracts from WT and PDE2 TG mice.
Specific PDE2 hydrolysis activity (A, B) was measured in heart extracts with radioenzymatic assay with 1 µM of cAMP (A) and 5 µM of cGMP (B) as substrate. Data are shown as mean±SEM, N=5 hearts for each group. Statistical significance was determined with Student's t-test, ***p<0.001 *vs.* WT.

Conclusion: cAMP- and cGMP-PDE2 hydrolytic activity is strongly increased in PDE2 TG mice as compared to WT mice.

III.2 Effect of PDE2 overexpression on exercise capacity

PDE2 overexpression exerts an effect similar to β-blockers on the heart. One of the limitations of β-blockers is a reduction in the exercise capacity resulting in a poor quality of life. To determine whether PDE2 overexpression decreases exercise capacity, we subjected mice to a forced treadmill activity and we calculated a maximal running distance.

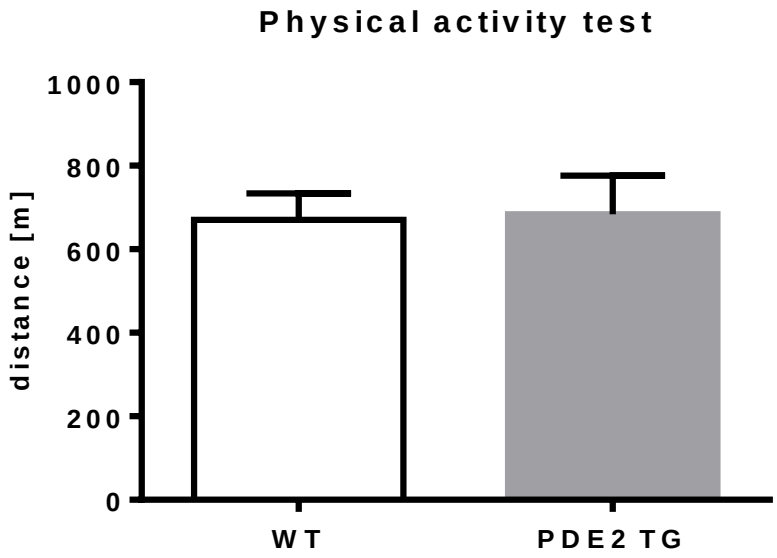

Figure 28: Similar training capacity of WT and PDE2 TG mice.
Forced treadmill activity is expressed as means of maximal running distance. Values are means±SEM, N=4 animals for each group. Statistical significance were determined by Student's t-test.

Conclusion: PDE2 overexpression does not change training capacity.

III.3 Effect of PDE2 overexpression on heart rate and developed pressure in isolated hearts

To determine whether higher contraction force in PDE2 TG mice is due to lower heart rate, hearts from WT and PDE2 TG mice were isolated and perfused using the Langendorff system. Hearts from WT and PDE2 TG mice were electrically paced at the same heart rate (450 bpm) and we measured left ventricular developed pressure (LVDP).

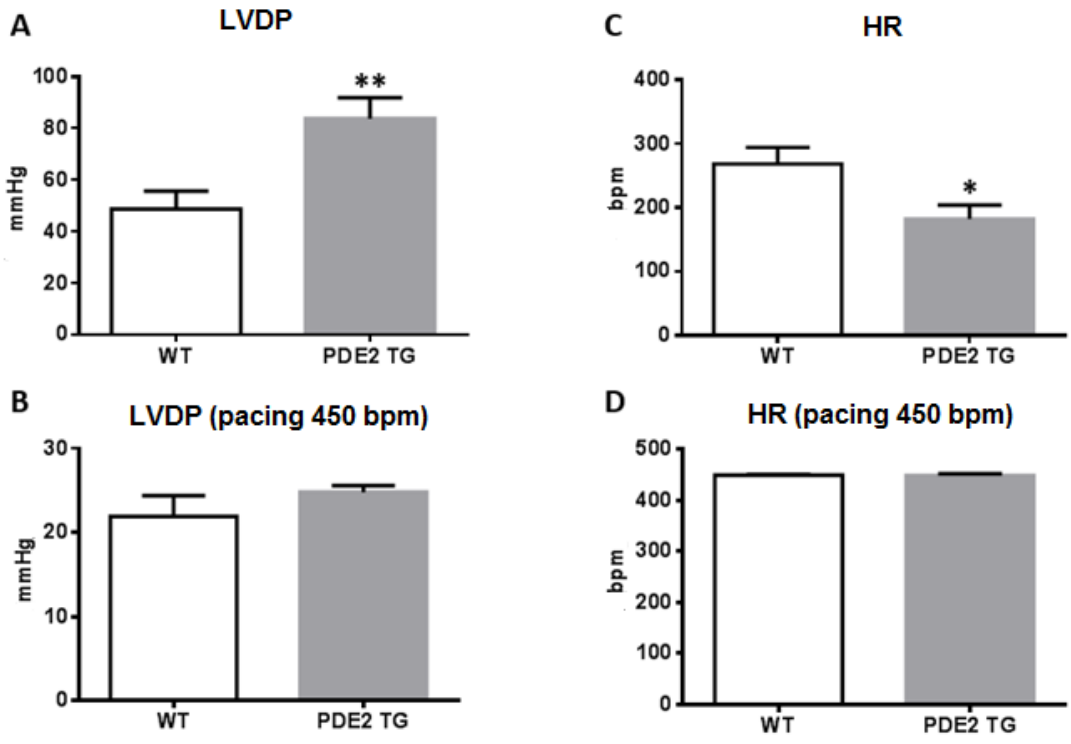

Figure 29: The higher contractility in PDE2 TG mice is due to lower heart rate.
Hearts from WT and PDE2 TG mice were isolated and perfused using the Langendorff system. Left ventricular developed pressure (LVDP) (A, B) and heart rate (HR) (C, D) were determined without (A, C) or with electrically pacing at 450 bpm (B, D). Data are shown as mean ± SEM, N=4 animals for each group. Statistical significance was determined by Student's t-test: * $p<0.05$, ** $p<0.01$ *vs.* WT.

Conclusion: The higher contractility of PDE2 TG *vs.* WT mice is observed in spontaneously beating hearts (Figure 29A) but not anymore when comparing LVDP between WT and PDE2 TG hearts paced at the same frequency (Figure 29B). We can thus conclude that the higher contractility in PDE2 TG mice is due to the lower heart rate observed in these animals (Figure 29C).

Then, we determined the effect of PDE2 overexpression on heart rate and contractility under β-AR stimulation (using increasing concentration of ISO).

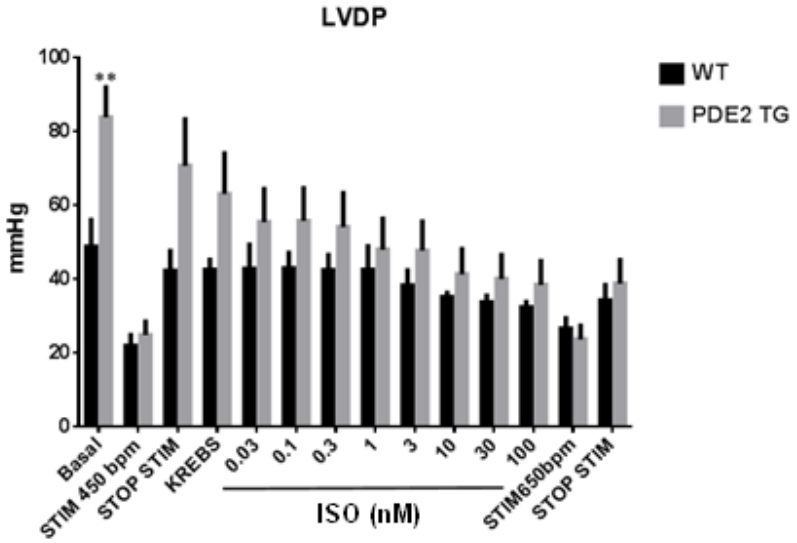

Figure 30: Contractility of Langendorff perfused hearts from WT and PDE2 TG mice during β-AR stimulation.

Hearts from WT and PDE2 TG mice were isolated and perfused with increasing concentrations of isoprenaline (ISO) using the Langendorff system. LV developed pressure (LVDP) was recorded. Data are shown as mean ± SEM, N=4-9 hearts for each condition. Statistical significance was determined by Student's t-test: **p<0.01 *vs.* WT.

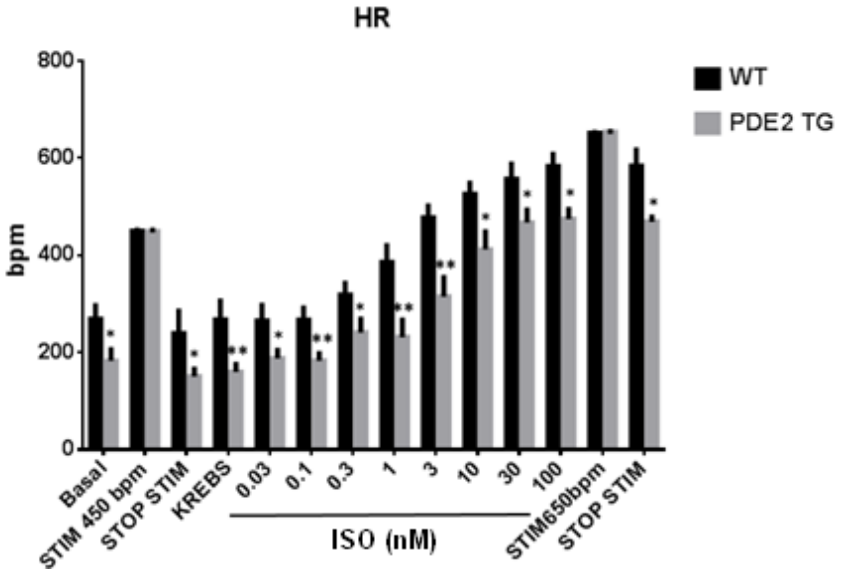

Figure 31: Lower heart rate in Langendorff perfused hearts from PDE2 TG *vs.* WT mice during β-AR stimulation.

Hearts from WT and PDE2 TG mice were isolated and perfused with increasing concentrations of isoprenaline (ISO) using the Langendorff system. Heart rate (HR) was recorded. Data are

shown as mean ± SEM, N=4-9 hearts for each condition. Statistical significance was determined by Student's t-test: *p<0.05, **p<0.01 *vs.* WT. Same set of experiments as in Figure 30.

Next, to determine the myocardial workload, we calculated the rate pressure product (RPP). This index is a direct indication of the energy demand of the heart, thus is a good measure of the energy consumption of the heart.

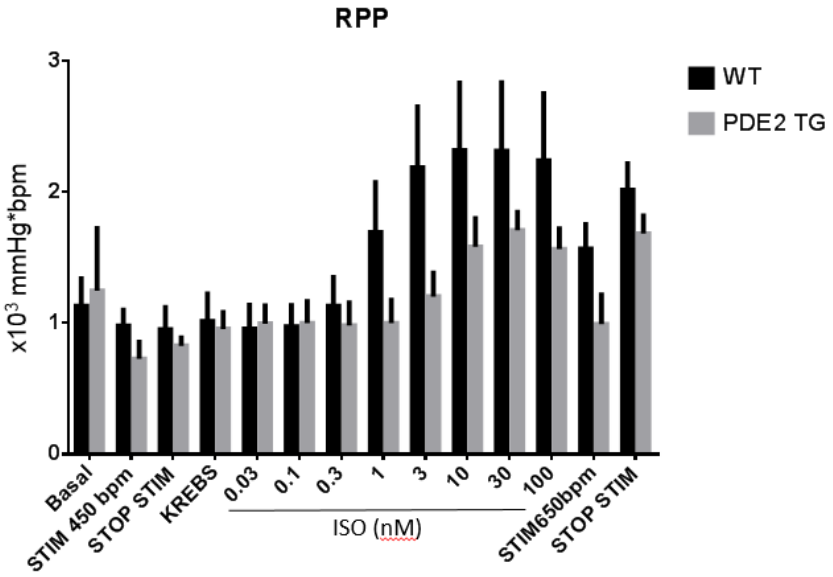

Figure 32: Rate pressure product in Langendorff perfused hearts from WT and PDE2 TG mice during β-AR stimulation.
Hearts from WT and PDE2 TG mice were isolated and perfused with increasing concentrations of isoprenaline (ISO) using the Langendorff system. Rate pressure product (RPP) was calculated as the product of LVDP (from data in Figure 30) and HR (from data in Figure 31). Data are shown as mean ± SEM, N=4-9 hearts for each condition. The differences were not statistically significance (Student's t-test).

Conclusion: ISO resulted in a stimulatory effect on the HR. HR was significantly lower in hearts isolated from PDE2 TG mice as compared to WT (Figure 31) at all concentration of ISO. ISO had the expected positive inotropic effect at all concentration. The contractile responses of isolated hearts from PDE2 TG and WT mice to ISO were not significantly different (Figure 30). However there is a tendency toward higher LVDP in PDE2 TG hearts. Similarly, there was no significant difference in changes of RPP in response to ISO (Figure 32) but with a tendency toward lower RPP in PDE2 TG hearts suggesting a lower myocardial oxygen consumptions by PDE2 TG hearts.

III.4 Effects of PDE2 overexpression on cardiac remodeling

To determine the long-term effects of PDE2 overexpression on cardiac morphology and to see whether higher contraction force in PDE2 TG mice is associated with cardiac hypertrophy, we measured heart-weight-to-body-weight ratio in WT and PDE2 TG mice at different ages: 10, 54 and 104 weeks.

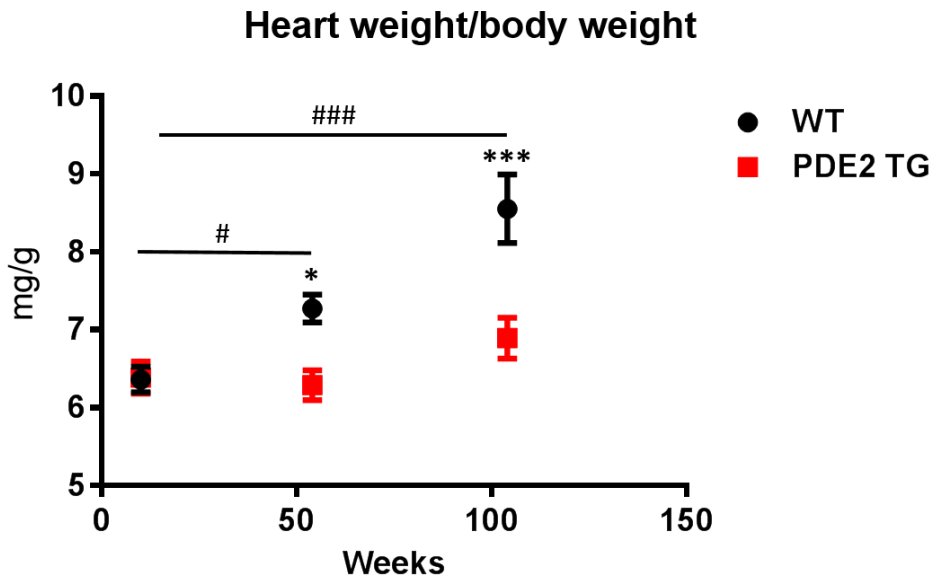

Figure 33: Heart weight to body weight ratio.
Heart weight to body weight ratio was measured in WT and PDE2 TG mice at different ages: 10, 54 and 104 weeks. Weight of the heart was determined after isolation at sacrifice and the ratio to animal's body weight was calculated. Data are shown as mean±SEM, N=6-14 animals per each group. Statistical significance was determined by Two way ANOVA followed by Sidak's test, *p<0.05 PDE2, ***p<0.001 TG *vs.* WT, $^{\#}$p<0.05, $^{\#\#\#}$p<0.001 WT *vs.* HW/BW ratio at age of 10 weeks.

Conclusion: Ageing is classically associated with a development of cardiac hypertrophy in mice (Elias *et al.*, 1977; Loffredo *et al.*, 2013). While we confirmed this observation and found an increase in the relative cardiac mass with age in WT animals, we found that heart-weight-to-body-weight ratio did not increase in PDE2 TG mice. Thus, PDE2 overexpression protects the heart against age-dependent hypertrophic growth. Also, these results demonstrate that the higher contraction force is not due to increased cardiac mass.

To determine whether PDE2 overexpression has an impact on myocardial remodeling, we measured left ventricular interstitial fibrosis determined as the collagen volume fraction of myocardial tissue.

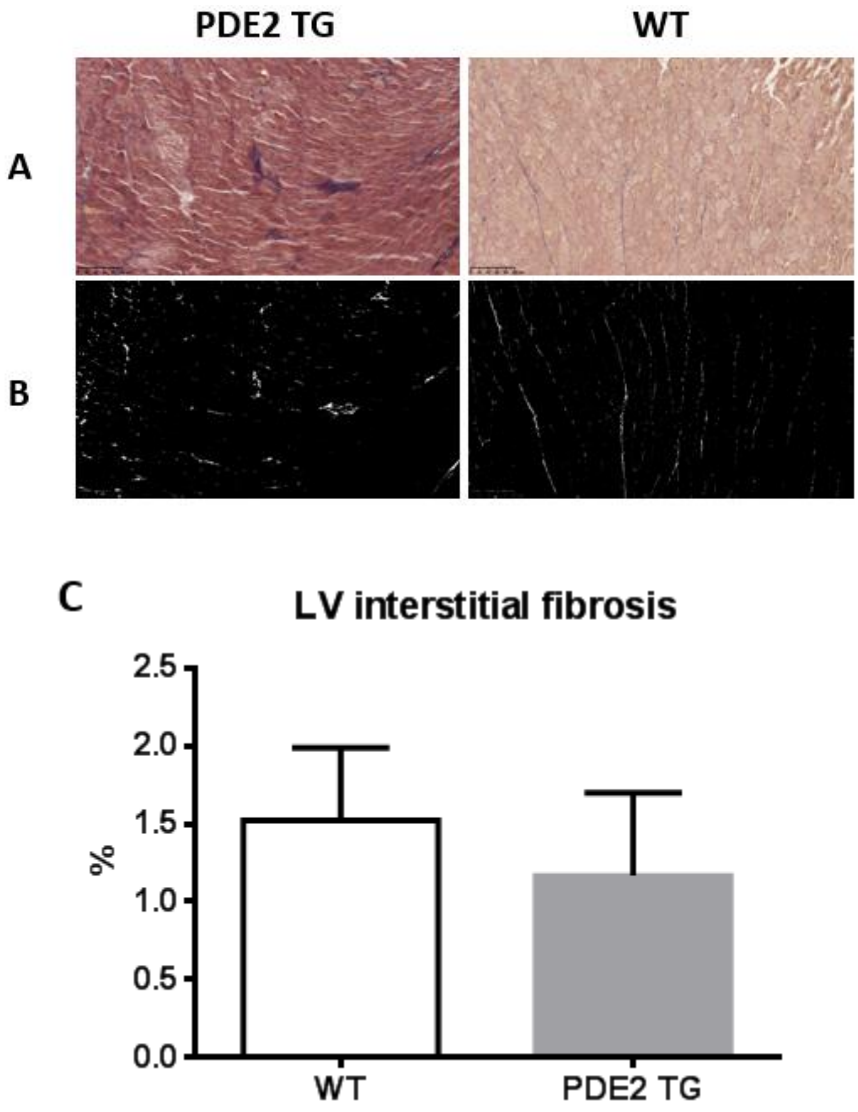

Figure 34: Left ventricular interstitial fibrosis by Masson's Trichrome Staining.
Representative images of hematoxylin and Masson's trichrome staining in WT and PDE2 TG mice. Blue color in A and white colour in B indicate the interstitial collagen fibril deposition. C, Data are shown as mean±SEM, N=4 animals for each group. There was no statistically significant difference between the two mouse models (Student's t-test).

Conclusion: PDE2 overexpression does not increase left ventricular interstitial fibrosis.

Then, we measured gene expression level of hypertrophic markers, ANP and BNP, in WT and PDE2 TG mice. We determined also the level of circulating BNP in blood serum in WT and PDE2 TG mice.

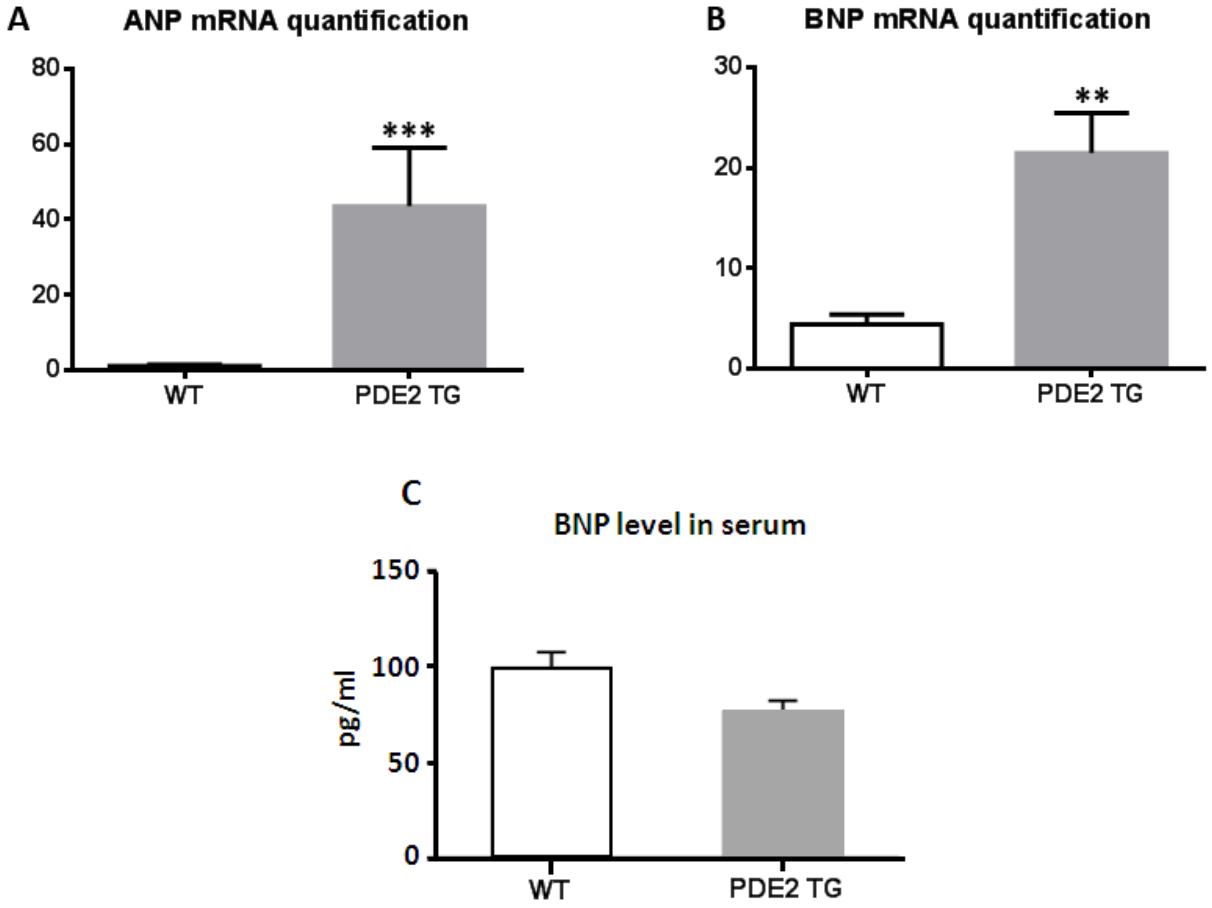

Figure 35: ANP and BNP quantification.
mRNA quantification of ANP and BNP from heart tissue (A, B) and circulating BNP level measured in serum (C). Data are presented as mean±SEM, n=4 animals for each group. Statistical significance was determined with Student's t-test: **p<0.01, ***p<0.001 *vs.* WT.

Conclusion: ANP and BNP expression levels are increased in PDE2 TG mice, even though this is not associated with cardiac hypertrophy.

III.5 Effect of PDE2 overexpression on the cardiac hypertrophy induced by a chronic isoproterenol infusion

To characterize the contribution of PDE2 to cardiac function under chronic β-AR stimulation, WT and PDE2 TG mice were exposed to a chronic ISO infusions (subcutaneously implanted minipumps, 60 mg/kg/d for 14 days) or NaCl (0.9%) as control.

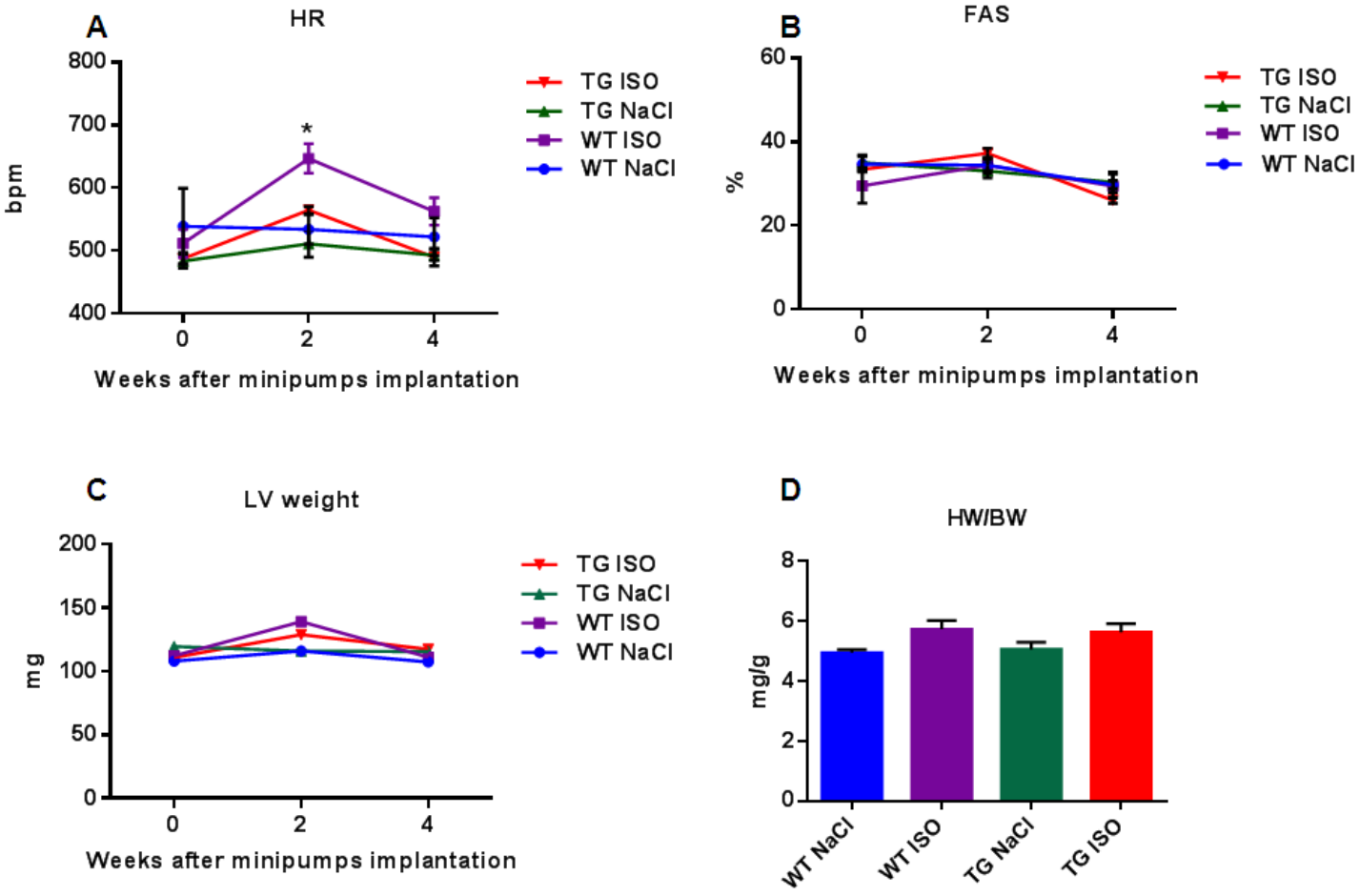

Figure 36: Lower heart rate in PDE2 TG mice chronically treated with ISO.
Effect of PDE2 overexpression in mice exposed to chronic ISO infusions for 14 days (60 mg/kg/day) or treated with a vehicle (0.9% NaCl). Animals were anaesthetized and monitored by echocardiography before implantation of minipumps, and 2 and 4 weeks after implantation. A: heart rate (HR), B: fractional area shortening (FAS), C: left ventricle (LV) weight, D: weight of the heart was determined after isolation at sacrifice and the ratio to animal's body weight was calculated. Data are shown as mean±SEM, n=3-8 animals per each group. Statistical significance was determined by Two-way ANOVA with Sidak's multiple comparison test: * $p<0.05$ TG ISO *vs.* WT ISO.

Then, we measured collagen volume fraction in myocardial tissue to evaluate the amount of interstitial fibrosis.

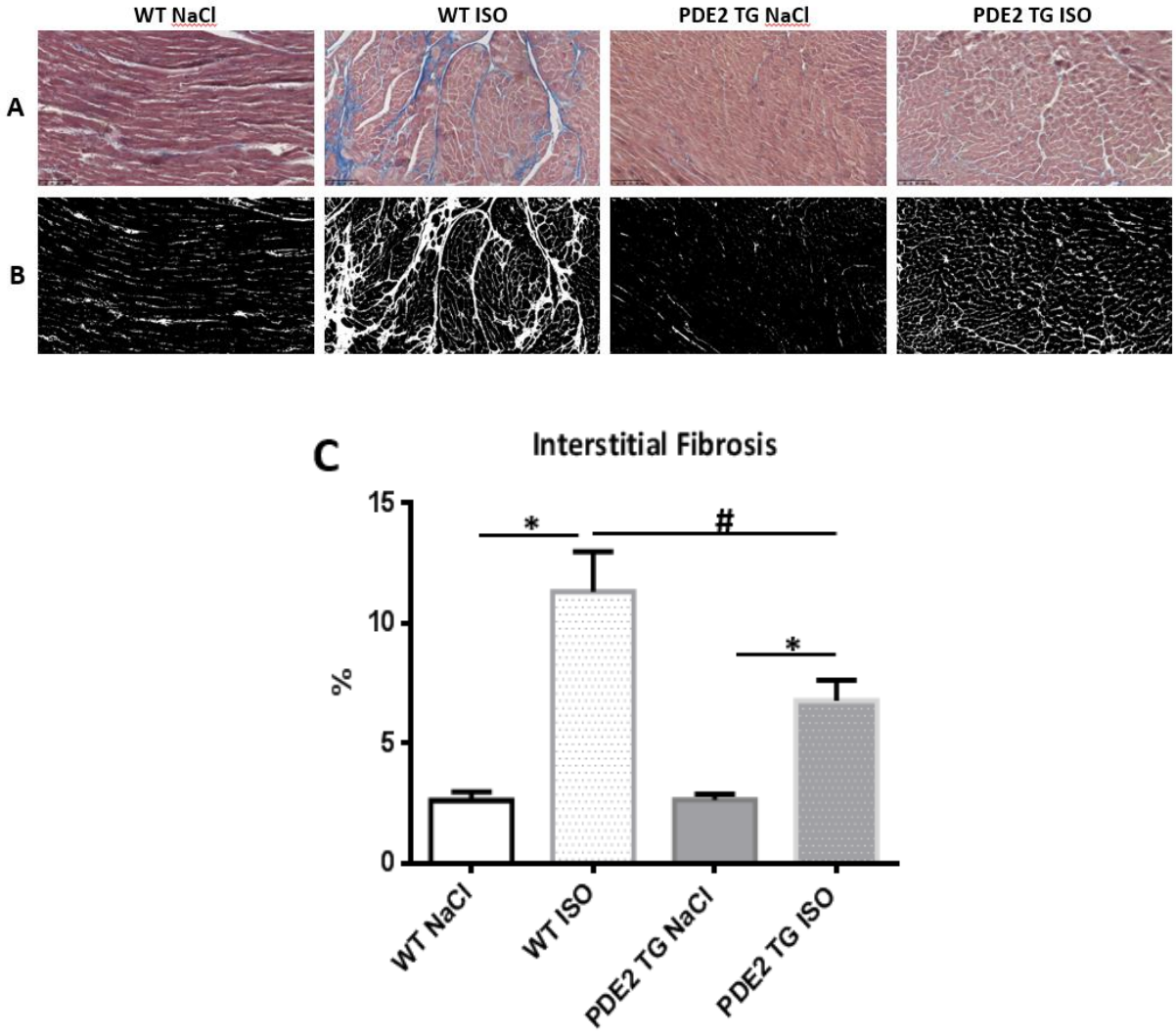

Figure 37: Left ventricular interstitial fibrosis determined by Masson's Trichrome Staining.
Representative images of hematoxylin and Masson's trichrome staining in WT and PDE2 TG mice exposed to chronic isoprenaline (ISO) infusion (Minipumps). Blue colour in **A** and white colour in **B** indicate the interstitial collagen fibril deposition. **C**, Data are shown as mean± SEM , N=3-4 animals for each group. Statistical significance was determined by one-way ANOVA followed by Newman-Keuls multiple comparison: * $p<0.05$ ISO *vs.* NaCl, # $p<0.05$ WT ISO *vs.* TG ISO.

Conclusion: When WT and PDE2 TG mice were challenged by a chronic (2-week) ISO stimulation, there was no real difference in fractional area shortening (FAS), LV weight, or heart-

weight-to-body-weight ratio. The only functional difference was a lower heart rate in PDE2 TG mice even during ISO stimulation. Interestingly, in this experimental model of chronic β-AR stimulation, PDE2 TG mice were less prone to fibrosis than WT mice, which suggests that PDE2 overexpression protects the heart from myocardial cell death.

III.6 Effect of PDE2 overexpression on expression level of other PDE isoforms

High PDE2 overexpression can lead to compensation of other PDE isoforms. To measure expression level of other PDE isoforms, we performed Western Blot using specific antibodies for PDE4A, B and D isoforms and PDE3A and PDE3B isoforms.

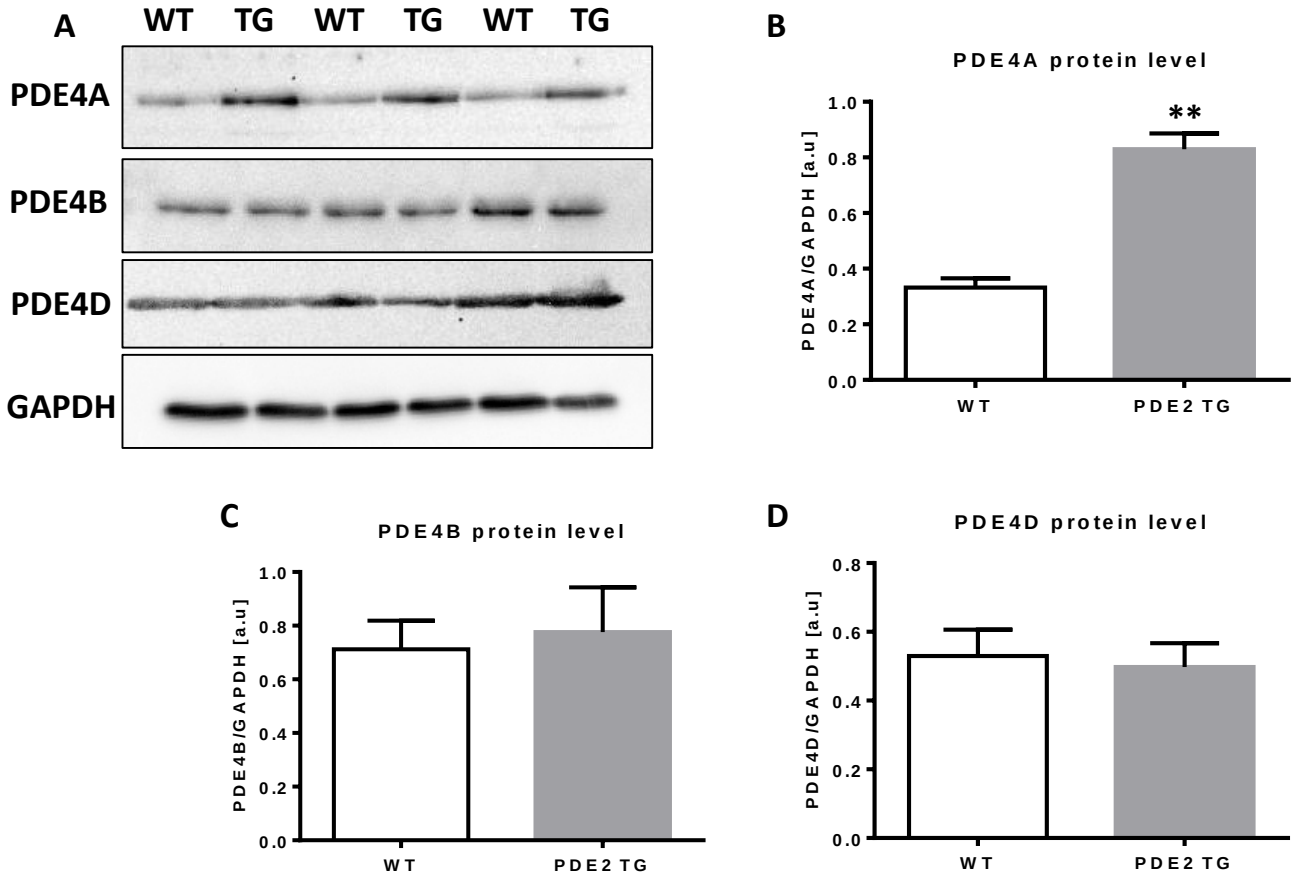

Figure 38: PDE4 isoform expression in heart extracts from WT and PDE2 TG mice.
PDE2 TG mice show a higher expression of PDE4A isoform. Lysates prepared from ventricular myocardium were analyzed by immunoblot with the indicated specific antibodies. Protein expression was normalized to GAPDH. Representative immunoblots (A) and quantification of protein level (B-D). Data are presented as mean±SEM, n=3 animals for each group. Statistical significance was determined with Student's t-test: **p<0.01 *vs.* WT.

Conclusion: PDE2 overexpression does not modify the level of PDE4B and PDE4D protein expression but increases ~2.5-fold PDE4A expression level.

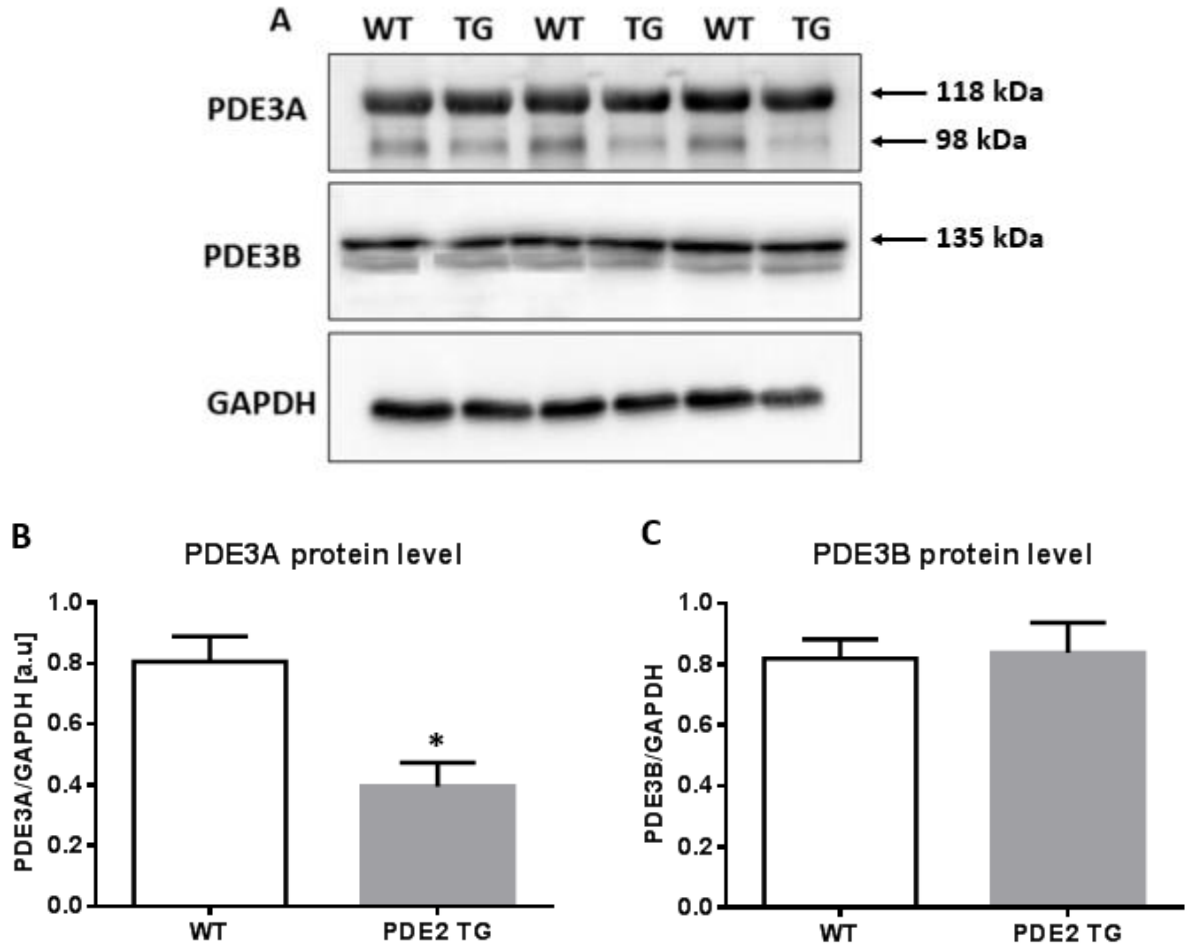

Figure 39: PDE3 isoform expression level in heart extracts from WT and PDE2 TG mice.
PDE2 TG mice show a lower expression of PDE3A 98 kDa isoform. Lysates prepared from ventricular myocardium were analyzed by immunoblot with the indicated specific antibodies. Protein expression was normalized to GAPDH. Representative immunoblots (A) and quantification of protein level (B-C). Data are presented as mean±SEM, n=3 animals for each group. Statistical significance was determined with Student's t-test: *p<0.05 *vs.* WT.

Conclusion: PDE2 overexpression does not modify the level of PDE3B protein expression but reduces ~2-fold PDE3A 98 kDa isoform expression level without differences in PDE3A 118 kDa. It can be due to subcellular localization of these two isoforms of PDE3A (Yan *et al.*,

2007*a*). Studies on human myocardium showed that PDE3A 118 kDa isoform is present in both the microsomal and cytosolic fraction, while PDE3A 94 kDa isoform absolutely in the cytosolic fraction of human myocardium (Smith *et al.*, 1993; Wechsler *et al.*, 2002; Movsesian *et al.*, 2009). Most of PDEs are expressed as a multiple variants because of use of different promoters and alternative splicing which explains the presence of multiple immunoreactive bands detected in Western Blot (Abi-Gerges *et al.*, 2009).

III.7 Effect of PDE2 overexpression on phosphorylation level of MyBP-C

Phosphorylation of MyBP-C, predominantly by PKA, plays an essential role in modulating contractility in response to β-AR stimulation. We determine the level of phosphorylation of MyBP-C in heart extracts from WT and PDE2 TG mice by Western Blot.

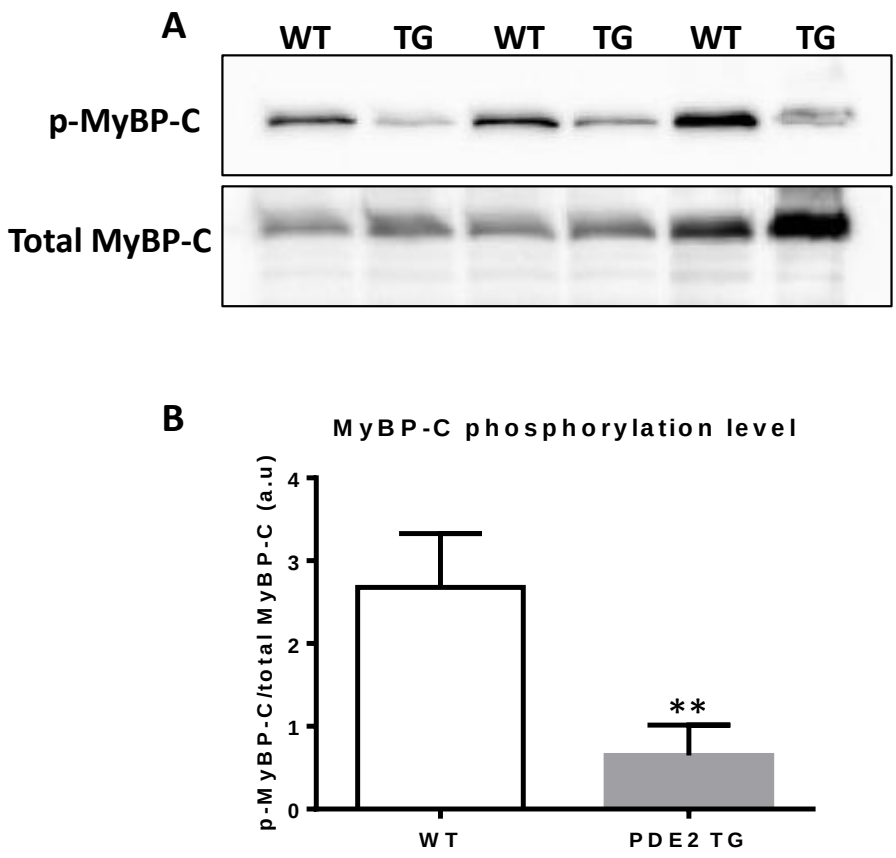

Figure 40: Phosphorylation level of MyBP-C in heart extracts from WT and PDE2 TG mice.

Lysates prepared from ventricular myocardium were analyzed by immunoblots (A) and quantification of phosphorylation level (B). Data are presented as mean±SEM, n=3 animals for each group. Statistical significance was determined with Student's t-test: ** $p<0.01$ *vs.* WT.

Conclusion: Phosphorylation level of MyBP-C is decreased in heart extracts from PDE2 TG mice.

Discussion and perspectives

I. Discussion

Among the seven families of PDEs expressed in the heart, the role of PDE3 and PDE4 in cAMP signaling was largely studied, as well as the role of PDE5 in cGMP signaling. Some studies showed altered PDE expression and activity in a number of cardiovascular diseases including heart failure (Abi-Gerges *et al.,* 2009). Moreover, inhibitors of PDE3 and PDE5 are used as therapeutic agents in cardiovascular diseases. Inhibitors of PDE3 are positive inotropes and vasodilators and have been used in acute heart failure. PDE5 controls degradation of cGMP in vascular smooth muscle cells and inhibitors are used to treat pulmonary hypertension and erectile dysfunction.

PDE2 that degrades cAMP and cGMP and is activated by cGMP is less studied. Yet, recent studies showed that expression and activity of PDE2 were increased in left ventricular myocardium from patients with terminal HF (Mehel *et al.*, 2013) and in a model of cardiac hypertrophy in rat (Mokni *et al.,* 2010). The pathophysiological consequences of PDE2 upregulation remain unclear.

To determine the pathophysiological consequences of PDE2 upregulation, we generated, in collaboration with Prof. Ali El-Armouche, a transgenic mouse with cardiac specific overexpression of PDE2.

Effect of PDE2 overexpression on cardiac function

To determine the effect of PDE2 overexpression on cardiac function, we performed experiments *in vivo*. Heart weight and contractility were studied using echocardiography. We showed that PDE2 TG mice displayed a decrease in basal and β-AR maximal stimulated heart rate. Basal contraction force measured as fractional area shortening was increased in PDE2 TG mice, but we did not observe difference between PDE2 TG and WT mice in maximal contractility. Experiments performed on isolated heart using Langendorff setup showed that, when hearts isolated from PDE2 TG and WT mice were paced at the same heart rate, developed pressure remained unchanged, suggesting that the higher contractility in PDE2 TG mice is due to lower heart rate. This can be explained by Frank-Starling law. Increase in cavity volume in the heart during ventricular filling generates more wall tension to produce the same pressure inside the cavity (Bollensdorff *et al.*, 2011). It has been also demonstrated that PDE2 is present in central

sinoatrial node tissue and may play a role in shaping the heart rate response via cGMP signaling pathway (Herring *et al.*, 2001). In addition, PDE2 has been showed to modulate $I_{Ca,L}$ in human atrial cells (Rivet-Bastide *et al.*, 1997; Vandecasteele *et al.*, 2001).

We showed also that higher contraction force in PDE2 TG mice was not related to cardiac hypertrophy. Left ventricular weight-to-body-weight-ratio and heart-weight-to-body-weight ratio (Additional results, Figure 33) did not differ between PDE2 TG and WT mice at the age of 10 weeks and were lower in elderly PDE2 TG mice as compared to WT.

Recently, Zoccarato et al. showed that PDE2 emerges as a key regulator of cardiac hypertrophy *in vitro* and *in vivo* and overexpression of PDE2 is sufficient *per se* to induce hypertrophy. They showed also that specific inhibition of PDE2 can counteract cardiac hypertrophic growth (Zoccarato *et al.*, 2015).

In our study, we did not observe negative short and long-term effects of PDE2 overexpression on functional and morphological parameters. In the publication of Zoccarato et al, there is a lack of echocardiographic data on heart rate and contraction force that would make an easier comparison between the two studies. In addition, inhibition of PDE2 with Bay 60-7550 at a concentration of 10 µM as used in their study (compared to 100 nM in our study) can inhibit also other PDE isoforms besides PDE2.

Our results are in line with the study published by Mehel et al., who showed beneficial effects of PDE2 upregulation in pathological hypertrophy (Mehel *et al.*, 2013).

We analyzed also the effect of PDE2 overexpression on cardiac function including in elderly mice. We showed that the lower heart rate and the higher basal contractility were preserved in elderly PDE2 TG mice without any indication of hypertrophy.

Next, we determined the effect of PDE2 overexpression under acute β-adrenergic stimulation. Echocardiographic analysis showed a lower maximal heart rate in PDE2 TG mice compared to WT, also in mice exposed to chronic ISO infusions (Additional results, Figure 36A). We analyzed also occurrence of arrhythmic events upon β-AR stimulation and the total number of arrhythmias was significantly lower in PDE2 TG mice.

Effect of PDE2 overexpression on cAMP level, Ca^{2+} cycling and Ca^{2+} handling proteins

To determine the impact of PDE2 overexpression on cAMP/PKA signaling pathway, we performed experiments *in vitro* on isolated adult mouse ventricular myocytes.

We measured real time changes in β-AR induced cAMP level by FRET technique. The response to a short application of ISO was markedly blunted in cardiomyocytes isolated from PDE2 TG mice.

Then, we studied the consequences of reduced cAMP level on cellular Ca^{2+} handling. We measured the L-type Ca^{2+} current with the patch-clamp technique. We showed that PDE2 overexpression markedly blunted the β-AR induced increase in $I_{Ca,L}$ in PDE2 TG mice. This finding is in line with data published by Mehel et al. (Mehel *et al.*, 2013). It has been also demonstrated that PDE2 controls $I_{Ca,L}$ in frog ventricular myocytes and human atrial myocytes (Hartzell & Fischmeister, 1986; Méry *et al.*, 1993*a*; Rivet-Bastide *et al.*, 1997).

Then, we measured simultaneously sarcomere shortening and Ca^{2+} transients in electrically stimulated cardiomyocytes using the IonOptix system. Accordingly, the response of Ca^{2+} transient and contractility to increasing concentrations of ISO were markedly blunted in PDE2 TG mice.

Next, we determined diastolic Ca^{2+} leak from SR via RyR2 and performed analysis of key Ca^{2+} handling proteins. We found that SR Ca^{2+} leak is reduced in PDE2 TG mice. We did not observe differences between PDE2 TG and WT mice in expression of SERCA2a, PLB or RyR2. In agreement with the observed reduction in SR Ca^{2+} leak in PDE2 TG mice, we found a decrease in RyR2 phosphorylation at the CaMKII phosphorylation site, but not at PKA site. PLB phosphorylation was significantly reduced at both S16 and T17 sites. We also found a reduction in the phosphorylation level of MyBP-C in PDE2 TG mice (Additional results, Figure 40).

It has been shown that increase in SR Ca^{2+} leak results in reduction of systolic functions and contributes to diastolic dysfunctions. Ca^{2+} waves can cause delayed and afterdepolarizations and trigger arrhythmias (Bers, 2014). CaMKII is implicated in the induction of SR Ca^{2+} leak and ventricular arrhythmias (Anderson, 2005). CaMKII has been shown to bind and phosphorylate RyR2 at a unique residue (S^{2814}). CaMKII-dependent phosphorylation of RyR2 increases the open probability of RyR2 at the single channel level (Wehrens *et al.*, 2004). It has been also demonstrated that overexpression of CaMKII in cardiac myocytes leads to an increase in the

frequency of Ca^{2+} sparks (Maier *et al.*, 2003). Thus, the anti-arrhythmic effect of PDE2 overexpression is likely related to the reduced phosphorylation of RyR2 by CaMKII and reduction in SR Ca^{2+} leak.

PDE2 overexpression as potential therapeutic strategy in HF

In our study, we showed that the effect of PDE2 is similar to a β-blocker treatment and increase in myocardial PDE2 levels may constitute an important defense mechanism by antagonizing β-AR/cAMP mediated cardiac toxicity. β-AR blockade is one of the most effective therapy in HF. However, the use of β-blockers in patients decreases contractility acutely in normal and failing hearts (Reiken *et al.*, 2003) and has deleterious effect on exercise capacity (Provencher *et al.*, 2006). In our study, we did not observe initial depression of contractile performance and negative influence on exercise capacity (Additional results, Figure 28). Thus, our study opens an interesting hypothesis that PDE2 activation may have therapeutical application in HF.

II. Perspectives

Effect of PDE2 overexpression on heart rate

In our study, we showed for the first time that cardiac specific overexpression of PDE2 leads to a decrease in basal as well as β-AR stimulated heart rate. However, we did not explain the underlying mechanisms of this finding.

Physiological heart beating is generated in in pacemaker cells located in the sinoatrial node (SAN). cAMP leads to increase in sinoatrial membrane currents directly or indirectly via PKA (DiFrancesco & Tortora, 1991). The high activity of adenylyl cyclase in SAN results in a considerable amount of cAMP. This cAMP is hydrolyzed by PDEs, thus preventing a high sinoatrial beating (Vinogradova *et al.*, 2008). It has been shown that PDE2 is expressed in SAN of mice (Hua et al, 2012). Study on SAN and atrial myocytes using specific PDE2 inhibitor (EHNA 10 µM) showed that PDE2 inhibition resulted in increase in spontaneous action potential (AP) frequency in mouse SAN myocytes, suggesting that PDE2 contributes to the regulation of AP properties under basal conditions. It has also been demonstrated that inhibition of PDE2 in mouse atrial myocytes increased AP duration, indicating that PDE2 regulates atrial AP properties (Hua *et al.*, 2012).

Based on these results, it would be interesting to determine the effect of PDE2 overexpression on AP in SAN and atrial myocytes, to understand better the effect of PDE2 upregulation on heart rate.

Recently, PDE2 has been shown to be upregulated in cardiac stellate ganglia in prehypertensive SHR rats (Li *et al.*, 2015). It has been also shown that the action of BNP in cardiac neurons is regulated by PDE2A family. BNP binds to NPR-A resulting in pGC stimulation. Newly synthesized cGMP activates PDE2 to hydrolyze cGMP and limit the increase in PKG activity. In addition, PKG inhibits Ca^{2+} current through phosphorylation of voltage-gated Ca^{2+} channels resulting in decrease in the intracellular Ca^{2+} transient. This leads to decrease in norepinephrine release from synaptic vesicles and reduces the heart rate response to sympathetic stimulation (Li *et al.*, 2015).

This study gives new insights into a putative role for PDE2 in heart rate regulation. However, in our PDE2 TG mouse model, the transgene is under the control of the αMHC promoter, which is a

cardiac promoter and makes it thus very unlikely that PDE2 is also overexpressed in cardiac neurons. Moreover, PDE2 overexpression in cardiac neurons would increase the release of norepinephrine and hence increase heart rate, which is quite opposite to what we observe in the PDE2 TG mice.

Effect of PDE2 overexpression on cGMP signaling pathway

PDE2 is a critical component of the cGMP/cAMP crosstalk. We demonstrated that PDE2 overexpression has protective effect against ventricular arrhythmia during excessive sympathetic stress. It may therefore constitute an up to now unconsidered link between ANP/BNP coupled cGMP enhancement and the protection against toxic sympathetic effects by acting as cGMP controlled intracellular sympathetic blockade.

In our study, we showed an elevated expression of ANP and BNP (Additional results, Figure 35). Natriuretic peptides (NPs) have been shown to be cardioprotective because of their antihypertrophic effect and beneficial action on neurohormonal control (Wada *et al.*, 1994; Rosenkranz *et al.*, 2003). The physiological effects of NPs occur via binding to pGC-coupled natriuretic peptide receptors, leading to PKG and PDE modulation (Omori & Kotera, 2007; Castro *et al.*, 2010) that leads to the regulation of intracellular Ca^{2+} level. Upregulation of NPs is a compensatory mechanism to improve hemodynamic and myocardial function as well as to inhibit cardiac sympathetic nervous system to slow the progression of hypertrophy and HF (Molkentin, 2003).

While we observed an increase in ANP and BNP gene expression in PDE2 TG, this was not associated with cardiac hypertrophy or adverse cardiac remodeling. However, it is necessary to study the effect of PDE2 overexpression on cGMP signaling pathway including measurement of cGMP levels in cardiac tissue and/or in cardiomyocytes isolated from WT and PDE2 TG mice, measurement of expression level of key components of cGMP signaling pathway and expression level of natriuretic peptide receptors.

Effect of PDE2 and PDE4 overexpression on cardiac function

In our laboratory, we generated a mouse model with cardiac specific overexpression of PDE4B (PDE4B TG mouse). Recently, it has been found that PDE4B expression is decreased in pathological cardiac hypertrophy (Abi-Gerges *et al.*, 2009). Moreover, PDE4B is colocalized with the LTCC and PDE4B KO mice have a higher response of $I_{Ca,L}$ to ISO and a higher

sensitivity to catecholamine-induced arrhythmias (Leroy *et al.*, 2011). This suggests that the decreased PDE4B observed in pathological hypertrophy may participate in the dysregulation of intracellular Ca^{2+} homeostasis and lead to cardiac arrhythmias in HF.

When comparing PDE2 TG and PDE4B TG mice, we found a similar inhibitory effect on the β-AR stimulation of contractility, Ca^{2+} transients, cAMP and $I_{Ca,L}$ at the cellular level, but PDE4B TG mice had no change in heart rate and, unlike PDE2 TG mice, developed hypertrophy under basal conditions.

It would thus be interesting to determine why PDE2 and PDE4B overexpression exert different effect on cardiac function.

It has been shown that PDE4B are colocalized along T-tubule membrane in adult mouse ventricular myocytes and regulate L-type Ca^{2+} current in this compartment (Leroy *et al.*, 2011), whereas PDE2 is mainly associated with membrane structures: plasma membrane, sarcoplasmic reticulum, Golgi and nuclear envelope (Lugnier, 2006). Different subcellular localization of these two enzymes could thus explain why their cardiac overexpression leads to different functional effects.

To test this hypothesis, we could compare basal and β-AR stimulated conditions in cells from PDE2 TG and PDE4B TG mice which have been detubulated, e.g. with formamide (Brette *et al.*, 2002). It can be also interesting to compare the effect of PDE2 and PDE4 overexpression in mice subjected to transaortic constriction (animal model of HF). HF is characterized by remodeling of cardiomyocyte structure including loss of T-tubules and Z-grooves (Gorelik *et al.*, 2013).

Cardiac specific PDE2 overexpression as potential new therapy in HF

Our study demonstrates that higher PDE2 abundance protects the heart against ventricular arrhythmias and exerts anti-adrenergic effect similar to beta-blockers and could constitute a defense mechanism antagonizing the cellular toxicity linked to over-activation of the β-AR/cAMP cascade. PDE2 overexpression may thus be a potential therapy to prevent HF progression and associated arrhythmias.

However, studies on large animals are necessary. The role of each PDE isoform can vary among mammalian species and our results may not recapitulate in humans in all details.

The critical point of this study is to find a way to upregulate PDE2 in the human heart. One of the therapeutic strategy is to target PDE2 with specific activators. An *in silico* high throughput screening based on the binding of molecules on the GAF-B domain of PDE2 has been performed on a large library of molecules. Then hits were tested with a PDE2 activity assay and the efficacy of potential activators was compared to 5 µM cGMP (C. Nicolas, unpublished). This project was supported by LabEx LERMIT. So far, we do not have any confirmed hits.

The second therapeutic strategy is to develop gene therapy with cardiac targeted overexpression of PDE2. In our laboratory, we have a project focused on cardiac gene therapy performed with adeno-associated virus (AAV) encoding PDE2A (J.-P. Margaria). AAV is a small, nonpathogenic human virus, belonging to the *Parvovirus* family and characterized by its high efficiency of transduction of cardiac tissue (Zacchigna *et al.*, 2014).

Preliminary results from experiments performed in C57BL/6 mice tail-injected with AAV9-PDE2A showed a two-fold increase of PDE2 expression in heart tissue. Moreover, injected mice were subjected to a chronic infusion of isoproterenol (60 mg/kg/day) for 2 weeks and PDE2 overexpression was able to improve both morphometric and functional cardiac parameters (J-P. Margaria, unpublished). These premilinary results need to be confirmed but are already promising.

Bibliography

Abi-Gerges A, Richter W, Lefebvre F, Mateo P, Varin A, Heymes C, Samuel J-L, Lugnier C, Conti M, Fischmeister R & Vandecasteele G (2009). Decreased expression and activity of cAMP phosphodiesterases in cardiac hypertrophy and its impact on beta-adrenergic cAMP signals. *Circ Res* **105,** 784–792.

Acin-Perez R, Russwurm M, Günnewig K, Gertz M, Zoidl G, Ramos L, Buck J, Levin LR, Rassow J, Manfredi G & Steegborn C (2011). A phosphodiesterase 2A isoform localized to mitochondria regulates respiration. *J Biol Chem* **286,** 30423–30432.

Andersen MB, Simonsen U, Wehland M, Pietsch J & Grimm D (2016). LCZ696 (Valsartan/Sacubitril)--A Possible New Treatment for Hypertension and Heart Failure. *Basic Clin Pharmacol Toxicol* **118,** 14–22.

Anderson ME (2005). Calmodulin kinase signaling in heart: an intriguing candidate target for therapy of myocardial dysfunction and arrhythmias. *Pharmacol Ther* **106,** 39–55.

Andrée B, Hillemann T, Kessler-Icekson G, Schmitt-John T, Jockusch H, Arnold HH & Brand T (2000). Isolation and characterization of the novel popeye gene family expressed in skeletal muscle and heart. *Dev Biol* **223,** 371–382.

Anon (n.d.). Biology, Solomon Berg Martin 8th Edition. Available at: http://fr.slideshare.net/nicolledb05/biology-solomon-berg-martin-8th-edition [Accessed June 12, 2016].

Arumugam S, Sreedhar R, Thandavarayan RA, Karuppagounder V, Krishnamurthy P, Suzuki K, Nakamura M & Watanabe K (2016). Angiotensin receptor blockers: Focus on cardiac and renal injury. *Trends Cardiovasc Med* **26,** 221–228.

Ashman DF, Lipton R, Melicow MM & Price TD (1963). Isolation of adenosine 3', 5'-monophosphate and guanosine 3', 5'-monophosphate from rat urine. *Biochem Biophys Res Commun* **11,** 330–334.

Azevedo MF, Faucz FR, Bimpaki E, Horvath A, Levy I, de Alexandre RB, Ahmad F, Manganiello V & Stratakis CA (2014). Clinical and molecular genetics of the phosphodiesterases (PDEs). *Endocr Rev* **35,** 195–233.

Baillie GS, Scott JD & Houslay MD (2005). Compartmentalisation of phosphodiesterases and protein kinase A: opposites attract. *FEBS Lett* **579,** 3264–3270.

Baillie GS, Sood A, McPhee I, Gall I, Perry SJ, Lefkowitz RJ & Houslay MD (2003). beta-Arrestin-mediated PDE4 cAMP phosphodiesterase recruitment regulates beta-adrenoceptor switching from Gs to Gi. *Proc Natl Acad Sci U S A* **100,** 940–945.

Baker AJ (2014). Adrenergic signaling in heart failure: a balance of toxic and protective effects. *Pflüg Arch Eur J Physiol* **466,** 1139–1150.

Bayram M, De Luca L, Massie MB & Gheorghiade M (2005). Reassessment of dobutamine, dopamine, and milrinone in the management of acute heart failure syndromes. *Am J Cardiol* **96,** 47G–58G.

Beavo JA (1995). Cyclic nucleotide phosphodiesterases: functional implications of multiple isoforms. *Physiol Rev* **75,** 725–748.

Beavo JA, Hardman JG & Sutherland EW (1971). Stimulation of adenosine 3',5'-monophosphate hydrolysis by guanosine 3',5'-monophosphate. *J Biol Chem* **246,** 3841–3846.

Beca S, Aschars-Sobbi R, Panama BK & Backx PH (2011). Regulation of murine cardiac function by phosphodiesterases type 3 and 4. *Curr Opin Pharmacol* **11,** 714–719.

Bedioune I, Bobin P, Karam S, Lindner M, Mika D, Lechêne P, Leroy J, Fischmeister R & Vandecasteele G (2016). Phosphodiestérases des nucléotides cycliques□: rôle dans le coeur et potentiel thérapeutique. *Biol Aujourd'hui*.

Bender AT & Beavo JA (2006). Cyclic nucleotide phosphodiesterases: molecular regulation to clinical use. *Pharmacol Rev* **58,** 488–520.

Bender AT, Ostenson CL, Giordano D & Beavo JA (2004). Differentiation of human monocytes in vitro with granulocyte-macrophage colony-stimulating factor and macrophage colony-stimulating factor produces distinct changes in cGMP phosphodiesterase expression. *Cell Signal* **16,** 365–374.

Benkusky NA, Weber CS, Scherman JA, Farrell EF, Hacker TA, John MC, Powers PA & Valdivia HH (2007). Intact beta-adrenergic response and unmodified progression toward heart failure in mice with genetic ablation of a major protein kinase A phosphorylation site in the cardiac ryanodine receptor. *Circ Res* **101,** 819–829.

Bennett HS & Porter KR (1953). An electron microscope study of sectioned breast muscle of the domestic fowl. *Am J Anat* **93,** 61–105.

Bentley JK, Juilfs DM & Uhler MD (2001). Nerve growth factor inhibits PC12 cell PDE 2 phosphodiesterase activity and increases PDE 2 binding to phosphoproteins. *J Neurochem* **76,** 1252–1263.

Bernstein D (2002). Cardiovascular and metabolic alterations in mice lacking beta1- and beta2-adrenergic receptors. *Trends Cardiovasc Med* **12,** 287–294.

Bers DM (2002). Cardiac excitation-contraction coupling. *Nature* **415,** 198–205.

Bers DM (2014). Cardiac sarcoplasmic reticulum calcium leak: basis and roles in cardiac dysfunction. *Annu Rev Physiol* **76,** 107–127.

Bers DM & Perez-Reyes E (1999). Ca channels in cardiac myocytes: structure and function in Ca influx and intracellular Ca release. *Cardiovasc Res* **42,** 339–360.

Blumenthal DK, Stull JT & Gill GN (1978). Phosphorylation of cardiac troponin by guanosine 3':5'-monophosphate-dependent protein kinase. *J Biol Chem* **253,** 324–326.

Boess FG, Hendrix M, van der Staay F-J, Erb C, Schreiber R, van Staveren W, de Vente J, Prickaerts J, Blokland A & Koenig G (2004). Inhibition of phosphodiesterase 2 increases neuronal cGMP, synaptic plasticity and memory performance. *Neuropharmacology* **47,** 1081–1092.

Bollensdorff C, Lookin O & Kohl P (2011). Assessment of contractility in intact ventricular cardiomyocytes using the dimensionless "Frank–Starling Gain" index. *Pflugers Arch* **462,** 39–48.

Boularan C & Gales C (2015). Cardiac cAMP: production, hydrolysis, modulation and detection. *Front Pharmacol* **6,** 203.

Brette F, Komukai K & Orchard CH (2002). Validation of formamide as a detubulation agent in isolated rat cardiac cells. *Am J Physiol Heart Circ Physiol* **283,** H1720-1728.

Brette F, Leroy J, Le Guennec J-Y & Sallé L (2006). Ca2+ currents in cardiac myocytes: Old story, new insights. *Prog Biophys Mol Biol* **91,** 1–82.

Bristow MR, Ginsburg R, Umans V, Fowler M, Minobe W, Rasmussen R, Zera P, Menlove R, Shah P & Jamieson S (1986). Beta 1- and beta 2-adrenergic-receptor subpopulations in nonfailing and failing human ventricular myocardium: coupling of both receptor subtypes to muscle contraction and selective beta 1-receptor down-regulation in heart failure. *Circ Res* **59,** 297–309.

Brodde O-E, Bruck H & Leineweber K (2006). Cardiac adrenoceptors: physiological and pathophysiological relevance. *J Pharmacol Sci* **100,** 323–337.

Bubb KJ, Trinder SL, Baliga RS, Patel J, Clapp LH, MacAllister RJ & Hobbs AJ (2014). Inhibition of phosphodiesterase 2 augments cGMP and cAMP signaling to ameliorate pulmonary hypertension. *Circulation* **130,** 496–507.

Butcher RW & Sutherland EW (1962). Adenosine 3',5'-phosphate in biological materials. I. Purification and properties of cyclic 3',5'-nucleotide phosphodiesterase and use of this enzyme to characterize adenosine 3',5'-phosphate in human urine. *J Biol Chem* **237,** 1244–1250.

Buxton IL & Brunton LL (1983). Compartments of cyclic AMP and protein kinase in mammalian cardiomyocytes. *J Biol Chem* **258,** 10233–10239.

Cabrera-Vera TM, Vanhauwe J, Thomas TO, Medkova M, Preininger A, Mazzoni MR & Hamm HE (2003). Insights into G protein structure, function, and regulation. *Endocr Rev* **24,** 765–781.

Calderone A, Thaik CM, Takahashi N, Chang DL & Colucci WS (1998). Nitric oxide, atrial natriuretic peptide, and cyclic GMP inhibit the growth-promoting effects of norepinephrine in cardiac myocytes and fibroblasts. *J Clin Invest* **101,** 812–818.

Calejo AI & Taskén K (2015). Targeting protein-protein interactions in complexes organized by A kinase anchoring proteins. *Front Pharmacol* **6,** 192.

Castro LRV, Schittl J & Fischmeister R (2010). Feedback control through cGMP-dependent protein kinase contributes to differential regulation and compartmentation of cGMP in rat cardiac myocytes. *Circ Res* **107,** 1232–1240.

Castro LRV, Verde I, Cooper DMF & Fischmeister R (2006). Cyclic guanosine monophosphate compartmentation in rat cardiac myocytes. *Circulation* **113,** 2221–2228.

Chambers RJ, Abrams K, Garceau NY, Kamath AV, Manley CM, Lilley SC, Otte DA, Scott DO, Sheils AL, Tess DA, Vellekoop AS, Zhang Y & Lam KT (2006). A new chemical tool for exploring the physiological function of the PDE2 isozyme. *Bioorg Med Chem Lett* **16,** 307–310.

Charbonneau H, Prusti RK, LeTrong H, Sonnenburg WK, Mullaney PJ, Walsh KA & Beavo JA (1990). Identification of a noncatalytic cGMP-binding domain conserved in both the cGMP-stimulated and photoreceptor cyclic nucleotide phosphodiesterases. *Proc Natl Acad Sci U S A* **87,** 288–292.

Chen H, Wild C, Zhou X, Ye N, Cheng X & Zhou J (2014). Recent advances in the discovery of small molecules targeting exchange proteins directly activated by cAMP (EPAC). *J Med Chem* **57,** 3651–3665.

Cheng X, Ji Z, Tsalkova T & Mei F (2008). Epac and PKA: a tale of two intracellular cAMP receptors. *Acta Biochim Biophys Sin* **40,** 651–662.

Christ T, Molenaar P, Klenowski PM, Ravens U & Kaumann AJ (2011). Human atrial β1L-adrenoceptor but not β3-adrenoceptor activation increases force and Ca2+ current at physiological temperature. *Br J Pharmacol* **162,** 823–839.

Conti M & Beavo J (2007). Biochemistry and physiology of cyclic nucleotide phosphodiesterases: essential components in cyclic nucleotide signaling. *Annu Rev Biochem* **76,** 481–511.

Conti M, Richter W, Mehats C, Livera G, Park J-Y & Jin C (2003). Cyclic AMP-specific PDE4 phosphodiesterases as critical components of cyclic AMP signaling. *J Biol Chem* **278,** 5493–5496.

Cooper GM (2000). *The Cell*, 2nd edn. Sinauer Associates.

Corbin JD, Turko IV, Beasley A & Francis SH (2000). Phosphorylation of phosphodiesterase-5 by cyclic nucleotide-dependent protein kinase alters its catalytic and allosteric cGMP-binding activities. *Eur J Biochem FEBS* **267,** 2760–2767.

Coudray C, Charon C, Komas N, Mory G, Diot-Dupuy F, Manganiello V, Ferre P & Bazin R (1999). Evidence for the presence of several phosphodiesterase isoforms in brown adipose tissue of Zucker rats: modulation of PDE2 by the fa gene expression. *FEBS Lett* **456,** 207–210.

Daaka Y, Luttrell LM & Lefkowitz RJ (1997). Switching of the coupling of the beta2-adrenergic receptor to different G proteins by protein kinase A. *Nature* **390,** 88–91.

Das A, Durrant D, Salloum FN, Xi L & Kukreja RC (2015). PDE5 inhibitors as therapeutics for heart disease, diabetes and cancer. *Pharmacol Ther* **147,** 12–21.

Davare MA, Avdonin V, Hall DD, Peden EM, Burette A, Weinberg RJ, Horne MC, Hoshi T & Hell JW (2001). A beta2 adrenergic receptor signaling complex assembled with the Ca2+ channel Cav1.2. *Science* **293,** 98–101.

Dedkova EN & Blatter LA (2013). Calcium signaling in cardiac mitochondria. *J Mol Cell Cardiol* **58,** 125–133.

Degerman E, Belfrage P & Manganiello VC (1997*a*). Structure, localization, and regulation of cGMP-inhibited phosphodiesterase (PDE3). *J Biol Chem* **272,** 6823–6826.

Degerman E, Belfrage P & Manganiello VC (1997*b*). Structure, localization, and regulation of cGMP-inhibited phosphodiesterase (PDE3). *J Biol Chem* **272,** 6823–6826.

Denbow CE (2000). Beta-adrenergic blockade in the treatment of congestive heart failure. *West Indian Med J* **49,** 102–107.

Derbyshire ER & Marletta MA (2012). Structure and regulation of soluble guanylate cyclase. *Annu Rev Biochem* **81,** 533–559.

Dessy C, Moniotte S, Ghisdal P, Havaux X, Noirhomme P & Balligand JL (2004). Endothelial beta3-adrenoceptors mediate vasorelaxation of human coronary microarteries through nitric oxide and endothelium-dependent hyperpolarization. *Circulation* **110,** 948–954.

Dickinson NT, Jang EK & Haslam RJ (1997). Activation of cGMP-stimulated phosphodiesterase by nitroprusside limits cAMP accumulation in human platelets: effects on platelet aggregation. *Biochem J* **323 (Pt 2),** 371–377.

Diebold I, Djordjevic T, Petry A, Hatzelmann A, Tenor H, Hess J & Görlach A (2009). Phosphodiesterase 2 mediates redox-sensitive endothelial cell proliferation and angiogenesis by thrombin via Rac1 and NADPH oxidase 2. *Circ Res* **104,** 1169–1177.

DiFrancesco D & Tortora P (1991). Direct activation of cardiac pacemaker channels by intracellular cyclic AMP. *Nature* **351,** 145–147.

Dittrich M, Jurevicius J, Georget M, Rochais F, Fleischmann B, Hescheler J & Fischmeister R (2001). Local response of L-type Ca(2+) current to nitric oxide in frog ventricular myocytes. *J Physiol* **534,** 109–121.

Dodge KL, Khouangsathiene S, Kapiloff MS, Mouton R, Hill EV, Houslay MD, Langeberg LK & Scott JD (2001). mAKAP assembles a protein kinase A/PDE4 phosphodiesterase cAMP signaling module. *EMBO J* **20,** 1921–1930.

Dodge-Kafka KL (2006). Compartmentation of Cyclic Nucleotide Signaling in the Heart: The Role of A-Kinase Anchoring Proteins. *Circ Res* **98,** 993–1001.

Dodge-Kafka KL, Soughayer J, Pare GC, Carlisle Michel JJ, Langeberg LK, Kapiloff MS & Scott JD (2005). The protein kinase A anchoring protein mAKAP coordinates two integrated cAMP effector pathways. *Nature* **437,** 574–578.

Efendiev R & Dessauer CW (2011). A kinase-anchoring proteins and adenylyl cyclase in cardiovascular physiology and pathology. *J Cardiovasc Pharmacol* **58,** 339–344.

El-Armouche A & Eschenhagen T (2009). Beta-adrenergic stimulation and myocardial function in the failing heart. *Heart Fail Rev* **14,** 225–241.

Elias MF, Elias PK, Pentz CA & Sorrentino RN (1977). Heart/body weight ratios for aging high and low blood pressure mice. *Exp Aging Res* **3,** 231–238.

Elkayam U (1998). Calcium channel blockers in heart failure. *Cardiology* **89 Suppl 1,** 38–46.

Elkayam U, Shotan A, Mehra A & Ostrzega E (1993). Calcium channel blockers in heart failure. *J Am Coll Cardiol* **22,** 139A–144A.

Emorine LJ, Marullo S, Briend-Sutren MM, Patey G, Tate K, Delavier-Klutchko C & Strosberg AD (1989). Molecular characterization of the human beta 3-adrenergic receptor. *Science* **245,** 1118–1121.

Erneux C, Couchie D & Dumont JE (1980). Characterization of horse thyroid cyclic nucleotide phosphodiesterases. *Eur J Biochem FEBS* **104,** 297–304.

Erneux C, Miot F, Boeynaems JM & Dumont JE (1982). Paradoxical stimulation by 1-methyl-3-isobutylxanthine of rat liver cyclic AMP phosphodiesterase activity. *FEBS Lett* **142,** 251–254.

Eschenhagen T (2013). PDE4 in the human heart - major player or little helper? *Br J Pharmacol* **169,** 524–527.

Eskandari N, Mirmosayyeb O, Bordbari G, Bastan R, Yousefi Z & Andalib A (2015). A short review on structure and role of cyclic-3',5'-adenosine monophosphate-specific phosphodiesterase 4 as a treatment tool. *J Res Pharm Pract* **4,** 175–181.

Espinasse I, Iourgenko V, Defer N, Samson F, Hanoune J & Mercadier JJ (1995). Type V, but not type VI, adenylyl cyclase mRNA accumulates in the rat heart during ontogenic development. Correlation with increased global adenylyl cyclase activity. *J Mol Cell Cardiol* **27,** 1789–1795.

Favot L, Keravis T, Holl V, Le Bec A & Lugnier C (2003). VEGF-induced HUVEC migration and proliferation are decreased by PDE2 and PDE4 inhibitors. *Thromb Haemost* **90,** 334–343.

Fiedler B & Wollert KC (2004). Interference of antihypertrophic molecules and signaling pathways with the Ca2+-calcineurin-NFAT cascade in cardiac myocytes. *Cardiovasc Res* **63,** 450–457.

Fimia GM & Sassone-Corsi P (2001). Cyclic AMP signalling. *J Cell Sci* **114,** 1971–1972.

Fischmeister R, Castro L, Abi-Gerges A, Rochais F & Vandecasteele G (2005). Species- and tissue-dependent effects of NO and cyclic GMP on cardiac ion channels. *Comp Biochem Physiol A Mol Integr Physiol* **142,** 136–143.

Fischmeister R, Castro LRV, Abi-Gerges A, Rochais F, Jurevicius J, Leroy J & Vandecasteele G (2006). Compartmentation of cyclic nucleotide signaling in the heart: the role of cyclic nucleotide phosphodiesterases. *Circ Res* **99,** 816–828.

Fischmeister R & Hartzell HC (1987). Cyclic guanosine 3',5'-monophosphate regulates the calcium current in single cells from frog ventricle. *J Physiol* **387,** 453–472.

Fisher DA, Smith JF, Pillar JS, St Denis SH & Cheng JB (1998). Isolation and characterization of PDE9A, a novel human cGMP-specific phosphodiesterase. *J Biol Chem* **273,** 15559–15564.

Flynn R & Altier C (2013). A macromolecular trafficking complex composed of β_2-adrenergic receptors, A-Kinase Anchoring Proteins and L-type calcium channels. *J Recept Signal Transduct Res* **33,** 172–176.

Francis SH, Blount MA & Corbin JD (2011). Mammalian cyclic nucleotide phosphodiesterases: molecular mechanisms and physiological functions. *Physiol Rev* **91,** 651–690.

Freihat L, Muleya V, Manallack DT, Wheeler JI & Irving HR (2014). Comparison of moonlighting guanylate cyclases: roles in signal direction? *Biochem Soc Trans* **42,** 1773–1779.

Frey N, Katus HA, Olson EN & Hill JA (2004). Hypertrophy of the heart: a new therapeutic target? *Circulation* **109,** 1580–1589.

Frey N & Olson EN (2003). Cardiac hypertrophy: the good, the bad, and the ugly. *Annu Rev Physiol* **65,** 45–79.

Fu Q, Chen X & Xiang YK (2013). Compartmentalization of β-adrenergic signals in cardiomyocytes. *Trends Cardiovasc Med* **23,** 250–256.

Fu Q & Xiang YK (2015). Trafficking of β-Adrenergic Receptors: Implications in Intracellular Receptor Signaling. *Prog Mol Biol Transl Sci* **132,** 151–188.

Fu Y, Westenbroek RE, Scheuer T & Catterall WA (2014). Basal and β-adrenergic regulation of the cardiac calcium channel CaV1.2 requires phosphorylation of serine 1700. *Proc Natl Acad Sci U S A* **111,** 16598–16603.

Fuller MD, Emrick MA, Sadilek M, Scheuer T & Catterall WA (2010). Molecular mechanism of calcium channel regulation in the fight-or-flight response. *Sci Signal* **3,** ra70.

Gautel M & Djinović-Carugo K (2016). The sarcomeric cytoskeleton: from molecules to motion. *J Exp Biol* **219,** 135–145.

Gauthier C, Langin D & Balligand JL (2000). Beta3-adrenoceptors in the cardiovascular system. *Trends Pharmacol Sci* **21,** 426–431.

Gauthier C, Leblais V, Kobzik L, Trochu JN, Khandoudi N, Bril A, Balligand JL & Le Marec H (1998). The negative inotropic effect of beta3-adrenoceptor stimulation is mediated by activation of a nitric oxide synthase pathway in human ventricle. *J Clin Invest* **102,** 1377–1384.

Gauthier C, Tavernier G, Charpentier F, Langin D & Le Marec H (1996). Functional beta3-adrenoceptor in the human heart. *J Clin Invest* **98,** 556–562.

Geoffroy V, Fouque F, Nivet V, Clot J-P, Lugnier C, Desbuquois B & Benelli C (1999). Activation of a cGMP-stimulated cAMP phosphodiesterase by protein kinase C in a liver Golgi–endosomal fraction. *Eur J Biochem* **259,** 892–900.

Gileadi O (2014). Structures of soluble guanylate cyclase: implications for regulatory mechanisms and drug development. *Biochem Soc Trans* **42,** 108–113.

Gloerich M & Bos JL (2010). Epac: defining a new mechanism for cAMP action. *Annu Rev Pharmacol Toxicol* **50,** 355–375.

Goaillard JM, Vincent PV & Fischmeister R (2001). Simultaneous measurements of intracellular cAMP and L-type Ca2+ current in single frog ventricular myocytes. *J Physiol* **530,** 79–91.

Gorelik J, Wright PT, Lyon AR & Harding SE (2013). Spatial control of the βAR system in heart failure: the transverse tubule and beyond. *Cardiovasc Res* **98,** 216–224.

Gorre F & Vandekerckhove H (2010). Beta-blockers: focus on mechanism of action. Which beta-blocker, when and why? *Acta Cardiol* **65,** 565–570.

Granzier HL & Labeit S (2004). The giant protein titin: a major player in myocardial mechanics, signaling, and disease. *Circ Res* **94,** 284–295.

Gu J, Noe A, Chandra P, Al-Fayoumi S, Ligueros-Saylan M, Sarangapani R, Maahs S, Ksander G, Rigel DF, Jeng AY, Lin T-H, Zheng W & Dole WP (2010). Pharmacokinetics and pharmacodynamics of LCZ696, a novel dual-acting angiotensin receptor-neprilysin inhibitor (ARNi). *J Clin Pharmacol* **50,** 401–414.

Guellich A, Mehel H & Fischmeister R (2014). Cyclic AMP synthesis and hydrolysis in the normal and failing heart. *Pflüg Arch Eur J Physiol* **466,** 1163–1175.

Gupta DK & Wang TJ (2015). Natriuretic Peptides and Cardiometabolic Health. *Circ J Off J Jpn Circ Soc* **79,** 1647–1655.

Haghighi K, Bidwell P & Kranias EG (2014). Phospholamban interactome in cardiac contractility and survival: A new vision of an old friend. *J Mol Cell Cardiol* **77,** 160–167.

Hamad AM, Clayton A, Islam B & Knox AJ (2003). Guanylyl cyclases, nitric oxide, natriuretic peptides, and airway smooth muscle function. *Am J Physiol Lung Cell Mol Physiol* **285,** L973-983.

Hammond J & Balligand J-L (2012). Nitric oxide synthase and cyclic GMP signaling in cardiac myocytes: from contractility to remodeling. *J Mol Cell Cardiol* **52,** 330–340.

Han X, Kobzik L, Balligand JL, Kelly RA & Smith TW (1996). Nitric oxide synthase (NOS3)-mediated cholinergic modulation of Ca2+ current in adult rabbit atrioventricular nodal cells. *Circ Res* **78,** 998–1008.

Hanoune J & Defer N (2001). Regulation and role of adenylyl cyclase isoforms. *Annu Rev Pharmacol Toxicol* **41,** 145–174.

Hartzell HC & Fischmeister R (1986). Opposite effects of cyclic GMP and cyclic AMP on Ca2+ current in single heart cells. *Nature* **323,** 273–275.

Harvey RD & Hell JW (2013). CaV1.2 signaling complexes in the heart. *J Mol Cell Cardiol* **58,** 143–152.

Hayes JS, Bowling N, King KL & Boder GB (1982). Evidence for selective regulation of the phosphorylation of myocyte proteins by isoproterenol and prostaglandin E1. *Biochim Biophys Acta* **714,** 136–142.

He H, Giordano FJ, Hilal-Dandan R, Choi DJ, Rockman HA, McDonough PM, Bluhm WF, Meyer M, Sayen MR, Swanson E & Dillmann WH (1997). Overexpression of the rat sarcoplasmic reticulum Ca2+ ATPase gene in the heart of transgenic mice accelerates calcium transients and cardiac relaxation. *J Clin Invest* **100,** 380–389.

Heikaus CC, Pandit J & Klevit RE (2009). Cyclic nucleotide binding GAF domains from phosphodiesterases: structural and mechanistic insights. *Struct Lond Engl 1993* **17,** 1551–1557.

Hell JW (2010). Beta-adrenergic regulation of the L-type Ca2+ channel Ca(V)1.2 by PKA rekindles excitement. *Sci Signal* **3,** pe33.

Herring N, Rigg L, Terrar DA & Paterson DJ (2001). NO-cGMP pathway increases the hyperpolarisation-activated current, I(f), and heart rate during adrenergic stimulation. *Cardiovasc Res* **52,** 446–453.

Herrmann S, Schnorr S & Ludwig A (2015). HCN channels--modulators of cardiac and neuronal excitability. *Int J Mol Sci* **16,** 1429–1447.

van der Heyden MAG, Wijnhoven TJM & Opthof T (2005). Molecular aspects of adrenergic modulation of cardiac L-type Ca2+ channels. *Cardiovasc Res* **65,** 28–39.

Hofmann F (2005). The biology of cyclic GMP-dependent protein kinases. *J Biol Chem* **280,** 1–4.

Hollenberg SM (2007). Vasodilators in acute heart failure. *Heart Fail Rev* **12,** 143–147.

Hou J & Kang YJ (2012). Regression of pathological cardiac hypertrophy: signaling pathways and therapeutic targets. *Pharmacol Ther* **135,** 337–354.

Houser SR (2014). Role of RyR2 phosphorylation in heart failure and arrhythmias: protein kinase A-mediated hyperphosphorylation of the ryanodine receptor at serine 2808 does not alter cardiac contractility or cause heart failure and arrhythmias. *Circ Res* **114,** 1320–1327; discussion 1327.

Houslay MD & Adams DR (2003). PDE4 cAMP phosphodiesterases: modular enzymes that orchestrate signalling cross-talk, desensitization and compartmentalization. *Biochem J* **370,** 1–18.

Hua R, Adamczyk A, Robbins C, Ray G & Rose RA (2012). Distinct patterns of constitutive phosphodiesterase activity in mouse sinoatrial node and atrial myocardium. *PloS One* **7,** e47652.

Huang ZM, Gold JI & Koch WJ (2011). G protein-coupled receptor kinases in normal and failing myocardium. *Front Biosci Landmark Ed* **16,** 3047–3060.

Huke S & Bers DM (2008). Ryanodine receptor phosphorylation at Serine 2030, 2808 and 2814 in rat cardiomyocytes. *Biochem Biophys Res Commun* **376,** 80–85.

Hutson PH et al. (2011). The selective phosphodiesterase 9 (PDE9) inhibitor PF-04447943 (6-[(3S,4S)-4-methyl-1-(pyrimidin-2-ylmethyl)pyrrolidin-3-yl]-1-(tetrahydro-2H-pyran-4-yl)-1,5-dihydro-4H-pyrazolo[3,4-d]pyrimidin-4-one) enhances synaptic plasticity and cognitive function in rodents. *Neuropharmacology* **61,** 665–676.

Huxley H & Hanson J (1954). Changes in the cross-striations of muscle during contraction and stretch and their structural interpretation. *Nature* **173,** 973–976.

Hwang PM & Sykes BD (2015). Targeting the sarcomere to correct muscle function. *Nat Rev Drug Discov* **14,** 313–328.

Ibrahim M, Gorelik J, Yacoub MH & Terracciano CM (2011). The structure and function of cardiac t-tubules in health and disease. *Proc Biol Sci* **278,** 2714–2723.

Iffland A, Kohls D, Low S, Luan J, Zhang Y, Kothe M, Cao Q, Kamath AV, Ding Y-H & Ellenberger T (2005). Structural determinants for inhibitor specificity and selectivity in PDE2A using the wheat germ in vitro translation system. *Biochemistry (Mosc)* **44,** 8312–8325.

Imbrogno S, Gattuso A, Mazza R, Angelone T & Cerra MC (2015). β3 -AR and the vertebrate heart: a comparative view. *Acta Physiol Oxf Engl* **214,** 158–175.

Inserte J, Hernando V, Ruiz-Meana M, Poncelas-Nozal M, Fernández C, Agulló L, Sartorio C, Vilardosa U & Garcia-Dorado D (2014). Delayed phospholamban phosphorylation in post-conditioned heart favours Ca2+ normalization and contributes to protection. *Cardiovasc Res* **103,** 542–553.

Jaber M, Koch WJ, Rockman H, Smith B, Bond RA, Sulik KK, Ross J, Lefkowitz RJ, Caron MG & Giros B (1996). Essential role of beta-adrenergic receptor kinase 1 in cardiac development and function. *Proc Natl Acad Sci U S A* **93,** 12974–12979.

Jaleel M, Saha S, Shenoy AR & Visweswariah SS (2006). The kinase homology domain of receptor guanylyl cyclase C: ATP binding and identification of an adenine nucleotide sensitive site. *Biochemistry (Mosc)* **45,** 1888–1898.

Ji Y, Lalli MJ, Babu GJ, Xu Y, Kirkpatrick DL, Liu LH, Chiamvimonvat N, Walsh RA, Shull GE & Periasamy M (2000). Disruption of a single copy of the SERCA2 gene results in altered Ca2+ homeostasis and cardiomyocyte function. *J Biol Chem* **275,** 38073–38080.

Jiang D, Xiao B, Yang D, Wang R, Choi P, Zhang L, Cheng H & Chen SRW (2004). RyR2 mutations linked to ventricular tachycardia and sudden death reduce the threshold for store-overload-induced Ca2+ release (SOICR). *Proc Natl Acad Sci U S A* **101,** 13062–13067.

Jiang LH, Gawler DJ, Hodson N, Milligan CJ, Pearson HA, Porter V & Wray D (2000). Regulation of cloned cardiac L-type calcium channels by cGMP-dependent protein kinase. *J Biol Chem* **275,** 6135–6143.

Juilfs DM, Fülle HJ, Zhao AZ, Houslay MD, Garbers DL & Beavo JA (1997). A subset of olfactory neurons that selectively express cGMP-stimulated phosphodiesterase (PDE2) and guanylyl cyclase-D define a unique olfactory signal transduction pathway. *Proc Natl Acad Sci U S A* **94,** 3388–3395.

Jurevicius J & Fischmeister R (1996). cAMP compartmentation is responsible for a local activation of cardiac Ca2+ channels by beta-adrenergic agonists. *Proc Natl Acad Sci U S A* **93,** 295–299.

Jurevičius J, Skeberdis VA & Fischmeister R (2003). Role of cyclic nucleotide phosphodiesterase isoforms in cAMP compartmentation following β2-adrenergic stimulation of ICa,L in frog ventricular myocytes. *J Physiol* **551,** 239–252.

Jurevicius J, Skeberdis VA & Fischmeister R (2003). Role of cyclic nucleotide phosphodiesterase isoforms in cAMP compartmentation following beta2-adrenergic stimulation of ICa,L in frog ventricular myocytes. *J Physiol* **551,** 239–252.

Kadambi VJ, Ponniah S, Harrer JM, Hoit BD, Dorn GW, Walsh RA & Kranias EG (1996). Cardiac-specific overexpression of phospholamban alters calcium kinetics and resultant cardiomyocyte mechanics in transgenic mice. *J Clin Invest* **97,** 533–539.

Kanwar M, Walter C, Clarke M & Patarroyo-Aponte M (2016). Targeting heart failure with preserved ejection fraction: current status and future prospects. *Vasc Health Risk Manag* **12,** 129–141.

Kass DA (2012). Cardiac role of cyclic-GMP hydrolyzing phosphodiesterase type 5: from experimental models to clinical trials. *Curr Heart Fail Rep* **9,** 192–199.

Kass DA, Champion HC & Beavo JA (2007). Phosphodiesterase type 5: expanding roles in cardiovascular regulation. *Circ Res* **101,** 1084–1095.

Kawasaki H, Springett GM, Mochizuki N, Toki S, Nakaya M, Matsuda M, Housman DE & Graybiel AM (1998). A family of cAMP-binding proteins that directly activate Rap1. *Science* **282,** 2275–2279.

Kaye DM, Wiviott SD & Kelly RA (1999). Activation of nitric oxide synthase (NOS3) by mechanical activity alters contractile activity in a Ca2+-independent manner in cardiac myocytes: role of troponin I phosphorylation. *Biochem Biophys Res Commun* **256,** 398–403.

Keef KD, Hume JR & Zhong J (2001). Regulation of cardiac and smooth muscle Ca(2+) channels (Ca(V)1.2a,b) by protein kinases. *Am J Physiol Cell Physiol* **281,** C1743-1756.

Kemp CD & Conte JV (2012). The pathophysiology of heart failure. *Cardiovasc Pathol* **21,** 365–371.

Kentish JC, McCloskey DT, Layland J, Palmer S, Leiden JM, Martin AF & Solaro RJ (2001). Phosphorylation of troponin I by protein kinase A accelerates relaxation and crossbridge cycle kinetics in mouse ventricular muscle. *Circ Res* **88,** 1059–1065.

Keravis T & Lugnier C (2012). Cyclic nucleotide phosphodiesterase (PDE) isozymes as targets of the intracellular signalling network: benefits of PDE inhibitors in various diseases and perspectives for future therapeutic developments. *Br J Pharmacol* **165,** 1288–1305.

Kerfant B-G, Zhao D, Lorenzen-Schmidt I, Wilson LS, Cai S, Chen SRW, Maurice DH & Backx PH (2007). PI3Kgamma is required for PDE4, not PDE3, activity in subcellular microdomains containing the sarcoplasmic reticular calcium ATPase in cardiomyocytes. *Circ Res* **101,** 400–408.

Kirk JA, Holewinski RJ, Crowgey EL & Van Eyk JE (2016). Protein kinase G signaling in cardiac pathophysiology: Impact of proteomics on clinical trials. *Proteomics* **16,** 894–905.

Kirstein M, Rivet-Bastide M, Hatem S, Bénardeau A, Mercadier JJ & Fischmeister R (1995). Nitric oxide regulates the calcium current in isolated human atrial myocytes. *J Clin Invest* **95,** 794–802.

Kılıçkıran Avcı B, İkitimur B, Karadağ B & Öngen Z (2014). Renin-angiotensin system blockade in the treatment of heart failure and the role of valsartan in this treatment. *Anadolu Kardiyol Derg AKD Anatol J Cardiol* **14 Suppl 2,** S1-8.

Klarenbeek J, Goedhart J, van Batenburg A, Groenewald D & Jalink K (2015). Fourth-generation epac-based FRET sensors for cAMP feature exceptional brightness, photostability and dynamic range: characterization of dedicated sensors for FLIM, for ratiometry and with high affinity. *PloS One* **10,** e0122513.

Klarenbeek JB, Goedhart J, Hink MA, Gadella TWJ & Jalink K (2011). A mTurquoise-based cAMP sensor for both FLIM and ratiometric read-out has improved dynamic range. *PloS One* **6,** e19170.

Knight W & Yan C (2013). Therapeutic potential of PDE modulation in treating heart disease. *Future Med Chem* **5,** 1607–1620.

Knowles JW, Esposito G, Mao L, Hagaman JR, Fox JE, Smithies O, Rockman HA & Maeda N (2001). Pressure-independent enhancement of cardiac hypertrophy in natriuretic peptide receptor A-deficient mice. *J Clin Invest* **107,** 975–984.

Kobiałka M & Gorczyca WA (2000). Particulate guanylyl cyclases: multiple mechanisms of activation. *Acta Biochim Pol* **47,** 517–528.

Kohout TA & Lefkowitz RJ (2003). Regulation of G protein-coupled receptor kinases and arrestins during receptor desensitization. *Mol Pharmacol* **63,** 9–18.

Kots AY, Martin E, Sharina IG & Murad F (2009). A short history of cGMP, guanylyl cyclases, and cGMP-dependent protein kinases. *Handb Exp Pharmacol*1–14.

Kranias EG & Hajjar RJ (2012). Modulation of cardiac contractility by the phospholamban/SERCA2a regulatome. *Circ Res* **110,** 1646–1660.

Krendel M & Mooseker MS (2005). Myosins: tails (and heads) of functional diversity. *Physiol Bethesda Md* **20,** 239–251.

Kuhn M (2003). Structure, regulation, and function of mammalian membrane guanylyl cyclase receptors, with a focus on guanylyl cyclase-A. *Circ Res* **93,** 700–709.

Kuo JF & Greengard P (1969). Cyclic nucleotide-dependent protein kinases. IV. Widespread occurrence of adenosine 3',5'-monophosphate-dependent protein kinase in various tissues and phyla of the animal kingdom. *Proc Natl Acad Sci U S A* **64,** 1349–1355.

Lanfear DE, Hasan R, Gupta RC, Williams C, Czerska B, Tita C, Bazari R & Sabbah HN (2009). Short term effects of milrinone on biomarkers of necrosis, apoptosis, and inflammation in patients with severe heart failure. *J Transl Med* **7,** 67.

Langendorff O (1898). *Untersuchungen Am Überlebenden Säugetierherzen Pflüg Arch*291–332.

Lanner JT, Georgiou DK, Joshi AD & Hamilton SL (2010). Ryanodine receptors: structure, expression, molecular details, and function in calcium release. *Cold Spring Harb Perspect Biol* **2,** a003996.

Latek D, Modzelewska A, Trzaskowski B, Palczewski K & Filipek S (2012). G protein-coupled receptors--recent advances. *Acta Biochim Pol* **59,** 515–529.

Laurent A-C, Breckler M, Berthouze M & Lezoualc'h F (2012). Role of Epac in brain and heart. *Biochem Soc Trans* **40,** 51–57.

Layland J, Li J-M & Shah AM (2002). Role of cyclic GMP-dependent protein kinase in the contractile response to exogenous nitric oxide in rat cardiac myocytes. *J Physiol* **540,** 457–467.

Layland J, Solaro RJ & Shah AM (2005). Regulation of cardiac contractile function by troponin I phosphorylation. *Cardiovasc Res* **66,** 12–21.

Leblais V, Jo S-H, Chakir K, Maltsev V, Zheng M, Crow MT, Wang W, Lakatta EG & Xiao R-P (2004). Phosphatidylinositol 3-kinase offsets cAMP-mediated positive inotropic effect via inhibiting Ca2+ influx in cardiomyocytes. *Circ Res* **95,** 1183–1190.

Lee DI et al. (2015). Phosphodiesterase 9A controls nitric-oxide-independent cGMP and hypertrophic heart disease. *Nature* **519,** 472–476.

Lee DI & Kass DA (2012). Phosphodiesterases and cyclic GMP regulation in heart muscle. *Physiol Bethesda Md* **27,** 248–258.

Lehnart SE, Wehrens XHT, Reiken S, Warrier S, Belevych AE, Harvey RD, Richter W, Jin S-LC, Conti M & Marks AR (2005). Phosphodiesterase 4D deficiency in the ryanodine-receptor complex promotes heart failure and arrhythmias. *Cell* **123,** 25–35.

Leroy J, Richter W, Mika D, Castro LRV, Abi-Gerges A, Xie M, Scheitrum C, Lefebvre F, Schittl J, Mateo P, Westenbroek R, Catterall WA, Charpentier F, Conti M, Fischmeister R & Vandecasteele G (2011). Phosphodiesterase 4B in the cardiac L-type Ca^{2+} channel complex regulates Ca^{2+} current and protects against ventricular arrhythmias in mice. *J Clin Invest* **121,** 2651–2661.

Levy FO (2013). Cardiac PDEs and crosstalk between cAMP and cGMP signalling pathways in the regulation of contractility. *Naunyn Schmiedebergs Arch Pharmacol* **386,** 665–670.

Lezoualc'h F, Fazal L, Laudette M & Conte C (2016). Cyclic AMP Sensor EPAC Proteins and Their Role in Cardiovascular Function and Disease. *Circ Res* **118,** 881–897.

Li D, Lu C-J, Hao G, Wright H, Woodward L, Liu K, Vergari E, Surdo NC, Herring N, Zaccolo M & Paterson DJ (2015). Efficacy of B-Type Natriuretic Peptide Is Coupled to Phosphodiesterase 2A in Cardiac Sympathetic Neurons. *Hypertension* **66,** 190–198.

Liao R, Podesser BK & Lim CC (2012). The continuing evolution of the Langendorff and ejecting murine heart: new advances in cardiac phenotyping. *Am J Physiol Heart Circ Physiol* **303,** H156-167.

Lin DTS, Fretier P, Jiang C & Vincent SR (2010). Nitric oxide signaling via cGMP-stimulated phosphodiesterase in striatal neurons. *Synap N Y N* **64,** 460–466.

Lincoln TM & Corbin JD (1978). Purified cyclic GMP-dependent protein kinase catalyzes the phosphorylation of cardiac troponin inhibitory subunit (TN-1). *J Biol Chem* **253,** 337–339.

Linder JU & Schultz JE (2008). Versatility of signal transduction encoded in dimeric adenylyl cyclases. *Curr Opin Struct Biol* **18,** 667–672.

Lindner E (1957). [Submicroscopic morphology of the cardiac muscle]. *Z Für Zellforsch Mikrosk Anat Vienna Austria 1948* **45,** 702–746.

Lissandron V & Zaccolo M (2006). Compartmentalized cAMP/PKA signalling regulates cardiac excitation-contraction coupling. *J Muscle Res Cell Motil* **27,** 399–403.

Loffredo FS et al. (2013). Growth differentiation factor 11 is a circulating factor that reverses age-related cardiac hypertrophy. *Cell* **153,** 828–839.

Lopez MJ, Wong SK, Kishimoto I, Dubois S, Mach V, Friesen J, Garbers DL & Beuve A (1995). Salt-resistant hypertension in mice lacking the guanylyl cyclase-A receptor for atrial natriuretic peptide. *Nature* **378,** 65–68.

Lugnier C (2006). Cyclic nucleotide phosphodiesterase (PDE) superfamily: a new target for the development of specific therapeutic agents. *Pharmacol Ther* **109,** 366–398.

Lugnier C (2011). PDE inhibitors: a new approach to treat metabolic syndrome? *Curr Opin Pharmacol* **11,** 698–706.

Lugnier C, Keravis T, Le Bec A, Pauvert O, Proteau S & Rousseau E (1999). Characterization of cyclic nucleotide phosphodiesterase isoforms associated to isolated cardiac nuclei. *Biochim Biophys Acta* **1472,** 431–446.

Lugnier C, Muller B, Le Bec A, Beaudry C & Rousseau E (1993). Characterization of indolidan- and rolipram-sensitive cyclic nucleotide phosphodiesterases in canine and human cardiac microsomal fractions. *J Pharmacol Exp Ther* **265,** 1142–1151.

Luo W, Grupp IL, Harrer J, Ponniah S, Grupp G, Duffy JJ, Doetschman T & Kranias EG (1994). Targeted ablation of the phospholamban gene is associated with markedly enhanced myocardial contractility and loss of beta-agonist stimulation. *Circ Res* **75,** 401–409.

Lymperopoulos A, Rengo G & Koch WJ (2013). Adrenergic Nervous System in Heart Failure Pathophysiology and Therapy. *Circ Res* **113,** 739–753.

Maack C & O'Rourke B (2007). Excitation-contraction coupling and mitochondrial energetics. *Basic Res Cardiol* **102,** 369–392.

MacFarland RT, Zelus BD & Beavo JA (1991). High concentrations of a cGMP-stimulated phosphodiesterase mediate ANP-induced decreases in cAMP and steroidogenesis in adrenal glomerulosa cells. *J Biol Chem* **266,** 136–142.

Maier LS, Zhang T, Chen L, DeSantiago J, Brown JH & Bers DM (2003). Transgenic CaMKIIdeltaC overexpression uniquely alters cardiac myocyte Ca2+ handling: reduced SR Ca2+ load and activated SR Ca2+ release. *Circ Res* **92,** 904–911.

Mann DL (1999). Mechanisms and models in heart failure: A combinatorial approach. *Circulation* **100,** 999–1008.

Marbán E (2002). Cardiac channelopathies. *Nature* **415,** 213–218.

Marks AR (2013). Calcium cycling proteins and heart failure: mechanisms and therapeutics. *J Clin Invest* **123,** 46–52.

Martinez SE, Beavo JA & Hol WGJ (2002*a*). GAF domains: two-billion-year-old molecular switches that bind cyclic nucleotides. *Mol Interv* **2,** 317–323.

Martinez SE, Wu AY, Glavas NA, Tang X-B, Turley S, Hol WGJ & Beavo JA (2002*b*). The two GAF domains in phosphodiesterase 2A have distinct roles in dimerization and in cGMP binding. *Proc Natl Acad Sci U S A* **99,** 13260–13265.

Martins TJ, Mumby MC & Beavo JA (1982). Purification and characterization of a cyclic GMP-stimulated cyclic nucleotide phosphodiesterase from bovine tissues. *J Biol Chem* **257,** 1973–1979.

Marx SO, Reiken S, Hisamatsu Y, Jayaraman T, Burkhoff D, Rosemblit N & Marks AR (2000). PKA phosphorylation dissociates FKBP12.6 from the calcium release channel (ryanodine receptor): defective regulation in failing hearts. *Cell* **101,** 365–376.

Mattiazzi A & Kranias EG (2014). The role of CaMKII regulation of phospholamban activity in heart disease. *Front Pharmacol* **5,** 5.

Maurice DH, Ke H, Ahmad F, Wang Y, Chung J & Manganiello VC (2014). Advances in targeting cyclic nucleotide phosphodiesterases. *Nat Rev Drug Discov* **13,** 290–314.

Maurice DH, Palmer D, Tilley DG, Dunkerley HA, Netherton SJ, Raymond DR, Elbatarny HS & Jimmo SL (2003). Cyclic nucleotide phosphodiesterase activity, expression, and targeting in cells of the cardiovascular system. *Mol Pharmacol* **64,** 533–546.

Mehel H et al. (2013). Phosphodiesterase-2 is up-regulated in human failing hearts and blunts β-adrenergic responses in cardiomyocytes. *J Am Coll Cardiol* **62,** 1596–1606.

Méry PF, Frace AM, Hartzell HC & Fischmeister R (1993*a*). A comparative analysis of the time course of cardiac Ca2+ current response to rapid applications of beta-adrenergic and dihydropyridine agonists. *Naunyn Schmiedebergs Arch Pharmacol* **348,** 197–206.

Méry PF, Lohmann SM, Walter U & Fischmeister R (1991). Ca2+ current is regulated by cyclic GMP-dependent protein kinase in mammalian cardiac myocytes. *Proc Natl Acad Sci U S A* **88,** 1197–1201.

Méry PF, Pavoine C, Belhassen L, Pecker F & Fischmeister R (1993*b*). Nitric oxide regulates cardiac Ca2+ current. Involvement of cGMP-inhibited and cGMP-stimulated phosphodiesterases through guanylyl cyclase activation. *J Biol Chem* **268,** 26286–26295.

Méry PF, Pavoine C, Pecker F & Fischmeister R (1995). Erythro-9-(2-hydroxy-3-nonyl)adenine inhibits cyclic GMP-stimulated phosphodiesterase in isolated cardiac myocytes. *Mol Pharmacol* **48,** 121–130.

Métrich M, Morel E, Berthouze M, Pereira L, Charron P, Gomez A-M & Lezoualc'h F (2009). Functional characterization of the cAMP-binding proteins Epac in cardiac myocytes. *Pharmacol Rep PR* **61,** 146–153.

Michel MC, Ochodnicky P & Summers RJ (2010). Tissue functions mediated by β3-adrenoceptors—findings and challenges. *Naunyn Schmiedebergs Arch Pharmacol* **382,** 103–108.

Mika D, Bobin P, Pomérance M, Lechêne P, Westenbroek RE, Catterall WA, Vandecasteele G, Leroy J & Fischmeister R (2013). Differential regulation of cardiac excitation-contraction coupling by cAMP phosphodiesterase subtypes. *Cardiovasc Res* **100,** 336–346.

Mika D, Leroy J, Vandecasteele G & Fischmeister R (2012). PDEs create local domains of cAMP signaling. *J Mol Cell Cardiol* **52,** 323–329.

Milano CA, Allen LF, Rockman HA, Dolber PC, McMinn TR, Chien KR, Johnson TD, Bond RA & Lefkowitz RJ (1994). Enhanced myocardial function in transgenic mice overexpressing the beta 2-adrenergic receptor. *Science* **264,** 582–586.

Miller CL, Oikawa M, Cai Y, Wojtovich AP, Nagel DJ, Xu X, Xu H, Florio V, Rybalkin SD, Beavo JA, Chen Y-F, Li J-D, Blaxall BC, Abe J & Yan C (2009). Role of Ca2+/calmodulin-stimulated cyclic nucleotide phosphodiesterase 1 in mediating cardiomyocyte hypertrophy. *Circ Res* **105,** 956–964.

Mokni W, Keravis T, Etienne-Selloum N, Walter A, Kane MO, Schini-Kerth VB & Lugnier C (2010). Concerted regulation of cGMP and cAMP phosphodiesterases in early cardiac hypertrophy induced by angiotensin II. *PloS One* **5,** e14227.

Molina CE, Leroy J, Richter W, Xie M, Scheitrum C, Lee I-O, Maack C, Rucker-Martin C, Donzeau-Gouge P, Verde I, Llach A, Hove-Madsen L, Conti M, Vandecasteele G & Fischmeister R (2012). Cyclic adenosine monophosphate phosphodiesterase type 4 protects against atrial arrhythmias. *J Am Coll Cardiol* **59,** 2182–2190.

Molkentin JD (2003). A friend within the heart: natriuretic peptide receptor signaling. *J Clin Invest* **111,** 1275–1277.

Molkentin JD (2004). Calcineurin-NFAT signaling regulates the cardiac hypertrophic response in coordination with the MAPKs. *Cardiovasc Res* **63,** 467–475.

Mongillo M, Tocchetti CG, Terrin A, Lissandron V, Cheung Y-F, Dostmann WR, Pozzan T, Kass DA, Paolocci N, Houslay MD & Zaccolo M (2006). Compartmentalized phosphodiesterase-2 activity blunts beta-adrenergic cardiac inotropy via an NO/cGMP-dependent pathway. *Circ Res* **98,** 226–234.

Moniotte S, Vaerman JL, Kockx MM, Larrouy D, Langin D, Noirhomme P & Balligand JL (2001). Real-time RT-PCR for the detection of beta-adrenoceptor messenger RNAs in small human endomyocardial biopsies. *J Mol Cell Cardiol* **33,** 2121–2133.

Morimoto S (2008). Sarcomeric proteins and inherited cardiomyopathies. *Cardiovasc Res* **77,** 659–666.

Movsesian M (2016). Novel approaches to targeting PDE3 in cardiovascular disease. *Pharmacol Ther*; DOI: 10.1016/j.pharmthera.2016.03.014.

Movsesian M, Stehlik J, Vandeput F & Bristow MR (2009). Phosphodiesterase inhibition in heart failure. *Heart Fail Rev* **14,** 255–263.

Mullershausen F, Friebe A, Feil R, Thompson WJ, Hofmann F & Koesling D (2003). Direct activation of PDE5 by cGMP: long-term effects within NO/cGMP signaling. *J Cell Biol* **160,** 719–727.

Najafi A, Sequeira V, Kuster DWD & van der Velden J (2016). β-adrenergic receptor signalling and its functional consequences in the diseased heart. *Eur J Clin Invest* **46,** 362–374.

Nikolaev VO, Bünemann M, Schmitteckert E, Lohse MJ & Engelhardt S (2006). Cyclic AMP imaging in adult cardiac myocytes reveals far-reaching beta1-adrenergic but locally confined beta2-adrenergic receptor-mediated signaling. *Circ Res* **99,** 1084–1091.

Nikolaev VO, Gambaryan S, Engelhardt S, Walter U & Lohse MJ (2005). Real-time monitoring of the PDE2 activity of live cells: hormone-stimulated cAMP hydrolysis is faster than hormone-stimulated cAMP synthesis. *J Biol Chem* **280,** 1716–1719.

Nishikimi T, Maeda N & Matsuoka H (2006). The role of natriuretic peptides in cardioprotection. *Cardiovasc Res* **69,** 318–328.

O'Brien F, Venturi E & Sitsapesan R (2015). The ryanodine receptor provides high throughput Ca2+-release but is precisely regulated by networks of associated proteins: a focus on proteins relevant to phosphorylation. *Biochem Soc Trans* **43,** 426–433.

Oda T, Iwasa M, Aihara T, Maéda Y & Narita A (2009). The nature of the globular- to fibrous-actin transition. *Nature* **457,** 441–445.

Okumura S, Kawabe J, Yatani A, Takagi G, Lee M-C, Hong C, Liu J, Takagi I, Sadoshima J, Vatner DE, Vatner SF & Ishikawa Y (2003). Type 5 adenylyl cyclase disruption alters not only sympathetic but also parasympathetic and calcium-mediated cardiac regulation. *Circ Res* **93,** 364–371.

Omori K & Kotera J (2007). Overview of PDEs and their regulation. *Circ Res* **100,** 309–327.

Opie LH, Commerford PJ, Gersh BJ & Pfeffer MA (2006). Controversies in ventricular remodelling. *Lancet Lond Engl* **367,** 356–367.

Orchard C & Brette F (2008). t-Tubules and sarcoplasmic reticulum function in cardiac ventricular myocytes. *Cardiovasc Res* **77,** 237–244.

Osadchii OE (2007). Myocardial phosphodiesterases and regulation of cardiac contractility in health and cardiac disease. *Cardiovasc Drugs Ther Spons Int Soc Cardiovasc Pharmacother* **21,** 171–194.

Ostrom RS, Violin JD, Coleman S & Insel PA (2000). Selective enhancement of beta-adrenergic receptor signaling by overexpression of adenylyl cyclase type 6: colocalization of receptor and adenylyl cyclase in caveolae of cardiac myocytes. *Mol Pharmacol* **57,** 1075–1079.

Ozawa T (2010). Modulation of ryanodine receptor Ca2+ channels (Review). *Mol Med Rep* **3,** 199–204.

Packer M, Carver JR, Rodeheffer RJ, Ivanhoe RJ, DiBianco R, Zeldis SM, Hendrix GH, Bommer WJ, Elkayam U & Kukin ML (1991). Effect of oral milrinone on mortality in severe chronic heart failure. The PROMISE Study Research Group. *N Engl J Med* **325,** 1468–1475.

Padayatti PS, Pattanaik P, Ma X & van den Akker F (2004*a*). Structural insights into the regulation and the activation mechanism of mammalian guanylyl cyclases. *Pharmacol Ther* **104,** 83–99.

Padayatti PS, Pattanaik P, Ma X & van den Akker F (2004*b*). Structural insights into the regulation and the activation mechanism of mammalian guanylyl cyclases. *Pharmacol Ther* **104,** 83–99.

Pandit J, Forman MD, Fennell KF, Dillman KS & Menniti FS (2009). Mechanism for the allosteric regulation of phosphodiesterase 2A deduced from the X-ray structure of a near full-length construct. *Proc Natl Acad Sci U S A* **106,** 18225–18230.

Parissis JT, Farmakis D & Nieminen M (2007). Classical inotropes and new cardiac enhancers. *Heart Fail Rev* **12,** 149–156.

Pavan B, Biondi C & Dalpiaz A (2009). Adenylyl cyclases as innovative therapeutic goals. *Drug Discov Today* **14,** 982–991.

Perera RK & Nikolaev VO (2013). Compartmentation of cAMP signalling in cardiomyocytes in health and disease. *Acta Physiol Oxf Engl* **207,** 650–662.

Perino A et al. (2011). Integrating Cardiac PIP3 and cAMP Signaling through a PKA Anchoring Function of p110γ. *Mol Cell* **42,** 84–95.

Petersen JW & Felker GM (2008). Inotropes in the management of acute heart failure. *Crit Care Med* **36,** S106-111.

Piper S & McDonagh T (2014). The role of intravenous vasodilators in acute heart failure management. *Eur J Heart Fail* **16,** 827–834.

Podda MV & Grassi C (2014). New perspectives in cyclic nucleotide-mediated functions in the CNS: the emerging role of cyclic nucleotide-gated (CNG) channels. *Pflüg Arch Eur J Physiol* **466,** 1241–1257.

Podzuweit T, Nennstiel P & Müller A (1995). Isozyme selective inhibition of cGMP-stimulated cyclic nucleotide phosphodiesterases by erythro-9-(2-hydroxy-3-nonyl) adenine. *Cell Signal* **7,** 733–738.

Porter KR & Palade GE (1957). Studies on the endoplasmic reticulum. III. Its form and distribution in striated muscle cells. *J Biophys Biochem Cytol* **3,** 269–300.

Potter LR (2011). Guanylyl cyclase structure, function and regulation. *Cell Signal* **23,** 1921–1926.

Poulos TL (2006). Soluble guanylate cyclase. *Curr Opin Struct Biol* **16,** 736–743.

Provencher S, Herve P, Jais X, Lebrec D, Humbert M, Simonneau G & Sitbon O (2006). Deleterious effects of beta-blockers on exercise capacity and hemodynamics in patients with portopulmonary hypertension. *Gastroenterology* **130,** 120–126.

Pyriochou A & Papapetropoulos A (2005). Soluble guanylyl cyclase: more secrets revealed. *Cell Signal* **17,** 407–413.

Qvigstad E, Moltzau LR, Aronsen JM, Nguyen CHT, Hougen K, Sjaastad I, Levy FO, Skomedal T & Osnes J-B (2010). Natriuretic peptides increase beta1-adrenoceptor signalling in failing hearts through phosphodiesterase 3 inhibition. *Cardiovasc Res* **85,** 763–772.

Rababa'h A, Singh S, Suryavanshi SV, Altarabsheh SE, Deo SV & McConnell BK (2015). Compartmentalization role of A-kinase anchoring proteins (AKAPs) in mediating protein kinase A (PKA) signaling and cardiomyocyte hypertrophy. *Int J Mol Sci* **16,** 218–229.

Rall TW & Sutherland EW (1958). Formation of a cyclic adenine ribonucleotide by tissue particles. *J Biol Chem* **232,** 1065–1076.

Reiken S, Wehrens XHT, Vest JA, Barbone A, Klotz S, Mancini D, Burkhoff D & Marks AR (2003). β-Blockers Restore Calcium Release Channel Function and Improve Cardiac Muscle Performance in Human Heart Failure. *Circulation* **107,** 2459–2466.

Rivet-Bastide M, Vandecasteele G, Hatem S, Verde I, Bénardeau A, Mercadier JJ & Fischmeister R (1997). cGMP-stimulated cyclic nucleotide phosphodiesterase regulates the basal calcium current in human atrial myocytes. *J Clin Invest* **99,** 2710–2718.

Robertson IM, Sun Y-B, Li MX & Sykes BD (2010). A structural and functional perspective into the mechanism of Ca2+-sensitizers that target the cardiac troponin complex. *J Mol Cell Cardiol* **49,** 1031–1041.

Rochais F, Abi-Gerges A, Horner K, Lefebvre F, Cooper DM., Conti M, Fischmeister R & Vandecasteele G (2006). A specific pattern of phosphodiesterases controls the cAMP signals generated by different Gs-coupled receptors in adult rat ventricular myocytes. *Circ Res* **98,** 1081–1088.

Rochais F, Vandecasteele G, Lefebvre F, Lugnier C, Lum H, Mazet J-L, Cooper DMF & Fischmeister R (2004). Negative feedback exerted by cAMP-dependent protein kinase and cAMP phosphodiesterase on subsarcolemmal cAMP signals in intact cardiac myocytes: an in vivo study using adenovirus-mediated expression of CNG channels. *J Biol Chem* **279,** 52095–52105.

Rockman HA, Hamilton RA, Jones LR, Milano CA, Mao L & Lefkowitz RJ (1996). Enhanced myocardial relaxation in vivo in transgenic mice overexpressing the beta2-adrenergic receptor is associated with reduced phospholamban protein. *J Clin Invest* **97,** 1618–1623.

de Rooij J, Zwartkruis FJ, Verheijen MH, Cool RH, Nijman SM, Wittinghofer A & Bos JL (1998). Epac is a Rap1 guanine-nucleotide-exchange factor directly activated by cyclic AMP. *Nature* **396,** 474–477.

Rosenkranz AC, Woods RL, Dusting GJ & Ritchie RH (2003). Antihypertrophic actions of the natriuretic peptides in adult rat cardiomyocytes: importance of cyclic GMP. *Cardiovasc Res* **57,** 515–522.

Rosman GJ, Martins TJ, Sonnenburg WK, Beavo JA, Ferguson K & Loughney K (1997). Isolation and characterization of human cDNAs encoding a cGMP-stimulated 3',5'-cyclic nucleotide phosphodiesterase. *Gene* **191,** 89–95.

Rossi AE & Dirksen RT (2006). Sarcoplasmic reticulum: the dynamic calcium governor of muscle. *Muscle Nerve* **33,** 715–731.

Rozec B & Gauthier C (2006). beta3-adrenoceptors in the cardiovascular system: putative roles in human pathologies. *Pharmacol Ther* **111,** 652–673.

Rybalkin SD, Yan C, Bornfeldt KE & Beavo JA (2003). Cyclic GMP phosphodiesterases and regulation of smooth muscle function. *Circ Res* **93,** 280–291.

Rybin VO, Pak E, Alcott S & Steinberg SF (2003). Developmental changes in beta2-adrenergic receptor signaling in ventricular myocytes: the role of Gi proteins and caveolae microdomains. *Mol Pharmacol* **63,** 1338–1348.

Rybin VO, Xu X, Lisanti MP & Steinberg SF (2000). Differential targeting of beta -adrenergic receptor subtypes and adenylyl cyclase to cardiomyocyte caveolae. A mechanism to functionally regulate the cAMP signaling pathway. *J Biol Chem* **275,** 41447–41457.

Sadana R & Dessauer CW (2009). Physiological roles for G protein-regulated adenylyl cyclase isoforms: insights from knockout and overexpression studies. *Neurosignals* **17,** 5–22.

Schindler RF, Poon KL, Simrick S & Brand T (2012). The Popeye domain containing genes: essential elements in heart rate control. *Cardiovasc Diagn Ther* **2,** 308–319.

Schindler RFR & Brand T (2016). The Popeye domain containing protein family - A novel class of cAMP effectors with important functions in multiple tissues. *Prog Biophys Mol Biol* **120,** 28–36.

Schlossmann J & Hofmann F (2005). cGMP-dependent protein kinases in drug discovery. *Drug Discov Today* **10,** 627–634.

Schröder F, Klein G, Fiedler B, Bastein M, Schnasse N, Hillmer A, Ames S, Gambaryan S, Drexler H, Walter U, Lohmann SM & Wollert KC (2003). Single L-type Ca(2+) channel regulation by cGMP-dependent protein kinase type I in adult cardiomyocytes from PKG I transgenic mice. *Cardiovasc Res* **60,** 268–277.

Seybold J, Thomas D, Witzenrath M, Boral S, Hocke AC, Bürger A, Hatzelmann A, Tenor H, Schudt C, Krüll M, Schütte H, Hippenstiel S & Suttorp N (2005). Tumor necrosis factor-alpha-dependent expression of phosphodiesterase 2: role in endothelial hyperpermeability. *Blood* **105,** 3569–3576.

Shannon TR, Ginsburg KS & Bers DM (2002). Quantitative assessment of the SR Ca2+ leak-load relationship. *Circ Res* **91,** 594–600.

Sharma S, Kumar K, Deshmukh R & Sharma PL (2013). Phosphodiesterases: Regulators of cyclic nucleotide signals and novel molecular target for movement disorders. *Eur J Pharmacol* **714,** 486–497.

Shiels HA & Galli GLJ (2014). The sarcoplasmic reticulum and the evolution of the vertebrate heart. *Physiol Bethesda Md* **29,** 456–469.

Shimizu K, Shintani Y, Ding W-G, Matsuura H & Bamba T (2002). Potentiation of slow component of delayed rectifier K(+) current by cGMP via two distinct mechanisms: inhibition of phosphodiesterase 3 and activation of protein kinase G. *Br J Pharmacol* **137,** 127–137.

Singh A, Laribi S, Teerlink JR & Mebazaa A (2016). Agents with vasodilator properties in acute heart failure. *Eur Heart J*; DOI: 10.1093/eurheartj/ehv755.

Skeberdis VA, Gendviliene V, Zablockaite D, Treinys R, Macianskiene R, Bogdelis A, Jurevicius J & Fischmeister R (2008). beta3-adrenergic receptor activation increases human atrial tissue contractility and stimulates the L-type Ca2+ current. *J Clin Invest* **118,** 3219–3227.

Skrzypiec-Spring M, Grotthus B, Szelag A & Schulz R (2007). Isolated heart perfusion according to Langendorff---still viable in the new millennium. *J Pharmacol Toxicol Methods* **55,** 113–126.

Smith CJ, Krall J, Manganiello VC & Movsesian MA (1993). Cytosolic and sarcoplasmic reticulum-associated low Km, cGMP-inhibited cAMP phosphodiesterase in mammalian myocardium. *Biochem Biophys Res Commun* **190,** 516–521.

Smith PK, Krohn RI, Hermanson GT, Mallia AK, Gartner FH, Provenzano MD, Fujimoto EK, Goeke NM, Olson BJ & Klenk DC (1985). Measurement of protein using bicinchoninic acid. *Anal Biochem* **150,** 76–85.

Soderling SH, Bayuga SJ & Beavo JA (1998). Identification and characterization of a novel family of cyclic nucleotide phosphodiesterases. *J Biol Chem* **273,** 15553–15558.

Soeller C & Cannell MB (1999). Examination of the transverse tubular system in living cardiac rat myocytes by 2-photon microscopy and digital image-processing techniques. *Circ Res* **84,** 266–275.

Solaro RJ, Henze M & Kobayashi T (2013). Integration of troponin I phosphorylation with cardiac regulatory networks. *Circ Res* **112,** 355–366.

Soler F, Fernández-Belda F, Pérez-Schindler J, Handschin C, Fuente T & Hernandez-Cascales J (2015). PDE2 activity differs in right and left rat ventricular myocardium and differentially regulates β2 adrenoceptor-mediated effects. *Exp Biol Med Maywood NJ* **240,** 1205–1213.

Song W, Wang H & Wu Q (2015). Atrial natriuretic peptide in cardiovascular biology and disease (NPPA). *Gene* **569,** 1–6.

Soni S, Scholten A, Vos MA & van Veen TAB (2014). Anchored protein kinase A signalling in cardiac cellular electrophysiology. *J Cell Mol Med* **18,** 2135–2146.

Sonnenburg WK, Mullaney PJ & Beavo JA (1991). Molecular cloning of a cyclic GMP-stimulated cyclic nucleotide phosphodiesterase cDNA. Identification and distribution of isozyme variants. *J Biol Chem* **266,** 17655–17661.

Sperelakis N & Rubio R (1971). An orderly lattice of axial tubules which interconnect adjacent transverse tubules in guinea-pig ventricular myocardium. *J Mol Cell Cardiol* **2,** 211–220.

Stangherlin A, Gesellchen F, Zoccarato A, Terrin A, Fields LA, Berrera M, Surdo NC, Craig MA, Smith G, Hamilton G & Zaccolo M (2011). cGMP signals modulate cAMP levels in a compartment-specific manner to regulate catecholamine-dependent signaling in cardiac myocytes. *Circ Res* **108,** 929–939.

Stangherlin A & Zaccolo M (2012). cGMP-cAMP interplay in cardiac myocytes: a local affair with far-reaching consequences for heart function. *Biochem Soc Trans* **40,** 11–14.

Steegborn C (2014). Structure, mechanism, and regulation of soluble adenylyl cyclases - similarities and differences to transmembrane adenylyl cyclases. *Biochim Biophys Acta* **1842,** 2535–2547.

Steinberg SF (1999). The molecular basis for distinct beta-adrenergic receptor subtype actions in cardiomyocytes. *Circ Res* **85,** 1101–1111.

Straub F (1942). Actin. *Stud Inst Med Chem Univ Szeged*3–15.

Stroop SD, Charbonneau H & Beavo JA (1989). Direct photolabeling of the cGMP-stimulated cyclic nucleotide phosphodiesterase. *J Biol Chem* **264,** 13718–13725.

Surks HK (2007). cGMP-dependent protein kinase I and smooth muscle relaxation: a tale of two isoforms. *Circ Res* **101,** 1078–1080.

Swedberg K (1998). History of Beta blockers in congestive heart failure. *Heart Br Card Soc* **79,** S29-30.

Takimoto E (2012). Cyclic GMP-dependent signaling in cardiac myocytes. *Circ J Off J Jpn Circ Soc* **76,** 1819–1825.

Takimoto E, Champion HC, Belardi D, Moslehi J, Mongillo M, Mergia E, Montrose DC, Isoda T, Aufiero K, Zaccolo M, Dostmann WR, Smith CJ & Kass DA (2005*a*). cGMP catabolism by phosphodiesterase 5A regulates cardiac adrenergic stimulation by NOS3-dependent mechanism. *Circ Res* **96,** 100–109.

Takimoto E, Champion HC, Li M, Belardi D, Ren S, Rodriguez ER, Bedja D, Gabrielson KL, Wang Y & Kass DA (2005*b*). Chronic inhibition of cyclic GMP phosphodiesterase 5A prevents and reverses cardiac hypertrophy. *Nat Med* **11,** 214–222.

Tamura N, Ogawa Y, Chusho H, Nakamura K, Nakao K, Suda M, Kasahara M, Hashimoto R, Katsuura G, Mukoyama M, Itoh H, Saito Y, Tanaka I, Otani H, Katsuki M & Nakao K (2000). Cardiac fibrosis in mice lacking brain natriuretic peptide. *Proc Natl Acad Sci U S A* **97,** 4239–4244.

Tang C-M & Insel PA (2004). GPCR expression in the heart; “new” receptors in myocytes and fibroblasts. *Trends Cardiovasc Med* **14,** 94–99.

Taskén K & Aandahl EM (2004). Localized effects of cAMP mediated by distinct routes of protein kinase A. *Physiol Rev* **84,** 137–167.

Taylor MRG & Bristow MR (2004). The emerging pharmacogenomics of the beta-adrenergic receptors. *Congest Heart Fail Greenwich Conn* **10,** 281–288.

Terasaki WL & Appleman MM (1975). The role of cyclic GMP in the regulation of cyclic AMP hydrolysis. *Metabolism* **24,** 311–319.

Thompson WJ & Appleman MM (1971). Characterization of cyclic nucleotide phosphodiesterases of rat tissues. *J Biol Chem* **246,** 3145–3150.

Tresguerres M, Levin LR & Buck J (2011). Intracellular cAMP signaling by soluble adenylyl cyclase. *Kidney Int* **79,** 1277–1288.

Tsai EJ & Kass DA (2009). Cyclic GMP signaling in cardiovascular pathophysiology and therapeutics. *Pharmacol Ther* **122,** 216–238.

Turko IV, Francis SH & Corbin JD (1998). Binding of cGMP to both allosteric sites of cGMP-binding cGMP-specific phosphodiesterase (PDE5) is required for its phosphorylation. *Biochem J* **329 (Pt 3),** 505–510.

Turnham RE & Scott JD (2016). Protein kinase A catalytic subunit isoform PRKACA; History, function and physiology. *Gene* **577,** 101–108.

Vandecasteele G, Verde I, Rücker-Martin C, Donzeau-Gouge P & Fischmeister R (2001). Cyclic GMP regulation of the L-type Ca(2+) channel current in human atrial myocytes. *J Physiol* **533,** 329–340.

Vandeput F, Krall J, Ockaili R, Salloum FN, Florio V, Corbin JD, Francis SH, Kukreja RC & Movsesian MA (2009). cGMP-Hydrolytic Activity and Its Inhibition by Sildenafil in Normal and Failing Human and Mouse Myocardium. *J Pharmacol Exp Ther* **330,** 884–891.

Vandeput F, Wolda SL, Krall J, Hambleton R, Uher L, McCaw KN, Radwanski PB, Florio V & Movsesian MA (2007). Cyclic nucleotide phosphodiesterase PDE1C1 in human cardiac myocytes. *J Biol Chem* **282,** 32749–32757.

van der Velden J (2011). Diastolic myofilament dysfunction in the failing human heart. *Pflüg Arch Eur J Physiol* **462,** 155–163.

Vinogradova TM, Sirenko S, Lyashkov AE, Younes A, Li Y, Zhu W, Yang D, Ruknudin AM, Spurgeon H & Lakatta EG (2008). Constitutive phosphodiesterase activity restricts spontaneous beating rate of cardiac pacemaker cells by suppressing local Ca2+ releases. *Circ Res* **102,** 761–769.

Volpe M, Carnovali M & Mastromarino V (2016). The natriuretic peptides system in the pathophysiology of heart failure: from molecular basis to treatment. *Clin Sci Lond Engl 1979* **130,** 57–77.

Wada A, Tsutamoto T, Matsuda Y & Kinoshita M (1994). Cardiorenal and neurohumoral effects of endogenous atrial natriuretic peptide in dogs with severe congestive heart failure using a specific antagonist for guanylate cyclase-coupled receptors. *Circulation* **89,** 2232–2240.

Wahl-Schott C, Fenske S & Biel M (2014). HCN channels: new roles in sinoatrial node function. *Curr Opin Pharmacol* **15,** 83–90.

Walsh DA & Van Patten SM (1994). Multiple pathway signal transduction by the cAMP-dependent protein kinase. *FASEB J Off Publ Fed Am Soc Exp Biol* **8,** 1227–1236.

Wang J, Wu X, Hu X & Jiang H (2015). Selectively inhibiting PDE5: a novel therapeutic target for reversing cardiac remodeling in heart failure. *Int J Cardiol* **178,** 210–211.

Wechsler J, Choi Y-H, Krall J, Ahmad F, Manganiello VC & Movsesian MA (2002). Isoforms of cyclic nucleotide phosphodiesterase PDE3A in cardiac myocytes. *J Biol Chem* **277,** 38072–38078.

Weeks KL & McMullen JR (2011). The athlete's heart vs. the failing heart: can signaling explain the two distinct outcomes? *Physiol Bethesda Md* **26,** 97–105.

Wegener JW, Nawrath H, Wolfsgruber W, Kühbandner S, Werner C, Hofmann F & Feil R (2002). cGMP-dependent protein kinase I mediates the negative inotropic effect of cGMP in the murine myocardium. *Circ Res* **90,** 18–20.

Wehrens XHT, Lehnart SE, Reiken SR & Marks AR (2004). Ca2+/calmodulin-dependent protein kinase II phosphorylation regulates the cardiac ryanodine receptor. *Circ Res* **94,** e61-70.

Weishaar RE, Kobylarz-Singer DC, Steffen RP & Kaplan HR (1987). Subclasses of cyclic AMP-specific phosphodiesterase in left ventricular muscle and their involvement in regulating myocardial contractility. *Circ Res* **61,** 539–547.

Wobst J, Rumpf PM, Dang TA, Segura-Puimedon M, Erdmann J & Schunkert H (2015). Molecular variants of soluble guanylyl cyclase affecting cardiovascular risk. *Circ J Off J Jpn Circ Soc* **79,** 463–469.

Wollert KC, Yurukova S, Kilic A, Begrow F, Fiedler B, Gambaryan S, Walter U, Lohmann SM & Kuhn M (2003). Increased effects of C-type natriuretic peptide on contractility and calcium regulation in murine hearts overexpressing cyclic GMP-dependent protein kinase I. *Br J Pharmacol* **140,** 1227–1236.

Woo AYH & Xiao R (2012). β-Adrenergic receptor subtype signaling in heart: from bench to bedside. *Acta Pharmacol Sin* **33,** 335–341.

Wu AY, Tang X-B, Martinez SE, Ikeda K & Beavo JA (2004). Molecular Determinants for Cyclic Nucleotide Binding to the Regulatory Domains of Phosphodiesterase 2A. *J Biol Chem* **279,** 37928–37938.

Wykes V, Bellamy TC & Garthwaite J (2002). Kinetics of nitric oxide-cyclic GMP signalling in CNS cells and its possible regulation by cyclic GMP. *J Neurochem* **83,** 37–47.

Xiang Y, Rybin VO, Steinberg SF & Kobilka B (2002). Caveolar localization dictates physiologic signaling of beta 2-adrenoceptors in neonatal cardiac myocytes. *J Biol Chem* **277,** 34280–34286.

Xiang YK (2011). Compartmentalization of beta-adrenergic signals in cardiomyocytes. *Circ Res* **109,** 231–244.

Xiao B, Jiang MT, Zhao M, Yang D, Sutherland C, Lai FA, Walsh MP, Warltier DC, Cheng H & Chen SRW (2005). Characterization of a novel PKA phosphorylation site, serine-2030, reveals no PKA hyperphosphorylation of the cardiac ryanodine receptor in canine heart failure. *Circ Res* **96,** 847–855.

Yan C, Miller CL & Abe J (2007*a*). Regulation of phosphodiesterase 3 and inducible cAMP early repressor in the heart. *Circ Res* **100,** 489–501.

Yan L, Vatner DE, O'Connor JP, Ivessa A, Ge H, Chen W, Hirotani S, Ishikawa Y, Sadoshima J & Vatner SF (2007*b*). Type 5 adenylyl cyclase disruption increases longevity and protects against stress. *Cell* **130,** 247–258.

Yanaka N, Kurosawa Y, Minami K, Kawai E & Omori K (2003). cGMP-phosphodiesterase activity is up-regulated in response to pressure overload of rat ventricles. *Biosci Biotechnol Biochem* **67,** 973–979.

Yang L, Liu G, Zakharov SI, Bellinger AM, Mongillo M & Marx SO (2007). Protein kinase G phosphorylates Cav1.2 alpha1c and beta2 subunits. *Circ Res* **101,** 465–474.

Yoo B, Lemaire A, Mangmool S, Wolf MJ, Curcio A, Mao L & Rockman HA (2009). Beta1-adrenergic receptors stimulate cardiac contractility and CaMKII activation in vivo and enhance cardiac dysfunction following myocardial infarction. *Am J Physiol Heart Circ Physiol* **297,** H1377-1386.

Zacchigna S, Zentilin L & Giacca M (2014). Adeno-Associated Virus Vectors as Therapeutic and Investigational Tools in the Cardiovascular System. *Circ Res* **114,** 1827–1846.

Zaccolo M (2006). Phosphodiesterases and compartmentalized cAMP signalling in the heart. *Eur J Cell Biol* **85,** 693–697.

Zaccolo M & Pozzan T (2002). Discrete microdomains with high concentration of cAMP in stimulated rat neonatal cardiac myocytes. *Science* **295,** 1711–1715.

Zafrir B & Amir O (2012). Beta blocker therapy, decompensated heart failure, and inotropic interactions: current perspectives. *Isr Med Assoc J IMAJ* **14,** 184–189.

Zhang KYJ, Card GL, Suzuki Y, Artis DR, Fong D, Gillette S, Hsieh D, Neiman J, West BL, Zhang C, Milburn MV, Kim S-H, Schlessinger J & Bollag G (2004). A glutamine switch mechanism for nucleotide selectivity by phosphodiesterases. *Mol Cell* **15,** 279–286.

Zhang KYJ, Ibrahim PN, Gillette S & Bollag G (2005). Phosphodiesterase-4 as a potential drug target. *Expert Opin Ther Targets* **9,** 1283–1305.

Zhang M & Kass DA (2011). Phosphodiesterases and cardiac cGMP: evolving roles and controversies. *Trends Pharmacol Sci* **32,** 360–365.

Zhao CY, Greenstein JL & Winslow RL (2016). Roles of phosphodiesterases in the regulation of the cardiac cyclic nucleotide cross-talk signaling network. *J Mol Cell Cardiol* **91,** 215–227.

Zoccarato A et al. (2015). Cardiac Hypertrophy Is Inhibited by a Local Pool of cAMP Regulated by Phosphodiesterase 2. *Circ Res* **117,** 707–719.